Advanced echocardiography and cardiac magnetic resonance in congenital heart disease

Insights in right ventricular mechanics and clinical implications

Annelies van der Hulst

Advanced echocardiography and cardiac magnetic resonance in congenital heart disease

Insights in right ventricular mechanics and clinical implications

Proefschrift

Ter verkrijging van
De graad van Doctor aan de Universiteit Leiden,
Op gezag van Rector Magnificus prof. mr. P.F. van der Heijden,
Volgens besluit van het College voor Promoties
Te verdedigen op donderdag 20 oktober 2011
klokke 15.00 uur

door

Anna Elisabeth van der Hulst
Geboren te Meppel in 1980

The project was supported by a grant from the Willem Alexander Kinderfonds, Leiden, the Netherlands.

The printing of this thesis was financially supported by the J.E. Jurriaanse Stichting, by the Division of Image Processing (LKEB) of the Leiden University Medical Center and by stichting Imago.

Financial support by the Dutch Heart Foundation for the publication of this thesis is gratefully acknowledged.

Cover and lay out by Anna Gerdien Bruna, Bruna & Bruna
Printed by GVO drukkers & vormgevers B.V

ISBN: 978-90-9026340-3

PROMOTIECOMMISSIE

Promotores:	Prof. dr. N. A. Blom Prof. dr. J.J. Bax Prof. dr. A. de Roos
Co-promotor:	dr. A.A.W. Roest
Overige leden:	Prof. dr. B.J.M. Mulder (Academisch Medisch Centrum, Amsterdam) Prof. dr. W.A. Helbing (Erasmus Medisch Centrum, Rotterdam) Prof. dr. M.G. Hazekamp Prof. dr. L. Mertens (Hospital for Sick Children, Toronto, Canada)

CONTENTS

CHAPTER 1

General Introduction

Advances in clinical, surgical and peri-operative knowledge have led to an increased survival of patients with congenital heart disease (CHD). As a result, the population with CHD has doubled over the last decades, and a growing extent of patients are surviving into late adulthood.(1) However, despite the improvements in clinical and surgical care, progressive heart failure remains a major cause of death during late follow-up of patients with complex CHD.(2) In adult (non-CHD) patients with heart failure, the recent advent of cardiac resynchronization therapy (CRT) has improved the clinical outcome of heart failure in patients with poor left ventricular (LV) ejection fraction and a wide QRS complex. CRT typically involves atrial-synchronized biventricular pacing, and improves LV function by inducing a more synchronous contraction pattern. Consequently, CRT has resulted in improvements in heart failure symptoms (New York Heart Association (NYHA) functional class, exercise capacity or quality of life) and all-cause mortality of heart failure patients.(3-7) Currently, CRT is a class I indication for adult non-CHD patients with NYHA functional class III or IV despite optimized pharmacological therapy, LV ejection fraction <35% and QRS duration >120 ms.(8,9)

The excellent outcomes obtained with CRT in adult non-CHD patients have raised interest to apply this therapy in CHD patients with heart failure. However, the etiologies of heart failure differ substantially between 'acquired' heart disease and CHD. An important subgroup of CHD patients with heart failure during follow-up are those with failure of the RV, of which the majority are patients with corrected Tetralogy of Fallot (cToF).(10) RV dysfunction is an important predictor of poor clinical outcome in these patients.(11) The RV differs importantly from the LV from an anatomical, embryological and functional point of view. The RV shape has a complex geometry, with a crescent shape when viewed in cross-section and a more triangular shape when viewed from the side. Embryologically, the RV can be divided into three sections; the sinus (inlet), the apical trabecular part, and the infundibulum (outlet).(12,13) Functionally, the RV is coupled to the pulmonary circulation which is highly distensible and has a low resistance.

Accordingly, the mechanical activation of the RV and its relation with myocardial performance, and hence the appropriate therapeutic strategies in RV failure may be different from the LV. Various advanced echocardiographic and cardiac magnetic resonance (CMR) imaging techniques have recently been developed, allowing comprehensive assessment of global and regional myocardial performance, motion and deformation. With the use of these imaging techniques, the mechanical activation pattern of the RV can be characterized in detail. Comprehensive knowledge on RV mechanics and performance may guide clinical decision-making with regard to therapeutic strategies in patients with RV failure, including the application of CRT.

Right ventricular imaging: echocardiography

Echocardiography is a readily available, non-invasive imaging tool that is routinely used in clinical practice for repeated cardiac imaging during follow-up of CHD patients. Various advanced echocardiographic imaging modalities allow a detailed characterization of myocardial performance, motion and deformation of the RV. **Tissue Doppler imaging** (TDI) enables the assessment of RV mechanics by measuring myocardial velocities and the temporal occurrence of myocardial motion with high temporal resolution. With the use of TDI, the velocity of the myocardium with respect to the transducer is measured. The assessment of peak systolic velocities at the basal RV free wall with TDI has shown to be of incremental value to conventional echocardiography to assess global and regional ventricular performance in various clinical conditions.(14,15) Furthermore, with TDI, the temporal occurrence of mechanical events can be measured, by calculating the time of the events relative to the onset of the QRS complex on the electrocardiogram. The assessment of timings of peak systolic velocities provides insight into electromechanical coupling and possible mechanical dyssynchrony.(16)

Another advanced echocardiographic technique is two-dimensional strain imaging or **speckle-tracking strain imaging.** Speckle tracking strain imaging permits multidirectional and angle-independent assessment of myocardial deformation. With this echocardiographic technique, the so-called speckles (natural acoustic markers equally distributed within the myocardium in 2-dimensional gray-scale echocardiographic images) are tracked frame-by-frame throughout the cardiac cycle. The change of their position relative to their original position is used to calculate myocardial strain. The assessment of myocardial strain has demonstrated to be useful to detect subclinical cardiac dysfunction in several clinical conditions.(17,18) Similar to TDI, with speckle-tracking strain imaging, the timing of peak systolic strain may be assessed, providing insight into possible dyssynchrony. Furthermore, speckle-tracking strain imaging permits imaging of torsional mechanics. LV twist takes into account the complex helical disposition of the myofibers and is a sensitive index of LV performance. By evaluating RV and LV strain, LV apical and basal rotation and LV twist, the ventricular-ventricular interaction between the LV and RV may be assessed at a regional level.

Finally, reliable assessment of volumes and ejection fraction of the RV is of clinical importance in CHD patients with RV failure. Quantification of RV volumes by two-dimensional echocardiography is hampered by the complex ventricular geometry. **Real-time three-dimensional echocardiography** of the RV overcomes this problem by imaging the entire RV in a three-dimensional volume. Furthermore, real-time three-dimensional echocardiography enables computation of regional volumes and function of the various RV segments: RV inlet, apical trabecular part and RV outlet.

Right ventricular imaging: cardiac magnetic resonance

CMR is a versatile non-invasive imaging technique during clinical follow-up of post-operative CHD patients.(19) With echocardiography, imaging of the RV is hampered by its complex geometry and its anterior position within the chest. CMR is independent of geometrical assumptions and of the acoustic window. Currently, CMR is the reference standard to quantify RV volumes and function, as well for the quantification of flow over the cardiac valves.(19) In addition, various advanced CMR techniques have enabled insight into ventricular mechanics. With the use of **Tissue-velocity magnetic resonance imaging** (TV-MRI), myocardial velocities can be assessed. TV-MRI has been validated against TDI for the assessment of myocardial velocities and timings of peak systolic velocities in the LV.(20-23) In CHD patients undergoing routine CMR evaluation, the validation of TV-MRI to assess myocardial velocities of the RV would permit a comprehensive assessment of ventricular volumes, function and myocardial velocities during a single integrated MRI examination. The evaluation of systolic velocities provides insight into ventricular performance

and possible dyssynchrony. In addition, the evaluation of diastolic velocities with TV-MRI or TDI yields a detailed quantitative assessment of RV diastolic function at a regional level, which can provide insight into the pathophysiological mechanism leading to RV dysfunction in CHD patients. In cToF patients, pulmonary regurgitation is a common hemodynamic lesion. Pulmonary regurgitation is an important cause of RV dilatation and RV failure. Therefore, reliable assessment of pulmonary flow has important clinical implications. Furthermore, comprehensive quantification of pulmonary regurgitation with CMR provides the opportunity to investigate the complex relationship among chronic volume overload, RV mechanics, and RV failure. Two-dimensional velocity-encoded CMR, the current reference standard for assessing PV flow, is hampered by cardiac motion, because the acquisition plane is fixed throughout the cardiac cycle. **Three-dimensional three-directional velocity-encoded flow imaging** (3D flow) has recently been introduced for the assessment of transvalvar flow.(24-26) The use of 3D velocity-encoded MR imaging resolves the problem of valvar annulus motion owing to retrospective valve tracking and velocity-encoding in three orthogonal directions. Furthermore, 3D flow imaging allows simultaneous assessment of flow over all four cardiac valves. This simultaneous assessment enables evaluation of global RV diastolic function of in cToF patients with pulmonary regurgitation. In the presence of pulmonary regurgitation, the flow pattern over the tricuspid valve does not reflect RV relaxation, since RV filling occurs also from the pulmonary regurgitation. Summation of the 3D time-resolved diastolic flow curves of the pulmonary valve and tricuspid valve permits the reconstruction of RV time-volume curves.(27) From the time-volume curve of the RV, global RV diastolic function can be comprehensively appreciated.

Prediction of outcome of CHD patients with echocardiography

In current clinical practice, echocardiography plays a central role to routinely assess cardiac anatomy and function during follow-up of CHD patients. The advent of new echocardiographic imaging modalities provides novel anatomical, functional or electromechanical parameters, which may improve clinical-decision making by predicting outcome in the individual patient. (14,15,17,18) Hence, novel imaging techniques may refine risk stratifications in known clinical protocols. Conversely, when new therapeutic strategies emerge (such as CRT for heart failure or pulmonary valve replacement for pulmonary regurgitation), conventional as well as novel imaging techniques may aid the selection of patients that are most likely to benefit from these new interventions. Accordingly, an important goal of clinical research on cardiac imaging techniques is to ultimately gain insight into the clinical implications with respect to patient outcome and to refine therapeutic and interventional protocols.

Objectives and outline of this thesis

The objective of this thesis was to obtain insight into the electromechanical activation of the RV in CHD patients as well as in healthy subjects. Furthermore, the relation between global RV performance and electromechanical activation was investigated with various non-invasive echocardiographic and CMR imaging techniques. Finally, the clinical role of echocardiography to predict outcome in CHD patients was explored.

Part 1 of this thesis focuses on the various advanced echocardiographic imaging tools to assess RV and LV mechanics in CHD patients. **Chapter 2.1** provides an overview on the application of CRT in CHD and pediatric patients and on the echocardiographic techniques to assess cardiac dyssynchrony. In **chapter 2.2**, the normal timings of peak systolic velocities and intra-ventricular time differences within the LV and RV in healthy children of various ages are investigated with TDI. **Chapter 2.3** describes the mechanical activation sequence of the RV, as assessed with speckle tracking strain imaging, and its relation with myocardial performance in healthy controls as well as in cToF patients. **Chapter 2.4** provides insight into ventricular-ventricular interactions with speckle tracking strain imaging and evaluation of torsional mechanics in healthy subjects and in CHD patients with a dilated RV. Finally, in **chapter 2.5,** a segmental analysis of RV dilatation and ejection fraction is performed and validated with real-time three-dimensional echocardiography, and the adaptive response of the various RV segments to chronic volume overload is investigated. Subsequently, Part 2 of this thesis focuses on CMR imaging of the RV in CHD patients. **Chapter 3.1** provides an overview on the role of CMR during follow-up of post-operative CHD patients. **Chapter 3.2** describes a study on the validation of TV-MRI against TDI to assess regional systolic myocardial velocities and the mechanical activation sequence of the RV. **Chapter 3.3** addresses the feasibility of TV-MRI and TDI to assess regional diastolic velocities at the RV in cToF patients. Furthermore, the clinical use of the assessment of regional diastolic velocities with TV-MRI is addressed in this chapter. In **chapter 3.4,** 3D flow is comprehensively validated against 2D flow and planimetric CMR for the assessment of pulmonary and tricuspid flow. In addition, a clinical application of 3D flow is provided that can reliably assess diastolic RV function in the presence of pulmonary regurgitation. Finally, part 3 of this thesis provides insight into the clinical application of echocardiography to predict outcome during long-term follow-up of CHD patients. In **chapter 4.1,** the predictive value of a residual pulmonary stenosis, as assessed with echo Doppler echocardiography in cToF patients is demonstrated. In **chapter 4.2**, TDI is used to predict atrial arrhythmia during follow-up of adult CHD patients. In **chapter 5,** the summary and conclusions of this thesis are provided.

REFERENCE LIST

1 Marelli AJ, Mackie AS, Ionescu-Ittu R, et al. Congenital heart disease in the general population: changing prevalence and age distribution. Circulation 2007;115:163-72.

2 Oechslin EN, Harrison DA, Connelly MS, et al. Mode of death in adults with congenital heart disease. Am J Cardiol 2000;86:1111-6.

3 Auricchio A, Stellbrink C, Sack S, et al. Long-term clinical effect of hemodynamically optimized cardiac resynchronization therapy in patients with heart failure and ventricular conduction delay. J Am Coll Cardiol 2002;39:2026-33.

4 Bristow MR, Saxon LA, Boehmer J, et al. Cardiac-resynchronization therapy with or without an implantable defibrillator in advanced chronic heart failure. N Engl J Med 2004;350:2140-50.

5 Cazeau S, Leclercq C, Lavergne T, et al. Effects of multisite biventricular pacing in patients with heart failure and intraventricular conduction delay. N Engl J Med 2001;344:873-80.

6 Cleland JG, Daubert JC, Erdmann E, et al. The effect of cardiac resynchronization on morbidity and mortality in heart failure. N Engl J Med 2005;352:1539-49.

7 Young JB, Abraham WT, Smith AL, et al. Combined cardiac resynchronization and implantable cardioversion defibrillation in advanced chronic heart failure: the MIRACLE ICD Trial. JAMA 2003;289:2685-94.

8 Epstein AE, DiMarco JP, Ellenbogen KA, et al. ACC/AHA/HRS 2008 Guidelines for Device-Based Therapy of Cardiac Rhythm Abnormalities: a report of the American College of Cardiology/American Heart Association Task Force on Practice Guidelines (Writing Committee to Revise the ACC/AHA/NASPE 2002 Guideline Update for Implantation of Cardiac Pacemakers and Antiarrhythmia Devices) developed in collaboration with the American Association for Thoracic Surgery and Society of Thoracic Surgeons. J Am Coll Cardiol 2008;51:e1-62.

9 Vardas PE, Auricchio A, Blanc JJ, et al. Guidelines for cardiac pacing and cardiac resynchronization therapy: The Task Force for Cardiac Pacing and Cardiac Resynchronization Therapy of the European Society of Cardiology. Developed in collaboration with the European Heart Rhythm Association. Eur Heart J 2007;28:2256-95.

10 Gatzoulis MA, Balaji S, Webber SA, et al. Risk factors for arrhythmia and sudden cardiac death late after repair of tetralogy of Fallot: a multicentre study. Lancet 2000;356:975-81.

11 Geva T, Sandweiss BM, Gauvreau K, et al. Factors associated with impaired clinical status in long-term survivors of tetralogy of Fallot repair evaluated by magnetic resonance imaging. J Am Coll Cardiol 2004;43:1068-74.

12 Anderson RH, Ho SY. What is a ventricle? Ann Thorac Surg 1998;66:616-20.

13 Sheehan F, Redington A. The right ventricle: anatomy, physiology and clinical imaging. Heart 2008;94:1510-5.

14 Alam M, Wardell J, Andersson E, et al. Right ventricular function in patients with first inferior myocardial infarction: assessment by tricuspid annular motion and tricuspid annular velocity. Am Heart J 2000;139:710-5.

15 Meluzin J, Spinarova L, Bakala J, et al. Pulsed Doppler tissue imaging of the velocity of tricuspid annular systolic motion; a new, rapid, and non-invasive method of evaluating right ventricular systolic function. Eur Heart J 2001;22:340-8.

16 Ypenburg C, Westenberg JJ, Bleeker GB, et al. Noninvasive imaging in cardiac resynchronization therapy--part 1: selection of patients. Pacing Clin Electrophysiol 2008;31:1475-99.

17 Delgado V, Ypenburg C, van Bommel RJ, et al. Assessment of left ventricular dyssynchrony by speckle tracking strain imaging comparison between longitudinal, circumferential, and radial strain in cardiac resynchronization therapy. J Am Coll Cardiol 2008;51:1944-52.

18 Hare JL, Brown JK, Marwick TH. Association of myocardial strain with left ventricular geometry and progression of hypertensive heart disease. Am J Cardiol 2008;102:87-91.

19 Pennell DJ, Sechtem UP, Higgins CB, et al. Clinical indications for cardiovascular magnetic resonance (CMR): Consensus Panel report. J Cardiovasc Magn Reson 2004;6:727-65.

20 Delfino JG, Bhasin M, Cole R, et al. Comparison of myocardial velocities obtained with magnetic resonance phase velocity mapping and tissue Doppler imaging in normal subjects and patients with left ventricular dyssynchrony. J Magn Reson Imaging 2006;24:304-11.

21 Marsan NA, Westenberg JJ, Tops LF, et al. Comparison between tissue Doppler imaging and velocity-encoded magnetic resonance imaging for measurement of myocardial velocities, assessment of left ventricular dyssynchrony, and estimation of left ventricular filling pressures in patients with ischemic cardiomyopathy. Am J Cardiol 2008;102:1366-72.

22 Paelinck BP, de Roos A, Bax JJ, et al. Feasibility of tissue magnetic resonance imaging: a pilot study in comparison with tissue Doppler imaging and invasive measurement. J Am Coll Cardiol 2005;45:1109-16.

23 Westenberg JJ, Lamb HJ, van der Geest RJ, et al. Assessment of left ventricular dyssynchrony in patients with conduction delay and idiopathic dilated cardiomyopathy: head-to-head comparison between tissue doppler imaging and velocity-encoded magnetic resonance imaging. J Am Coll Cardiol 2006;47:2042-8.

24 Roes SD, Hammer S, van der Geest RJ, et al. Flow Assessment Through Four Heart Valves Simultaneously Using 3-Dimensional 3-Directional Velocity-Encoded Magnetic Resonance Imaging With Retrospective Valve Tracking in Healthy Volunteers and Patients With Valvular Regurgitation. Invest Radiol 2009.

25 Westenberg JJ, Danilouchkine MG, Doornbos J, et al. Accurate and reproducible mitral valvular blood flow measurement with three-directional velocity-encoded magnetic resonance imaging. J Cardiovasc Magn Reson 2004;6:767-76.

26 Westenberg JJ, Roes SD, Ajmone MN, et al. Mitral valve and tricuspid valve blood flow: accurate quantification with 3D velocity-encoded MR imaging with retrospective valve tracking. Radiology 2008;249:792-800.

27 Helbing WA, Niezen RA, Le Cessie S, et al. Right ventricular diastolic function in children with pulmonary regurgitation after repair of tetralogy of Fallot: volumetric evaluation by magnetic resonance velocity mapping. J Am Coll Cardiol 1996;28:1827-35.

CHAPTER 2

Right ventricular imaging: echocardiography

2.1

Review: cardiac resynchronization therapy in pediatric and congenital heart disease patients

European Heart Journal 2011; doi: 10.1093/eurheartj/ehr093

A.E. van der Hulst
V. Delgado
N.A. Blom
N.R. van de Veire
M.J. Schalij
J. J. Bax
A.A.W. Roest
E.R. Holman

ABSTRACT

The number of patients with congenital heart disease (CHD) has significantly increased over the last decades. The CHD population has a high prevalence of heart failure during late follow-up and this is a major cause of mortality. Cardiac resynchronization therapy (CRT) may be a promising therapy to improve the clinical outcome of CHD and pediatric patients with heart failure. However, the CHD and pediatric population is a highly heterogeneous group with different anatomical substrates that may influence the effects of CRT. Echocardiography is the mainstay imaging modality to evaluate CHD and pediatric patients with heart failure and novel echocardiographic tools permit a comprehensive assessment of cardiac dyssynchrony that may help selecting candidates for CRT. This article reviews the role of CRT in the CHD and pediatric population with heart failure. The current inclusion criteria for CRT as well as the outcomes of different anatomical subgroups are evaluated. Finally, echocardiographic assessment of mechanical dyssynchrony in the CHD and pediatric population and its role in predicting response to CRT is comprehensively discussed.

INTRODUCTION

Heart failure is a major health burden with an estimated overall prevalence of 2-3%.(1) Cardiac resynchronization therapy (CRT) has improved the clinical outcome of drug refractory heart failure in patients with poor left ventricular ejection fraction (LVEF) and wide QRS complex. CRT improves LV function by inducing a more synchronous contraction. Consequently, CRT has resulted in improvements in heart failure symptoms (New York Heart Association (NYHA) functional class, exercise capacity or quality of life) and all-cause mortality of heart failure patients.(2-7) Currently, CRT is a class I indication for patients with NYHA functional class III or IV despite optimized pharmacological therapy, LVEF <35% and QRS duration >120 ms.(8;9)

Advances in cardiac surgery have led to an increased survival of patients with congenital heart disease (CHD). As a result, the prevalence of CHD in the pediatric population has doubled over the last decades.(10) Progressive heart failure is a major cause of death during late follow-up of patients with complex CHD.(11;12) The excellent outcomes obtained with CRT in adult patients have raised interest to apply this therapy in CHD and pediatric patients with heart failure. However, the current inclusion criteria for CRT in adult populations may not be directly applied to pediatric patients. Etiologies of heart failure differ substantially between adults and children, with CHD as the mainstay cause in the pediatric population.(13) In addition, within the CHD population there are several subgroups of patients according to (post-surgical) cardiac anatomy, including patients with a systemic LV, patients with a systemic right ventricle (RV) and patients with a single ventricle. These different groups may show different responses to CRT.(14-16) Therefore, a detailed evaluation prior to CRT implantation may be crucial to identify those who will benefit from this therapy within this heterogeneous group of patients.

Cardiac imaging plays a central role in the evaluation of CHD and pediatric patients before CRT device implantation. Accurate assessment of ventricular volumes and function is mandatory before CRT implantation to assess heart failure severity and to accurately follow-up ventricular function. In addition, assessment of cardiac anatomy is crucial to anticipate the ventricular pacing lead implantation approach (epicardial or transvenous). Furthermore, the study of ventricular mechanical dyssynchrony and identification of the latest activated areas may help to define the most suited position of the ventricular pacing lead and may provide meaningful insight into the effects of CRT in the CHD and pediatric population. Several echocardiographic methods have been proposed to evaluate ventricular mechanical dyssynchrony.(17) The assessment of ventricular dyssynchrony in the adult populations has been demonstrated useful to identify patients who will benefit from CRT, with subsequently a better clinical outcome.(17) However, the role of established dyssynchrony parameters based on tissue Doppler imaging (TDI), 2-dimensional (2D) speckle tracking and real-time 3-dimensional (RT3D) echocardiography to evaluate mechanical dyssynchrony has not been extensively studied in the CHD and pediatric population. This article reviews the role of CRT in chronic heart failure in the CHD and pediatric population, focusing particularly on the current inclusion criteria and outcomes of different anatomical subgroups. Finally, the different imaging

modalities to assess cardiac mechanical dyssynchrony in the CHD and pediatric population and their role in predicting response to CRT will be discussed.

EXPERIENCE OF CRT IN CHD AND PEDIATRIC PATIENTS

The main CRT trials on CHD and pediatric patients have included highly heterogeneous populations. According to an anatomical classification, different subgroups can be defined, including patients with:

- systemic LV failure,
- systemic RV failure,
- failure of the single ventricle.

The group of patients with **systemic LV failure** (Figure 1, panel A) consists of both pediatric patients with normal cardiac anatomy with heart failure due to cardiomyopathies or congenital atrioventricular block, and of patients (children and adults) with LV failure due to underlying CHD. Although the majority of evidence is based on case reports and small case series(18-25) several retrospective non-randomized trials including heterogeneous populations have reported favourable outcomes after CRT in this subgroup of patients.(14-16)

Failure of the systemic right ventricle (Figure 1, panel B) is commonly observed in patients with complete transposition of the great arteries who underwent atrial switch operation (Mustard or Senning procedure), and patients with congenital corrected transposition of the great arteries (double discordance).(26-28) A recent study evaluated the effects of CRT in eight patients with systemic RV failure. After a median follow-up of 17 months, RV ejection fraction significantly increased (mean change +10%, p=0.004) along with a decrease in QRS duration (from 161 ± 21 ms to 116 ± 22 ms, p<0.01).(29) Subsequent small studies further demonstrated favourable clinical outcomes in RV systemic failure patients treated with CRT, yielding improvements in NYHA functional class, RV ejection fraction and exercise performance.(14-16;21;30-33)

Finally, patients with **failure of the single ventricle** (Figure 1, panel C) may constitute the most challenging population. According to current surgical practice, most patients with one hypoplastic ventricle undergo surgical palliation by a Fontan procedure or total cavo-pulmonary connection. The systemic and pulmonary circulations are separated without interposition of a sub-pulmonary ventricle, and both caval veins are redirected to the pulmonary artery. The ventricle supporting the systemic circulation may be either of RV or LV morphology. Despite surgical intervention, heart failure is common in this subgroup of patients.(28) Bacha and colleagues studied the effects of post-operative CRT in 26 single-ventricle patients.(34) Multisite epicardial pacing with maximal distance between the wires yielded a significant reduction of QRS duration (from 94 ± 18 ms to 72 ± 11 ms, p<0.01) and a significant improvement in cardiac function.

The different anatomical classification of CHD patients may account for differences in response rates to CRT. In addition, cardiac anatomy may challenge lead implantation. In contrast to adult patients with heart failure, a surgical epicardial approach is commonly needed. Particularly, surgical

Table 1. Retrospective cohorts on CRT in CHD and pediatric patients

	CRT studies in CHD and pediatric populations		
	Dubin et al.(15)	**Cecchin et al.(14)**	**Janousek et al.(16)**
Number of patients (n)	103	60	109
Age range (y) **median**	0.3 – 55 13	0.4 – 43 15	0.2 – 74 17
Follow-up (mo)	4.8 ± 4	range: 1 – 64 median: 8.4†	range: n/a median: 7.5
Before CRT			
NYHA functional class n (%)			
I	15 (14)	16 (27)	
II	49 (48)	25 (42)	median: 2.5
III-IV	39 (38)	19 (32)	
Systemic ventricle EF (%)	26 ± 12	range: 8 – 70 median: 36	range: n/a median:27
QRS (ms)	166 ± 33	range: 95 – 210 median: 149	range: n/a median: 160
Successful implantations n (%)	n/a	49 (82)	93 (85)
Complications n (%)	20‡ (19)	6 (10)	10 (9)
After CRT			
NYHA functional class n (%)	n/a	n/a	median change -1.5
Systemic ventricle EF (%)	40 ± 15*	range: n/a median: 43*	median change +12
QRS (ms)	126 ± 24*	range: n/a median: 120*	range: n/a median:130*
Response rates defined as			
Systemic ventricle EF improvement n (%)	78 (76)	n/a	n/a
NYHA improvement ≥ 1 class n (%)	n/a	19 (32)	n/a
Systemic ventricle EF or NYHA improvement n (%)	n/a	39 (65)	79 (72)
Survival rate n (%)	98 (95)	65 (92)	102 (94)

Data of three retrospective CRT studies in CHD and pediatric populations. Continuous data are expressed in means ± standard deviation unless otherwise specified. Response rates are on an intention to treat basis, i.e. including the total amount of patients enrolled in the study, regardless of deaths, follow-up and unsuccessful implantations. Complications included: pocket hematomas, infection, lead issues, blood loss, ventricular arrhythmia, pneumothorax, pleural effusion, pulmonary edema, cardiac perforation, cardiovascular incidents and pacing threshold problems. Abbreviations: deaths: any deaths during follow-up period, EF: ejection fraction, mo: months, n/a: not available, NYHA: New York Heart Association functional class, successful implantation: all patients alive and receiving CRT at latest follow-up date, y: years. * statistical difference (p<0.05) as compared with data before CRT implantation. † majority of outcome data obtained at 3 months follow-up.‡ includes early complications (<30 days after CRT implantation).

Table 2. Response rates of retrospective cohorts on CRT in CHD and pediatric patients, according to anatomical subgroups

	CRT studies in CHD and pediatric populations		
	Dubin et al.(15)	Cecchin et al.(14)	Janousek et al.*(16)
Systemic LV n (%)	79 (77)	38 (63)	62 (67)
Increase LVEF (%)	n/a	median: 8*	median: 13*
Decrease QRS (ms)	n/a	median: 33*	median: 40*
Response rate defined as			
Increase LVEF n (%)	n/a	n/a	n/a
NYHA improvement ≥1 class n (%)	n/a	n/a	n/a
LVEF increase or NYHA improvement n (%)	n/a	n/a	43 (69)
Systemic RV n (%)	17 (16)	9 (15)	27 (29)
Increase RVEF (%)	13 ± 11*	median: 14	7*
Decrease QRS (ms)	38 ± 29*	median: 15	median: 21
Response rate defined as			
increase RVEF n (%)	n/a	n/a	n/a
NYHA improvement ≥1 class n (%)	13 (76)	n/a	n/a
RVEF increase or NYHA improvement n (%)	n/a	2 (22)	19 (70)
Single ventricle n (%)	7 (7)	13 (22)	4 (4)
Increase LVEF or RVEF (%)	7.3 ± 5.7	median: 10	n/a
Decrease QRS (ms)	45 ± 26*	median: 13	n/a
Response rate defined as			
LVEF or RVEF increase n (%)	n/a	10 (77)	n/a
NYHA improvement ≥1 class n (%)	2 (30)	7 (54)	2 (50)
RVEF/LVEF increase or NYHA improvement n (%)	n/a	n/a	3 (75)

Response rates after CRT in three retrospective studies in CHD and pediatric populations, displayed for every anatomical subgroup. Response percentages are on an intention to treat basis, i.e. including the total amount of patients enrolled in the study, regardless of deaths, follow-up and unsuccessful implantations.
Abbreviations: LVEF: left ventricular ejection fraction, NYHA: New York Heart Association class, RVEF: right ventricular ejection fraction.

* statistical difference ($p<0.05$) as compared with data before CRT Implantation.*patients with concurrent cardiac surgical procedure excluded

epicardial lead implantation may be preferred in small patients or in patients with a concomitant cardiac surgical indication. However, the three largest trials including CHD and pediatric patients report no differences in complications during CRT implantation or in clinical outcome between the patients with transvenous or epicardial lead implantation.(14-16)

Beyond the anatomical classification as described above, a substantial part of the studies on CRT in pediatric and CHD patients includes patients who previously underwent conventional single-site pacing for congenital or surgical atrioventricular block.(14-16) In these patients, chronic single-site ventricular pacing may cause failure of the systemic ventricle at long-term follow-up.(35-38) Several small series have reported promising results with significant clinical and echocardiographic improvement after CRT upgrading.(21;24;25;30;32;33;39-41) For example, Moak et al describe a series of 6 patients with LV failure after long-term single-site pacing. Along with clinical improvement in all patients, LVEF significantly increased (from 34 ± 6% to 60 ± 2%, p=0.003) after upgrade to CRT.41

OUTCOME OF CRT IN CHD AND PEDIATRIC PATIENTS

Beyond case reports and small case series, data on mid and long-term outcome, as well as survival and complication rates of CRT in pediatric patients are limited to three retrospective studies including patients with all anatomical substrates and etiologies (Table 1).

First, Dubin et al. described the outcomes of 103 CHD and pediatric patients in a multicenter study.(15) After a mean duration of 4.8 months follow-up, a reduction in QRS duration (from 166 ± 33 ms to 126 ± 24 ms, $p<0.01$) and an increase in ejection fraction of the systemic ventricle (from 26 ± 12% to 40 ± 15%, $p<0.05$) were observed after CRT. Finally, the survival rate in this cohort was 95%.

Second, Cecchin and colleagues reported mid-term outcomes of 60 CHD and pediatric patients treated with CRT.(14) Significant improvement in the ejection fraction of the systemic ventricle (from 36% to 43%, $p<0.01$) and decrease in QRS duration (from 149 ms to 120 ms, $p<0.01$) were reported. A total of 65 (92%) patients survived during follow-up.

Third, Janousek and co-workers performed a multicenter trial on CRT including 109 CHD and pediatric patients.(16) Similar to the other series, a significant improvement in ejection fraction of the systemic ventricle (from 27% to 39%, $p<0.01$) and decrease in QRS duration (from 160 ms to 130 ms, $p<0.01$) were noted. Finally, 94% of patients survived during follow-up.

In these three studies, response rates (based on intention to treat) ranged between 32% and 76%, depending on the established end points. Dubin and colleagues reported a response rate of 76%, defined as an improvement in ejection fraction of the systemic ventricle.(15) In the study by Cecchin and co-workers, 32% of patients exhibited an improvement in NYHA functional class, and 65% of patients improved in either NYHA functional class or ejection fraction of the systemic ventricle.(14) Finally, Janousek et al. defined response as improvement in NYHA functional class or ejection fraction of the systemic ventricle and reported a response rate of 72%.(16)

The different anatomical subgroups may account for differences in the response rates to CRT.

Figure 1. Anatomical subgroups of CHD and pediatric patients

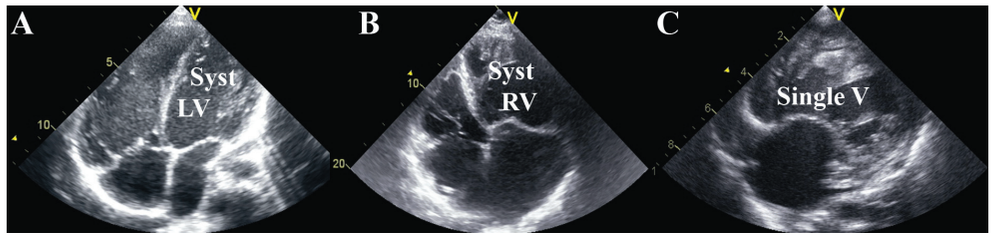

Panel A: Example of a CHD patient with a systemic left ventricle. Apical 4-camber viewof a patient after correction of tetralogy of Fallot.The left ventricle is the systemic ventricle in patients with tetralogy of Fallot. The right ventricle is dilated in this patient due to pulmonary regurgitation and subsequent chronic volume overload. In tetralogy of Fallot, systemic left ventricular failure may occur during late follow-up. **Panel B:** Example of a CHD patient with a systemic right ventricle. Apical 4-chamber view of a patient with congenital corrected transposition of the great arteries (double discordance). The (morphological) right ventricle is the systemic ventricle in patients with congenital corrected transposition of the great arteries. Note the trabecularization of the systemic right ventricle and the (more apical) septal insertion of the atrioventricular valve compared with the (morphological) left ventricle. Systemic right ventricular failure is a common problem in patients with congenital corrected transposition of the great arteries. **Panel C:** Example of a CHD patient with a singe ventricle. Apical "4-chamber" view of a patient with a hypoplastic left ventricle. The single ventricle is of right ventricular morphology. Note the very hypoplastic left ventricle. Failure of the single ventricle is common in patients with a hypoplastic left ventricle. Abbreviations: syst LV: systemic left ventricle, syst RV: systemic right ventricle, V: ventricle.

Figure 2. Atrioventricular dyssynchrony

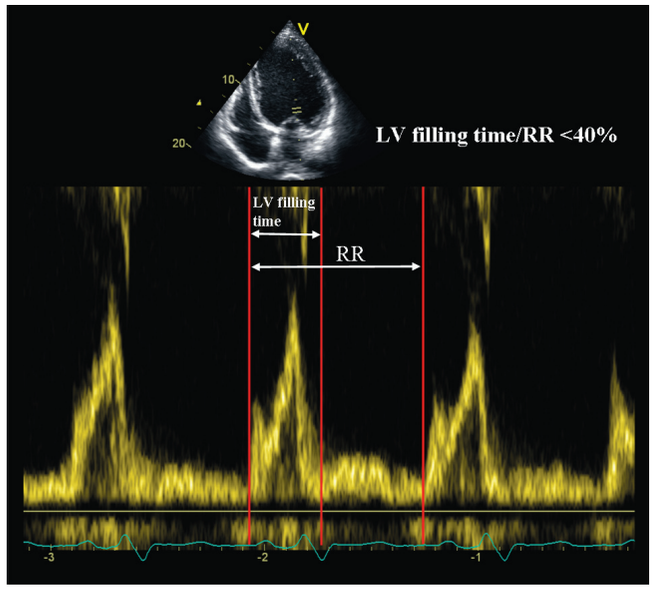

Example of a pediatric patient with idiopathic dilated cardiomyopathy and atrioventricular dyssynchrony as assessed with pulsed wave Doppler echocardiography. Left ventricular filling time is reduced (<40% of RR interval) and the early (E-wave) and late (A-wave) diastolic inflow waves are fused. Abbreviation: LV: left ventricle

Response rates of the anatomical subgroups are depicted in Table 2. The majority of patients had a systemic LV (63% to 77%). Janousek et al. reported a response rate of 69% in this subgroup, defined by an increase in either LVEF or NYHA functional class.(16)

The subgroup of patients with a systemic RV made up 15% to 29% of the cohorts (Table 3). Dubin and colleagues reported an improvement in NYHA functional class in 76% of this subgroup.(15) In addition, defining response rate by RV ejection fraction or NYHA functional class improvement, the trial by Cecchin et al. reported a response rate of 22%,(14) whereas Janousek and co-workers observed improvement in 70% of patients with a systemic RV.(16)

Single ventricle patients constituted 4% to 22% of the cohorts (Table 3). Improvement in NYHA functional class was observed in 30% to 54% of these patients.(14-16) In addition, Janousek et al. observed an echocardiographic or clinical response in 75% of the patients of this subgroup.(16)

Finally, 55 to 77% of patients in the three studies on CRT had a pacemaker before up-grading to

Figure 3. Inter-ventricular dyssynchrony

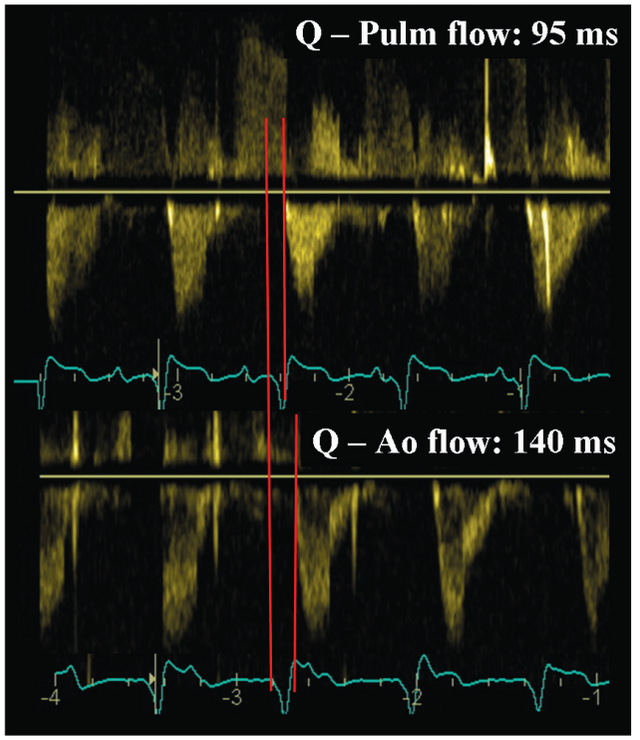

Example of inter-ventricular dyssynchrony in a patient with congenital atrioventricular block and chronic right ventricular pacing. Inter-ventricular dyssynchrony can be evaluated with pulsed wave Doppler echocardiography. The time from onset of the QRS complex to the onset of flow (pre-ejection interval) is measured in the pulmonary artery and in the left ventricular outflow tract. The difference between both pre-ejection times yields the so-called inter-ventricular mechanical delay (IVMD). In this example, the IVMD is 45 ms (>40 ms).(6) Abbreviations; Ao: aorta, Pulm: pulmonary artery.

CRT.(14-16) In the study of Janousek and colleagues, the patients with failure of the systemic LV who were upgraded from single-site pacing to biventricular pacing showed the highest response rate.(16) In addition, these patients showed a significantly larger improvement in NYHA functional class and a larger extent of LV reverse remodeling as compared with the rest of the study population.

Based on this clinical evidence, CRT may be a promising therapy to improve cardiac performance and clinical outcome of CHD and pediatric patients with heart failure. However, several issues need further investigation. First, the median follow-up duration of the three trials described is limited (4.8 to 8.4 months) (Table 1). Additional trials reporting on the long-term effects of CRT in CHD and pediatric patients are warranted. Furthermore, comparisons of the CRT response rate between heart failure adult patients and CHD and pediatric patients should take into consideration patient age and size related differences. Finally, current selection criteria remain controversial in CHD and pediatric patients, and accurate selection of patient subgroups that will benefit from CRT is warranted.

SELECTION OF CHD AND PEDIATRIC PATIENTS FOR CRT

Current inclusion criteria for CRT in the adult populations are: NYHA functional class III or IV despite optimal pharmacological therapy, LVEF <35% and QRS duration >120 ms.(8;9) However, the majority of the studies on CRT in CHD and pediatric populations have not applied these criteria prospectively.

NYHA functional class III or IV despite optimal pharmacological therapy is one of the inclusion criteria. In CRT trials enrolling CHD and pediatric populations, the majority of patients were in NYHA functional class I or II, indicating only mild heart failure. This discrepancy with the current guidelines likely resulted from a substantial proportion of CHD and pediatric patients with a concomitant indication for cardiac surgery (15% to 32%), ICD implantation or anti-bradycardia pacing (55-77%).(14-16) These concomitant indications may well have accelerated decision-making on CRT implantation during the same procedure in patients with only mild heart failure. In addition, Janousek et al. demonstrated that NYHA functional class is a strong determinant of CRT response in CHD and pediatric patients, with a higher favourable response rate in those patients with NYHA functional class I-II than in patients in NYHA functional class III-IV.(16) Indeed, the benefits of CRT in adult patients with mild symptomatic heart failure have been evaluated. The REsynchronization reVErses Remodeling in Systolic left vEntricular dysfunction (REVERSE) trial included over 600 heart failure patients in NYHA functional class I-II undergoing CRT implantation.(42) After 1 year follow-up, reverse LV remodeling and improved LVEF was observed, indicating a beneficial effect of CRT even with mild clinical heart failure. Therefore, the implantation of CRT at an early stage may help to prevent the progression and/or the development of heart failure. However, when CRT is considered in asymptomatic or mildly symptomatic patients, the possible effects of implantation of a device on quality of life need to be weighed against the benefits of CRT on cardiac performance. Importantly, in young pediatric patients, grading of heart failure by NYHA class may not be reliable.(43;44) In those patients, careful monitoring of ventricular performance by measuring ejection fraction may yield more reliable data about response to CRT.

Another inclusion criterion is LVEF <35%. The mean value of systemic ventricular ejection fraction in the three CHD and pediatric cohorts varied between 26% and 36%. Dubin et al. observed a lower baseline ejection fraction of the systemic ventricle in non responders (24 ± 11% versus 32 ± 14%, p=0.04).(15) However, evaluation of this parameter in the CHD and pediatric population is hampered by methodological difficulties. Although echocardiographic LVEF is reliable in patients with a systemic LV,(45) in patients with RV failure (systemic RV or single RV), standard echocardiography is less accurate for quantifying RV volumes and ejection fraction due to the complex RV geometry. In this regard, quantification with magnetic resonance imaging is currently preferred

Figure 4. Left ventricular dyssynchrony: M-mode septal-to-posterior wall motion delay

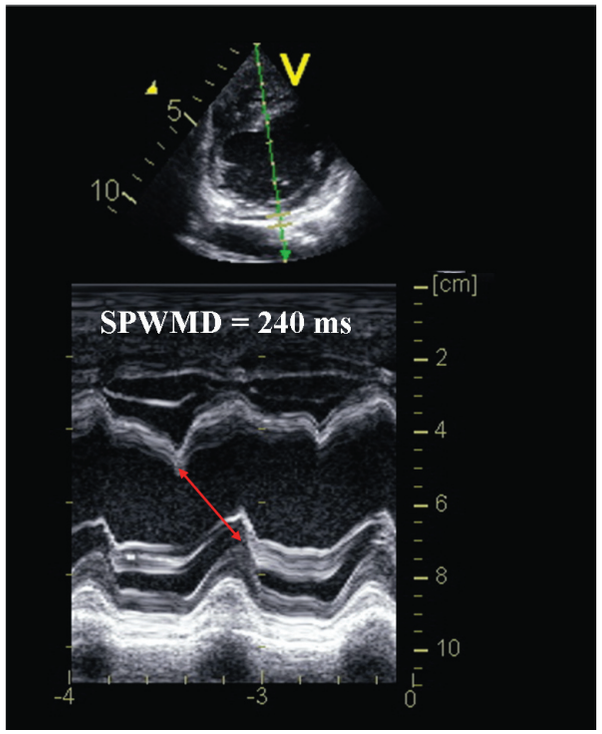

Example of left ventricular dyssynchrony in a patient with a truncus arteriosus after aortic and pulmonary valve replacement. The patient shows flattening of the septum in the parasternal short axis view due to right ventricular outflow obstruction. Left ventricular dyssynchrony is measured with M-mode septal-to-posterior wall motion delay (SPWMD). From the parasternal short-axis M-mode recording of the left ventricle, a delay of 240 ms is observed between the peak systolic inward motion of the septum and the peak systolic inward motion of the posterior wall. (SPWMD ≥130 ms indicates left ventricular dyssynchrony).(59) Abbreviations: SPWMD: septal-to-posterior wall motion delay.

over echocardiography since this imaging tool does not rely on geometrical assumptions.(46;47) Nevertheless, the majority of the CRT devices currently implanted are not compatible with magnetic resonance scanners and therefore, patient follow-up with this imaging technique is not feasible after device implantation.

Finally, CRT is indicated in patients with wide QRS complex. Current guidelines include width of the QRS complex >120 ms as a marker of electrical dyssynchrony. However, it has been shown that the relationship between electrical conduction delay and mechanical dyssynchrony is not straightforward.(2-6) In addition, the value of QRS complex duration to predict response to CRT may be suboptimal with a sensitivity and specificity of 54%.(48) The mean QRS duration in the three retrospective CHD and pediatric cohorts described above was >120 ms.(14-16) However, Dubin et al. stated that only 54% of included patients met the combined criteria of QRS >120 ms and systemic ventricle ejection fraction <35%. In addition, Pham et al. evaluated the effects of biventricular pacing in 19 CHD patients with a narrow QRS complex (96 ± 18 ms).(49) Temporary epicardial leads were implanted and several pacing modes, including biventricular pacing, were tested for 10 minutes each. Compared to conventional pacing modalities, biventricular pacing was associated with significant improvements in cardiac index in these patients with narrow QRS complex. Furthermore, various imaging studies in pediatric patients with dilated cardiomyopathy have demonstrated the presence of LV mechanical dyssynchrony despite narrow QRS complex.(50-52) These findings indicate that pediatric patients may benefit from CRT, even in the presence of a narrow QRS complex. Indeed, several adult trials included heart failure patients with narrow QRS complex and LV mechanical dyssynchrony, and observed favourable outcomes after CRT.(53;54)

As mentioned above, important differences with the current CRT inclusion criteria are observed in the pediatric cohorts, especially with regard to clinical heart failure classification and QRS duration. Moreover, the anatomical substrate may constitute an additional issue to be considered before CRT implantation in these populations. Cardiac imaging of ventricular function and mechanics (dyssynchrony) may provide additional insight into the effects of CRT and improve selection of CHD and pediatric patients who will benefit from CRT.

ECHOCARDIOGRAPHIC ASSESSMENT OF DYSSYNCHRONY

As mentioned before, prolonged QRS duration is the only criterion considered by current guidelines defining the presence of cardiac dyssynchrony. However, QRS duration might not be accurate enough to identify those patients who will benefit from CRT.(17) It has been demonstrated that the presence of mechanical dyssynchrony, rather than electrical dyssynchrony, may be a more robust parameter to select patients who will benefit from CRT.(17) Mechanical dyssynchrony may occur at different levels (atrioventricular, inter-ventricular and intra-ventricular(55)) and can be assessed with various cardiac imaging techniques. Echocardiography is the mainstay imaging modality to evaluate cardiac dyssynchrony and permits comprehensive assessment of these three different types of dyssynchrony.

Atrioventricular dyssynchrony

Atrioventricular dyssynchrony refers to a prolonged delay in atrioventricular sequential contraction, resulting from prolongation of the PR interval, QRS widening, or both.(56) With the use of pulsed-wave Doppler echocardiography, atrioventricular dyssynchrony can be assessed by measuring LV filling time from transmitral flow recordings. When the atrioventricular delay is prolonged, the early (E-wave) and late (A-wave) diastolic waves fuse and diastolic filling time of the ventricles is shortened.(56) In adult patients, a LV filling time/RR interval <40% indicates atrioventricular dyssynchrony (Figure 2).(56) In CHD and pediatric patients with LV systemic failure, no data on LV filling time are available so far. Nevertheless, surgical or congenital atrioventricular block may cause atrioventricular dyssynchrony and therefore the threshold of LV filling time/RR interval <40% needs investigation. However, in CHD patients with systemic RV failure, one small study provided data on RV filling time. Janousek et al. assessed RV filling time before and after CRT in eight patients with systemic RV failure and RBBB.(29) RV filling time was calculated from the transtricuspid pulsed-wave Doppler spectral signal. At 17 months follow-up, RV filling time (normalized for RR interval) had increased from 45.1 ± 6.5% to 50.0 ± 6.1% ($p<0.01$).

Inter-ventricular dyssynchrony

Inter-ventricular dyssynchrony refers to contraction delay between the RV and the LV. Several indexes have been proposed to assess this type of cardiac dyssynchrony. One of the first was the inter-ventricular mechanical delay (IVMD) assessed with pulsed-wave Doppler echocardiography. IVMD is obtained by calculating the difference between aortic and pulmonary pre-ejection intervals (the time from the onset of QRS to the onset of flow) (Figure 3). An IVMD >40 ms indicates inter-ventricular dyssynchrony.(6;56) The CARE-HF trial demonstrated the use of this index to predict response to CRT. Differences between CHD patients and adult heart failure patients may account for different IVMD cut-off values. For example, in patients with transposition of the great arteries (with normal LVEF), the aortic and pulmonary pre-ejection intervals differ from healthy individuals.(57) Furthermore, in patients with pulmonary stenosis, the pulmonary pre-ejection interval may be prolonged.(58) Little is known about IVMD cut-off values predicting response to CRT in pediatric and CHD patients.(24;29;31;39) The available studies included too few patients precluding to draw robust conclusions regarding the performance of this dyssynchrony index to predict response to CRT. However, a consistent reduction in IVMD after CRT was reported in the majority of patients.(24;29;31;39)

Intra-ventricular dyssynchrony: left ventricle

Intra-ventricular dyssynchrony of the LV (LV dyssynchrony) has shown to be an independent determinant of response to CRT and long-term survival in adult patients with heart failure. The assessment of LV dyssynchrony can be performed with various methods, evaluating time between mechanical events of two or more LV segments. Pitzalis et al. introduced the use of M-mode echocardiography to assess LV dyssynchrony.(59) From the parasternal short-axis view of the LV, the time difference between the maximal systolic inward motion of the septal and posterior wall was

Figure 5. Left ventricular dyssynchrony: Color-coded TDI septal-to-lateral wall motion delay

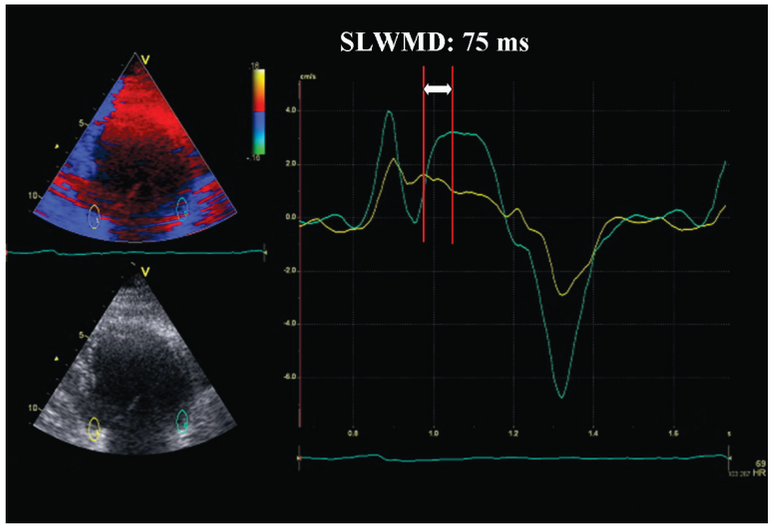

Left panel: Example of a patient with tricuspid atresia after Fontan procedure, with septal-to-lateral wall motion delay. Apical "4-chamber" view assessed with TDI. Two regions of interest are placed off-line at the basal septum (yellow) and left ventricular lateral wall (blue). **Right panel:** Time-velocity curves are reconstructed. The time difference between peak systolic velocity of the septal and lateral segments (septal-to-lateral wall motion delay) is 75 ms in this patient (>60 ms(62)). Abbreviations: SLWMD: septal-to-lateral wall motion delay. TDI: tissue Doppler imaging.

calculated: the so-called septal-to-posterior wall motion delay (SPWMD) (Figure 4). A cut-off value of SPWMD of ≥130 ms was proposed to predict response to CRT. In the CHD pediatric population several case reports and two small trials have used this index to evaluate the effects of CRT.(24;39;41;60;61) For example, Tomaske and colleagues described six children with CHD and systemic LV failure who were treated with CRT.(24) In these patients, SPWMD decreased from 312 ± 24 ms to 95 ± 57 ms (p=0.03) after one month follow-up, along with an improved LVEF (from 41 ± 6% to 53 ± 8%, p=0.03) and a trend towards a decreased LV end-diastolic volume (from 70 ± 22 ml/m^2 to 63 ± 18 ml/m^2, p=0.09).

The advent of TDI, measuring regional myocardial velocities, has provided useful parameters to assess LV dyssynchrony, identifying responders to CRT with high specificity and sensitivity.(17) Both pulsed-wave TDI and color-coded TDI can be used to assess LV dyssynchrony. Unlike pulsed-wave TDI, color-coded TDI can provide myocardial velocity tracings of two or more segments simultaneously (Figure 5). The feasibility and accuracy of color-coded TDI to evaluate LV dyssynchrony have been extensively explored in studies on CRT in the adult population.(17;62-64) One of the first indices was the time difference between peak systolic velocities of the septal and the lateral LV wall. From the apical 4-chamber view, the time difference between peak systolic velocity of the basal septal and basal lateral walls was calculated: the so-called septal-to-lateral wall delay.(62) A septal-to-lateral wall delay ≥60 ms predicted response to CRT with a sensitivity of 76% and a specificity of 78%.(62) Subsequently, a 4-segment model, including the basal segments of the septal, lateral, inferior and anterior walls was evaluated.(63) The maximum delay between peak systolic velocities among the four LV walls was calculated. A delay ≥65 ms predicted clinical and echocardiographic response to CRT with high sensitivity (92%) and specificity (92%).(63) Finally, Yu et al. proposed a 12-segment model, evaluating time to peak systolic velocity at six basal and six mid-myocardial segments of the LV.(64) A standard deviation ≥32.6 ms predicted LV reverse remodeling after CRT with a sensitivity and specificity of 100%.

Figure 6. Left ventricular dyssynchrony: TDI derived radial and longitudinal strain

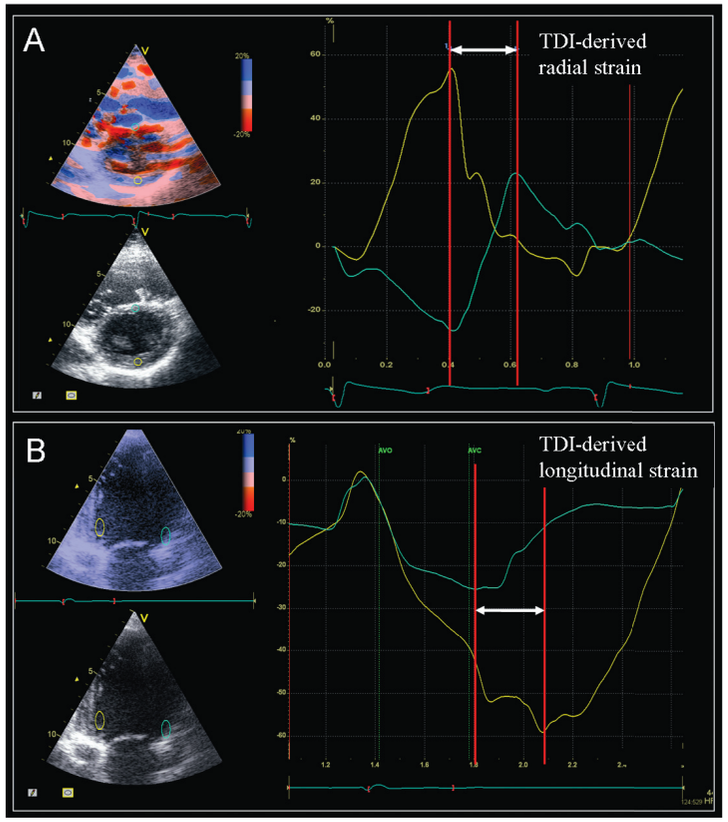

Panel A: Example of a postoperative tetralogy of Fallot patient with right ventricular dilatation and left ventricular dyssynchrony, assessed with TDI derived radial strain. **Left:** Regions of interest are placed at the septal (blue) and posterior (yellow) wall of the left ventricle. **Right:** Radial strain (thickening of myocardium) curve. Dyssynchrony can be quantified by measuring time between peak radial strain at the septal and posterior walls (white arrow). A delay between the septal and posterior wall >130 ms indicates radial dyssynchrony.(65) **Panel B:** Example of a patient with left ventricular dyssynchrony, assessed with TDI derived longitudinal strain. **Left:** Regions of interest are placed at the inferior (yellow) and anterior wall (blue). **Right:** Longitudinal strain (shortening of myocardium) curve. Dyssynchrony can be quantified by measuring time between peak radial strain at the septal and posterior walls (white arrow).(66) Abbreviation: TDI: tissue Doppler imaging.

Figure 7. Left ventricular dyssynchrony: two dimensional speckle tracking

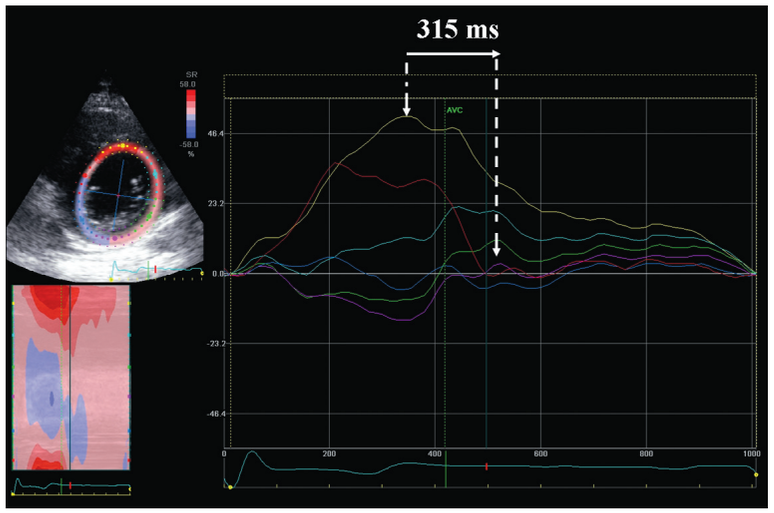

Example of a postoperative patient with atrioventricular septum defect and left ventricular dyssynchrony as assessed with two-dimensional speckle tracking radial strain. **Left panel**: A region of interest can be indicated in a two-dimensional gray scale image. The colors of the region of interest correspond with the colors of the time-strain curves in the right panel. **Right panel:** Time-radial strain curves of the different segments of the left ventricle. The time delay in peak radial strain between the antero-septal (yellow) and the posterior segments (purple curve) is 315 ms (≥130 ms), indicating the presence of significant left ventricular dysynchrony.(69)

In pediatric populations, the usefulness of these indices has been demonstrated in several case reports and one small trial.(19;20;24) Tomaske and co-workers applied a 4-segment TDI model in six CHD patients with systemic LV failure.(24) At baseline, the maximum intra-LV delay between two basal and two mid-ventricular LV segments in the apical 4-chamber view was 64 ± 10 ms and improved to 37 ± 8 ms after one month of CRT (p=0.03), along with an improved LV systolic performance.
In addition to myocardial velocity, myocardial strain can be obtained from color-coded TDI images (Figure 6). The advantage of strain imaging over myocardial velocity imaging is that strain indicates active myocardial deformation or contraction whereas velocity represents passive motion or displacement. Differences in time to peak strain can be calculated to quantify LV dyssynchrony. (65;66) TDI derived strain has been evaluated in a pediatric study.(67) Abd El Rahman and colleagues assessed TDI derived longitudinal strain in 25 patients (median 19 years, range 3-35 years) with tetralogy of Fallot and in 25 age-matched controls.(67) The mean time to peak strain was assessed at the LV free wall (basal, mid and apical) as well as at the septum, and the mean septal-to-LV free wall time delay was calculated. LV dyssynchrony was defined as a septal-to-LV free wall delay two standard deviations above the mean observed in controls (>25.8 ms). Accordingly, 52% of tetralogy of Fallot patients showed LV dyssynchrony. These patients had longer QRS duration (155 ± 19 ms vs. 136 ± 23 ms, p=0.018) and an impaired LV performance compared to patients without dyssynchrony, as assessed with the Tei index (Tei index in patients with LV dyssynchrony: 0.5 ± 0.08, Tei index in patients without LV dyssynchrony: 0.38 ± 0.06, p=0.004).

Figure 8. Left ventricular dyssynchrony assessed with real-time three-dimensional echocardiography

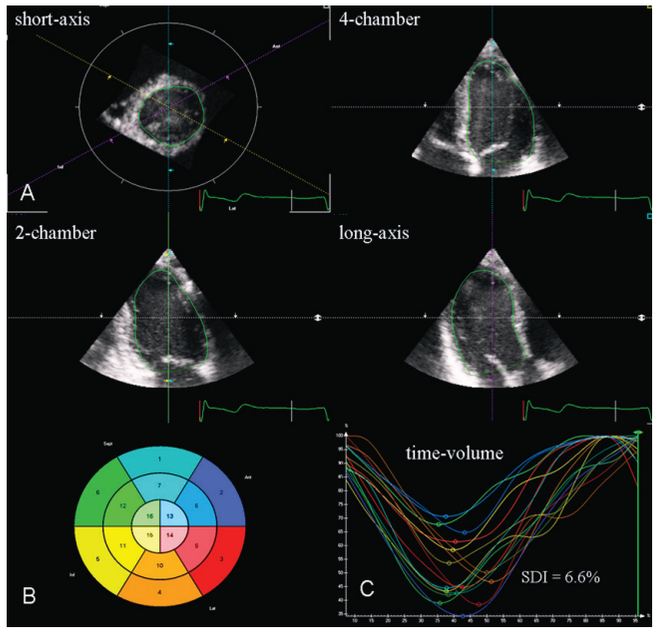

Example of a postoperative tetralogy of Fallot patient with left ventricular dyssynchrony, as assessed with real-time three-dimensional echocardiography. Contours are drawn at end-systole (**Panel A**) and end-diastole in the short-axis view, 4-chamber view, 2-chamber view and long-axis view. An automated tracking algorithm traces the myocardium throughout the cardiac cycle. The time-volume curves (**Panel C**) are displayed, depicting instantaneous volume of each of the left ventricular segments (**Panel B**), from which a systolic dyssynchrony index (standard deviation of time to minimum systolic volume of left ventricular segments) can be calculated. In this example, the systolic dyssynchrony index is 6.6%. A systolic dyssynchrony index >6.4% indicates left ventricular dyssynchrony.(75) Abbreviations: SDI: systolic dyssynchrony index.

Finally, the advent of novel echocardiographic techniques, including 2D strain and RT3DE has enabled assessment of dyssynchrony by evaluating active myocardial deformation (2D strain) or by evaluation of volumetric changes in a 3-dimensional fashion (RT3DE).
2D strain imaging or speckle-tracking strain imaging is a novel echocardiographic technique that permits multidirectional and angle-independent assessment of LV deformation. With this technique, the so-called speckles (natural acoustic markers equally distributed within the myocardium in 2D gray-scale images) are tracked frame-by-frame throughout the cardiac cycle. The change of their position relative to their original position is used to calculate myocardial strain. LV dyssynchrony can be characterized by evaluating radial strain (thickening of the myocardium in the short-axis views) (Figure 7). At the mid ventricular short-axis view of the LV, a maximum difference of ≥130 ms in time to peak strain between the antero-septal and the posterior LV segments has shown to predict favourable response to CRT in adult populations.(68;69) Other adult series have evaluated the use of circumferential (LV shortening along the short-axis curvature of the LV) and longitudinal strain to measure LV dyssynchrony and to evaluate the effects of CRT.(70;71) Tomaske

and co-workers investigated LV dyssynchrony by assessing 2D circumferential strain in 6 CHD patients who underwent CRT for systemic LV failure.(24) The maximum difference between the earliest and the latest activated segments and the standard deviation of time to peak strain of 12 segments were calculated at baseline and at one month follow-up. Both dyssynchrony parameters decreased significantly at one month follow-up after CRT (maximum difference decreased from 201 ± 35 ms to 99 ± 23 ms, p=0.03; the standard deviation decreased from 72 ± 14 ms to 40 ± 15 ms; p=0.03). Along with the mechanical resynchronization, the LVEF improved significantly at one month follow-up (from 41 ± 6% to 53 ± 8%, p=0.03).(24) In addition, 2D strain imaging permits evaluation of the latest activated areas where the LV pacing lead should ideally be placed. In adult populations, the position of the LV pacing lead concordant with the latest activated segment has demonstrated to be a determinant of positive response to CRT and superior long-term outcome.(72) In CHD and pediatric studies, the usefulness of this technique to identify the latest activated segment and to guide the LV lead placement has been also demonstrated.(73;74)
Finally, RT3DE provides regional time-volume curves for the evaluation of LV dyssynchrony (Figure 8). LV dyssynchrony is assessed by calculating the systolic dyssynchrony index (SDI). The standard deviation of time to minimum systolic volume of 16 LV segments is calculated. Marsan et al. demonstrated that a SDI cut-off value of 6.4% predicted long-term CRT response with high sensitivity (88%) and specificity (85%).(75) Concerning CHD patients, Bacha et al. performed RT3DE in 10 single ventricle patients who received multisite pacing post-operatively.(34) At 48 hours after CRT, the SDI of the single ventricle decreased significantly (from 10.3 ± 4.8 to 6.0 ± 1.4, p<0.05).
The proposed inter-ventricular dyssynchrony parameters in the adult trials resemble the observations on LV dyssynchrony in pediatric and CHD patients. However, the predictive value of inter-ventricular dyssynchrony of the LV in CHD and pediatric patients may vary in the various anatomical subgroups. Furthermore, several factors such as previous pacing strategies, the presence and location of scar tissue and hemodynamic abnormalities may influence the CRT response.(76) Additional trials are needed to establish cut-off values of LV dyssynchrony in CHD and pediatric patients, taking into consideration the various anatomical subgroups.

Intra-ventricular dyssynchrony: right ventricle

Similar to the assessment of intra-ventricular dyssynchrony of the LV in the adult population, intra-ventricular dyssynchrony of the RV has been studied in CHD patients with systemic RV failure. Van de Veire et al. assessed septal-to-lateral delay within the RV in the apical four-chamber view with color-coded TDI in a patient with RV-systemic failure who was upgraded from conventional pacing to CRT.(33) After two weeks, the RV septal-to-lateral delay decreased from 80 ms to completely synchronous contraction and exercise capacity improved significantly. In addition, Janousek et al. evaluated intra-ventricular dyssynchrony of the RV with TDI derived strain before and after CRT in eight patients with RV systemic failure.(29) RV dyssynchrony was quantified by measuring the largest delay in time to peak strain between four mid-ventricular RV segments (septal, lateral, anterior, posterior). After 4 days of CRT, RV dyssynchrony significantly reduced (from 138 ± 59 ms to 64 ± 21 ms, p=0.042). In addition, RVEF, as assessed with radionuclide angiography at 4 months follow-up, improved from 41.5% to 45.5% (p<0.01).
According to these data, assessment of intra-ventricular dyssynchrony of the RV could be useful in selecting patients with RV failure for CRT. However, unlike LV dyssynchrony assessment, characterization of RV dyssynchrony has been less explored(77-79), and additional studies evaluating RV dyssynchrony are needed to determine its value for predicting success of CRT in RV failure.

CONCLUSION AND FUTURE PERSPECTIVE

The beneficial effects of CRT on clinical outcomes and LV function of adult heart failure patients has encouraged the use of this therapy in other populations, such as CHD and pediatric patients.(14-16) The population with CHD is growing, and this subgroup of patients has a high prevalence of heart failure during late follow-up.(11) Although some studies have demonstrated the beneficial effects of CRT in CHD and pediatric patients, there are several concerns. First, the population of CHD and pediatric patients included in the studies is highly heterogeneous, comprising various anatomical substrates (systemic LV, systemic RV, single ventricle) and etiologies of heart failure (chronic single-site ventricular pacing).(14-16) Furthermore, heterogeneity in this population results from patient age and size variations. Second, the current adult selection criteria may not be suitable for the CHD and pediatric heart failure population. Only a minority of CHD and pediatric patients included in studies on CRT fulfilled the adult guidelines of QRS >120 ms, NYHA functional class III or IV and LVEF <35%.(14-16) Third, the various anatomical substrates may result in patterns of cardiac dyssynchrony that may not be accurately characterized with ECG criteria. The study of mechanical dyssynchrony with various imaging modalities may provide a more accurate definition of cardiac dyssynchrony and improve selection of those CHD and pediatric patients who have the highest likelihood of response to CRT. However, the feasibility and performance of the various dyssynchrony parameters in CHD and pediatric patients may differ from those observed in adult heart failure patients.
In conclusion, CRT may be a promising therapy to improve the clinical outcome of CHD and pediatric patients with heart failure. However, more studies are needed to establish appropriate guidelines for patient selection, taking into account the different anatomical subgroups.

REFERENCE LIST

1 Dickstein K, Cohen-Solal A, Filippatos G, et al. ESC Guidelines for the diagnosis and treatment of acute and chronic heart failure 2008: the Task Force for the Diagnosis and Treatment of Acute and Chronic Heart Failure 2008 of the European Society of Cardiology. Developed in collaboration with the Heart Failure Association of the ESC (HFA) and endorsed by the European Society of Intensive Care Medicine (ESICM). Eur Heart J 2008;29:2388-442.

2 Abraham WT, Fisher WG, Smith AL, et al. Cardiac resynchronization in chronic heart failure. N EnglJ Med 2002;346:1845-53.

3 Auricchio A, Stellbrink C, Sack S, et al. Long-term clinical effect of hemodynamically optimized cardiac resynchronization therapy in patients with heart failure and ventricular conduction delay. J Am Coll Cardiol 2002;39:2026-33.

4 Bristow MR, Saxon LA, Boehmer J, et al. Cardiac-resynchronization therapy with or without an implantable defibrillator in advanced chronic heart failure. N Engl J Med 2004;350:2140-50.

5 Cazeau S, Leclercq C, Lavergne T, et al. Effects of multisite biventricular pacing in patients with heart failure and intraventricular conduction delay. N Engl J Med 2001;344:873-80.

6 Cleland JG, Daubert JC, Erdmann E, et al. The effect of cardiac resynchronization on morbidity and mortality in heart failure. N Engl J Med 2005;352:1539-49.

7 Young JB, Abraham WT, Smith AL, et al. Combined cardiac resynchronization and implantable cardioversion defibrillation in advanced chronic heart failure: the MIRACLE ICD Trial. JAMA 2003;289:2685-94.

8 Epstein AE, DiMarco JP, Ellenbogen KA, et al. ACC/AHA/HRS 2008 Guidelines for Device-Based Therapy of Cardiac Rhythm Abnormalities: a report of the American College of Cardiology/American Heart Association Task Force on Practice Guidelines (Writing Committee to Revise the ACC/AHA/NASPE 2002 Guideline Update for Implantation of Cardiac Pacemakers and Antiarrhythmia Devices) developed in collaboration with the American Association for Thoracic Surgery and Society of Thoracic Surgeons. J Am Coll Cardiol 2008;51:e1-62.

9 Vardas PE, Auricchio A, Blanc JJ, et al. Guidelines for cardiac pacing and cardiac resynchronization therapy: The Task Force for Cardiac Pacing and Cardiac ResynchronizationTherapy of the European Society of Cardiology. Developed in collaboration with the European Heart Rhythm Association. Eur Heart J 2007;28:2256-95.

10 Marelli AJ, Mackie AS, Ionescu-Ittu R, et al. Congenital heart disease in the general population:changing prevalence and age distribution. Circulation 2007;115:163-72.

11 Oechslin EN, Harrison DA, Connelly MS, et al. Mode of death in adults with congenital heart disease. Am J Cardiol 2000;86:1111-6.

12 Verheugt CL, Uiterwaal CS, van d, V, et al. Mortality in adult congenital heart disease. Eur Heart J 2010;31:1220-9.

13 Rosenthal D, Chrisant MR, Edens E, et al. International Society for Heart and Lung Transplantation: Practice guidelines for management of heart failure in children. J Heart Lung Transplant 2004;23:1313-33.

14 Cecchin F, Frangini PA, Brown DW, et al. Cardiac resynchronization therapy (and multisite pacing) in pediatrics and congenital heart disease: five years experience in a single institution. J Cardiovasc Electrophysiol 2009;20:58-65.

15 Dubin AM, Janousek J, Rhee E, et al. Resynchronization therapy in pediatric and congenital heart disease patients: an international multicenter study. J Am Coll Cardiol 2005;46:2277-83.

16 Janousek J, Gebauer RA, Abdul-Khaliq H, et al. Cardiac resynchronisation therapy in paediatric and congenital heart disease: differential effects in various anatomical and functional substrates. Heart 2009;95:1165-71.

17 Ypenburg C, Westenberg JJ, Bleeker GB, et al. Noninvasive imaging in cardiac resynchronization therapy--part 1: selection of patients. Pacing Clin Electrophysiol 2008;31:1475-99.

18 Abdel-Rahman U, Kleine P, Seitz U, et al. Biventricular pacing for successful weaning from extracorporal circulation in an infant with complex tetralogy of fallot. Pediatr Cardiol 2002;23:553-4.

19 Blom NA, Bax JJ, Ottenkamp J, et al. Transvenous biventricular pacing in a child after congenital heart surgery as an alternative therapy for congestive heart failure. J Cardiovasc Electrophysiol 2003;14:1110-2.

20 Chen CA, Wang SS, Chiu SN, et al. Left ventricular reverse remodeling after successful cardiac resynchronization therapy in a 3-year-old girl with idiopathic dilated cardiomyopathy. Int J Cardiol 2007;117:e7-e9.

21 Khairy P, Fournier A, Thibault B, et al. Cardiac resynchronization therapy in congenital heart disease. Int J Cardiol 2006;109:160-8.

22 Nurnberg JH, Butter C, Abdul-Khaliq H, et al. Successful cardiac resynchronization therapy in a 9-year-old boy with dilated cardiomyopathy. Z Kardiol 2005;94:44-8.

23 Saito K, Ibuki K, Yoshimura N, et al. Successful cardiac resynchronization therapy in a 3-year-old girl with isolated left ventricular non-compaction and narrow QRS complex: a case report. Circ J 2009;73:2173-7.

24 Tomaske M, Breithardt OA, Balmer C, et al. Successful cardiac resynchronization with single-site left ventricular pacing in children. Int J Cardiol 2008;136:136-43.

25 Strieper M, Karpawich P, Frias P, et al. Initial experience with cardiac resynchronization therapy for ventricular dysfunction in young patients with surgically operated congenital heart disease. Am J Cardiol 2004;94:1352-4.

26 Dos L, Teruel L, Ferreira IJ, et al. Late outcome of Senning and Mustard procedures for correction of transposition of the great arteries. Heart 2005;91:652-6.

27 Moons P, Gewillig M, Sluysmans T, et al. Long term outcome up to 30 years after the Mustard or Senning operation: a nationwide multicentre study in Belgium. Heart 2004;90:307-13.

28 Piran S, Veldtman G, Siu S, et al. Heart failure and ventricular dysfunction in patients with single or systemic right ventricles. Circulation 2002;105:1189-94.

29 Janousek J, Tomek V, Chaloupecky VA, et al. Cardiac resynchronization therapy: a novel adjunct to the treatment and prevention of systemic right ventricular failure. J Am Coll Cardiol 2004;44:1927-31.

30 Cowburn PJ, Parker JD, Cameron DA, et al. Cardiac resynchronization therapy: retiming the failing right ventricle. J Cardiovasc Electrophysiol 2005;16:439-43.

31 Jauvert G, Rousseau-Paziaud J, Villain E, et al. Effects of cardiac resynchronization therapy on echocardiographic indices, functional capacity, and clinical outcomes of patients with a systemic right ventricle. Europace 2009;11:184-90.

32 Rodriguez-Cruz E, Karpawich PP, Lieberman RA, et al. Biventricular pacing as alternative therapy for dilated cardiomyopathy associated with congenital heart disease. Pacing Clin Electrophysiol 2001;24:235-7.

33 Van de Veire NR, Blom NA, Holman ER, et al. Triplane Tissue Doppler Imaging to Evaluate Mechanical Dyssynchrony Before and After Cardiac Resynchronization in a Patient with Congenitally Corrected Transposition of the Great Arteries. J Cardiovasc Electrophysiol 2006;18:222-5.

34 Bacha EA, Zimmerman FJ, Mor-Avi V, et al. Ventricular resynchronization by multisite pacing improves myocardial performance in the postoperative single-ventricle patient. Ann Thorac Surg 2004;78:1678-83.

35 Kim JJ, Friedman RA, Eidem BW, et al. Ventricular function and long-term pacing in children with congenital complete atrioventricular block. J Cardiovasc Electrophysiol 2007;18:373-7.

36 Moak JP, Barron KS, Hougen TJ, et al. Congenital heart block: development of late-onset cardiomyopathy, a previously underappreciated sequela. J Am Coll Cardiol 2001;37:238-42.

37 Udink ten Cate FE, Breur JM, Cohen MI, et al. Dilated cardiomyopathy in isolated congenital complete atrioventricular block: early and long-term risk in children. J Am Coll Cardiol 2001;37:1129-34.

38 Vatasescu R, Shalganov T, Paprika D, et al. Evolution of left ventricular function in paediatric patients with permanent right ventricular pacing for isolated congenital heart block: a medium term follow-up. Europace 2007;9:228-32.

39 Janousek J, Tomek V, Chaloupecky V, et al. Dilated cardiomyopathy associated with dual-chamber pacing in infants: improvement through either left ventricular cardiac resynchronization or programming the pacemaker off allowing intrinsic normal conduction. J Cardiovasc Electrophysiol 2004;15:470-4.

40 Kirsh JA, Stephenson EA, Redington AN. Images in cardiovascular medicine. Recovery of left ventricular

systolic function after biventricular resynchronization pacing in a child with repaired tetralogy of Fallot and severe biventricular dysfunction. Circulation 2006;113:e691-e692.
41 Moak JP, Hasbani K, Ramwell C, et al. Dilated cardiomyopathy following right ventricular pacing for AV block in young patients: resolution after upgrading to biventricular pacing systems. J Cardiovasc Electrophysiol 2006;17:1068-71.
42 Linde C, Abraham WT, Gold MR, et al. Randomized trial of cardiac resynchronization in mildly symptomatic heart failure patients and in asymptomatic patients with left ventricular dysfunction and previous heart failure symptoms. J Am Coll Cardiol 2008;52:1834-43.
43 Connolly D, Rutkowski M, Auslender M, et al. The New York University Pediatric Heart Failure Index: a new method of quantifying chronic heart failure severity in children. J Pediatr 2001;138:644-8.
44 Ross RD, Bollinger RO, Pinsky WW. Grading the severity of congestive heart failure in infants. Pediatr Cardiol 1992;13:72-5.
45 Lai WW, Geva T, Shirali GS, et al. Guidelines and standards for performance of a pediatric echocardiogram: a report from the Task Force of the Pediatric Council of the American Society of Echocardiography. J Am Soc Echocardiogr 2006;19:1413-30.
46 Helbing WA, Rebergen SA, Maliepaard C, et al. Quantification of right ventricular function with magnetic resonance imaging in children with normal hearts and with congenital heart disease. Am Heart J 1995;130:828-37.
47 van Straten A, Vliegen HW, Hazekamp MG, et al. Right ventricular function late after total repair of tetralogy of Fallot. Eur Radiol 2005;15:702-7.
48 Mollema SA, Bleeker GB, van der Wall EE, et al. Usefulness of QRS duration to predict response to cardiac resynchronization therapy in patients with end-stage heart failure. Am J Cardiol 2007;100:1665-70.
49 Pham PP, Balaji S, Shen I, et al. Impact of conventional versus biventricular pacing on hemodynamics and tissue Doppler imaging indexes of resynchronization postoperatively in children with congenital heart disease. J Am Coll Cardiol 2005;46:2284-9.
50 Friedberg MK, Silverman NH, Dubin AM, et al. Mechanical dyssynchrony in children with systolic dysfunction secondary to cardiomyopathy: a Doppler tissue and vector velocity imaging study. J Am Soc Echocardiogr 2007;20:756-63.
51 Friedberg MK, Roche SL, Balasingam M, et al. Evaluation of mechanical dyssynchrony in children with idiopathic dilated cardiomyopathy and associated clinical outcomes. Am J Cardiol 2008;101:1191-5.
52 Labombarda F, Blanc J, Pellissier A, et al. Health-e-Child Project: Mechanical Dyssynchrony in Children with Dilated Cardiomyopathy. J Am Soc Echocardiogr 2009;22:1289-95.
53 Bleeker GB, Schalij MJ, Molhoek SG, et al. Frequency of left ventricular dyssynchrony in patients with heart failure and a narrow QRS complex. Am J Cardiol 2005;95:140-2.
54 Yu CM, Lin H, Zhang Q, et al. High prevalence of left ventricular systolic and diastolic asynchrony in patients with congestive heart failure and normal QRS duration. Heart 2003;89:54-60.
55 Kass DA. Ventricular resynchronization: pathophysiology and identification of responders. Rev Cardiovasc Med 2003;4 Suppl 2:S3-S13.
56 Cazeau S, Bordachar P, Jauvert G, et al. Echocardiographic modeling of cardiac dyssynchrony before and during multisite stimulation: a prospective study. Pacing Clin Electrophysiol 2003;26:137-43.
57 Hirschfeld S, Meyer R, Schwartz DC, et al. Measurement of right and left ventricular systolic time intervals by echocardiography. Circulation 1975;51:304-9.
58 Ebeid MR, Ferrer PL, Robinson B, et al. Doppler echocardiographic evaluation of pulmonary vascular resistance in children with congenital heart disease. J Am Soc Echocardiogr 1996;9:822-31.
59 Pitzalis MV, Iacoviello M, Romito R, et al. Cardiac resynchronization therapy tailored by echocardiographic evaluation of ventricular asynchrony. J Am Coll Cardiol 2002;40:1615-22.
60 Roofthooft MT, Blom NA, Rijlaarsdam ME, et al. Resynchronization therapy after congenital heart surgery to improve left ventricular function. Pacing Clin Electrophysiol 2003;26:2042-4.
61 Takabayashi S, Shimpo H, Mitani Y, et al. Pediatric cardiac remodeling after cardiac resynchronization therapy. Pediatr Cardiol 2006;27:485-9.
62 Bax JJ, Marwick TH, Molhoek SG, et al. Left ventricular dyssynchrony predicts benefit of cardiac resynchronization therapy in patients with end-stage heart failure before pacemaker implantation. Am J Cardiol 2003;92:1238-40
63 Bax JJ, Bleeker GB, Marwick TH, et al. Left ventricular dyssynchrony predicts response and prognosis after cardiac resynchronization therapy. J Am Coll Cardiol 2004;44:1834-40.
64 Yu CM, Fung WH, Lin H, et al. Predictors of left ventricular reverse remodeling after cardiac resynchronization therapy for heart failure secondary to idiopathic dilated or ischemic cardiomyopathy. Am J Cardiol 2003;91:684-8.
65 Dohi K, Suffoletto MS, Schwartzman D, et al. Utility of echocardiographic radial strain imaging to quantify left ventricular dyssynchrony and predict acute response to cardiac resynchronization therapy. Am J Cardiol 2005;96:112-6.
66 Yu CM, Gorcsan J, III, Bleeker GB, et al. Usefulness of tissue Doppler velocity and strain dyssynchrony for predicting left ventricular reverse remodeling response after cardiac resynchronization therapy. Am J Cardiol 2007;100:1263-70.
67 Abd El Rahman MY, Hui W, Yigitbasi M, et al. Detection of left ventricular asynchrony in patients with right bundle branch block after repair of tetralogy of Fallot using tissue-Doppler imaging-derived strain. J Am Coll Cardiol 2005;45:915-21.
68 Delgado V, Ypenburg C, van Bommel RJ, et al. Assessment of left ventricular dyssynchrony by speckle tracking strain imaging comparison between longitudinal, circumferential, and radial strain in cardiac resynchronization therapy. J Am Coll Cardiol 2008;51:1944-52.
69 Suffoletto MS, Dohi K, Cannesson M, et al. Novel speckle-tracking radial strain from routine black-and-white echocardiographic images to quantify dyssynchrony and predict response to cardiac resynchronization therapy. Circulation 2006;113:960-8.
70 Becker M, Kramann R, Franke A, et al. Impact of left ventricular lead position in cardiac resynchronization therapy on left ventricular remodelling. A circumferential strain analysis based on 2D echocardiography. Eur Heart J 2007;28:1211-20.
71 Lim P, Buakhamsri A, Popovic ZB, et al. Longitudinal strain delay index by speckle tracking imaging: a new marker of response to cardiac resynchronization therapy. Circulation 2008;118:1130-7.
72 Ypenburg C, van Bommel RJ, Delgado V, et al. Optimal left ventricular lead position predicts reverse remodeling and survival after cardiac resynchronization therapy. J Am Coll Cardiol 2008;52:1402-9.
73 Gonzalez MB, Schweigel J, Kostelka M, et al. Cardiac resynchronization in a child with dilated cardiomyopathy and borderline QRS duration: speckle tracking guided lead placement. Pacing Clin Electrophysiol 2009;32:683-7.
74 Madriago E, Sahn DJ, Balaji S. Optimization of myocardial strain imaging and speckle tracking for resynchronization after congenital heart surgery in children. Europace 2010.
75 Marsan NA, Bleeker GB, Ypenburg C, et al. Real-time three-dimensional echocardiography as a novel approach to assess left ventricular and left atrium reverse remodeling and to predict response to cardiac resynchronization therapy. Heart Rhythm 2008;5:1257-64.
76 Janousek J, Gebauer RA. Cardiac resynchronization therapy in pediatric and congenital heart disease. Pacing Clin Electrophysiol 2008;31 Suppl 1:S21-S23.
77 Geva T, Powell AJ, Crawford EC, et al. Evaluation of regional differences in right ventricular systolic function by acoustic quantification echocardiography and cine magnetic resonance imaging. Circulation 1998;98:339-45.
78 Matsui H, Satomi G, Yasukochi S, et al. Evaluation of right ventricular contraction by myocardial strain in children using a two-dimensional tissue tracking method. Pediatr Cardiol 2008;29:377-81.
79 Uebing A, Gibson DG, Babu-Narayan SV, et al. Right ventricular mechanics and QRS duration in patients with repaired tetralogy of Fallot: implications of infundibular disease. Circulation 2007;116:1532-9.

2.2

Tissue Doppler imaging in the left ventricle and right ventricle in healthy children: normal age-related peak systolic velocities, timings, and time differences

Submitted

A.E. van der Hulst
V. Delgado
A.D.J. ten Harkel
L.M. Klitsie
L.H.P.M. Filippini
J.J. Bax
N.A. Blom
A.A.W. Roest

ABSTRACT

Background: Tissue Doppler imaging (TDI) enables assessment of velocities and timings within the left (LV) and right (RV) ventricle with high temporal resolution. Knowledge on normal age-related values of peak systolic velocities and timings in healthy children may optimize the benefit of device-based therapies in pediatric patients with heart failure.

Methods: A total of 123 healthy children (from 1 month to 18 years old) underwent TDI evaluation of the RV and LV. Peak systolic velocity and time to peak systolic velocity were assessed at the basal segments of the LV lateral wall, inter-ventricular septum (IVS), RV free wall (RVFW) and at the RVOT. Intra-ventricular time differences were calculated. Regression analysis was performed to assess the age-dependency of the ventricular mechanics.

Results: Median peak velocities were: LV lateral wall 6.3 cm/s, (inter-quartile-range: 5.1-7.9 cm/s), IVS: 6.0 cm/s (5.4-6.7 cm/s), RVFW: 10.2 cm/s (8.9-11.3 cm/s), RVOT 7.2 cm/s (6.0-8.2 cm/s). Timings of peak systolic velocities: LV lateral wall 101 ms (91-112 ms), IVS: 114 ms (100-128 ms), RVFW: 177 ms (157-194 ms), RVOT 100 ms (88-113 ms). Timings and peak velocities significantly increased with age at both ventricles. No relevant time difference was observed within the LV, whereas a considerable time delay was observed within the RV between the RVFW and the IVS (62 ms, IQR 45-74 ms) and between the RVFW and the RVOT (74 ms, IQR 59-93 ms).

Conclusions: The present evaluation provides TDI-derived reference values on LV and RV mechanics of healthy children. Within the LV, no relevant time difference was observed whereas a considerable mechanical delay is observed within the healthy RV.

INTRODUCTION

Echocardiographic tissue Doppler imaging (TDI) enables the assessment of left (LV) and right (RV) ventricular mechanics by measuring myocardial velocities and time to peak myocardial velocities with high temporal resolution. The assessment of peak systolic velocities of the LV and RV myocardium with TDI is of incremental value to conventional echocardiography to assess global and regional ventricular performance in various clinical conditions.(1-5) Furthermore, evaluation of the temporal occurrence of peak systolic velocities with TDI provides insight into electromechanical coupling and mechanical dyssynchrony.(6)

TDI-derived peak velocities and time-differences between peak systolic velocities within the myocardium of the LV and RV have been investigated in healthy children.(7-9) However, the absolute timings within the LV and the RV have not been reported. The advent of novel device-based therapies, such as cardiac resynchronization therapy (CRT), has encouraged the research on LV and RV mechanics with noninvasive imaging. Understanding LV and RV mechanics in healthy children may optimize the benefit of these therapies in patients with heart failure. Furthermore, in certain patients with congenital heart disease, RV outflow tract (RVOT) mechanics have an influence on global RV performance. Abnormal RVOT mechanics have been related to RV failure and poor clinical outcome. However, the reference values of normal peak systolic velocities and timings at the RVOT in healthy children have not been evaluated. Accurate standardization of reference values of TDI velocities at the RVOT would help to understand the mechanisms underlying RV failure in patients with congenital heart disease.(5,10,11)

Accordingly, the objectives of this evaluation were to assess peak systolic velocities, timings of peak systolic velocities and intra-ventricular time differences with TDI in the LV and RV of healthy children. In addition, the age-dependency of the peak systolic velocities, timings to peak systolic velocities and intra-ventricular time differences in healthy children were investigated.

METHODS

Study population

Healthy children of various ages (from 1 month to 18 years) were prospectively included in the current study. We did not include patients younger than 1 month since these young patients may still have a raised pulmonary pressure, which may interfere with the observed myocardial velocities. All subjects underwent transthoracic echocardiography and TDI. Conventional two-dimensional echocardiography confirmed structurally normal hearts. Peak systolic velocities and timings of peak systolic velocities at the LV and RV were assessed with TDI in all subjects. In addition, intra-ventricular time differences between the peak systolic velocities at the various LV and RV regions were calculated. Finally, the relationship between age and myocardial velocities, time to peak systolic velocity and the intra-ventricular time differences were evaluated. The study protocol was approved by our hospital institutional review board. All participants or their parents gave written informed consent.

Table 1. Ventricular mechanics as assessed by TDI

Peak systolic velocity (cm/s)	
Left ventricle	
LV lat	6.3 (5.1 – 7.9)
IVS	6.0 (5.4 – 6.7)
Right ventricle	
RVFW	10.2 (8.9 – 11.3)
RVOT	7.2 (6.0 – 8.2)
Timing peak systolic velocity (ms)	
Left ventricle	
LV lat	101 (91 – 112)
IVS	114 (100 – 128)
Right ventricle	
RVFW	177 (157 – 194)
RVOT	100 (88 – 113)
Intra-ventricular time differences (ms)	
Left ventricle	
LV lat - IVS	10 (0 – 20)
Right ventricle	
IVS - RVFW	62 (45 – 75)
RVOT - RVFW	74 (59 – 93)

Abbreviations: IVS: inter-ventricular septum, LV lat: left ventricular lateral wall, RVFW: right ventricular free wall, RVOT: right ventricular outflow tract.

Tissue Doppler imaging

Transthoracic echocardiography data were acquired using a commercially available system equipped with a 3.5 MHz transducer (Vivid-7.0.0, GE Vingmed Ultrasound AS, Horten, Norway). Standard two-dimensional gray-scale images were acquired from the parasternal (long- and short-axis) and apical views (4-chamber and long-axis) and digitally stored in cine-loop format. Acquisition of TDI images was performed with adjusted sector width and angle to align the ultrasound beam along the direction of the myocardial motion. The color frame rate was →120 frames/s, and at least three consecutive beats were recorded. Analyses were performed off-line using EchoPac version 108.1.5 (General Electric Medical Systems). Longitudinal myocardial velocity curves were obtained by placing regions of interest at the basal LV lateral wall (Figure 1, panel A), basal interventricular septum (IVS) (Figure 1, panel A) and basal RV free wall (RVFW) (Figure 1, panel B) in the 4-chamber view, and at the lateral wall of the RVOT (Figure 1, panel C) in a dedicated apical RVOT view, as previously reported. (5, 12) Semi-automated tissue tracking was used to maintain the region of interest within the sample area throughout the cardiac cycle. Peak systolic velocity was measured at all LV and RV regions. In addition, time from onset of the Q-wave of the ECG to peak systolic velocity was measured in all LV and RV basal segments. Finally, the LV intra-ventricular time difference was obtained by calculating the difference between time to peak systolic velo-

Figure 1. TDI images of LV and RV in a healthy child

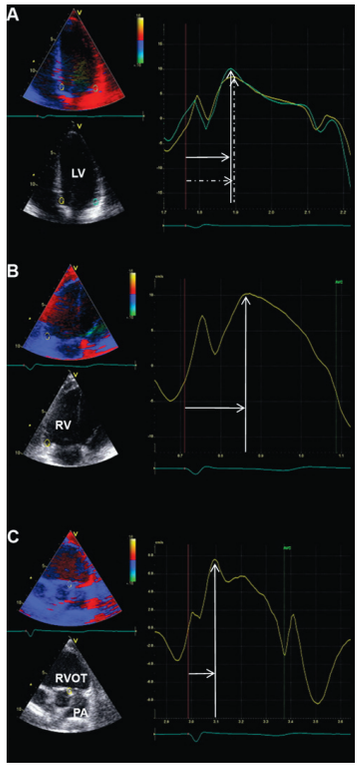

Panel A: TDI image of LV. Yellow region of interest is placed at the basal IVS. Blue region of interest is placed at the basal lateral wall. From the corresponding velocity curves the peak systolic velocity (vertical dotted arrow: peak systolic velocity IVS, vertical solid arrow: peak systolic velocity LV lateral wall) and time to peak systolic velocity (horizontal dotted arrow: time to peak systolic velocity IVS, horizontal solid arrow: time to peak systolic velocity LV lateral wall) can be derived.
Panel B: TDI image of RV. Yellow region of interest is placed at the basal free wall. From the corresponding velocity curve, the peak systolic velocity (vertical arrow) and time to peak systolic velocity (horizontal arrow) can be derived.
Panel C: TDI image of RVOT. Yellow region of interest is placed at the septal side of the RVOT, just below the pulmonary valve. From the corresponding velocity curve, the peak systolic velocity (vertical arrow) and time to peak systolic velocity (horizontal arrow) can be derived.
Abbreviations: IVS: inter-ventricular septum, LV: left ventricle, PA: pulmonary artery, RV: right ventricle, RVOT: right ventricular outflow tract.

city at the basal LV lateral segment and at the basal part of the IVS. The RV intra-ventricular time difference was calculated by measuring the time delay in peak systolic velocities between the basal part of the IVS and RVFW and between the RVOT and basal RVFW. Intra and inter observer agreement of all peak velocities and timings of peak velocities was assessed in a blinded manner in 15 randomly chosen subjects. Peak velocity and time to peak velocity at the different LV and RV regions was reassessed by the same and by an independent observer.

Statistical analysis

Continuous variables are expressed as median and inter-quartile range (IQR). Categorical variables are presented as numbers and percentages. Linear regression analysis was performed to evaluate the relation between age and peak systolic velocities, timings of velocities, and time differences. Intra observer and inter observer agreement was assessed by measuring the absolute difference between the repeated measurements in percent of the mean, averaged over the study subjects and presented as mean ± standard deviation. In addition, 95% reference intervals for the linear regression models were calculated. Data were analyzed using the SPSS 17.0 software (SPSS Inc, Chicago, Illinois). A p-value of <0.05 was considered statistically significant.

RESULTS

Study population characteristics

A total of 123 healthy children (56% male) were included. The median age at echocardiography was 6.3 years (IQR: 3.3-11.7 years) and children of all ages (1 month to 18 years) were represented in the present study. All subjects showed structurally normal hearts on echocardiography. The median heart rate during image acquisition was 90 min-¹ (IQR: 72-111/min-¹) and the median body surface area was 0.9 m^2 (IQR: 0.6-1.3 m2). The obtained TDI images had sufficient image quality for analysis in all subjects.

Peak systolic velocities

Table 1 summarizes the peak systolic velocities at the different LV and RV regions. The median peak systolic velocity at the LV lateral wall was 6.3 cm/s (IQR: 5.1-7.9 cm/s). At the IVS, peak systolic velocity was 6.0 cm/s (IQR: 5.4-6.7 cm/s). At the RVFW, the median peak systolic velocity was 10.2 cm/s (IQR 8.9-11.3 cm/s). Finally, the median peak systolic velocity at the RVOT was 7.2 cm/s (IQR 6.0-8.2 cm/s).
A significant relationship between age and peak systolic velocity measured at the LV lateral wall was observed (LV lateral wall: r=0.75, p<0.001) (Figure 2). At the IVS, this relationship, although modest, was also observed (IVS: r=0.54 p<0.001) (Figure 2). In contrast, the relationship between age and peak systolic velocity at the RVFW and at the RVOT was weak (RVFW: r=0.42 p<0.001, RVOT r=0.38, p<0.001) (Figure 3). The results of the intra observer and intra observer agreement for the peak velocities were: LV lateral wall: intra observer 7% ± 6%, inter observer: 9% ± 9%, IVS:

intra observer: 6% ± 5%, inter observer: 14% ± 13%, RVFW: intra observer: 10% ± 11%, inter observer: 17% ± 14%, RVOT: intra observer: 7% ± 6%, inter observer 12% ± 13 %.

Timings of peak systolic velocities

Timings of peak systolic velocities are summarized in Table 1. The median time to peak systolic velocity at the LV lateral wall was 101 ms (IQR: 91-112 ms). At the IVS, the median time to peak systolic velocity was 114 ms (IQR 100-118 ms). At the RVFW, the median time to peak systolic velocity was 177 ms (IQR 157-194 ms). The peak systolic velocity at the RVOT occurred prior to that of the RVFW, at 100 ms (IQR: 88-113 ms).

Time to peak systolic velocity at the LV lateral wall and IVS were significantly related with age (LV lateral wall: $r=0.57$, $p<0.001$, IVS: $r=0.41$, $p<0.01$) (Figure 4). Similarly, time to peak systolic velocity at the RVFW and RVOT increased significantly along with age (RVFW: $r=0.58$, $p<0.001$, RVOT: $r=0.70$, $p<0.001$) (Figure 5). The results of the intra observer and intra observer agreement for the timings of peak velocities were: LV lateral wall: intra observer 5% ± 4%, inter observer: 14% ± 13%, IVS: intra observer: 6% ± 5%, inter observer: 11% ± 8%, RVFW: intra observer: 7% ± 2%, inter observer: 7% ± 5%, RVOT: intra observer: 7% ± 5%, inter observer 9% ± 6 %.

Intra-ventricular time differences

Table 1 shows the median inter-ventricular time delays in the LV and RV in the healthy children. The median time delay between peak systolic velocity at the LV lateral wall and peak systolic velocity at the IVS was very small (median 10 ms, IQR 0-20 ms). In contrast, within the RV, the time difference between the IVS and the RVFW was 62 ms (IQR 45-75 ms), and the median time difference between the RVOT and the RVFW was 74 ms (IQR 59-93 ms). The observed small intra-ventricular time difference within the LV did not change with age. At the RV, the time delay between the IVS and the RVFW showed a weak correlation with age ($r=0.25$, $p<0.001$), whereas the time difference between the RVOT and the RVFW did not relate with age in the healthy subjects.

DISCUSSION

The present study provides age-related values for peak systolic velocities and timings of peak systolic velocities as assessed with TDI at the basal segments of the LV, RV and of the RVOT in healthy children. The results of the current study show that peak systolic velocities and time to peak systolic velocities increase with age in both ventricles. Furthermore, no intra-ventricular time differences between the basal LV lateral wall and IVS are observed at any age, whereas within the RV, a considerable time delay is present between the basal IVS and the basal RVFW, and between the basal RVFW and the RVOT. Finally, the intra-ventricular time differences within RV did not show relevant changes with age in healthy children.

Peak systolic velocities

The assessment of peak systolic velocities with TDI provides a quantitative measure of ventricular systolic function. Several studies have demonstrated the value of TDI-derived peak systolic velocities to quantify regional LV and RV ventricular performance in adults with various clinical conditions.(1-5) In pediatric patients, the assessment of peak systolic velocities has been shown to be a sensitive tool to detect myocardial dysfunction.(13,14) The current study provides age-related normal values of peak systolic velocities at the basal LV lateral wall, basal RVFW and at the RVOT with TDI. Peak velocities were highest at the basal RVFW (median 10.2 cm/s) and lowest at the LV lateral wall (median 6.0 cm/s). The observed pattern of different magnitudes of normal peak velocities among the basal LV lateral wall, basal IVS and basal RV is in agreement with previous investigations in children.(5,8,9,15) Furthermore, the observed normal peak velocities at the basal LV and RV increased significantly with age in the current study. This observation is in line with a previous study on the alterations of LV performance during cardiac maturation in healthy children.(16) Notomi and colleagues assessed LV performance in 45 healthy controls by measuring rotational mechanics with TDI. In their study, LV performance increased significantly with age.(16) In contrast, other studies have reported weaker(9) or non-significant(8) relationships between TDI-derived peak velocities at the basal RV and LV and age in healthy children. Kapusta et al. investigated age-related peak systolic velocities at the basal RFVW, IVS and LV lateral wall in 160 healthy children and observed no significant changes with age.(8) However, the age range (4-18 years) of the included subjects was significantly smaller as compared to the present study.

The current report is the first to investigate normal values of peak systolic velocities at the RVOT. The peak systolic velocity at the RVOT was lower than the velocity at the RVFW and showed a significant increase with age. Comprehensive insight into normal values of peak systolic velocities at the RVOT is of interest to evaluate patients with congenital heart disease, specifically those with tetralogy of Fallot.(11,17) Systolic dysfunction at the RVOT has been associated with reduced global performance of the RV.(11,17) Accordingly, the observed normal values on the peak systolic velocity at the RVOT provide a framework for future studies on patients with congenital heart disease and RV failure.

Timing of peak systolic velocities and intra-ventricular time

The assessment of timings of peak systolic velocities with TDI yields insight into electromechanical coupling and possible mechanical dyssynchrony. CRT targets dyssynchrony in patients with LV failure by inducing a more synchronous contraction. In pediatric patients, no guidelines for patient selection for CRT are available at present.(18-20) Knowledge on normal values of myocardial velocities, timings and time-differences within the LV as assessed with TDI could play an important role in defining appropriate recommendations for pediatric patients with LV failure who may benefit from CRT. However, a systematic description of the normal temporal occurrence of peak systolic velocities and time differences within the LV has not been previously reported in children. The present study provides insight into the normal electromechanical activation of the LV in children. With a median time difference of 10 ms between the time to peak velocity at the basal LV lateral wall

Figure 2. Relation between age and peak systolic velocity in the LV

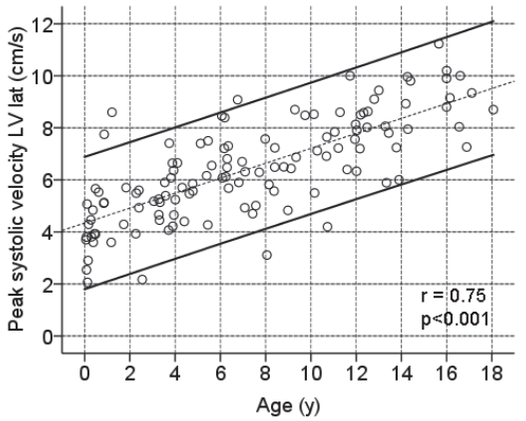

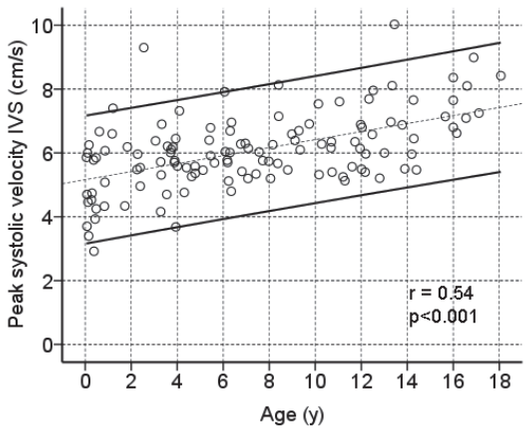

Upper: Scatter plot depicting linear relation and 95% reference intervals for age and peak systolic velocity at LV lateral wall. **Lower:** Scatter plot depicting linear relation and reference intervals between age and peak systolic velocity at IVS.
Abbreviations: IVS: inter-ventricular septum. LV lat: left ventricular lateral wall.

Figure 3. Relation between age and peak systolic velocity in the RV

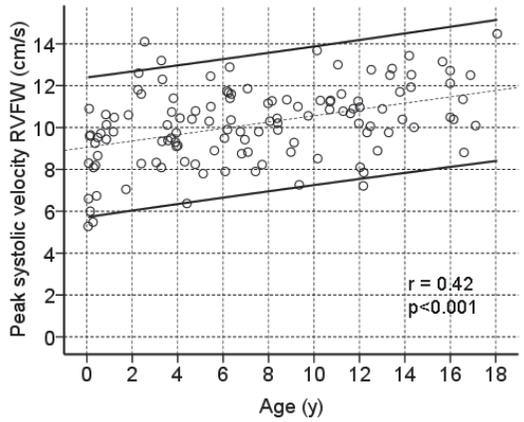

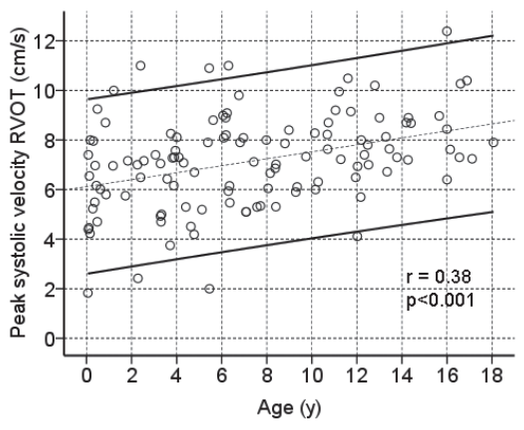

Upper: Scatter plot depicting linear relation and 95% reference intervals for age and peak systolic velocity at RVFW. **Lower:** Scatter plot depicting linear relation and reference intervals between age and peak systolic velocity at RVOT.
Abbreviations: RVFW: right ventricular free wall, RVOT: right ventricular outflow tract.

Figure 4. Relation between age and time to peak systolic velocity in the LV

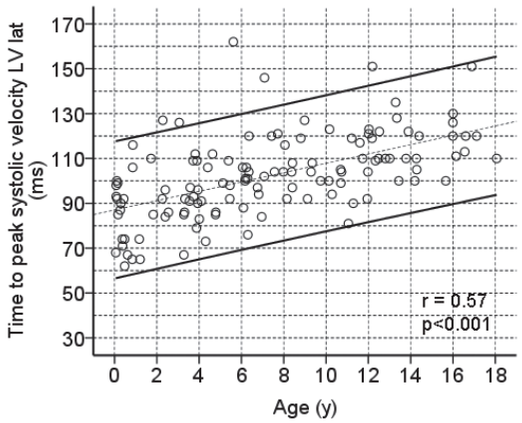

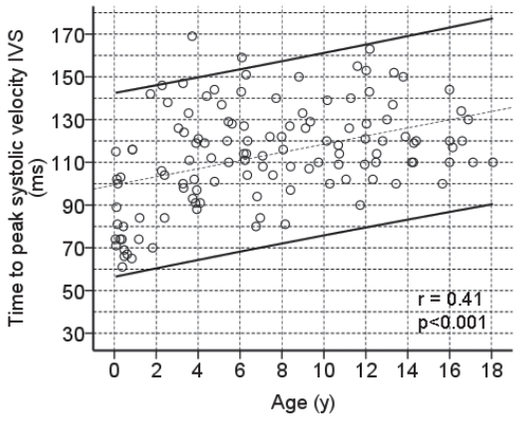

Upper: Scatter plot depicting linear relation and 95% reference intervals for age and time to peak systolic velocity at LV lateral wall. **Lower:** Scatter plot depicting linear relation and reference intervals between age and time to peak systolic velocity at IVS.
Abbreviations: IVS: inter-ventricular septum. LV lat: left ventricular lateral wall.

Figure 5. Relation between age and time to peak systolic velocity in the RV

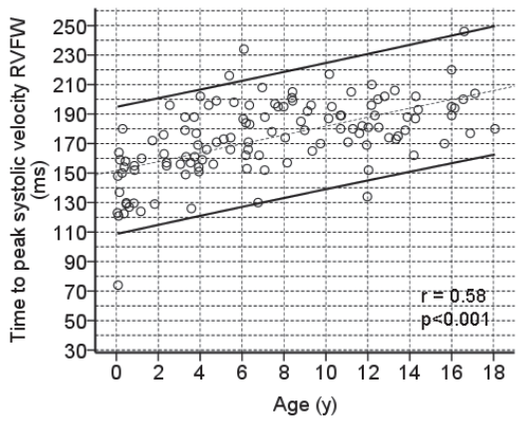

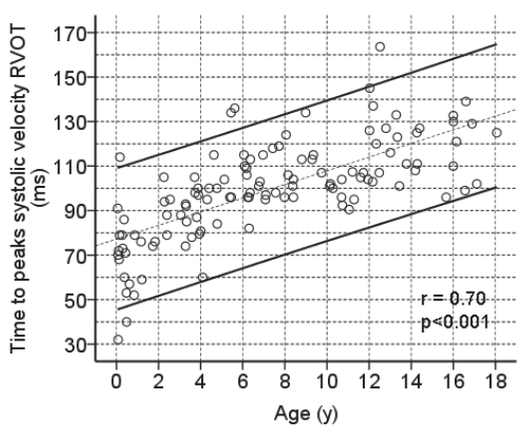

Upper: Scatter plot depicting linear relation and 95% reference intervals for age and time to peak systolic velocity at RVFW. **Lower:** Scatter plot depicting linear relation and reference intervals between age and time to peak systolic velocity at RVOT.
Abbreviations: RVFW: right ventricular free wall, RVOT: right ventricular outflow tract.

and the basal IVS, no significant time delay within the LV was observed at any age. These normative data are in line with the results of previous studies including adult population (15), and provide an empirical basis for future studies on LV dyssynchrony in pediatric candidates for CRT.

The RV differs greatly from the LV in terms of anatomy and function. Accordingly, the mechanical activation pattern of the RV may be different from that of the LV. In the current investigation, a significant IVS-to-RVFW delay was observed in the healthy subjects, with a median time difference of 62 ms. Albeit substantially smaller, the presence of an IVS-to-RVFW delay was previously observed with TDI by Hui et al. in a study on 98 healthy children.(7) Moreover, based on their observations, the authors proposed to consider as normal range any IVS-to-RVFW delay below 70 ms.(7) Of note, within the LV, a time delay of 70 ms would indicate significant dyssynchrony.(21) In addition, in the present study, the intra-ventricular time difference between the basal RVFW and RVOT was investigated, yielding a median intra-ventricular time delay of 74 ms. A previous study evaluating RV intra-ventricular timings assessed with TDI showed a similar activation pattern with a significant time delay between the RVOT and RVFW in healthy adults.(5) In the present study, the observed intra-ventricular time differences within the RV did not show a relevant relationship with age. Accordingly, significant intra-ventricular time differences between the IVS and RVFW and between the RVOT and RVFW are present in children of any age.

The presence of a mechanical delay within the RV may have important clinical implications. RV failure is common in pediatric patients with congenital heart disease(22-24) and the best therapeutic approach to RV failure remains incompletely elucidated. CRT has been evaluated as novel therapy for patients with RV failure.(19,25) However, the pathophysiological basis of CRT is the restoration of electromechanical dyssynchrony. With the observed mechanical delay within the healthy RV, this concept of resynchronization may not be applicable to the RV. The application of CRT in patients with RV failure warrants further studies on RV mechanics and its relation with RV performance.

Study limitations

The relatively small sample size of the study may constitute a limitation. Furthermore, the results of the present study were obtained with equipment from one vendor. A previous study demonstrated that for the assessment of myocardial velocities, different ultrasound systems from different vendors can not be used interchangeably.(26) Accordingly, the presented reference values should be interpreted with caution when using other equipment. Instead of TDI, speckle tracking strain analysis is increasingly used in clinical practice for evaluation of patients with heart failure who may benefit from CRT and early detection of subtle changes in myocardial performance. However, in the pediatric population, speckle tracking strain analysis has been less explored. The higher heart rates observed in small children may challenge the assessment of myocardial strain or even velocities with speckle tracking, a technique strongly dependent on frame rate. Therefore, for this population, TDI might be still preferable. However, additional studies using speckle tracking will confirm whether this technique provides the same results or not.

CONCLUSIONS

In conclusion, in the present study, reference values are provided on LV and RV peak systolic velocities and timings of peak systolic velocities as assessed with TDI in healthy children. Within the LV, no relevant time-differences were observed at any age. Within the RV of healthy children, an intrinsic time delay was observed, which has implications for future studies on device-based therapies for RV failure.

REFERENCE LIST

1 Alam M, Witt N, Nordlander R, et al. Detection of abnormal left ventricular function by Doppler tissue imaging in patients with a first myocardial infarction and showing normal function assessed by conventional echocardiography. Eur J Echocardiogr 2007;8:37-41.

2 Dagianti A, Vitarelli A, Conde Y, et al. Assessment of regional left ventricular function during exercise test with pulsed tissue Doppler imaging. Am J Cardiol 2000;86:30G-2G.

3 Meluzin J, Spinarova L, Bakala J, et al. Pulsed Doppler tissue imaging of the velocity of tricuspid annular systolic motion; a new, rapid, and non-invasive method of evaluating right ventricular systolic function. Eur Heart J 2001;22:340-8.

4 Mogelvang R, Sogaard P, Pedersen SA, et al. Cardiac dysfunction assessed by echocardiographic tissue Doppler imaging is an independent predictor of mortality in the general population. Circulation 2009;119:2679-85.

5 Uebing A, Gibson DG, Babu-Narayan SV, et al. Right ventricular mechanics and QRS duration in patients with repaired tetralogy of Fallot: implications of infundibular disease. Circulation 2007;116:1532-9.

6 Ypenburg C, Westenberg JJ, Bleeker GB, et al. Noninvasive imaging in cardiac resynchronization therapy--part 1: selection of patients. Pacing Clin Electrophysiol 2008;31:1475-99.

7 Hui W, Slorach C, Bradley TJ, et al. Measurement of right ventricular mechanical synchrony in children using tissue Doppler velocity and two-dimensional strain imaging. J Am Soc Echocardiogr 2010;23:1289-96.

8 Kapusta L, Thijssen JM, Cuypers MH, et al. Assessment of myocardial velocities in healthy children using tissue Doppler imaging. Ultrasound Med Biol 2000;26:229-37.

9 Swaminathan S, Ferrer PL, Wolff GS, et al. Usefulness of tissue Doppler echocardiography for evaluating ventricular function in children without heart disease. Am J Cardiol 2003;91:570-4.

10 Davlouros PA, Kilner PJ, Hornung TS, et al. Right ventricular function in adults with repaired tetralogy of Fallot assessed with cardiovascular magnetic resonance imaging: detrimental role of right ventricular outflow aneurysms or akinesia and adverse right-to-left ventricular interaction. J Am Coll Cardiol 2002;40:2044-52.

11 Wald RM, Haber I, Wald R, et al. Effects of regional dysfunction and late gadolinium enhancement on global right ventricular function and exercise capacity in patients with repaired tetralogy of Fallot. Circulation 2009;119:1370-7.

12 van der Hulst AE, Roest AA, Delgado V, Holman ER, de Roos A, Blom NA, et al. Relationship between temporal sequence of right ventricular deformation and right ventricular performance in patients with corrected tetralogy of Fallot. Heart 2011;3:231-6.

13 Hershenson JA, Zaidi AN, Texter KM, et al. Differences in tissue Doppler imaging between single ventricles after the fontan operation and normal controls. Am J Cardiol 2010;106:99-103.

14 Vitarelli A, Conde Y, Cimino E, et al. Quantitative assessment of systolic and diastolic ventricular function with tissue Doppler imaging after Fontan type of operation. Int J Cardiol 2005;102:61-9.

15 Marciniak M, Bijnens B, Baltabaeva A, et al. Interventricular interaction as a possible mechanism for the presence of a biphasic systolic velocity profile in normal left ventricular free walls. Heart 2008;94:1058-64.

16 Notomi Y, Srinath G, Shiota T, et al. Maturational and adaptive modulation of left ventricular torsional biomechanics: Doppler tissue imaging observation from infancy to adulthood. Circulation 2006;113:2534-41.

17 Oosterhof T, Mulder BJ, Vliegen HW, et al. Corrected tetralogy of Fallot: delayed enhancement in right ventricular outflow tract. Radiology 2005;237:868-71.

18 Cecchin F, Frangini PA, Brown DW, et al. Cardiac resynchronization therapy (and multisite pacing) in pediatrics and congenital heart disease: five years experience in a single institution. J Cardiovasc Electrophysiol 2009;20:58-65.

19 Dubin AM, Feinstein JA, Reddy VM, et al. Electrical resynchronization: a novel therapy for the failing right ventricle. Circulation 2003;107:2287-9.

20 Janousek J, Gebauer RA, Abdul-Khaliq H, et al. Cardiac resynchronisation therapy in paediatric and congenital heart disease: differential effects in various anatomical and functional substrates. Heart 2009;95:1165-71.

21 Bax JJ, Bleeker GB, Marwick TH, et al. Left ventricular dyssynchrony predicts response and prognosis after cardiac resynchronization therapy. J Am Coll Cardiol 2004;44:1834-40.

22 Dos L, Teruel L, Ferreira IJ, et al. Late outcome of Senning and Mustard procedures for correction of transposition of the great arteries. Heart 2005;91:652-6.

23 Geva T, Sandweiss BM, Gauvreau K, et al. Factors associated with impaired clinical status in long-term survivors of tetralogy of Fallot repair evaluated by magnetic resonance imaging. J Am Coll Cardiol 2004;43:1068-74.

24 Helbing WA, Rebergen SA, Maliepaard C, et al. Quantification of right ventricular function with magnetic resonance imaging in children with normal hearts and with congenital heart disease. Am Heart J 1995;130:828-37.

25 Cowburn PJ, Parker JD, Cameron DA, et al. Cardiac resynchronization therapy: retiming the failing right ventricle. J Cardiovasc Electrophysiol 2005;16:439-43.

26 Koopman LP, Slorach C, Manlhiot C, McCrindle BW, Friedberg MK, Mertens L, et al. Myocardial tissue Doppler velocity imaging in children: comparative study between two ultrasound systems. J Am Soc Echocardiogr 2010;23:929-37.

2.3

Relationship between temporal sequence of right ventricular deformation and right ventricular performance in patients with corrected tetralogy of Fallot

Heart 2010; 97: 231-236

A.E. van der Hulst
A.A.W. Roest
V. Delgado
E.R. Holman
A. de Roos
N.A. Blom
J.J. Bax

ABSTRACT

Objective: Right ventricular (RV) dysfunction is common in patients with corrected tetralogy of Fallot (cToF). Abnormalities in the temporal pattern of RV mechanical activation have been observed in cToF patients, however, the relationship with RV performance remains unclear. The present study characterizes RV performance and the temporal sequence of RV deformation in cToF patients and healthy controls.

Design and patients: Thirty-seven cToF patients were compared to 18 controls. Using two-dimensional speckle tracking analysis, global RV strain was assessed. In addition, time to peak strain, and the time difference between RV inlet and RV outlet (RV time delay) was assessed.

Main outcome measure: The relation between RV performance and RV time delay was assessed with linear regression analysis.

Results: RV strain was reduced in patients compared to controls (-20.9±4.3% vs. -30.7±3.4%, p<0.001). Time to peak strain at the RV inlet showed no differences (cToF patients: 406±55 ms, controls: 405±67 ms, p=0.429), whereas time to peak strain at the RV outlet was significantly delayed in cToF patients (RV outlet: 339±75 ms vs. 262±85 ms, p=0.003). Consequently, RV time delay was significantly shorter in cToF patients (RV time delay: 66±48 ms vs. 143±53 ms, p<0.001). A close relation between RV time delay and RV strain was observed (r=-0.70, p<0.001).

Conclusion: In cToF patients, RV outlet deformation is delayed, causing a reduction of RV time delay which is significantly related to impairment in RV performance.

INTRODUCTION

Right ventricular (RV) dysfunction is common after surgical correction of tetralogy of Fallot (cToF) (1,2) and is an important predictor of poor clinical outcome in these patients.(1) Although chronic volume overload due to pulmonary regurgitation is recognized as an important factor causing RV failure in cToF,(3) the exact pathophysiological mechanisms leading to RV failure remain poorly understood. Abnormalities in the temporal pattern of RV mechanical activation, in particular a delayed activation of the RV outflow tract,(4) have been proposed as one of the determinants of RV dysfunction in cToF patients. The complex geometry and myofiber arrangement of the RV challenges the assessment of RV systolic function and mechanical activation pattern. From an anatomical and embryological perspective, the RV can be divided into two sections; the sinus (inlet), and the infundibulum (outlet).(5,6) Previous studies have demonstrated the presence of temporal differences in motion between the RV inlet and outlet in cToF patients as well as in healthy subjects.(4,7) However, the characterization of the RV mechanical activation sequence with different imaging techniques provided conflicting data.(4,7,8) In addition, the relationship between the RV temporal mechanical activation pattern and RV performance has not been elucidated.

Two-dimensional speckle tracking strain imaging is a recently introduced echocardiographic imaging modality that permits angle-independent, multi-directional assessment of myocardial deformation.(9,10) Two-dimensional speckle tracking strain analysis has demonstrated to be a useful method for early detection of myocardial dysfunction.(11-14) In addition, two-dimensional strain analysis enables the assessment of the temporal occurrence of regional myocardial deformation.(15,16) Accordingly, the aim of the present study was to characterize the temporal sequence of RV deformation and RV performance in cToF patients and healthy controls with two-dimensional speckle tracking echocardiography and with cardiac magnetic resonance imaging (CMR). The temporal sequence of RV deformation was related to RV performance to comprehensively understand the determinants of RV dysfunction in cToF patients.

METHODS

Study population and study protocol

A total of 37 consecutive patients with cToF and pulmonary regurgitation (mean age 12.9±2.9 years) were prospectively enrolled in the present study. Patients were selected from the database of the Center of Congenital Heart disease Amsterdam-Leiden. Patients after pulmonary valve replacement were excluded. In addition, 18 healthy controls with a similar age and body surface area were included. The study protocol was approved by the institutional review board and all subjects gave written, informed consent. A standard 12-lead ECG with a paper speed of 25 mm/s and 1 mV/mm was acquired for every cToF patient and control subject. The maximum QRS width was calculated. In addition, patients and controls were evaluated with CMR, two-dimensional echocardiography and speckle tracking echocardiography. RV dimensions and ejection fraction

Table 1. Baseline characteristics and results of right ventricular echocardiography

Baseline characteristics	Patients	Controls	p-value
Number (n)	37	18	
Age (y)	12.9 ± 2.9	13.9 ± 2.4	0.151
Male/female n (%)	22/15 (60/40)	11/7 (39/61)	0.907
QRS (ms)	134 ± 19	93 ± 8	<0.001
BSA (m²)	1.4 ± 0.3	1.5 ± 0.3	0.067
Age at repair (y)	0.84 ± 0.6		
Type of repair n (%)			
Transannular patch	22 (59)		
RVOT patch	4 (11)		
AP patch	3 (8)		
Infundibulectomy	8 (22)		
CMR			
RV-EDV (ml/m²)	131 ± 36	98 ± 13	<0.001
RV-ESV (ml/m²)	67 ± 21	46 ± 10	<0.001
RV-EF (%)	50 ± 5	53 ± 4	0.009
Echocardiography			
Pulmonary regurgitation n (%)			
mild	10 (28)	0	
moderate	12 (33)	0	
severe	14 (39)	0	
Pulmonary stenosis n (%)			
none/mild (<20 mmHg)	18 (49)	18 (100)	
moderate (20-40 mmHg)	14 (38)	0	
severe (>40 mmHg)	5 (13)	0	
TAPSE (mm)	16 ± 3	22 ± 3	<0.001
RV global longitudinal strain (%)	-20.9 ± 4.3	-30.7 ± 3.4	<0.001

Abbreviations: AP: arteria pulmonalis, BSA: body surface area, CMR: cardiac magnetic resonance, EDV: end-diastolic volume, EF: ejection fraction, ESV: end-systolic volume, RV: right ventricle, RVOT: right ventricular outflow tract. TAPSE: tricuspid annular plane systolic excursion.

Table 2. Temporal sequence of time to peak strain at RV inlet and RV outlet

	Patients	Controls	p-value
RV inlet Ts-inlet (ms)	406 ± 55	405 ± 67	0.429
RV outlet Ts-outlet (ms)	339 ± 75	262 ± 85	0.003
RV inlet – RV outlet RV time delay (ms)	66 ± 48	143 ± 53	<0.001

Abbreviations: RV time delay: difference between Ts-inlet and Ts-outlet. RV: right ventricle, Ts-inlet: time from onset of QRS to peak systolic strain at the RV inlet, Ts-outlet: time from onset of QRS to peak systolic strain at the RV outlet.

were assessed with CMR. RV performance was furthermore evaluated with conventional two-dimensional echocardiography (tricuspid annular plane systolic excursion [TAPSE]) and with speckle tracking strain analysis (global longitudinal strain). In addition, the temporal sequence of myocardial deformation of the inlet and outlet components of the RV was studied with speckle tracking strain analysis. Finally, RV dimensions, as assessed with CMR, and RV performance, as assessed with 2-dimensional speckle tracking, were related to the temporal sequence of myocardial deformation of the RV components.

CMR

CMR was performed on a 1.5 Tesla pulsar gradient system (Intera, release 11; Philips Medical Systems, Best, the Netherlands) with 33 mT/m amplitude, 100 mT/m/ms slew rate, and 0.33 ms rise time. A five-element cardiac coil was used for signal reception. After acquiring scout images, multi-section transversal cine imaging was performed. A stack of slices was planned in the transversal plane, covering the RV throughout the cardiac cycle. Images were acquired with a steady-state free precession sequence during breath hold at end-expiration (repetition time 3.9 ms, echo time 1.5 ms, flip angle 50°, slice thickness 8 mm, matrix 160x256, field-of-view 350 mm, temporal resolution 25 ms). Images were analyzed using the MASS (Medis, Leiden, The Netherlands) software package. (17) RV volumes were calculated by manually tracing the endocardial borders at end-systole and end-diastole in all slices and multiplying the area with slice thickness. Subsequently, RV ejection fractions were automatically calculated by MASS. RV volumes were indexed for body surface area.

Conventional two-dimensional echocardiography

Transthoracic echocardiographic images were acquired by a single experienced sonographer using a commercially available system equipped with a 3.5 MHz transducer (Vivid-7.0.0, GE Vingmed Ultrasound AS, Horten, Norway). Subjects were in the left lateral decubitus position during image acquisition. Standard two-dimensional images and color Doppler data were acquired from the parasternal and apical views and digitally stored in cine-loop format. Analyses were performed off-line using EchoPac version 108.1.5 (General Electric Medical Systems). TAPSE was evaluated

by applying the anatomic M-mode to the free wall of the RV at the tricuspid annulus. Pulmonary regurgitation was evaluated on parasternal short axis images with color Doppler and continuous-wave Doppler echocardiography.(18) The maximum pressure gradient over the pulmonary valve was assessed with pulsed-wave Doppler on parasternal short axis images. Finally, pulmonary valve closure was defined on trans-pulmonary valve pulsed-wave Doppler flow recordings and was used as time reference to assess RV deformation parameters.

Two-dimensional speckle tracking

Global longitudinal RV systolic strain and the temporal sequence of RV deformation were evaluated with speckle tracking analysis at the 4-chamber view (Figure 1, panel A and B) and at a dedicated apical RV view, depicting both inlet and outlet components of the RV, as previously described (Figure 1, panel C).(4) Frame rates ranged from 40 to 100 frames/s. During analysis, the endocardial border was manually traced at end-systole and the region of interest width adjusted to include the entire myocardium. The software then automatically tracks and accepts segments of good tracking quality and rejects poorly tracked segments, while allowing the observer to manually override its decisions based on visual assessments of tracking quality. The automated algorithm subsequently tracks the myocardium of interest frame by frame providing time-strain curves. Peak systolic global longitudinal strain of the RV was measured from the time-strain curves obtained at the apical 4-chamber view, (Figure 1, panel B) as described reviously.(13,19) At the dedicated RV view, regional longitudinal time-strain curves of the inlet and outlet of the RV were obtained (Figure 1, panel C and D). From these curves, peak longitudinal strain of the RV outlet was obtained. In addition, the temporal sequence of RV deformation of the inlet and outlet of the RV was derived from the time-strain curves by measuring the following parameters: time from QRS onset to peak systolic regional strain at the RV inlet (Ts-inlet) and time from QRS onset to peak systolic regional strain of the RV outlet (Ts-outlet). Finally, the time difference between Ts-inlet and Ts-outlet (RV time delay) was calculated (Figure 1, panel D).

Intra- and inter-observer agreement of the measurements in the dedicated apical RV view was assessed in a blinded manner in 15 randomly chosen subjects. Ts-inlet, Ts-outlet and peak longitudinal strain at the RV outlet were re-measured by the same and by an independent observer.

Statistical analysis

Continuous variables are expressed as mean values ± standard deviation (SD) and were compared with the Mann-Whitney U-test. Categorical data are expressed as numbers and frequencies and were compared with the Fisher's exact test. QRS duration, RV dimensions (as assessed with CMR) and RV performance (as assessed with echocardiography) were related to the RV time delay by using linear regression analysis. Intra-observer and inter-observer agreement of Ts-inlet, Ts-outlet and peak longitudinal strain at the RV outlet was assessed using the intra-class correlation coefficient (ICC) for absolute agreement. All data were analyzed using software of SPSS version 16.0. Statistical significance was set at a p-value <0.05.

Figure 1. Two-dimensional speckle tracking at the RV free wall and at RV inlet and RV outlet

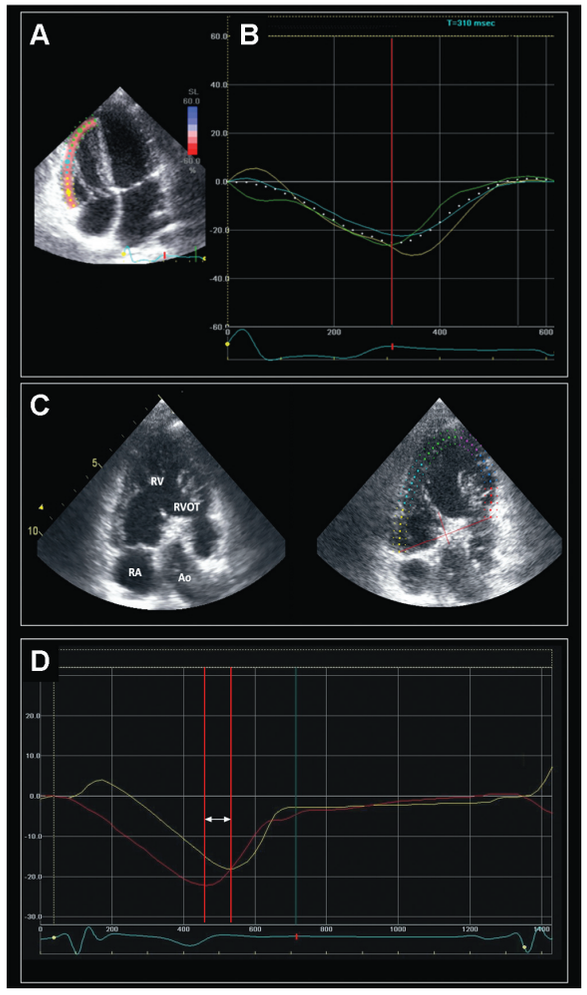

Panel A: Example of two-dimensional speckle tracking of the right ventricular (RV) free wall in the 4-chamber view of a corrected Tetralogy of Fallot (cToF) patient. The endocardium of the RV free wall is manually traced at end-systole. A region of interest, divided in a basal (yellow), a mid-ventricular (blue) and an apical region (green) is automatically displayed. **Panel B:** The software tracks the concerning myocardium frame by frame throughout the cardiac cycle, producing regional time-strain curves. A global time-strain curve (dotted line) is automatically calculated from a weighted average of the three regions, from which peak global strain can be derived (red line). **Panel C, left:** Example of dedicated apical RV view of a cToF patient, depicting the RV inlet and the RV outlet. **Right:** Example of placement of a region of interest for two-dimensional speckle tracking at the dedicated RV view in a cToF patient. The endocardium of the RV is manually traced at end-systole. A region of interest is automatically displayed. The automated tracking mechanism allows manual adjustment of width and position of the region of interest. **Panel D:** Example of time-strain curves of inlet and outlet of dedicated apical RV view in a cToF patient. Yellow curve; regional time-strain curve at the RV inlet. Red curve; regional time-strain curve at the RV outlet. Time to peak strain at the RV inlet (Ts-inlet), time to peak strain at the RV outlet (Ts-outlet) and RV time delay (difference between Ts-inlet and Ts-outlet, white arrows) can be derived. Abbreviations: Ao: Aorta, RA: Right atrium, RV: right ventricle, RVOT: right ventricular outflow tract.

RESULTS

Study population

The baseline characteristics of patients and controls are shown in Table 1. All patients were in New York Heart Association functional class I. Patients and controls did not differ in age, gender or body surface area. The QRS duration in cToF patients was significantly increased (134±19 ms vs. 93±8 ms, p<0.001). In all patients the acoustic window was satisfactory to provide sufficient quality for all images.

RV performance: CMR, conventional two-dimensional echocardiography and speckle tracking analysis

Table 1 outlines the RV dimensions and functional parameters as assessed with CMR and echocardiography. RV end-diastolic volume and RV end-systolic volume, as assessed with CMR, were significantly enlarged in cToF patients. In addition, RV ejection fraction was significantly reduced (50±5% vs. 53±4%, p=0.009). The mean TAPSE value, as assessed with echocardiography, was significantly reduced in patients as compared to controls (16±3 mm vs. 22±3 mm, p<0.001). Peak longitudinal strain of the RV outlet was significantly reduced in cToF patients (-16.4±5.4%, vs. -27.8±7.1%, p<0.001), with excellent intra- and inter-observer agreement (intra-observer ICC: 0.99, p<0.001, inter-observer ICC 0.86, p<0.001). Finally, global longitudinal strain of the RV was significantly impaired in cToF patients (-20.9±4.3% vs. -30.7±3.4%, p<0.001).

Temporal sequence of RV deformation

Analysis of the temporal sequence of myocardial deformation of the RV inlet and outlet and the RV time delay are shown in Table 2. In healthy controls and cToF patients, the peak strain of the RV outlet occurred earlier than the peak strain of the RV inlet. The time to peak systolic strain at the inlet was not significantly different between patients and controls (Ts-inlet: 406±55 ms vs. 405±67 ms, p=0.429). In contrast, time to peak systolic strain at the outlet was significantly longer in cToF patients as compared to controls (Ts-outlet: 339±75 ms vs. 262±85 ms, p=0.003). Consequently, cToF patients showed a significantly shorter RV time delay between the RV outlet and RV inlet than controls (RV time delay: 66±48 ms vs. 143±53 ms, p<0.001). Moreover, within patients, the RV time delay was significantly shorter in the patients with a patch (transannular or RV outflow tract patch, n=26), as compared with those without (50±28 ms vs. 101±65 ms, p=0.029). Intra- and inter-observer analysis of Ts-inlet and Ts-outlet yielded excellent agreements (Ts-inlet: intra-observer ICC 0.94, p<0.001, inter-observer ICC 0.95, p<0.001, Ts-outlet: intra-observer ICC 0.99, p<0.001, inter-observer ICC 0.95, p<0.001)

Relationship between RV time delay, QRS duration and CMR- and echocardiography-derived parameters

The relationship between the electrical (duration of QRS complex) and the mechanical (RV time delay) activation of the RV was evaluated. A weak correlation between QRS duration and RV time delay was observed (r=-0.37, p=0.006). In addition, the relationship between the RV mechanical

activation pattern and CMR-derived RV dimensions was assessed. Significant relations were observed between the RV time delay and RV end-diastolic volume (r=-0.45, p=0.001). Furthermore, the relation between RV time delay and degree of pulmonary regurgitation and stenosis, as assessed with echocardiography, was evaluated. Although RV longitudinal strain was related to degree of pulmonary stenosis (r=0.41, p=0.002), no significant relationship was noted between RV time delay and pulmonary stenosis (r=-0.23, p=0.099). In contrast, RV time delay was significantly related to degree of pulmonary regurgitation (r=-0.55, p <0.001). Finally, the relationship between RV time delay and RV performance, as assessed with TAPSE and two-dimensional speckle tracking, was evaluated. RV time delay was significantly related to TAPSE (r=0.53, p<0.001) (Figure 2, panel A). Moreover, a significant relation between RV time delay and global RV longitudinal strain was observed (r=-0.70, p<0.001) (Figure 2, panel B).

DISCUSSION

The current study demonstrated the presence of a time delay in RV longitudinal myocardial deformation between the outlet and inlet components in healthy controls as well as in cToF patients. Two-dimensional speckle tracking analysis showed that longitudinal RV outlet deformation preceded RV inlet deformation in healthy controls, and this sequence was also observed in the RV of cToF patients. However, in cToF patients, the RV outlet was activated significantly later than in healthy controls, reducing the time delay between the inlet and outlet components of the RV. This abnormal temporal activation of the RV was related to a significant deterioration of RV performance.

Temporal sequence of RV deformation in healthy subjects

The data of the present study show that longitudinal RV outlet deformation occurs prior to RV inlet deformation, which seems to conflict with the theory of a peristalsis-like contraction pattern of the RV segments. This peristalsis theory, postulating that the RV body contracts prior to the RV outflow tract, was originally derived from experimental animal data, using sonomicrometry to assess RV motion.(20-22) Data from these experiments do not uniformly point towards a peristalsis-like pattern of RV contraction. Importantly, two directions of movement of the RV outflow tract have been explored: transversal and longitudinal. In individuals with a structurally normal right ventricle, a peristalsis-like pattern of RV contraction was observed in the transversal direction with contraction of the RV body followed by contraction of the RV outflow tract.(21,22) However, in the longitudinal direction, the peristalsis-like pattern was not observed.(21,22) These findings were recently confirmed by Matsui and co-workers.(7) The authors assessed longitudinal shortening at the RV free wall and at the RV outflow tract with two-dimensional tissue tracking in healthy volunteers. Time to peak longitudinal strain at the RV outflow tract occurred prior to that of the RV free wall. In addition, changes in the transverse diameter of the RV outflow tract were tracked in time. Measuring in this direction, a peristalsis-like sequence of RV activation was observed: the time to minimal diameter of the RV outflow tract was delayed as compared with the RV free wall.

Figure 2. Relation between RV time delay and RV performance

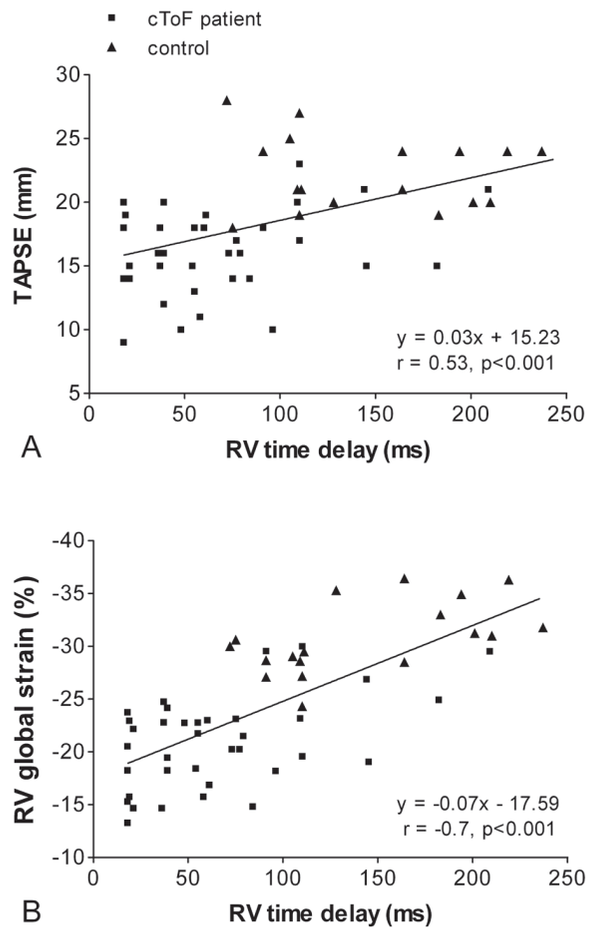

Scatter plots representing correlations between RV performance and RV time delay. **Panel A:** Correlation between RV time delay and TAPSE. **Panel B:** Correlation RV time delay and RV global strain. Abbreviations: RV: right ventricle, TAPSE: tricuspid annulus peak systolic excursion.

In addition, Uebing et al. provided further evidence on the longitudinal activation sequence of the RV in a subgroup of healthy volunteers.(4) Using tissue Doppler imaging, time to peak longitudinal velocity of the RV free wall and RV outflow tract were measured. This study showed that peak systolic longitudinal velocity of the RV outflow tract occurs prior to that of the RV free wall. In contrast, the study by Geva et al. assessed RV segmental volumes with echocardiography and MRI in healthy subjects and evaluated the activation sequence in the transverse direction.(8) In this direction, again, a peristalsis-like pattern of RV contraction was observed.
Based on this evidence and the data of the current study, a hypothetical model of the sequence of normal segmental RV contraction can be postulated, with early longitudinal and late transverse movement of the RV outflow tract. Nevertheless, additional studies to confirm this model of RV sequential contraction are warranted.

Delayed activation of RV outlet deformation in cToF patients

The RV outlet is involved in the surgical repair of tetralogy of Fallot to relieve pulmonary stenosis, by either infundibulectomy or RV outflow tract patch placement. The present study demonstrated that, similar to healthy patients, longitudinal RV outlet deformation in cToF patients occurs prior to RV inlet deformation. However, RV outlet deformation was significantly delayed in cToF patients, causing a reduced RV time delay. The longitudinal deformation of the RV outlet was even more delayed in patients that had undergone RV outflow tract or transannular patch placement. This effect after surgical repair in cToF patients confirms the findings of Uebing and colleagues.(4) In their study, the RV time delay observed in healthy subjects was reduced in cToF patients, which was mainly caused by a delayed longitudinal RV outlet motion. The presence of RV outflow tract damage due to a surgical patch or scar tissue presumably causes delayed RV outlet contraction. This finding confirms the importance of current surgical strategies, with an aim to preserve RV outflow tract integrity whenever possible.

Relationship between electrical and mechanical RV delay and RV performance

In the current study, the observed delay between RV inlet and RV outlet deformation was only weakly related with QRS duration. QRS prolongation reflects temporal differences in electrical activation within the myocardium, and is currently used as a marker for dyssynchrony in trials on cardiac resynchronization therapy (CRT) for left ventricular (LV) failure.(23,24) However, the relationship between QRS prolongation and intra-ventricular mechanical delay is not straightforward.(25) Moreover, the current study demonstrated the presence of an average mechanical delay of 140 ms within the RV of healthy subjects with a narrow QRS duration. Future studies are needed to further characterize the deformation pattern of the RV inlet and outlet in various age groups and etiologies.
The RV time delay was closely related with RV end-diastolic volume as assessed with CMR, as well as with degree of pulmonary regurgitation, indicating a relation between the observed mechanical abnormities and chronic volume overload. In addition, the RV mechanical time delay was significantly related with RV performance, as assessed with two-dimensional speckle tracking and TAPSE. According to our data, disappearance of the RV time delay is associated with a deterioration of RV performance. Furthermore, the presence of a mechanical delay in the structurally normal RV has important clinical implications for future treatment of RV dysfunction, in particular with CRT. Importantly, the concept is in contrast with reported data on LV performance, where LV dyssynchronous contraction leads to LV systolic dysfunction. In case of LV failure, CRT improves LV function by restoring synchronous LV contraction pattern.(26) However, based on the results of the present study, showing a mechanical time delay in longitudinal deformation of the healthy RV, these assumptions may not hold for RV motion patterns. The effects of CRT have been evaluated in patients with cToF and RV dysfunction.(27-30) However, a better understanding of the RV mechanical activation patterns and the presence of a physiological RV time delay between longitudinal deformation of the RV inlet and outlet may be essential to maximize the benefits of CRT.

Study limitations

Two-dimensional speckle tracking analysis is dependent on image quality and frame rate. In the present study, two-dimensional gray scale images were optimized to obtain the highest image quality at the highest frame rate possible to allow reliable analysis. In addition, assessment of exercise capacity was not performed in the current study. Additional studies investigating the relationship between the observed RV time delay and exercise capacity are warranted.

Conclusion

The presence of a mechanical time delay between the outlet and inlet components of the RV may be an important determinant of preserved RV function. Longitudinal deformation of the RV outlet precedes longitudinal deformation of the RV inlet in individuals with structurally normal right ventricles. In cToF patients, this mechanical sequence is also observed, however, RV outlet deformation is significantly delayed causing a reduction of RV time delay which is subsequently related to impairment in RV performance.

REFERENCE LIST

1 Geva T, Sandweiss BM, Gauvreau K, et al. Factors associated with impaired clinical status in long-term survivors of tetralogy of Fallot repair evaluated by magnetic resonance imaging. J Am Coll Cardiol 2004;43:1068-74.

2 Knauth AL, Gauvreau K, Powell AJ, et al. Ventricular size and function assessed by cardiac MRI predict major dverse clinical outcomes late after tetralogy of Fallot repair. Heart 2008;94:211-6.

3 Bouzas B, Kilner PJ, Gatzoulis MA. Pulmonary regurgitation: not a benign lesion. Eur Heart J 2005;26:433-9.

4 Uebing A, Gibson DG, Babu-Narayan SV, et al. Right ventricular mechanics and QRS duration in patients with repaired tetralogy of Fallot: implications of infundibular disease. Circulation 2007;116:1532-9.

5 Anderson RH, Ho SY. What is a ventricle? Ann Thorac Surg 1998;66:616-20.

6 Sheehan F, Redington A. The right ventricle: anatomy, physiology and clinical imaging. Heart 2008;94:1510-5.

7 Matsui H, Satomi G, Yasukochi S, et al. Evaluation of right ventricular contraction by myocardial strain in children using a two-dimensional tissue tracking method. Pediatr Cardiol 2008;29:377-81.

8 Geva T, Powell AJ, Crawford EC, et al. Evaluation of regional differences in right ventricular systolic function by acoustic quantification echocardiography and cine magnetic resonance imaging. Circulation 1998;98:339-45.

9 Amundsen BH, Helle-Valle T, Edvardsen T, et al. Noninvasive myocardial strain measurement by speckle tracking echocardiography: validation against sonomicrometry and tagged magnetic resonance imaging. J Am Coll Cardiol 2006;47:789-93.

10 Langeland S, D'hooge J, Wouters PF, et al. Experimental validation of a new ultrasound method for the imultaneous assessment of radial and longitudinal myocardial deformation independent of insonation angle. irculation 2005;112:2157-62.

11 Delgado V, Tops LF, van Bommel RJ, et al. Strain analysis in patients with severe aortic stenosis and preserved left ventricular ejection fraction undergoing surgical valve replacement. Eur Heart J 2009.

12 Hare JL, Brown JK, Marwick TH. Association of myocardial strain with left ventricular geometry and rogression of hypertensive heart disease. Am J Cardiol 2008;102:87-91.

13 Knirsch W, Dodge-Khatami A, Kadner A, et al. Assessment of myocardial function in pediatric patients with perated tetralogy of Fallot: preliminary results with 2D strain echocardiography. Pediatr Cardiol 2008;29:718-25.

14 Scherptong RW, Mollema SA, Blom NA, et al. Right ventricular peak systolic longitudinal strain is a sensitive marker for right ventricular deterioration in adult patients with tetralogy of Fallot. Int J Cardiovasc Imaging 2009;25:669-76.

15 Delgado V, Ypenburg C, van Bommel RJ, et al. Assessment of left ventricular dyssynchrony by speckle tracking strain imaging comparison between longitudinal, circumferential, and radial strain in cardiac resynchronization therapy. J Am Coll Cardiol 2008;51:1944-52.

16 Suffoletto MS, Dohi K, Cannesson M, et al. Novel speckle-tracking radial strain from routine black-and-white echocardiographic images to quantify dyssynchrony and predict response to cardiac resynchronization therapy. Circulation 2006;113:960-8.

17 van der Geest RJ, Buller VG, Jansen E, et al. Comparison between manual and semiautomated analysis of left ventricular volume parameters from short-axis MR images. J Comput Assist Tomogr 1997;21:756-65.

18 Li W, Davlouros PA, Kilner PJ, et al. Doppler-echocardiographic assessment of pulmonary regurgitation in adults with repaired tetralogy of Fallot: comparison with cardiovascular magnetic resonance imaging. Am Heart J 2004;147:165-72.

19 Teske AJ, De Boeck BW, Olimulder M, et al. Echocardiographic assessment of regional right ventricular function: a head-to-head comparison between 2-dimensional and tissue Doppler-derived strain analysis. J Am Soc Echocardiogr 2008;21:275-83.

20 Meier GD, Bove AA, Santamore WP, et al. Contractile function in canine right ventricle. Am J Physiol 1980;239:H794-H804.

21 Raines RA, LeWinter MM, Covell JW. Regional shortening patterns in canine right ventricle. Am J Physiol 1976;231:1395-400.

22 Santamore WP, Meier GD, Bove AA. Effects of hemodynamic alterations on wall motion in the canine right ventricle. Am J Physiol 1979;236:H254-H262.

23 Epstein AE, DiMarco JP, Ellenbogen KA, et al. ACC/AHA/HRS 2008 Guidelines for Device-Based Therapy of Cardiac Rhythm Abnormalities: a report of the American College of Cardiology/American Heart Association Task Force on Practice Guidelines (Writing Committee to Revise the ACC/AHA/NASPE 2002 Guideline Update for Implantation of Cardiac Pacemakers and Antiarrhythmia Devices) developed in collaboration with the American Association for Thoracic Surgery and Society of Thoracic Surgeons. J Am Coll Cardiol 2008;51:e1-62.

24 Vardas PE, Auricchio A, Blanc JJ, et al. Guidelines for cardiac pacing and cardiac resynchronization therapy: The Task Force for Cardiac Pacing and Cardiac Resynchronization Therapy of the European Society of Cardiology. Developed in collaboration with the European Heart Rhythm Association. Eur Heart J 2007;28:2256-95.

25 Bleeker GB, Schalij MJ, Molhoek SG, et al. Relationship between QRS duration and left ventricular dyssynchrony in patients with end-stage heart failure. J Cardiovasc Electrophysiol 2004;15:544-9.

26 Leclercq C, Kass DA. Retiming the failing heart: principles and current clinical status of cardiac resynchronization. J Am Coll Cardiol 2002;39:194-201.

27 Bordachar P, Iriart X, Chabaneix J, et al. Presence of ventricular dyssynchrony and haemodynamic impact of right ventricular pacing in adults with repaired Tetralogy of Fallot and right bundle branch block. Europace 2008;10:967-71.

28 Dubin AM, Feinstein JA, Reddy VM, et al. Electrical resynchronization: a novel therapy for the failing right ventricle. Circulation 2003;107:2287-9.

29 Stephenson EA, Cecchin F, Alexander ME, et al. Relation of right ventricular pacing in tetralogy of Fallot to electrical resynchronization. Am J Cardiol 2004;93:1449-52, A12.

30 Zimmerman FJ, Starr JP, Koenig PR, et al. Acute hemodynamic benefit of multisite ventricular pacing after congenital heart surgery. Ann Thorac Surg 2003;75:1775-80.

2.4

Relation of left ventricular twist and global strain with right ventricular dysfunction in patients after correction of tetralogy of Fallot

American Journal of Cardiology 2010; 106: 723-729

A.E. van der Hulst
V. Delgado
E.R. Holman
L.J.M. Kroft
A. de Roos
M.G. Hazekamp
N.A. Blom
J.J. Bax
A.A.W. Roest

ABSTRACT

Background: In patients with corrected tetralogy of Fallot (cToF), left ventricular (LV) dysfunction is closely related to right ventricular (RV) dysfunction, indicating adverse ventricular-ventricular interactions. However, the mechanism that links RV dysfunction to LV dysfunction remains unclear.

Methods: In this prospective study, 32 cToF patients and 19 controls were enrolled. With cardiac magnetic resonance imaging (CMR), biventricular ejection fractions were assessed. Using two-dimensional speckle tracking, global and regional RV and LV strain and LV twist were assessed. To detect and characterize ventricular-ventricular interaction, the relation between global and regional RV mechanics and global and regional LV mechanics was assessed.

Results: Global RV strain, global LV strain and LV twist were decreased in cToF patients. Global RV strain correlated with global LV strain ($r = 0.66$, $p < 0.001$) and LV twist ($r = -0.72$, $p < 0.001$) indicating the presence of adverse ventricular-ventricular interaction. Furthermore, close relations were observed between apical RV strain and apical LV strain ($r = 0.62$, $p < 0.001$) and apical LV rotation ($r = -0.67$, $p < 0.001$).

Conclusions: RV strain was significantly related to LV strain and LV twist in cToF patients and controls. Furthermore, apical RV strain correlated with apical LV strain and apical LV rotation, indicating adverse apical ventricular-ventricular interactions.

INTRODUCTION

Current surgical techniques have improved the clinical outcome of patients with tetralogy of Fallot.(1) However, after the third postoperative decade, the risk of death increases dramatically.(2) Recent studies have demonstrated that reduced left ventricular (LV) ejection fraction and right ventricular (RV) ejection fraction and older age at correction of tetralogy of Fallot (cToF) are strong independent determinants of poor clinical outcome in cToF patients.(3,4) In addition, several studies have demonstrated a close relationship between RV and LV ejection fraction in cToF patients(3,5) indicating the potential pathophysiologic role of ventricular-ventricular interactions that lead to clinical deterioration late after cToF. However, these ventricular-ventricular interactions have not been completely elucidated and, more importantly, the mechanism that links RV dysfunction to impairment of LV function remains unclear. Two-dimensional speckle tracking echocardiography has enabled assessment of multidirectional myocardial mechanics, providing information on complex RV and LV motion patterns. This imaging modality has demonstrated to be useful to detect subclinical cardiac dysfunction in several clinical conditions.(6,7) In the present study, two-dimensional speckle tracking echocardiography and cardiac magnetic resonance (CMR) were used to comprehensively characterize global and regional RV and LV performance in cToF patients and in healthy subjects. In addition, global and regional RV mechanics were related to global and regional LV mechanics to detect and characterize ventricular-ventricular interaction.

METHODS

Thirty-two consecutive cToF patients undergoing clinical CMR evaluation between July 2008 and July 2009 (age range 8-18 years) were prospectively recruited from an ongoing registry (Center for Congenital Heart Disease Amsterdam-Leiden). Exclusion criteria were previous pulmonary valve replacement and any contraindications for CMR, such as claustrophobia, cardiac devices or arrhythmia. In addition, 19 healthy subjects, matched by age and body surface area, without structural heart disease underwent echocardiography and CMR evaluation within the same time frame. Individuals with history of cardiomyopathy, valvular heart disease or arrhythmic disorders were excluded. CMR and transthoracic echocardiography were performed to study LV and RV performance and to assess ventricular-ventricular interactions. RV ejection fraction (EF), RV end-diastolic and end-systolic volume, LVEF and LV end-diastolic and end-systolic volume were assessed with CMR. RV and LV longitudinal strain and LV twist were evaluated with two-dimensional speckle tracking. Ventricular-ventricular interaction was studied by assessing the relationships between RV and LV strain and LV rotation. The study protocol was approved by the institutional review board and all subjects gave written, informed consent.

CMR was performed on a 1.5-Tesla pulsar gradient system (Intera, release 11; Philips Medical Systems, Best, the Netherlands) with 33 mT/m amplitude, 100 mT/m/ms slew rate, and 0.33 ms rise time. A five-element cardiac coil was used for signal reception. After acquiring a series of localizing thoracic scout images, multi-section transversal(8) cine imaging was performed. A stack of slices

Table 1. Patient and control characteristics

Variable	Patients (n=32)	Controls (n=19)	p-value
Age (years)	13.2 ± 2.9	14.1± 2.4	0.228
Male/female	19/13	12/7	0.693
Age at surgery (years)	0.9 ± 0.6	..	
Type of surgery			
Infundibulectomy	5 (15%	..	
RVOT patch	4 (13%)	..	
Transannular patch	20 (63%)	..	
AP patch	3 (9%)	..	
QRS (ms)	134 ± 19	94 ± 8	<0.001
BSA (m²)	1.4 ± 0.3	1.6 ± 0.3	0.113
BMI (kg/m²)	18.5 ± 4	19.4 ± 3	0.368
Pulmonary regurgitation			
Mild	8 (25%)	..	
Moderate	13 (41%)	..	
Severe	11 (34%)	..	
CMR parameters			
RV-EDV (ml/m²)	131± 30	98 ± 13	<0.001
RV-ESV (ml/m²)	110 ± 66	59 ± 46	<0.001
RVEF (%)	50 ± 5	53 ± 4	0.016
LV-EDV (ml/m²)	88 ± 20	95 ± 10	0.196
LV-ESV (ml/m²)	40 ± 13	42 ± 7	0.266
LVEF (%)	56 ± 5	56 ± 3	0.724

Abbreviations: AP: arteria pulmonalis; BSA: body surface area, BMI: body mass index, CMR: cardiac magnetic resonance, LV-EDV: left ventricular end-diastolic volume, LVEF: left ventricular ejection fraction, LV-ESV: left ventricular end-diastolic volume, NA: not applicable, RV-EDV: right ventricular end-systolic volume, RV-ESV: right ventricular end-systolic volume, RVEF: right ventricular ejection fraction; RVOT: right ventricular outflow tract. between RV time delay and TAPSE.

was planned in the transversal plane, covering both ventricles throughout the cardiac cycle. Images were acquired with a steady-state free precession sequence during breath hold at end-expiration with the settings: repetition time 3.9 ms, echo time 1.5 ms, flip angle 50°, slice thickness 8 mm, matrix 160 x 256, field-of-view 350 mm and temporal resolution 25 ms.

Images were analyzed using the MASS (Medis, Leiden, The Netherlands) software package.(9) LV and RV volumes were calculated by manually tracing the endocardial borders at end-systole and end-diastole in all slices and multiplying the area with slice thickness. Subsequently, LV and RV ejection fractions were automatically calculated by MASS. LV and RV volumes were indexed for body surface area.

All subjects were imaged in the left lateral decubitus position with a commercially available system (Vingmed Vivid 7, General Electrics Medical Systems, Milwaukee, Wisconsin, USA) equipped with

Table 2. Global and regional right ventricular and left ventricular longitudinal peak systolic

	Patients (n=32)	Controls (n=19)	p-value
2D speckle tracking parameters			
Global RV LPSS (%)	-20.5 ± 4.2	-30.7 ± 3.3	<0.001
Regional RV LPSS (%)			
basal	-21.9 ± 6.2	-28.0 ± 5.5	0.001
mid	-23.8 ± 3.7	-30.4 ± 4.2	<0.001
apical	-20.7 ± 6.9	-32.6 ± 4.7	<0.001
Global LV LPSS (%)	-17.2 ± 1.3	-20.4 ± 1.3	<0.001
Regional LV LPSS (%)			
basal	-18.6 ± 2.5	-19.2 ± 2.4	0.519
mid	-18.1 ± 2.1	-19.7 ± 2.7	0.014
apical	-15.9 ± 2.8	-22.1 ± 3.4	<0.001
LV twist (^{O})	8.8 ± 3.3	14.8 ± 3.2	<0.001
apical rotation (^{O})	5.6 ± 2.4	10.0 ± 2.0	<0.001
basal rotation (^{O})	-4.1 ± 2.0	-5.3 ± 2.3	0.073

Abbreviations: 2D: two-dimensional, LPSS: longitudinal peak systolic LV: left ventricle, RV: right ventricle.

a 3.5 MHz transducer. Standard two-dimensional images, Doppler and color Doppler data were acquired from the parasternal and apical views and digitally stored in cine-loop format. Analyses were performed off-line using EchoPac version 108.1.5 (General Electric Medical Systems). For speckle tracking analysis, standard two-dimensional gray-scale images with a frame rate ≥40 frames/s were used. Three cardiac cycles were obtained and stored in cine-loop format for offline analysis. All echocardiographic measurements were averaged from three cardiac cycles. The presence of pulmonary regurgitation was systematically evaluated with continuous-wave Doppler echocardiography, by measuring duration of pulmonary regurgitation, and color Doppler echocardiography, by measuring width of regurgitant jet, as previously described by Li et al.(10)

Global longitudinal RV strain was assessed with two-dimensional speckle tracking analysis in the apical 4-chamber view, measuring the longitudinal peak systolic strain of the RV free wall, as described previously (Figure 1A).(11) The weighted average of the 3 regional values of the RV free wall (basal, mid and apical segments) provided the value of global longitudinal RV strain. Regional longitudinal peak systolic strain of the RV was assessed at the basal, mid and apical components of the RV free wall. Intra- and inter-observer reproducibility for RV strain measurement have been previously reported showing small bias and no significant trend (-0.2 ± 3.6% and 0.6 ± 3.8%, respectively).(12)

Global longitudinal LV strain was measured at the apical long axis, 2- and 4-chamber views using automated function imaging, a novel two-dimensional speckle tracking algorithm.(13,14) The end-systolic frame is defined in the apical long-axis view. Closure of the aortic valve is marked and the software measures the time interval between the R-wave and aortic valve closure. This interval is used as a reference for the apical 2- and 4-chamber views. After defining the mitral annulus and the LV apex with three index points at the end-systolic frame in each apical view, the automated algorithm places the region of interest including the entire myocardial wall. The tracking algorithm follows the endocardium from this single frame throughout the cardiac cycle and allows for manual adjustment of the region of interest. The LV is divided into 6 segments in each view and the tracking quality is manually validated for each segment. The algorithm displays regional and global longitudinal LV peak strain in a 17-segment model "bull's eye" plot, with the average values of peak longitudinal strain for each view and the averaged global peak longitudinal strain for the entire LV (Figure 1B). Regional longitudinal LV strain was evaluated at the basal, mid and apical level by calculating the average strain values of the basal, mid and apical segments of the apical long axis, 2- and 4-chamber views. Intra- and inter-observer reproducibility for automated function imaging measurements have been previously reported with small bias and no significant trend (-0.3 ± 0.6% and -0.2 ± 2.6%, respectively).(13)

LV rotation was measured at the apical and basal level in the parasternal short-axis view using two-dimensional speckle tracking. The basal plane was identified by the presence of the mitral valve. The apical plane was defined as the smallest cavity during systole below the papillary muscles. Off-line, the endocardial border was traced at an end-systolic frame and the region of interest was placed to fit the entire myocardium. Subsequently, LV rotation of both apical and basal planes was automatically calculated. Counterclockwise rotation provided a positive value, whereas clockwise rotation provided a negative value, as viewed from the apex. LV twist was defined as the maximal net difference in rotation between the LV apex and base at isochronal time points (Figure 1C).(15)

Statistical analysis

Continuous variables are expressed as means ± standard deviations. Comparisons between patients and controls were analyzed using a Mann-Whitney U-test. Categorical variables are presented as numbers and percentages and were compared with Fisher's exact test. The relations between LVEF, RVEF and global LV and RV strain, and between RV end-diastolic volume, RV end systolic volume and global RV strain were evaluated with linear regression. Differences in RV apical strain between controls and subgroups of cToF patients with mild, moderate and severe pulmonary regurgitation were assessed with the Kruskal-Wallis test. Furthermore, linear regression analysis was used to assess the relationship between global RV strain and global LV strain and LV twist. In addition, regional ventricular-ventricular interaction was studied, by evaluating the relation between RV strain and LV strain and rotation at the basal and apical level with linear regression. To analyze whether surgical technique could determine RV and LV strain or LV rotational mechanics, univariate regression analysis was performed. A p-value of <0.05 was considered statistically significant.

Figure 1. Two-dimensional speckle tracking echocardiography for right ventricular longitudinal strain, left ventricular longitudinal strain and left ventricular twist analysis

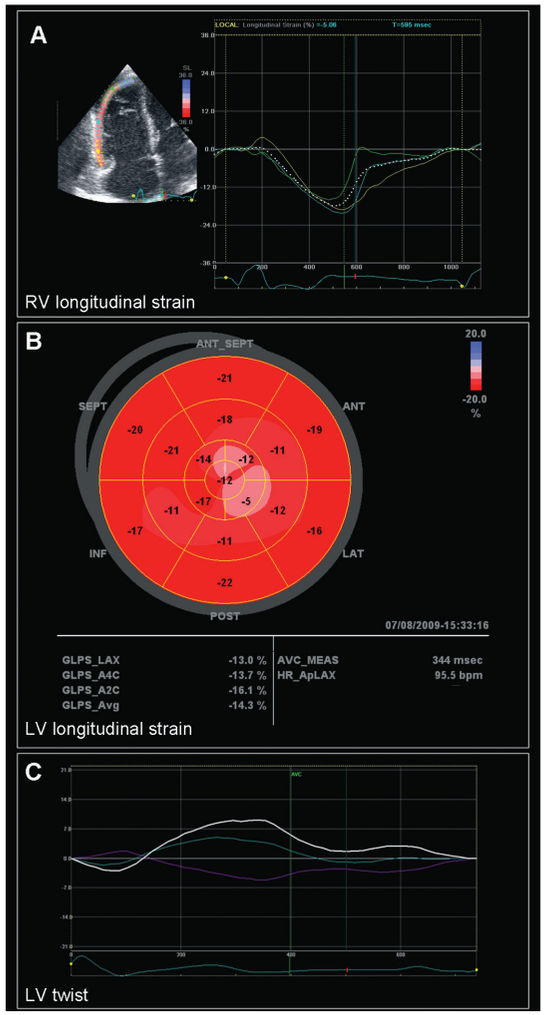

Panel A. Example of two-dimensional speckle tracking of right ventricular longitudinal strain in a corrected tetralogy of Fallot patient. Global and segmental strain curves are automatically calculated providing global and regional peak systolic longitudinal strain. Global right ventricular strain: white dotted curve, apical right ventricular strain: green curve, mid right ventricular strain: blue curve, basal right ventricular strain: yellow curve.
Panel B. Example of "bull's eye" plot of left ventricular longitudinal strain of a corrected tetralogy of Fallot patient. Longitudinal strain is most reduced at the apical level.
Panel C. Example of apical and basal rotation and left ventricular twist of a corrected tetralogy of Fallot patient. Left ventricular twist is reduced, mainly due to reduced apical rotation. Basal rotation: purple curve, apical rotation: blue curve, left ventricular twist: white curve. Abbreviations: A2C: apical 2-chamber view, A4C: apical 4-chamber view, AFI: automated functional imaging, AVC_AUTO: aortic valve closure detected automatically, AVC_MEAS: aortic valve closure detected manually, Avg: average peak strain of the LV, cToF: corrected tetralogy of Fallot, GLPS: global longitudinal peak strain, LAX: apical long axis view, LV: left ventricle HR_ApLAX: heart rate during acquisition of the apical long axis view, RV: right ventricle.

Figure 2. Global and regional left ventricular longitudinal strain and left ventricular twist

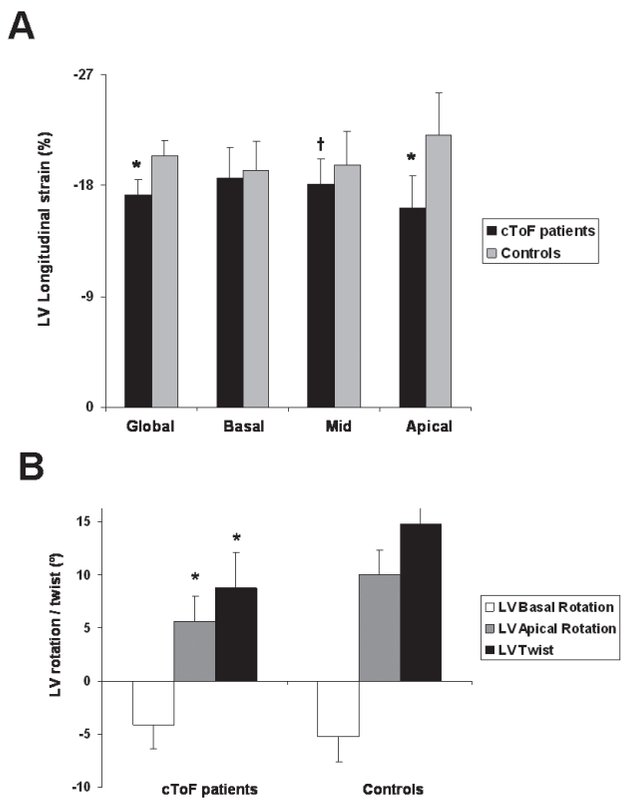

Panel A: Bar-graph presenting the global left ventricular longitudinal strain and regional left ventricular longitudinal strain at the basal, mid and apical levels in corrected tetralogy of Fallot patients and controls. A significantly decreased global strain is observed in the patients, mainly caused by a significantly reduced strain at the apical and mid level of the left ventricle.*p < 0.0001 vs. controls; †p = 0.014 vs. controls. **Panel B:** Bar-graph presenting left ventricular basal and apical rotation and left ventricular twist in corrected tetralogy of Fallot patients and controls. Rotation at the basal level is clockwise and expressed as a negative value, whereas apical rotation is counterclockwise and expressed as a positive value. In the patients, left ventricular twist is significantly reduced, mainly because of a significantly decreased rotation at the apical level. * p < 0.0001 vs. controls.
Abbreviations: cToF: corrected tetralogy of Fallot, LV: left ventricle.

Figure 3. Ventricular-ventricular interactions

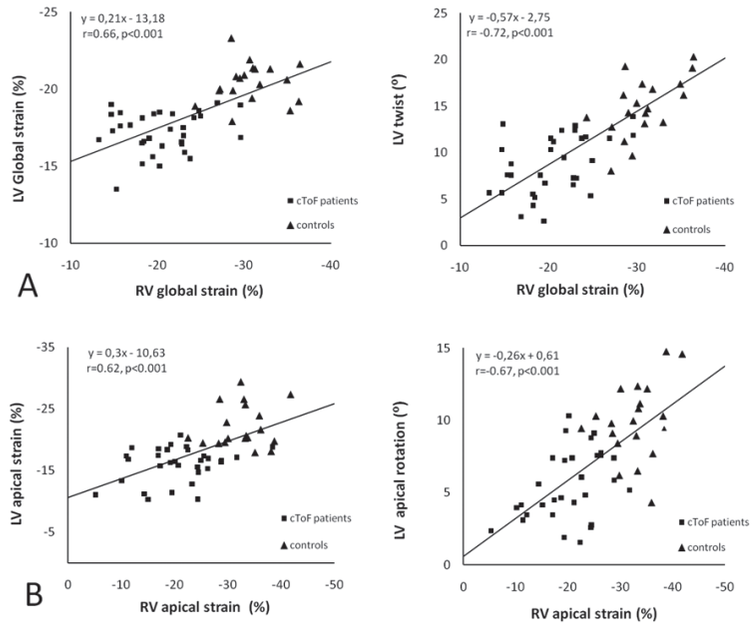

Scatter-plots presenting correlations between right ventricular global strain and left ventricular global strain nd left ventricular twist (Panel A). Panel B presents the correlation between right ventricular apical strain and left ventricular apical strain, and between right ventricular apical strain and left ventricular apical rotation.
Abbreviations: cToF: corrected tetralogy of Fallot: LV: left ventricle, RV: right ventricle.

RESULTS

Characteristics of cToF patients and healthy subjects are displayed in Table 1. All patients were in New York Heart Association functional class I. Baseline characteristics were not significantly different between cToF patients and healthy controls with the exception of QRS duration (patients: 134 ± 19 ms vs. controls: 94 ± 8 ms, p < 0.001). RV end-diastolic volume and RV end-systolic volume were larger in cToF patients and RVEF was significantly reduced. LV dimensions and LVEF did not differ in cToF patients as compared to controls.

The assessment of RV function with two-dimensional speckle tracking demonstrated significantly reduced global longitudinal RV strain in cToF patients (-20.5 ± 4.2% vs. -30.7 ± 3.3%, p < 0.001) as compared to controls (Table 2). When assessing regional longitudinal RV strain, cToF patients had significantly reduced strain in all segments of the RV free wall (basal, mid and apical) (Table 2). In addition, RV apical longitudinal strain was significantly different in controls and in cToF patients with mild, moderate and severe pulmonary regurgitation (-32.6 ± 4.7 %, -20.2 ± 9.6 %, -23.6 ± 6 % and -18.0 ± 5.3 %, respectively; p < 0.001).

Two-dimensional speckle tracking analysis demonstrated a significant impairment in global longitudinal LV strain in cToF patients (-17.2 ± 1.3% vs. -20.4 ± 1.3%, p < 0.001) (Table 2 and Figure 2A). Assessment of regional longitudinal LV strain revealed that in cToF patients strain was significantly reduced at the mid level (-18.1 ± 2.1 vs. -19.7 ± 2.7, p = 0.014) and apical level (-15.9 ± 2.8% vs. -19.8 ± 2.9, p < 0.001). In contrast, longitudinal LV strain at the basal level was not significantly different (Table 2, Figure 2A).

The assessment of LV rotation and twist demonstrated a significantly reduced LV apical rotation in cToF patients as compared to controls (5.6 ± 2.4o vs. 10.0 ± 2.0o, p < 0.001) whereas no differences were observed in LV basal rotation (-4.1 ± 2.0o vs. -5.3 ± 2.3o, p = 0.073) (Table 2). This resulted in a significantly reduced LV twist in cToF patients (8.8 ± 3.3o vs. 14.8 ± 3.2o, p < 0.001) (Figure 2B).

In addition, the influence of the surgical technique (the use of an RVOT patch or transannular patch) on RV and LV performance was evaluated by univariate regression analysis. Surgical technique did not determine RV or LV performance (RV global longitudinal strain: r = 0.14; p = 0.458, RV apical longitudinal strain: r = 0.26; p = 0.159, LV global longitudinal strain: r = 0.15; p = 0.425, LV apical longitudinal strain: r = 0.01; p = 0.959, LV twist: r = 0.16; p = 0.379, LV apical rotation: r = 0. 21; p = 0.251).

The assessment of global ventricular-ventricular interaction showed that LVEF and RVEF were closely related (r = 0.63, p<0.001). In addition, global longitudinal RV strain correlated significantly with global longitudinal LV strain (r = 0.66, p < 0.001) and with LV twist (r = -0.72, p < 0.001) (Figure 3A). Evaluation of regional ventricular-ventricular interaction revealed that apical longitudinal RV strain was significantly correlated with apical longitudinal LV strain (r = 0.62, p < 0.001) and with apical LV rotation (r = -0.67, p < 0.001) (Figure 3B). In contrast, no significant correlations were found between the basal longitudinal RV strain and basal longitudinal LV strain (r = 0.13, p = 0.394) and basal LV rotation (r = 0.23, p = 0.116).

DISCUSSION

The present study demonstrated that cToF patients in the first post-operative decades have a significantly reduced RVEF and preserved LVEF, as assessed with CMR. However, the evaluation of myocardial deformation with two-dimensional speckle tracking confirmed the RV dysfunction observed with CMR and revealed the presence of LV subclinical dysfunction, with impairment in global longitudinal LV strain and LV twist. In addition, regional analysis with two-dimensional speckle tracking revealed a homogeneous reduction of longitudinal RV strain in all segments, whereas the LV showed a significant impairment in longitudinal strain and rotational mechanics only at the mid and apical levels. More important, a close relationship was observed between global RV and LV mechanics, demonstrated with both CMR and two-dimensional speckle tracking. When assessing regional performance, this close relationship was most pronounced at the apical levels of the RV and LV. These findings indicate the presence of adverse ventricular-ventricular interactions

and provide new insights into the pathophysiological mechanisms that link RV dysfunction to LV dysfunction. Evaluation of global and regional RV performance in cToF patients may be challenging with two-dimensional echocardiography. Currently, CMR is the gold standard for evaluation of RV dimensions and ejection fraction.(16) In addition, recent CMR volumetric analyses of the different components of the RV (inlet, apical trabecular and outlet) have provided meaningful insight into the adaptive response of the RV to volume overload.(17) This adaptive response relied mostly on the RV apical trabecular component that accounted for the largest increase in volume.(17) In addition, a close relationship between the function of the apical trabecular component and global RV function (r^2 = 0.69) was observed, whereas no relationship was found between the function of the RV inlet and outlet and global RV function.(17) This indicates that global RV performance strongly depends on the function of the RV apical component. With the use of two-dimensional speckle tracking, the present study confirmed and extended previous findings. Although a homogeneous reduction in strain at the three different RV levels was observed, only the deterioration of RV apical strain was related to impairment in LV mechanics, indicating an adverse ventricular-ventricular interaction at this level. The assessment of LV systolic dysfunction in cToF patients is crucial as it is the strongest determinant of poor clinical outcome in these patients.(3,4) LV systolic dysfunction is usually observed late after surgical correction and is related to RV dysfunction.(3) However, there is a paucity of data on the time course of LV dysfunction in cToF patients and whether this could be detected at an early age with more sensitive methods than LVEF.(18-20) The present study demonstrated that in cToF patients with preserved LVEF, a significantly impaired global longitudinal LV strain was observed. Therefore, subclinical LV systolic dysfunction is already present in the first post-operative decades. In addition, two-dimensional speckle tracking echocardiography enables assessment of LV torsional mechanics by evaluating LV apical and basal rotation. LV twist is a comprehensive index of LV performance and takes into account the complex helical disposition of the myofibers. At present, LV torsional mechanics in cToF patients have not been extensively studied. The present study provides new insights into this field. In cToF patients with preserved LVEF, LV twist was significantly reduced. This reduction was secondary to a significant reduction in LV apical rotation, whereas LV basal rotation was preserved. These results indicate that impairment in LV performance may start at the apical level.

Finally, LV twist and LV apical rotation were closely related to global and apical RV strain, demonstrating the presence of adverse ventricular-ventricular interactions. As previously indicated, changes in the geometry of the RV apical trabecular component as a consequence of volume overload may induce alterations in the apical LV geometry that could lead to reduced apical LV performance. Sheehan et al. studied the geometric changes of the RV caused by chronic volume overload in cToF patients and observed that the RV cross-sectional area was only significantly enlarged at the apical level.(21) This apical RV dilatation may lead to distortion of the apical LV geometry and altered fiber orientation at the apex of the heart. Consequently, regional strain and rotation at the LV apex may decrease at an earlier stage than the LV basal segments. In addition, at a late stage of the disease, changes in myofiber orientation of the interventricular septum may further decrease RV and LV performance, especially in patients with increased pulmonary vascular resistance.(22)

The relatively small sample size of the study may constitute a limitation. Furthermore, objective assessment of exercise capacity was not performed. Finally, RV myocardial fibrosis and its potential influence on RV performance were not evaluated. Additional studies relating the location and extent of RV fibrosis to RV performance as assessed with myocardial deformation imaging are warranted.

The findings of the current study have important clinical implications. In cToF patients with significant pulmonary regurgitation, an early detection of RV and LV dysfunction by means of myocardial strain and LV torsional mechanics may indicate the need of pulmonary valve replacement in order to reverse RV and LV dysfunction and to improve late clinical outcome. Additional studies investigating the prognostic value of these RV and LV mechanical parameters are warranted.

REFERENCE LIST

1 Bacha EA, Scheule AM, Zurakowski D, et al. Long-term results after early primary repair of tetralogy of Fallot. J Thorac Cardiovasc Surg 2001;122:154-61.

2 Nollert G, Fischlein T, Bouterwek S, et al. Long-term survival in patients with repair of tetralogy of Fallot: 36-year follow-up of 490 survivors of the first year after surgical repair. J Am Coll Cardiol 1997;30:1374-83.

3 Geva T, Sandweiss BM, Gauvreau K, et al. Factors associated with impaired clinical status in long-term survivors of tetralogy of Fallot repair evaluated by magnetic resonance imaging. J Am Coll Cardiol 2004;43:1068-74.

4 Ghai A, Silversides C, Harris L, et al. Left ventricular dysfunction is a risk factor for sudden cardiac death in adults late after repair of tetralogy of Fallot. J Am Coll Cardiol 2002;40:1675-80.

5 Tzemos N, Harris L, Carasso S, et al. Adverse left ventricular mechanics in adults with repaired tetralogy of Fallot. Am J Cardiol 2009;103:420-5.

6 Delgado V, Tops LF, van Bommel RJ, et al. Strain analysis in patients with severe aortic stenosis and preserved left ventricular ejection fraction undergoing surgical valve replacement. Eur Heart J 2009.

7 Hare JL, Brown JK, Marwick TH. Association of myocardial strain with left ventricular geometry and progression of hypertensive heart disease. Am J Cardiol 2008;102:87-91.

8 Fratz S, Schuhbaeck A, Buchner C, et al. Comparison of accuracy of axial slices versus short-axis slices for measuring ventricular volumes by cardiac magnetic resonance in patients with corrected tetralogy of fallot. Am J Cardiol 2009;103:1764-9.

9 van der Geest RJ, Buller VG, Jansen E, et al. Comparison between manual and semiautomated analysis of left ventricular volume parameters from short-axis MR images. J Comput Assist Tomogr 1997;21:756-65.

10 Li W, Davlouros PA, Kilner PJ, et al. Doppler-echocardiographic assessment of pulmonary regurgitation in adults with repaired tetralogy of Fallot: comparison with cardiovascular magnetic resonance imaging. Am Heart J 2004;147:165-72.

11 Knirsch W, Dodge-Khatami A, Kadner A, et al. Assessment of myocardial function in pediatric patients with operated tetralogy of Fallot: preliminary results with 2D strain echocardiography. Pediatr Cardiol 2008;29:718-25.

12 van RJ, Mollema SA, Delgado V, et al. Relation of immediate decrease in ventricular septal strain after alcohol septal ablation for obstructive hypertrophic cardiomyopathy to long-term reduction in left ventricular outflow tract pressure gradient. Am J Cardiol 2009;103:1592-7.

13 Delgado V, Mollema SA, Ypenburg C, et al. Relation between global left ventricular longitudinal strain assessed with novel automated function imaging and biplane left ventricular ejection fraction in patients with coronary artery disease. J Am Soc Echocardiogr 2008;21:1244-50.

14 Reisner SA, Lysyansky P, Agmon Y, et al. Global longitudinal strain: a novel index of left ventricular systolic function. J Am Soc Echocardiogr 2004;17:630-3.

15 Bertini M, Nucifora G, Marsan NA, et al. Left ventricular rotational mechanics in acute myocardial infarction and in chronic (ischemic and nonischemic) heart failure patients. Am J Cardiol 2009;103:1506-12.

16 Lai WW, Gauvreau K, Rivera ES, et al. Accuracy of guideline recommendations for two-dimensional quantification of the right ventricle by echocardiography. Int J Cardiovasc Imaging 2008;24:691-8.

17 Bodhey NK, Beerbaum P, Sarikouch S, et al. Functional analysis of the components of the right ventricle in the setting of tetralogy of Fallot. Circ Cardiovasc Imaging 2008;1:141-7.

18 Abd El Rahman MY, Abdul-Khaliq H, Vogel M, et al. Relation between right ventricular enlargement, QRS duration, and right ventricular function in patients with tetralogy of Fallot and pulmonary regurgitation after surgical repair. Heart 2000;84:416-20.

19 Schamberger MS, Hurwitz RA. Course of right and left ventricular function in patients with pulmonary insufficiency after repair of Tetralogy of Fallot. Pediatr Cardiol 2000;21:244-8.

20 Weidemann F, Eyskens B, Mertens L, et al. Quantification of regional right and left ventricular function by ultrasonic strain rate and strain indexes after surgical repair of tetralogy of Fallot. Am J Cardiol 2002;90:133-8.

21 Sheehan FH, Ge S, Vick GW, III, et al. Three-dimensional shape analysis of right ventricular remodeling in repaired tetralogy of Fallot. Am J Cardiol 2008;101:107-13.

22 Buckberg GD. The ventricular septum: the lion of right ventricular function, and its impact on right ventricular restoration. Eur J Cardiothorac Surg 2006;29 Suppl 1:S272-S278

2.5

Real-time three-dimensional echocardiography: segmental analysis of the right ventricle in patients with tetralogy of Fallot

Journal of the American Society of Echocardiography: Accepted

A.E. van der Hulst
A.A.W. Roest
E.R. Holman
A. de Roos
N.A. Blom
J. J. Bax
V. Delgado

ABSTRACT

Background: Accurate assessment of right ventricular (RV) function and dimensions has important prognostic implications in patients with repaired tetralogy of Fallot (ToF). 3-dimensional imaging is the preferred methodology to evaluate RV function. Novel post-processing software applications to evaluate 3-dimensional data have provided insight into RV function and dimensions by analyzing the various RV components (inlet, apical trabecular, outlet). The present study aimed to characterize regional RV function and dimensions with real-time 3-dimensional echocardiography (RT3DE) in repaired ToF patients.

Methods: Forty-one repaired ToF patients (age range 8-18 years) and 20 control subjects were enrolled. Global and segmental RV volumes and ejection fraction (EF) were assessed with RT3DE and compared between repaired ToF patients and controls.

Results: RT3DE segmental analysis demonstrated that the apical trabecular region was the most remodeled RV component in repaired ToF patients, with significantly increased end-diastolic volume and end-systolic volume as compared to controls (59 ± 19 ml vs. 41 ± 16 and 36 ± 13 ml vs. 24 ± 8 ml, respectively; p=0.001 for both). However, EF was preserved at that region. In contrast, EF was reduced at the RV inlet and outlet: (inlet: 53 ± 6% vs. 58 ± 7%, p=0.003, outlet: 44 ± 16% vs. 52 ± 10, p=0.032).

Conclusions: Repaired ToF patients show characteristic RV remodeling as assessed with RT3DE. At the apical trabecular part the largest volumes were observed as compared with control patients, whereas EF at the inlet and outlet components was significantly impaired. RT3DE may facilitate future studies on segmental RV volumes and function in repaired ToF patients.

INTRODUCTION

Right ventricular (RV) dilatation and subsequent RV failure in patients with repaired tetralogy of Fallot (ToF) are associated with poor clinical outcome.[1] The clinical management of these patients is highly determined by RV dimensions and function.[1-3] Evaluation of RV volumes using conventional 2-dimensional echocardiography is hampered by the complex geometry of the RV.[4] Recently, real-time 3-dimensional echocardiography (RT3DE) has overcome some of the limitations of 2-dimensional echocardiography to assess RV volumes and function.[5-9] The feasibility and accuracy of RT3DE for RV volume assessment have been demonstrated in several studies including repaired ToF patients.[5-9]

From an embryological and anatomical perspective, the RV can be divided into three sections; the inlet, the apical trabecular part, and the outlet.[10, 11] Recent studies in repaired ToF patients using magnetic resonance imaging have shown that the three different components of the RV show a different volumetric and functional response to volume overload.[12, 13] The performance of RT3DE to assess the various RV components has not been evaluated so far. Accordingly, the objective of the current study was to evaluate the feasibility of a novel semi-automated software algorithm based on RT3DE to assess the dimensions and function of the various components of the RV. Furthermore, the contribution of the various RV components to the global RV volume and function was evaluated in repaired ToF patients and compared with a group of control subjects.

METHODS

Study population and protocol

A total of 41 consecutive repaired ToF patients (mean age 13.1 ± 2.8 years, 56% male) and 20 healthy controls, matched for age, gender and body surface area, were prospectively enrolled in the present study. All patients and controls were evaluated with standard two-dimensional echocardiography and RT3DE. Particularly, global and segmental RV volumes and ejection fraction were assessed with RT3DE. Using dedicated software, RT3DE RV data were segmented off-line in three different functional regions: inlet, apical trabecular and outlet. The contribution of each functional component to global RV volume and function was compared between repaired ToF patients and healthy controls. The study protocol was approved by the institutional review board and all subjects gave written, informed consent.

RT3DE image acquisition and analysis

Transthoracic RT3DE images of the RV were acquired by a single experienced sonographer using a commercially available system equipped with a 3V phased array transducer (Vivid-7.0.0, GE Vingmed Ultrasound AS, Horten, Norway). Patients and control subjects were imaged in the left lateral decubitus position. To encompass the full RV volume into the dataset, six ECG-gated sub-volumes were acquired to form a larger pyramidal volume including the entire RV. Images were acquired during a single breath-hold in end-expiration to avoid translational motion. Compression and gain settings were adjusted to optimize image quality and subsequent endocardial border visualization. RT3DE RV datasets were stored digitally and quantitative analysis of the 3-dimensional RV volumes was performed offline using commercially available semi-automated software (TomTec Imaging Systems, Unterschleissheim, Germany).

Global assessment of RV volumes and function

From the RT3DE RV full-volume datasets, first, the software algorithm automatically displayed the RV volume in three imaging planes (4-chamber, sagittal and coronal plane; Figure 1). In these planes, manual identification of three anatomic landmarks (center of the tricuspid annulus, center of the mitral valve annulus, left ventricular apex) was performed. Subsequently, the endocardial RV border was manually traced at end-systole and end-diastole in the 4-chamber, sagittal and coronal planes. During contour tracing, the apical trabeculae were included in the chamber volume. The automated algorithm tracked the endocardial borders frame-by-frame throughout the cardiac cycle. After automated endocardial border tracking, the algorithm displayed the frame-by-frame endocardial contour position in a cine-loop. The dynamic change of the endocardial border and the apical trabeculae could be appreciated in this cine loop, and the contours were adjusted when necessary. Finally, the software automatically calculated RV end-diastolic volume (EDV), RV end-systolic volume (ESV) and RV ejection fraction (EF).

Regional assessment of RV volumes and function

The algorithm for segmental analysis of the RV is displayed in Figure 2. After manual tracing of the endocardial borders of the full RV volume in the 4-chamber view, sagittal RV view and coronal RV view, the software identified three anatomical landmarks (lateral wall of the tricuspid annulus, lateral wall of the pulmonary annulus and apex). On the basis of these anatomical landmarks defined by the observer, three surface landmarks were subsequently identified mathematically by the automated software (landmark A to landmark C, Figure 2) Landmark A was defined as the region at 50 percent of the distance between the tricuspid valve border (lateral wall of tricuspid annulus) and the apex. Landmark B was defined as the region at 50 percent of the distance between the pulmonary valve border (lateral wall of pulmonary valve annulus) and the apex. Landmark C was defined as the as the region at 50 percent of the distance between the tricuspid valve border and the pulmonary valve border. From these surface landmarks, the three RV regions (inlet, apical trabecular and outlet) were automatically identified. Subsequently, the software provided volume computations for the three sub-volumes in every time-frame, from which EDV (largest volume), ESV (smallest volume) and EF ([ESV/EDV] *100%) were derived for each RV functional component.

Statistical analysis

Continuous variables are expressed as mean ± standard deviation. Categorical variables are presented as numbers and percentages. Differences between repaired ToF patients and controls

Table 1. Patient and control characteristics

	cToF patients (n=41)	controls (n=20)	p-value
age (y)	13.1 ± 2.8	13.8 ± 2.5	0.202
male/female n (%)	23/18 (56/44)	13/7 (65/35)	0.507
BSA (ml/m²)	1.4 ± 0.3	1.5 ± 0.3	0.129
QRS (ms)	134 ± 19	94 ± 8	<0.001
Type of surgery*			
transannular patch	26 (65)	..	
infundibulectomy	8 (20)	..	
RVOT or PA patch	6 (15)	..	
Pulmonary regurgitation			
none/mild	12 (29)	..	
moderate	11 (27)	..	
severe	18 (44)	..	
RT3DE			
RV EDV (ml)	164 ± 48	133 ± 50	0.026
RV ESV (ml)	89 ± 26	64 ± 24	0.001
RV EF (%)	46 ± 8	52 ± 5	0.007

Abbreviations: BSA: body surface area, EDV: end diastolic volume, EF: ejection fraction, ESV: end systolic volume, PA: pulmonary artery, RT3DE : real-time 3-dimensional echocardiography, RV: right ventricle, RVOT: right ventricular outflow tract. * information about type of surgery was not available in one patient.

Table 2. RT3DE RV segmental analysis

	repaired ToF patients (n=41)	controls (n=20)	p-value
RV inlet			
EDV (ml)	67 ± 25	63 ± 27	0.546
ESV (ml)	31 ± 10	26 ±12	0.098
EF (%)	53 ± 6	58 ± 7	0.003
RV apical trabecular			
EDV (ml)	59 ± 19	41 ± 16	0.001
ESV (ml)	36 ± 13	24 ± 8	0.001
EF (%)	39 ± 12	39 ± 12	0.916
RV outlet			
EDV (ml)	38 ± 13	36 ± 21	0.728
ESV (ml)	21 ± 9	17 ± 9	0.099
EF (%)	44 ± 16	52 ± 10	0.032

Abbreviations: EDV: end diastolic volume, EF: ejection fraction, ESV: end systolic volume, RV: right ventricle, RT3DE: real-time 3-dimensional echocardiography.

Figure 1. RT3DE analysis of the RV

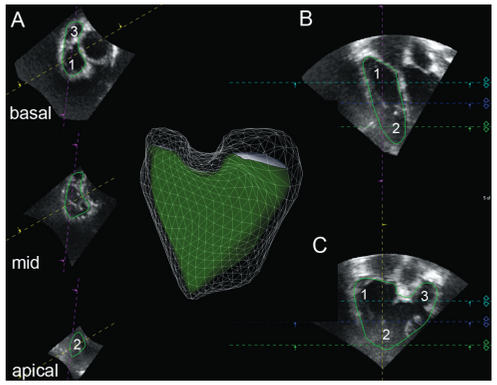

Example of RT3DE image analysis of the full RV volume showing the final step of the software algorithm. **Panel A**: sagittal view of the RV at three levels (basal, mid ventricular and apical). **Panel B**: 4-chamber view of the RV. **Panel C:** coronal view of the RV. The observer can scroll through the reconstructed 3D surface contours by moving the sagittal imaging planes in the apical-to-basal direction (light blue, dark blue and green dotted lines), and by rotating the coronal plane and 4-chamber plane (yellow dotted lines). Manual correction of the endocardial contour position can be performed when needed in any view and any phase of the cardiac cycle. Finally, the software automatically displays the reconstructed full RV volume (center) and the volumes and ejection fraction are automatically displayed (not shown).
Abbreviations: (1): inlet, (2) apical trabecular, (3) outlet, RT3DE: real-time 3-dimensional echocardiography, RV: right ventricle.

Figure 2. Identification of the RV functional segments with automated software.

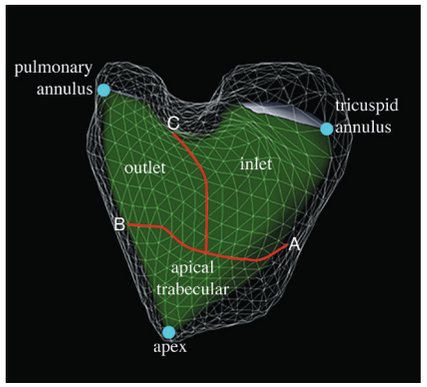

Identification of the RV functional segments with the automated software. After manual tracing of the endocardial borders of the full RV volume in the 4-chamber view, sagittal RV view and coronal RV view, the software automatically identifies 3 surface landmarks (landmark A to landmark C) on the 3-dimensional RV volume. **Landmark A** is defined as the region at 50 percent of the distance between the tricuspid valve border (lateral wall of tricuspid annulus) and the apex. **Landmark B** is defined as the region at 50 percent of the distance between the pulmonary valve border (lateral wall of pulmonary valve annulus) and the apex. **Landmark C** is defined as the as the region at 50 percent of the distance between the tricuspid valve border and the pulmonary valve border. Subsequently, the three RV regions, (inlet, apical trabecular and outlet) are identified in the 3D volume by the algorithm as indicated in the figure.

were analyzed using the unpaired t-test. Categorical data were analyzed with the Chi-square test. To assess the inter-observer agreement of RT3DE, Bland-Altman analysis was performed. Furthermore, the coefficient of variation was calculated (the absolute difference between the observers in percentage of the study population average). Data were analyzed using the SPSS 17.0 software (SPSS Inc, Chicago, Illinois). A p-value of <0.05 was considered statistically significant.

RESULTS

Study population

Table 1 summarizes the clinical and echocardiographic characteristics of patients and controls, and the surgical details of the repaired ToF patients. In all patients, surgical repair was performed through an atrial incision. An additional commisurotomy or valvotomy of the pulmonary valve was performed in two patients who received a RVOT or pulmonary artery patch. None of the patients showed a hemodynamically significant residual ventricular septum defect at the time of inclusion. By definition, there were no significant differences between patients and controls in terms of age, gender and body surface area. QRS duration was significantly increased in repaired ToF patients (134 ± 19 ms vs. 94 ± 8 ms, p<0.001). In repaired ToF patients, global RV volumes as assessed with RT3DE were significantly increased (RV EDV: 164 ± 48 ml vs. 133 ± 50 ml, p=0.026, RV ESV: 89 ± 26 ml vs. 64 ± 24 ml p=0.001) and global RV EF was significantly reduced (46 ± 8% vs. 52 ± 5 %, p=0.007) as compared to control subjects. None of the included repaired ToF patients showed an aneurysmatic RVOT.

Segmental analysis of RV volumes with RT3DE

Table 2 outlines the segmental analysis of the RV in repaired ToF patients and control subjects. At the RV inlet, the EDV and ESV were not different between repaired ToF patients and controls. In contrast, EF at the RV inlet was significantly reduced in repaired ToF patients as compared to controls (53 ± 6% vs. 58 ± 7%, respectively; p=0.003). At the apical trabecular segment of the RV, repaired ToF patients had a larger EDV compared to healthy controls (59 ± 19 ml vs. 41 ± 16, respectively; p=0.001). In addition, the ESV was significantly larger at the apical trabecular segment (ESV apical trabecular: 36 ± 13 ml vs. 24 ± 8 ml, p=0.001) whereas the segmental EF was not different between patients and controls at this region (Table 2). Finally, at the RV outlet, segmental volumes were not significantly different between patients and controls (Table 2). However, the EF at the outflow tract was significantly reduced in repaired ToF patients compared to controls (44 ± 16% vs. 52 ± 10, p=0.032).

Reproducibility

Measuring inter-observer agreement of RT3DE for full RV volume assessment with Bland Altman analysis, small differences and tight limits of agreement were observed (Figure 3). (EDV: -1.6 ± 20 ml, ESV 2.6 ± 7 ml, EF: -3.5 ± 5 %). Furthermore, the inter-observer agreement of the assessment with Bland Altman analysis of the segmental RV volumes with RT3DE showed small differences

Figure 3. Inter-observer agreement of RT3DE for RV full volume assessment

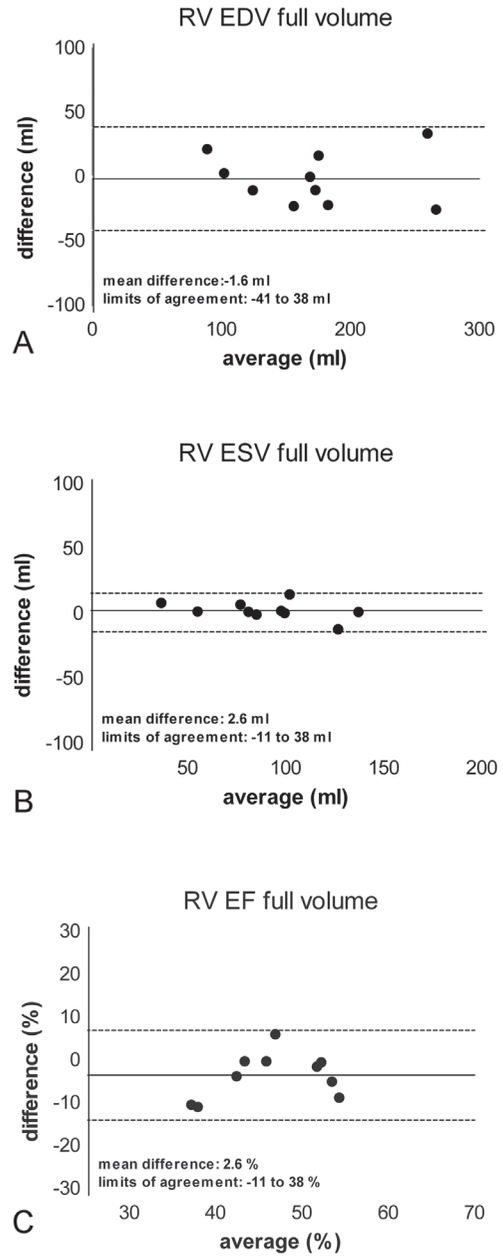

Panel A. Bland Altman plot showing average difference and limits of agreement for the assessment of RV EDV.
Panel B. Bland Altman plot showing average difference and limits of agreement for the assessment of RV ESV.
Panel C. Bland Altman plot showing average difference and limits of agreement for the assessment of RV EF.
Abbreviations: EDV: end diastolic volume, ESV: end systolic volume, EF: ejection fraction. RV: right ventricle

Figure 4. Inter-observer agreement of RT3DE assessment of the RV inlet

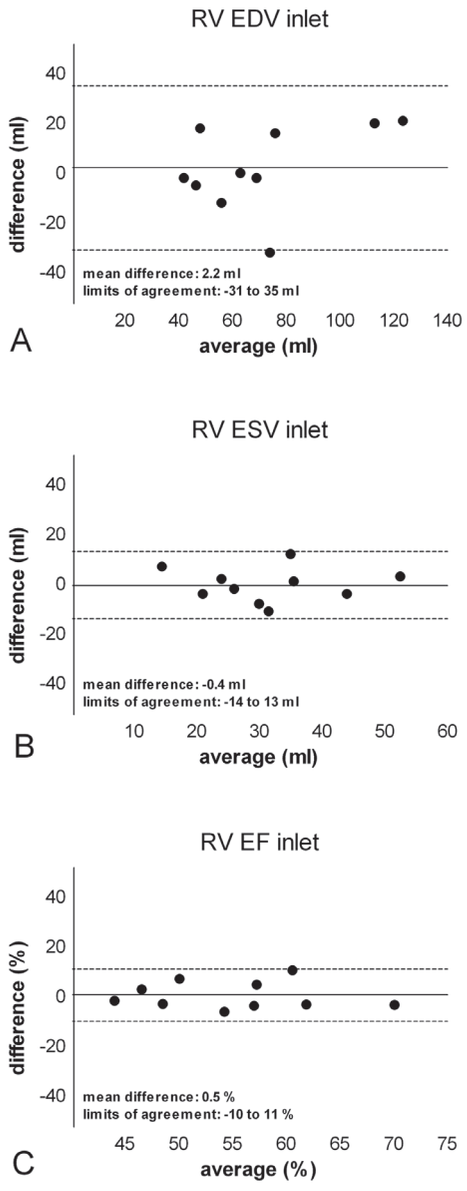

Panel A. Bland Altman plot showing average difference and limits of agreement for the assessment of EDV at the RV inlet. **Panel B.** Bland Altman plot showing average difference and limits of agreement for the assessment of ESV at the RV inlet. **Panel C.** Bland Altman plot showing average difference and limits of agreement for the assessment of EF at the RV inlet. Abbreviations: EDV: end diastolic volume, ESV: end systolic volume, EF: ejection fraction. RV: right ventricle

Figure 5. Inter-observer agreement of RT3DE assessment of the RV apical trabecular segment

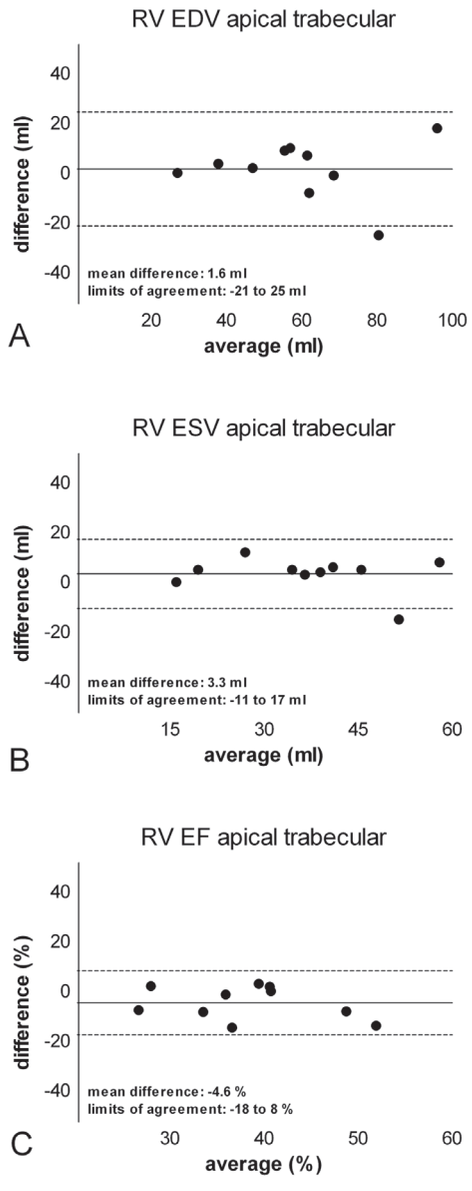

Panel A. Bland Altman plot showing average difference and limits of agreement for the assessment of EDV at the apical trabecular segment. **Panel B.** Bland Altman plot showing average difference and limits of agreement for the assessment of ESV at the apical trabecular segment. **Panel C.** Bland Altman plot showing average difference and limits of agreement for the assessment of EF at the apical trabecular segment. Abbreviations: EDV: end diastolic volume, ESV: end systolic volume, EF: ejection fraction. RV: right ventricle

Figure 6. Inter-observer agreement of RT3DE assessment of the RV outlet

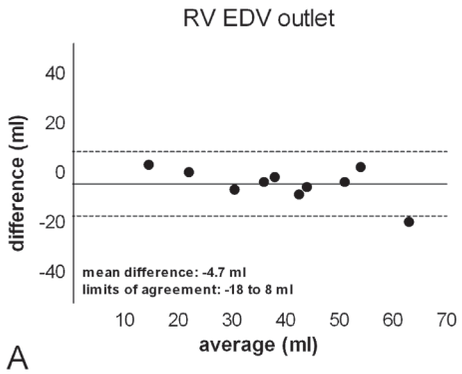

A

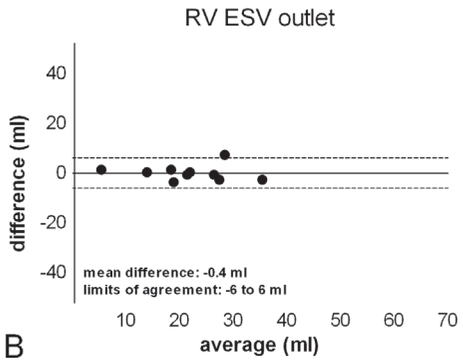

B

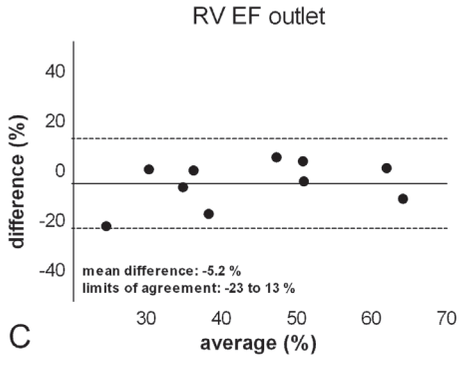

C

Panel A. Bland Altman plot showing average difference and limits of agreement for the assessment of EDV at the RV outlet. **Panel B**. Bland Altman plot showing average difference and limits of agreement for the assessment of ESV at the RV outlet. **Panel C.** Bland Altman plot showing average difference and limits of agreement for the assessment of EF at the RV outlet. Abbreviations: EDV: end diastolic volume, ESV: end systolic volume, EF: ejection fraction. RV: right ventricle

with fair limits of agreement: (Figure 4, Figure 5 and Figure 6) (RV inlet: EDV: 2.2 ± 33 ml, ESV: -0.2 ± 13 ml, EF: 0.5 ± 11%; RV apical trabecular: EDV: 1.6 ± 23 ml, ESV: 3.3 ± 14 ml, EF: -4.6 ± 12%; RV outlet: EDV: -4.7 ± 12 ml, ESV: -0.4 ± 6 ml , EF: -5.2 ± 18%).

In addition, the coefficients of variation for the RT3DE measurements were: EDV: 11 ± 7%; ESV: 7 ± 7%; EF: 9 ± 8%. Furthermore, the coefficient of variation calculations of the assessment of segmental RV volumes with RT3DE yielded the following: RV inlet: EDV: 20 ± 17%, ESV: 21 ± 15%, EF: 8 ± 5%; RV apical trabecular: 18 ± 17%, ESV: 22 ± 16 %, EF: 15 ± 16%; RV outlet: EDV 16 ± 16%, ESV: 11 ± 11%, EF: 15 ± 16 %.

DISCUSSION

The present investigation demonstrated the feasibility of a novel semi-automated software based on RT3DE to assess volumes and function of the inlet, apical trabecular and outlet regions of the RV in healthy subjects and in repaired ToF patients. In repaired ToF patients, the various RV components showed different contributions to the global RV volumes and EF. Specifically, the apical trabecular part was significantly more dilated as compared to the other regions while EF was preserved. In contrast, at the RV inlet and outlet, volume dilatation was limited whereas the segmental EF was significantly impaired.

RT3DE of the RV

Reliable assessment of RV volumes during follow-up of congenital heart disease patients has clinical and prognostic significance.[1-3, 14, 15] Magnetic resonance imaging is currently the reference standard to asses RV volumes and function.[16] A recent study by Sheehan et al. introduced a fast and accurate magnetic resonance imaging-based algorithm to analyze the volume and shape of the RV.[17] The algorithm uses a database with data on RV shape variations in healthy volunteers and patients. Nevertheless, magnetic resonance image acquisition is a time-consuming and expensive imaging technique. Moreover, as a result of the long acquisition time, sedation is required during magnetic resonance imaging in young congenital heart disease patients. Echocardiography is fast, safe and readily available for repeated assessment of ventricular function during routine clinical follow-up. However, the complex morphology of the RV hampers reliable evaluation of RV volumes and function with 2-dimensional echocardiography.[4] Novel RT3DE has enabled accurate assessment of RV volumes and function with few geometric assumptions.[5-9] RT3DE has been validated against magnetic resonance imaging to measure global RV volumes and function in patients with various pathologies, including repaired ToF.[6-9] For example, van der Zwaan et al. performed a direct comparison between RT3DE and magnetic resonance imaging to assess RV volumes and ejection fraction in patients with congenital heart disease.[18] RT3DE provided a fast and reproducible assessment of RV volumes with a fair to good accuracy as compared to magnetic resonance imaging. Furthermore, the authors demonstrated a good test-retest variability of RT3DE in a subsequent study including patients with congenital heart disease and healthy subjects.[19] In addition, Grewal et al. showed strong correlations and good agreement between RT3DE and magnetic resonance

imaging to assess RV volumes in patients with repaired ToF.[20] The current investigation showed a good inter-observer reproducibility of RT3DE for the assessment of global RV volumes in repaired ToF patients and control subjects. In addition, similar to previous studies, the present investigation demonstrated that repaired ToF patients had significant larger global RV volumes and reduced EF compared with healthy controls.[21] Therefore, RT3DE may be a valuable imaging technique to accurately evaluate repaired ToF patients and facilitate clinical decision-making.

RT3DE segmental analysis of the RV

The adaptive response of the RV to chronic overload remains incompletely understood. In a recent magnetic resonance imaging investigation, Sheehan and colleagues have shown that the remodeled RV exhibits significant changes in geometry and 3-dimensional shape.[13] The cross-sectional RV shape was analyzed from apex to base in repaired ToF patients with RV dilation. Specifically, repaired ToF patients showed dilatation of the apex, bulging at the base, and significant shape change (from crescent to rectangular shape).[13] Accordingly, comprehensive evaluation of the various RV components may yield a better understanding of RV dilatation and dysfunction. Based on embryological and functional observations, the segmental approach of the RV identifies the inlet, apical trabecular and outlet components as separate entities within the RV.[10] This approach was initially applied to comprehensively describe congenital malformed ventricles.[10] Recently, Bodhey and colleagues demonstrated the role of this segmental analysis in the clinical assessment of RV dilatation in repaired ToF patients.[12] Using magnetic resonance imaging, marked differences among the RV components were observed, with the apical trabecular part as the most dilated component in repaired ToF patients with volume overload.[12] In the present study, the inlet, apical trabecular and outlet components of the RV were analyzed by novel RT3DE software in repaired ToF patients and controls. The identification of true anatomical structures that define the various RV segments, such as the parietal band, conal septum, septal band, moderator band and the papillary muscle insertions is not always feasible with echocardiography. Therefore, in the present study we applied a standardized automated software algorithm to identify the various RV segments, as opposed to a manual identification of the segments which may lead to significant error when anatomical landmarks are not correctly identified. The results indicate that RT3DE segmental analysis of the RV is feasible and has fair to good reproducibility. Furthermore, similar to the observations by Bodhey and co-workers[12], the most pronounced volume increase was observed at the apical trabecular part of the RV, whereas segmental EF was preserved. Accordingly, the apical trabecular part seems to play a central role in the adaptive response to volume overload in repaired ToF patients. Furthermore, despite the preserved EF at the apical trabecular segment, the altered apical geometry may distort regional fiber orientation, which could ultimately have a deleterious effect on systolic performance of the RV.[22-24]

At the inlet and outlet components of the RV, a limited contribution to the RV dilatation was observed. This observation is in agreement with a previous investigation.[12] The RV inlet and RV outlet components have a close anatomical relationship with the fibrous tricuspid and pulmonary annuli as well as with the left ventricle. Consequently, the amount of remodeling may be limited due the narrow configuration of the inlet and outlet components as compared to the apical trabecular segment of the RV.[12] Finally, the RT3DE segmental analysis showed an impaired EF at the inlet and outlet components. Both RV segments are involved in the surgical repair of ToF patients (closure of the ventricular septum defect at the inlet, relief of pulmonary stenosis at the outlet). The clinical implications of systolic dysfunction at the RV outlet have been the focus of extensive research in repaired ToF patients. Functional abnormalities of the RV outlet relate to surgical scarring and patch placement at that level, and have been shown to relate with outcome in repaired ToF patients.[25, 26]

Study limitations

The present study has several limitations. RV endocardial border detection in patients with a dilated RV is challenging, as the endocardial border may be blurred due to the increased distance from the transducer to the RV wall.[8] Furthermore, the feasibility of the software algorithm to assess the dimensions and function of the various components of the RV was not previously validated against a reference method. Therefore, the results of the present study may not be comparable when different and larger populations are evaluated. Nevertheless, the results are in agreement with previous studies[12, 25, 26], confirming thus the reliability of the methodology. However, we acknowledge that the present results should be extended and confirmed in larger populations. Furthermore, the inter-observer reproducibility of the algorithm in terms of segmental analysis is not optimal. Technological developments with accurate definition of anatomical landmarks may help to overcome this limitation.

Conclusion

Patients with repaired ToF show a characteristic RV remodeling as assessed with RT3DE. The apical trabecular part showed the largest volumes as compared with control patients. However, the function of the inlet and outlet components were significantly impaired. RT3DE can facilitate future studies on segmental RV volumes and function in patients with repaired ToF. However, additional studies are needed in order to validate current RT3DE based algorithms.

REFERENCE LIST

1 Gatzoulis MA, Balaji S, Webber SA, Siu SC, Hokanson JS, Poile C, et al. Risk factors for arrhythmia and sudden cardiac death late after repair of tetralogy of Fallot: a multicentre study. Lancet 2000;356:975-81.

2 de Ruijter FT, Weenink I, Hitchcock FJ, Meijboom EJ, Bennink GB. Right ventricular dysfunction and pulmonary valve replacement after correction of tetralogy of Fallot. Ann Thorac Surg 2002;73:1794-800.

3 Vliegen HW, van Straten A, de Roos A, Roest AA, Schoof PH, Zwinderman AH, et al. Magnetic resonance imaging to assess the hemodynamic effects of pulmonary valve replacement in adults late after repair of tetralogy of fallot. Circulation 2002;106:1703-7.

4 Helbing WA, Bosch HG, Maliepaard C, Rebergen SA, van der Geest RJ, Hansen B, et al. Comparison of echocardiographic methods with magnetic resonance imaging for assessment of right ventricular function in children. Am J Cardiol 1995;76:589-94.

5 Friedberg MK, Su X, Tworetzky W, Soriano BD, Powell AJ, Marx GR. Validation of 3D echocardiographic assessment of left ventricular volumes, mass, and ejection fraction in neonates and infants with congenital heart disease: a comparison study with cardiac MRI. Circ Cardiovasc Imaging 2010;3:735-42.

6 Iriart X, Montaudon M, Lafitte S, Chabaneix J, Reant P, Balbach T, et al. Right ventricle three-dimensional echography in corrected tetralogy of fallot: accuracy and variability. Eur J Echocardiogr 2009;10:784-92.

7 Khoo NS, Young A, Occleshaw C, Cowan B, Zeng IS, Gentles TL. Assessments of right ventricular volume and function using three-dimensional echocardiography in older children and adults with congenital heart disease: comparison with cardiac magnetic resonance imaging. J Am Soc Echocardiogr 2009;22:1279-88.

8 Shimada YJ, Shiota M, Siegel RJ, Shiota T. Accuracy of right ventricular volumes and function determined by three-dimensional echocardiography in comparison with magnetic resonance imaging: a meta-analysis study. J Am Soc Echocardiogr 2010;23:943-53.

9 van der Zwaan HB, Helbing WA, Boersma E, Geleijnse ML, McGhie JS, Soliman OI, et al. Usefulness of real-time three-dimensional echocardiography to identify right ventricular dysfunction in patients with congenital heart disease. Am J Cardiol 2010;106:843-50.

10 Anderson RH, Ho SY. What is a ventricle? Ann Thorac Surg 1998;66:616-20.

11 Sheehan F, Redington A. The right ventricle: anatomy, physiology and clinical imaging. Heart 2008;94:1510-5.

12 Bodhey NK, Beerbaum P, Sarikouch S, Kropf S, Lange P, Berger F, et al. Functional analysis of the components of the right ventricle in the setting of tetralogy of Fallot. Circ Cardiovasc Imaging 2008;1:141-7.

13 Sheehan FH, Ge S, Vick GW, III, Urnes K, Kerwin WS, Bolson EL, et al. Three-dimensional shape analysis of right ventricular remodeling in repaired tetralogy of Fallot. Am J Cardiol 2008;101:107-13.

14 Oosterhof T, van Straten A, Vliegen HW, Meijboom FJ, van Dijk AP, Spijkerboer AM, et al. Preoperative thresholds for pulmonary valve replacement in patients with corrected tetralogy of Fallot using cardiovascular magnetic resonance. Circulation 2007;116:545-51.

15 Therrien J, Provost Y, Merchant N, Williams W, Colman J, Webb G. Optimal timing for pulmonary valve replacement in adults after tetralogy of Fallot repair. Am J Cardiol 2005;95:779-82.

16 Pennell DJ, Sechtem UP, Higgins CB, Manning WJ, Pohost GM, Rademakers FE, et al. Clinical indications for cardiovascular magnetic resonance (CMR): Consensus Panel report. J Cardiovasc Magn Reson 2004;6:727-65.

17 Sheehan FH, Kilner PJ, Sahn DJ, Vick GW, III, Stout KK, Ge S, et al. Accuracy of knowledge-based reconstruction for measurement of right ventricular volume and function in patients with tetralogy of Fallot. Am J Cardiol 2010;105:993-9.

(18) van der Zwaan HB, Helbing WA, McGhie JS, Geleijnse ML, Luijnenburg SE, Roos-Hesselink JW, et al. Clinical value of real-time three-dimensional echocardiography for right ventricular quantification in congenital heart disease: validation with cardiac magnetic resonance imaging. J Am Soc Echocardiogr 2010;23:134-40.

19 van der Zwaan HB, Geleijnse ML, Soliman OI, McGhie JS, Wiegers-Groeneweg EJ, Helbing WA, et al. Test-retest variability of volumetric right ventricular measurements using real-time three-dimensional echocardiography. J Am Soc Echocardiogr 2011;24:671-9.

20 Grewal J, Majdalany D, Syed I, Pellikka P, Warnes CA. Three-dimensional echocardiographic assessment of right ventricular volume and function in adult patients with congenital heart disease: comparison with magnetic resonance imaging. J Am Soc Echocardiogr 2010;23:127-33.

21 Bouzas B, Kilner PJ, Gatzoulis MA. Pulmonary regurgitation: not a benign lesion. Eur Heart J 2005;26:433-9.

22 Plunkett MD, Buckberg GD. Pathophysiologic implications of the helical ventricular myocardial band: considerations for right ventricular restoration. Semin Thorac Cardiovasc Surg Pediatr Card Surg Annu 2007;68-75.

23 Sanchez-Quintana D, Anderson RH, Ho SY. Ventricular myoarchitecture in tetralogy of Fallot. Heart 1996;76:280-6.

24 van der Hulst AE, Delgado V, Holman ER, Kroft LJ, de RA, Hazekamp MG, et al. Relation of left ventricular twist and global strain with right ventricular dysfunction in patients after operative "correction" of tetralogy of fallot. Am J Cardiol 2010;106:723-9.

25 Davlouros PA, Kilner PJ, Hornung TS, Li W, Francis JM, Moon JC, et al. Right ventricular function in adults with repaired tetralogy of Fallot assessed with cardiovascular magnetic resonance imaging: detrimental role of right ventricular outflow aneurysms or akinesia and adverse right-to-left ventricular interaction. J Am Coll Cardiol 2002;40:2044-52.

26 Oosterhof T, Mulder BJ, Vliegen HW, de Roos A. Corrected tetralogy of Fallot: delayed enhancement in right ventricular outflow tract. Radiology 2005;237:868-71.

CHAPTER 3

Right ventricular imaging: cardiac magnetic resonance

3.1

Review: cardiac magnetic resonance imaging in postoperative congenital heart disease patients

Journal of Magnetic Resonance Imaging: Invited

A.E. van der Hulst
A.A.W. Roest
J.J.M. Westenberg
L.J.M. Kroft
A. de Roos

ABSTRACT

The survival of patients with congenital heart disease (CHD) has greatly improved over the last decades. Nevertheless, lifelong follow-up is required in postoperative CHD patients, and noninvasive imaging plays an important role during follow-up. Cardiac magnetic resonance (CMR) imaging enables comprehensive imaging of cardiac function and anatomy, and helps to detect patients who need re-intervention and to predict clinical outcome. Postoperative CHD patients who are frequently referred for CMR evaluation include those with coarctation of the aorta, tetralogy of Fallot, transposition of the great arteries and single ventricle patients after the Fontan procedure. This article reviews the current clinical role of CMR in these various subgroups of postoperative CHD patients. Furthermore, an overview of novel CMR applications and their clinical value in CHD patients is provided.

INTRODUCTION

Advances in diagnostic, surgical and peri-operative knowledge have greatly improved the survival of patients with congenital heart disease (CHD). As a result, the population with CHD has doubled over the last decades.(1) In addition, the age distribution of the CHD patients is changing with an increasing number of patients aging into adulthood.(1,2) However, surgical intervention may not lead to complete correction of CHD and re-interventions are frequently needed, especially in patients with complex CHD.(3) Therefore, extensive life-long follow-up is required in CHD patients to monitor ventricular, valvar and electrophysiological function and to detect any cardiovascular or non-cardiovascular sequelae.(4)

Cardiac magnetic resonance imaging (CMR) is a non-invasive imaging technique that plays an important role during clinical follow-up of postoperative CHD patients.(5) CMR is not hampered by geometrical assumptions or by the acoustic window, which may limit echocardiographic imaging in postoperative CHD patients as a result of abnormal cardiac anatomy or scar tissue. Moreover, as no ionizing radiation is needed, the application of CMR is safe and can be used for repeated evaluation of CHD patients during long-term follow-up. CMR provides various acquisition schemes such as black-blood spin echo (BBSE), bright-blood gradient echo (GRE) imaging, phase-encoded flow imaging, three-dimensional contrast-enhanced angiography (3D-MRA) and late gadolinium-enhanced imaging. The various schemes make CMR a versatile imaging technique for a wide range of cardiovascular indications.

In postoperative CHD patients, MRI can provide valuable information on cardiac anatomy, ventricular function, valvar function and on the presence and location of myocardial scar tissue. Within the population of postoperative CHD patients, the diagnostic subgroups most frequently referred for CMR evaluation include those with coarctation of the aorta, tetralogy of Fallot (ToF), transposition of the great arteries and single ventricle patients after the Fontan procedure. (6,7) This article provides an overview of the role of CMR during follow-up of postoperative CHD patients. The various CMR acquisition schemes and their applications in postoperative CHD patients are reviewed, with specific attention to the most frequently referred subgroups of CHD patients. Finally, we provide a concise overview of novel CMR applications and their clinical value in postoperative CHD patients.

TECHNICAL ASPECTS

Several technical aspects and acquisition schemes apply to CMR imaging. First, specific technical adaptations are needed with regard to cardiac and respiratory motion during image acquisition. In addition, a range of CMR-specific pulse sequences are used to image the various aspects of the heart that are of use in clinical practice.

During CMR assessment, motion synchronization is needed to avoid respiratory and cardiac motion artifacts. To compensate for respiratory motion, various strategies (signal averaging, breath

holding, respiratory gating or single shot imaging) can be applied. To compensate for cardiac motion, the ECG signal is used. Typically, the R-wave of the ECG at the beginning of the cardiac cycle is used as reference point. ECG-synchronized MR imaging may be performed prospectively (i.e. ECG-triggering; the pulse events needed for data acquisition start at a fixed time after the R-wave), or retrospectively (i.e. ECG-gating; continuous data acquisition throughout multiple cardiac cycles with subsequent retrospective sorting of the obtained data based on its relative position within the cardiac cycle).

Although many acquisition schemes may be applied for the clinical evaluation of postoperative CHD patients, most clinical imaging protocols are commonly composed from the following range of techniques: BBSE imaging, bright-blood GRE cine imaging, phase-encoded flow imaging, 3D-MRA, and late gadolinium-enhanced imaging.(8-10)

Black-blood spin echo (BBSE)

BBSE in postoperative CHD patients is mostly performed to evaluate cardiac anatomy. For this purpose, static T1 weighted images are obtained with short echo times. BBSE images have high tissue-to-blood contrast, with intense signal from cardiac tissue (appearing grey-to-white) and no signal from the moving blood pool (appearing black). Currently, the most commonly used pulse sequence for BBSE imaging combines a black-blood double inversion preparation sequence with a turbo or fast spin echo acquisition. The double inversion preparation sequence nulls the signal from the blood in the imaged slice, improving contrast in the image, whereas the turbo or fast spin echo sequence shortens the acquisition time.(11) In CHD patients, multi-slice BBSE anatomic imaging is routinely used to characterize cardiac and extra-cardiac anatomy (Figure 1), although it is increasingly being replaced by bright-blood GRE imaging. BBSE is particularly useful to evaluate the spatial relationships between airways and blood vessels, such as in CHD patients with anomalies of the aortic vessels (eg. coarctation, right sided aorta, double aortic arch) or pulmonary vessels (anomalous pulmonary venous connection, Fontan circulation).(12) In the presence of intra-cardiac metal devices such as sternal wires or intravascular stents, BBSE is less affected by metallic artifacts than bright-blood GRE.(11)

Bright-blood gradient echo cine imaging

Bright blood GRE imaging yields T1 weighted images, with blood appearing white, hence the name "bright blood". In current clinical practice, bright-blood GRE image acquisition is essentially obtained by the 'balanced steady state free precession' (balanced SSFP) technique. Balanced SSFP is a fast gradient echo technique providing images with high spatial and temporal resolution. (13) Contrast in balanced SSFP images is generated by the differences in T1/T2 ratio in the imaged tissues. Balanced SSFP imaging yields a high signal from blood or fat (which have a short T1 time), hence appearing white in the reconstructed images, whereas other tissues, such as myocardium, will appear gray. Like BBSE, balanced SSFP allows imaging of cardiac anatomy. Moreover, balanced SSFP is specifically useful for the assessment of ventricular function(14,15). With whole-heart multi-slice balanced SSFP cine images, ventricular volumes (end-diastolic volume, end-systolic volume, stroke volume), ejection fraction and ventricular mass can be reliably assessed (Figure 2).(14,15) Since multiple contiguous parallel slices covering the entire ventricle are obtained, geometrical assumptions of ventricular shape are avoided. This is particularly important for the assessment of reliable ventricular volumes and ejection fraction in CHD patients, as these patients may have an abnormal ventricular shape.(14) The analysis of left ventricular (LV) volumes and function is preferably performed in balanced SSFP cine images acquired in the short axis, but may also be derived from axial images. In contrast, the RV has a more complex ventricular shape and coarse endocardial trabeculations, which complicates the identification of the endocardial border in the short axis during image analysis. Therefore, CMR assessment of volume and function of the RV may be more reliable when imaged in the axial plane (Figure 2).(16) Moreover, imaging in the axial plane provides additional valuable information regarding spatial relationships between the heart and its surrounding structures, as well as diagnostic information of the surrounding structures (e.g. pulmonary artery stenosis, conduit obstruction, pleura effusion). Finally, with bright-blood GRE cine acquisition, the presence of turbulent flow may be identified. Turbulent flow causes local signal loss during GRE acquisition, resulting in a black 'flow void' in the image.

Figure 1. Example of black blood spin echo image

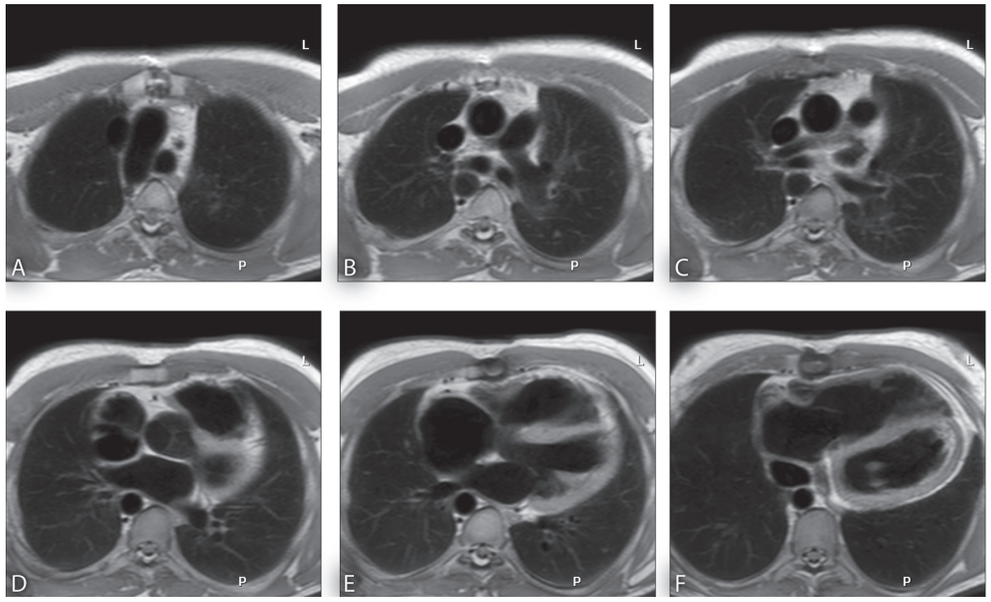

Repaired tetralogy of Fallot. BBSE images in a 36-year old male. Axial images with view from below showing the spatial relationships between the heart, large vessels, and airways. Right aortic arch (a) and right descending aorta (b-f). Normal diameter of left pulmonary artery (b), but relatively small caliber right pulmonary artery (c), as complication after Waterston shunt in the past. Dilated right ventricular outflow tract (d) and dilated right ventricle with some right ventricular hypertrophy (e,f). Note that this is accompanied with slight ventral displacement of the left thoracic chest wall (c-e). The left ventricle was also enlarged (f). Patient had moderate-to-severe pulmonary regurgitation of 45%.

Accordingly, valvar regurgitation, stenosis, or turbulent flow over a ventricular septum defect may be identified with GRE cine imaging. However, the balanced SSFP technique is less sensitive for the identification of turbulent flow as compared to the conventional GRE techniques. Furthermore, to obtain quantitative flow measures, phase-encoded imaging is required.

Phase-encoded flow imaging

In contrast with BBSE and bright-blood GRE imaging, which rely on signal intensity for image reconstruction, flow imaging encodes the phase of moving spins in the structures of interest linearly to the velocity of their movement. Intravascular protons that flow along a magnetic gradient obtain phase-shifts that are proportional to their flow velocity. Therefore, after the application of a magnetic gradient along the flow direction, the flow velocity of the blood can be derived by analyzing the phase-shifts at a plane of interest.(17)

Phase-encoded flow imaging is used to measure flow volumes, regurgitation fraction and peak flow velocities. Phase-encoded flow imaging can be performed in any arbitrary direction, perpendicular to an acquisition plane (i.e. through-plane encoding), or in a combination of directions (i.e., 2D in-plane encoding or 3D encoding).

Through-plane phase-encoded flow imaging enables the assessment of flow volumes across cardiac valves and vessels. For this purpose, the imaging plane is positioned perpendicular to the flow at the level of the valve or vessel of interest. Data acquisition with retrospective ECG-gating results in a time series of reconstructed phase-encoded images covering the full cardiac cycle. From these images, flow velocity curves are reconstructed from which flow volumes and regurgitation volumes can be derived (Figure 3). In CHD patients, through-plane flow imaging can furthermore be used to quantify shunt volumes, measuring the ratio between pulmonary flow volume (Qp) and aortic flow volume (Qs).(18) In the absence of a shunt, the aortic flow volume should equal the pulmonary flow volume, and the Qp/Qs ration is equal to 1. In general, a Qp/Qs ratio over 1.5 represents a large left-to-right shunt that indicates the need for (re)intervention. Similarly, the relative flow volume to each lung can be measured to assess the hemodynamic significance of branch pulmonary artery stenosis.(19,20)

3D gadolinium-enhanced angiography (3D-MRA)

3D-MRA provides three-dimensional images of the pulmonary and aortic vessels. 3D-MRA images are obtained by a T1-weighted sequence applied shortly after intravenous administration of a gadolinium-based contrast agent. The intravascular gadolinium-chelate shortens the T1 time of the surrounding tissue (blood) resulting in increased signal intensity, delineating bright blood against virtually no background tissue signal (Figure 4). 3D-MRA provides images with high resolution and is suitable for characterization of complex intravascular anatomy of the aorta and pulmonary vessels. In CHD patients, 3D-MRA is of great value to detect vascular anomalies, such as major aorta-to-pulmonary collateral arteries (MAPCAs).(21) Furthermore, during long-term follow-up of postoperative CHD patients, 3D-MRA is an important imaging tool for the evaluation of (re) stenosis, aneurysms, or for the evaluation of surgical shunts.(22,23)

Figure 2. Assessment of biventricular volumes and function with balanced steady state free precession

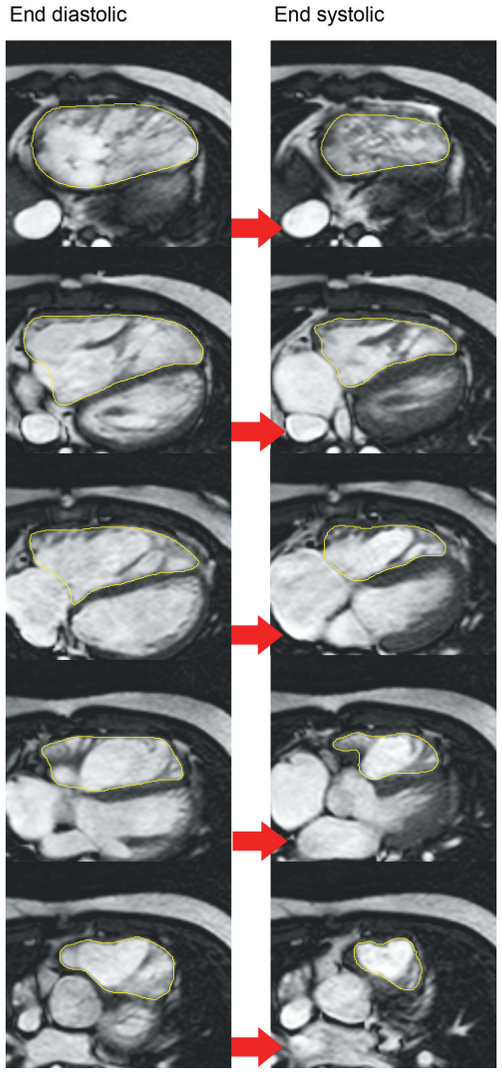

Schematic representation of assessment of volumes and function of right ventricle with axial balanced SSFP cine imaging in a 15 year old patient with tetralogy of Fallot. The right ventricle is dilated and ejection fraction is impaired. Multiple cines with contiguous parallel slices covering the whole heart are obtained. Five axial slices are displayed from inferior (top) to superior (bottom). Right ventricular volumes are obtained by manually tracing the endocardial borders at end-diastole (left panels) and end-systole (right panels) on all axial slices and multiplying the area by the slice thickness (Simpson's rule). Subsequently, stroke volumes and ejection fraction can be calculated.

Figure 3. Phase-encoded flow imaging

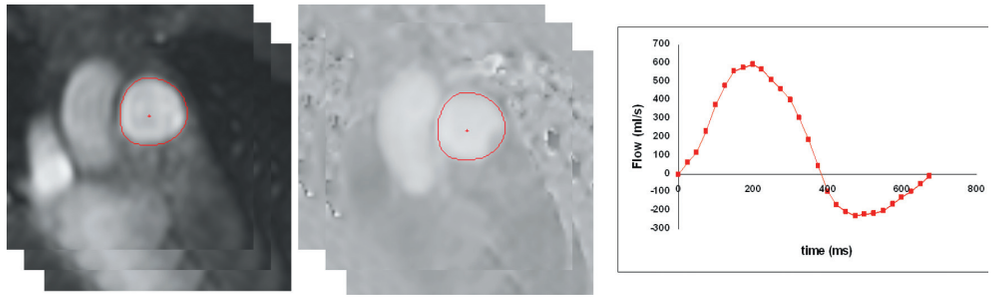

Schematic representation of phase-encoded flow imaging across the pulmonary artery. The imaging plane is positioned perpendicular to the pulmonary artery, midway between the PV and the bifurcation at end diastole. Velocity is encoded in one direction during free breathing. Consecutive modulus (anatomic) images (left panel) and phase-encoded images (middle) are obtained, covering the full cardiac cycle. The inner border of the pulmonary artery is traced (red trace) during every phase in the modulus image and copied to the corresponding phase-encoded images. Time - flow velocity curves (right panel) can be reconstructed, from which the following parameters can be calculated: Right ventricular stroke volume, regurgitation volume, and regurgitation fraction across the pulmonary valve.

Late gadolinium-enhanced imaging

Following 3D-MRA, late gadolinium-enhanced imaging may be performed. Images are acquired approximately ten minutes after intravenous gadolinium-chelate contrast agent administration. Late gadolinium-enhanced imaging enables the detection and quantification of myocardial fibrosis or scar tissue. The imaging sequence takes advantage of the T1 shortening effect of gadolinium and of the differences in 'wash-out' kinetics of the gadolinium-chelate between viable and non-viable myocardium. To obtain the late gadolinium-enhanced images, an inversion-recovery, T1 weighted GRE image is acquired. Myocardial fibrotic regions or scar tissue have a delayed wash-out of the contrast agent and appear bright; i.e. "late enhancement", whereas contrast agent in normal and/or viable tissue has been washed out (no enhancement).(24) Although limited data are available at present in CHD patients, late gadolinium-enhanced myocardial viability imaging may be of use in various postoperative CHD patients to quantify scar tissue.(25,26)

CMR IN POSTOPERATIVE CHD PATIENTS

The subgroups of postoperative CHD patients most frequently referred for CMR evaluation include those with coarctation of the aorta, ToF patients, patients after correction of transposition of the great arteries and single ventricle patients after the Fontan procedure.(6,7) The various subgroups require specific CMR imaging protocols based on postoperative anatomy and the specific clinical problems that may be encountered during follow-up.

Coarctation of the aorta

Coarctation of the aorta is characterized by stenosis of the aortic lumen. The stenotic region is

Figure 4. 3D-MRA in repaired tetralogy of Fallot

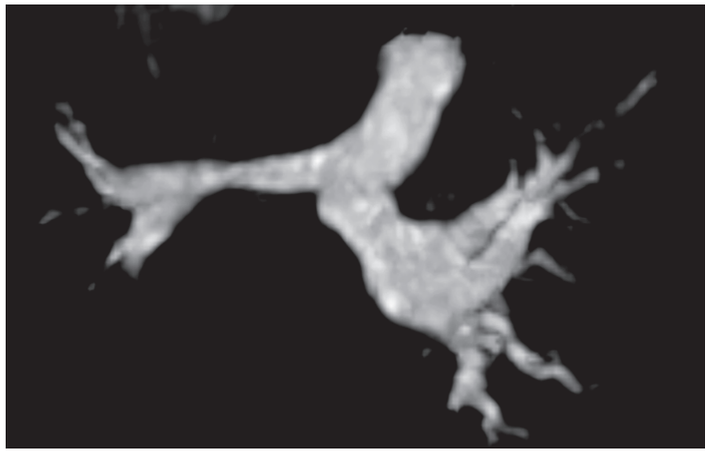

Gadolinium-contrast agent enhanced 3D-MRA in a 36-year old male (same patient as in Figure 1). 3D frontal view, oblique from below, showing the pulmonary trunk and pulmonary arteries. Note the small diameter of the right pulmonary artery as complication after Waterston shunt in the past (i.e. connection between the ascending aorta and right pulmonary artery), compare with the left pulmonary artery. Note that the intravascular anatomy is better delineated by 3D-MRA than by BBSE imaging (compare with Figure 1).

typically located just distal to the left subclavian artery at the insertion of the ductus arteriosus (Figure 5). Coarctation severity may vary from a mild focal stenosis (presenting in young adults with hypertension) to a severe obstruction with an additional hypoplastic aortic arch (presenting in infants with severe systemic hypo-perfusion at the time of the physiologic closure of the ductus arteriosus). Coarctation of the aorta is associated with cardiac and vascular anomalies, of which a bicuspid aortic valve is the most common anomaly (75%).(27) Even in the absence of symptoms, relief of a significant hemodynamic coarctation (as indicated by a pressure gradient over the coarctation >20 mmHg, as assessed by catheterization) is indicated due to a high incidence of complications (including congestive heart failure, aortic rupture and infective endocarditis) if left untreated.(28) Relief of the obstruction may be performed surgically by resection of the stenotic region followed by end-to-end anastomosis or, less frequently, by the use of prosthetic material or a subclavian flap.(27,29) Alternatively, in older patients, an endovascular approach may be used with transcatheter stenting or balloon angioplasty.(27,30,31) Common problems in postoperative coarctation patients include aneurysm formation at the surgical site, re-coarctation with hypertension and subsequent LV dysfunction and collateral artery formation.(30,31)

During long term follow-up of postoperative coarctation patients, CMR imaging of the aortic arch should be routinely performed to detect aneurysm formation or re-coarcation.(5,32) Aneurysm formation at the region of coarctation correction is observed in up to 30% of postoperative patients, with the highest incidence after the use of prosthetic material.(33) To appreciate aortic aneurysms or re-coarctation, anatomical BBSE images may be obtained by planning a stack of slices in the oblique sagittal plane through the aortic arch. However, when the coarctation

Figure 5. Aortic coarctation

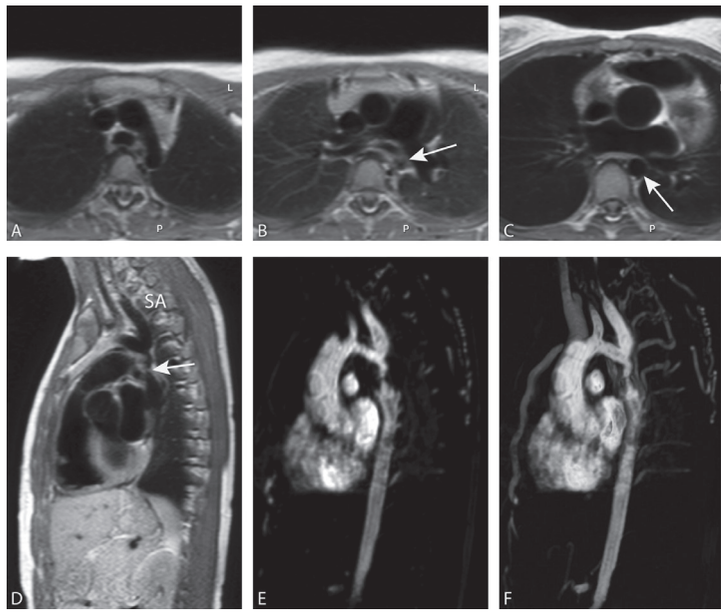

CMR images in a 13-year old female with recently discovered coarctation. BBSE images in axial orientation with view from below (a-c) and sagittal image with left lateral view showing the aortic arch with mildly hypoplastic descending aortic arch (a) and the aorta at the narrowest part of the coarctation (arrow in b, d) at the classic location distal from the origin of the left subclavian artery (SA, in d). Descending aorta distal from the coarctation (arrow, c). MRA showing the coarctation in original 2.8 mm slice image (e) and in thick 29 mm 3D maximum intensity projection image (f). Note the enlarged intercostal arteries and enlarged mammary artery that serve as collateral arteries as to bypass the coarctation (f).

tissue is thin or membranous, it may not be projected on BBSE images due to partial volume effects. Alternatively, bright-blood GRE cine imaging may yield a turbulent flow void at the site of obstruction. In case of re-coarctation, quantification of the hemodynamic severity is necessary to investigate the need for intervention. Although cardiac catheterization is currently the reference standard to quantify hemodynamic severity, it is an invasive procedure requiring ionizing radiation. Alternatively, for initial assessment of the hemodynamic significance of re-coarctation, CMR may be used (Figure 6). CMR has various approaches to non-invasively characterize coarctation severity. With 3D-MRA, the exact diameter, length, and location of the (re-)coarctation is visualized and can be measured. In addition, with 3D-MRA, the presence of collateral arteries is shown. In the presence of collateral arteries coarctation severity can be assessed by measuring collateral flow volume with the use of phase-contrast flow imaging. For this purpose, the aortic flow volume just proximal to the coarctation region is measured and compared with the flow volume in the descending aorta at the level of the diaphragm. In the presence of collaterals, the flow volume is increased at the distal aorta. The percent increase in volume provides a quantitative measurement of (re-)coarctation severity.(34) In addition,

Figure 6. Aortic coarctation severity by flow measures

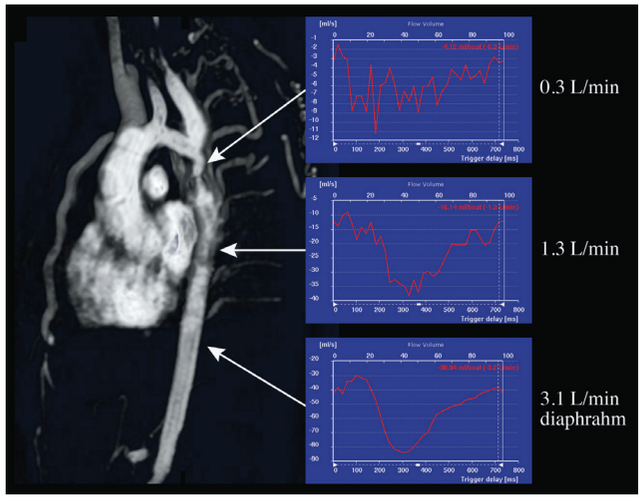

MR images in a 13-year old female, same patient as in figure 5. 3D-MRA showing the locations for flow measurements with resulting flow volumes through the aorta. Flow was measured by velocity encoded imaging, immediately proximal to the coarctation, half-way below the coarctation, and at the level of the diaphragm. Note that the aortic flow increases from proximal to distal that indicates retrograde collateral flow towards the aorta. At the level of the diaphragm approximately 90% of flow through the aorta is due to collateral retrograde flow via chest-wall- and intercostal arteries. Output at the level of the aortic valve was 5.6 L/min.

Figure 7. Transposition of the great arteries after arterial switch

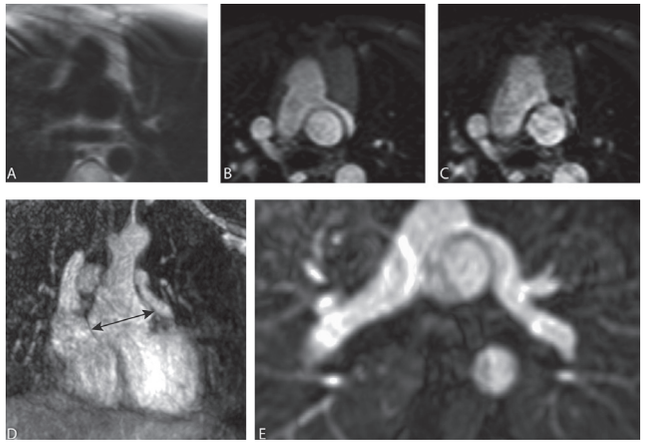

CMR images in a 12-year old male with transposition of the great arteries after arterial switch. Axial black blood image with view from below (a) and MRA (e) showing the spatial relationships between the pulmonary trunk and ascending aorta. Lecompte maneuver locates the pulmonary trunk in front of the ascending aorta with the pulmonary arteries on either side of the aorta (a-c, e). Left pulmonary artery is partially obstructed due to the position of the main pulmonary artery in relation to the aorta. Axial GRE cine end-diastolic (b) and end-systolic (c) images showing the dynamic character of obstruction within the cardiac cycle. The neo-aortic root in this child was enlarged to 39 mm (d).

another study validated CMR against catheterization to assess re-coarctation severity in 31 patients.(35) 3D-MRA was used to assess the diameter of the narrowest coarctation segment. Additionally, with phase-encoded flow MRI at the thoracic descending aorta, the deceleration velocity of flow was obtained as a quantitative measure of flow obstruction. Using this combined approach, CMR could differentiate between a transcatheter pressure gradient >20 mmHg or below 20 mmHg with high sensitivity (95%) and specificity (82%).(35)

Tetralogy of Fallot

Tetralogy of Fallot (ToF) is the most common complex congenital heart disease with an incidence of 420 per million live births.(36) In ToF patients, an anterior displacement of the RV outflow septum causes a ventricular septum defect, overriding of the aorta, pulmonary stenosis, and subsequent RV hypertrophy. Surgical repair of ToF involves closure of the ventricular septum defect and relief of the pulmonary stenosis by infundibular resection, valvulotomy and/or patch placement. The long term survival after surgical correction of ToF is excellent. Nevertheless, postoperative ToF patients may present with a range of functional and hemodynamic sequelae during follow-up. CMR plays an important role to assess these abnormalities.

After surgical relief of the pulmonary stenosis, pulmonary regurgitation is common in ToF patients.(37) As a result of the pulmonary regurgitation, longstanding chronic volume overload may cause RV dilatation and subsequent RV dysfunction (Figure 1 and Figure 2).(38) Severe RV dilatation in postoperative ToF patients is associated with ventricular arrhythmia and sudden death.(37) Therefore, in postoperative ToF patients with moderate or severe pulmonary regurgitation fraction (≥25%) and severe right RV dilatation (RV end-diastolic volume >160-170 ml/m^2 or RV end-systolic volume >82-85 ml/m^2) or clinical symptoms, pulmonary valve replacement is recommended in order to improve clinical outcome.(39-41) CMR is currently the method of choice to quantify pulmonary regurgitation and to assess RV volumes and function. Sequential assessment of ventricular volumes and function with bright blood GRE cine images and assessment of pulmonary regurgitation with phase-encoded images is therefore crucial for clinical decision-making with regard to pulmonary valve replacement in postoperative ToF patients.

Furthermore, during CMR imaging of postoperative ToF patients, specific attention should be paid to the right ventricular outflow tract (RVOT). As a result of regional surgical manipulation, regional wall motion abnormalities at the RVOT are observed in more than 50% of patients and are independently related with RV dilatation.(42) RVOT akinesia or dyskinesia may be assessed with bright blood GRE cine imaging in the oblique sagittal plane through the RVOT or in the midventricular short axis.(25,42,43) In addition, several studies have demonstrated the presence of fibrotic or scar tissue at the RVOT, as indicated by late enhancement imaging.(25,43,44) Recently, two independent imaging studies on postoperative ToF patients illustrated that both regional RVOT dysfunction and late RVOT enhancement independently relate to global RV function, exercise capacity and ventricular arrhythmia.(43,44) These findings emphasize the importance of comprehensive RVOT imaging using bright blood GRE cine images and late gadolinium-enhanced imaging. RVOT imaging is furthermore important for the selection of ToF patients suitable for percutaneous valve replacement.(45) Currently, this transcatheter technique to replace the pulmonary valve may be performed in patients without a transannular patch who previously underwent surgical pulmonary valve replacement.(46) The percutaneously placed pulmonary valve needs safe anchoring at the RVOT and therefore, specific anatomic properties of the RVOT are required. Schievano et al. have shown that morphological characterization of the RVOT, as assessed by 3D-MRA, greatly aids in selecting patients for percutaneous pulmonary valve replacement.(45)

In addition, progressive aortic regurgitation, aortic dilatation and LV dysfunction may occur in ToF patients. Accordingly, LV function and aortic root dimensions need a comprehensive evaluation during CMR imaging of ToF patients.(47) Grotenhuis et al. demonstrated an association between aortic regurgitation and a reduced aortic elasticity in cToF patients.(47) Ultimately, reduced aortic elasticity and regurgitation may lead to LV dysfunction in ToF patients.(47) Furthermore, recent trials on LV dysfunction in postoperative ToF patients have demonstrated a close correlation between RV and LV performance, especially at the apical level. These results indicate an important role of ventricular-ventricular interaction in the pathophysiological mechanism leading to LV dysfunction in ToF patients.(48,49) Finally, stenotic lesions, such as conduit obstruction or stenosis at the main or branch pulmonary arteries are frequently encountered in postoperative ToF patients. These lesions may aggravate pulmonary regurgitation or cause asymmetric lung perfusion and reduced exercise capacity.(50) BBSE and 3D-MRA provide an anatomic evaluation of the pulmonary arteries (Figure 1 and Figure 4). Furthermore, phase-contrast flow imaging of the pulmonary arteries has been validated against perfusion scintigraphy to accurately assess differential lung flow over both branch pulmonary arteries.(20)

Transposition of the great arteries

The population of postoperative patients with transposition of the great arteries consist of three subgroups of patients: those with D-transposition of the great arteries who underwent arterial switch operation, D-transposition patients after atrial switch operation (Mustard or Senning procedure), and patients with “congenitally corrected” transposition of the great arteries (L-transposition). The latter two subgroups have the morphological RV sustaining the systemic circulation, which largely determines the role of CMR during follow-up in these patients.

<u>D-transposition of the great arteries after arterial switch</u>

Patients with D-transposition of the great arteries have a discordant ventriculo-arterial connection. In these patients, the aorta arises from the morphological RV and the pulmonary artery arises from the morphological LV. The ‘D’ refers to the (normal) dextro-position of the embryonic bulboventricular loop (i.e. the morphological RV is on the right side). In patients with D-transposition, the atrial situs and the atrio-ventricular connections are normal. Common associated cardiac lesions include a ventricular septum defect and pulmonary outflow obstruction. In the absence of a sufficient shunt between the pulmonary and systemic circulation (such as a patent ductus arteriosus, a ventricular septum defect or an atrial septum defect), neonates with D-transposition present with severe cyanosis at the time of the physiological closure of the ductus

Figure 8. Transposition of the great arteries after atrial switch

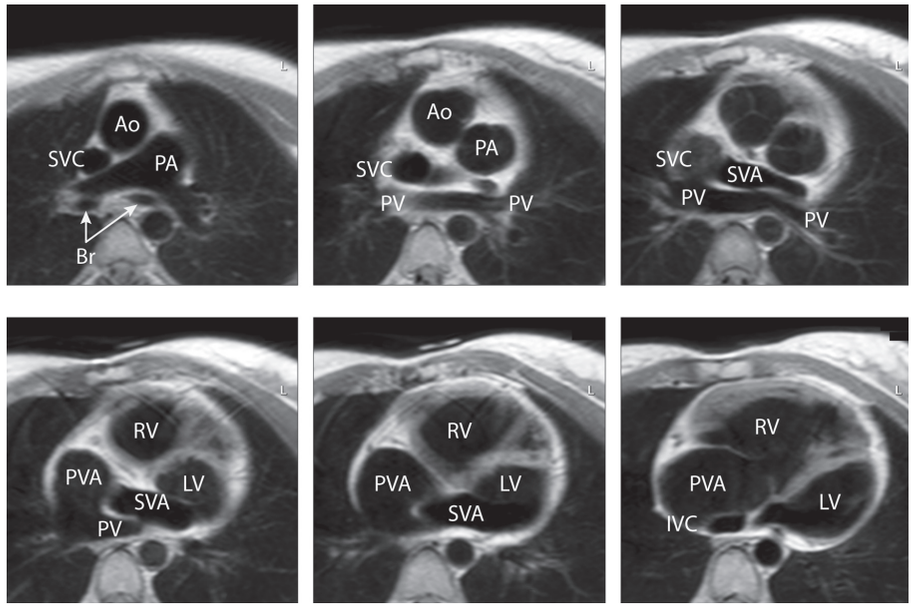

MR images in 36-year old female with transposition of the great arteries after Senning repair, axial black blood images with view from below. The aorta (Ao) is located above the right ventricle (RV) that sustains the systemic circulation. The pulmonary artery (PA) is located above the left ventricle (LV) that sustains the pulmonary circulation. Blood from the superior vena cava (SVC) and inferior vena cava (IVC) is directed to the systemic venous atrium (SVA), that is connected to the LV. Blood from the pulmonary veins (PV) is directed to the pulmonary venous atrium (PVA), that is connected to the RV. Note RV hypertrophy caused by systemic pressure. PVA and right ventricle are enlarged due to longstanding tricuspid regurgitation. Br: bronchus

arteriosus. In these patients, atrial balloon septostomy (Rashkind procedure) may be performed to create or enlarge an atrial septum defect.(51) Currently, the arterial switch operation is the surgical procedure of choice to anatomically correct patients with D-transposition of the great arteries. During this procedure, both arteries are transected above the sinuses and subsequently switched and re-anastomosed to the correct ventricle (Figure 7).(52) Subsequently, the coronary arteries are re-implanted in the neo-aorta.(52)

Survival is excellent after the arterial switch operation.(53) However, during long term follow-up, several complications may be encountered, including RVOT obstruction or supra-valvar pulmonary stenosis, dilatation of the neo-aortic root, neo-aortic regurgitation, and coronary artery stenosis.(53) As a result of these complications, re-interventions are frequently performed during follow-up.(53) The most common indications for re-intervention after arterial switch operation are RVOT obstruction and supra-valvar pulmonary stenosis, accounting for 40% of all reoperations.(54) Two types of pulmonary artery obstruction may be observed. First, a circumferential narrowing at the suture line of the pulmonary artery anastomosis may develop. Second, as a result of surgical manipulation, tension and flattening of pulmonary arteries may cause obstruction. Furthermore,

aortic dilatation and regurgitation during follow-up may be caused by abnormalities of the neo-aortic root in postoperative D-transposition (Figure 7, panel D).(55) After the arterial switch operation, the native pulmonary trunk and native pulmonary valve (neo-aortic root and valve) are functioning in the systemic circulation. The smooth muscle in the vessel wall of the pulmonary root is structurally different from that of the aortic root.(56) In addition, a diminished amount of collagen in the arterial wall of both great arteries of patients with D-transposition has been demonstrated.(56) As a result, the compliance of the pulmonary trunk in patients with D-transposition may be reduced. Accordingly, even in the absence of significant pulmonary artery stenosis, increased peak flow velocities in the pulmonary trunk have been demonstrated in patients after arterial switch operation.(57)

To appreciate possible pulmonary or RVOT stenosis and neo-aortic dilatation during CMR evaluation of postoperative D-transposition patients, specific attention should be paid to the LV and RV outflow tracts. Oblique sagittal and oblique coronal bright-blood GRE cines through the LV outflow tract and RVOT enable assessment of the regional diameters and geometry.(58,59) Furthermore, multi-slice axial bright-blood GRE cines from the diaphragm up to the transverse aorta permits dynamic imaging of the supra-valvar aortic and pulmonary artery regions as well as assessment of ventricular volumes and function. In addition, with the use of 3D-MRA, more distal (branch) pulmonary artery stenosis can be identified. Finally, aortic and pulmonary valve competence and velocity can be quantified by phase-encoded flow imaging.(59)

Finally, stenosis of the coronary arteries at the site of the surgical anastomosis may occur after arterial switch operation.(60) Although those patients are often asymptomatic, they may be at risk for ischemia during follow-up.(61,62) CMR enables various approaches for the detection of coronary artery disease, including late enhancement MRI, stress MRI (by supine bycicle ergometry or dobutamine infusion), contrast-enhanced myocardial perfusion MRI, coronary angiography MRI and coronary flow MRI.(5) Various authors have demonstrated the feasibility of these imaging techniques to detect coronary stenosis in young asymptomatic patients after the arterial switch operation. As a result, these imaging protocols are increasingly being incorporated into the CMR protocols of patients after arterial switch operation.(5) However, at present, the clinical implications of the detection of coronary obstruction with CMR in asymptomatic patients after arterial switch operation remains under investigation.(62-64)

<u>D-transposition of the great arteries after atrial switch</u>

Before the introduction of the arterial switch operation, which was first performed by Jatene in 1975(52), D-transposition of the great arteries was surgically corrected at the atrial level. During atrial correction of D-transposition, a surgical baffle is constructed within the atria, redirecting the systemic venous blood to the LV and the pulmonary venous blood to the RV (Figure 8). The atrial baffle may be constructed with synthetic or pericardial tissue (Mustard procedure), or, alternatively, native atrial tissue is used (Senning procedure). In patients with D-transposition after atrial switch, the RV is supporting the systemic circulation. Consequently, the RV functions as a high pressure pump with increased oxygen demand, making it vulnerable for failure and/or ischemia.(65) In a follow-up study including 91 patients with D-transposition after the Mustard procedure, over 50%

Figure 9. Example of pulse wave velocity assessment with CMR

From: Grotenhuis et al. J. Magn. Reson. Imaging 2009;30:521–526. Copyright by Wiley-Blackwell.

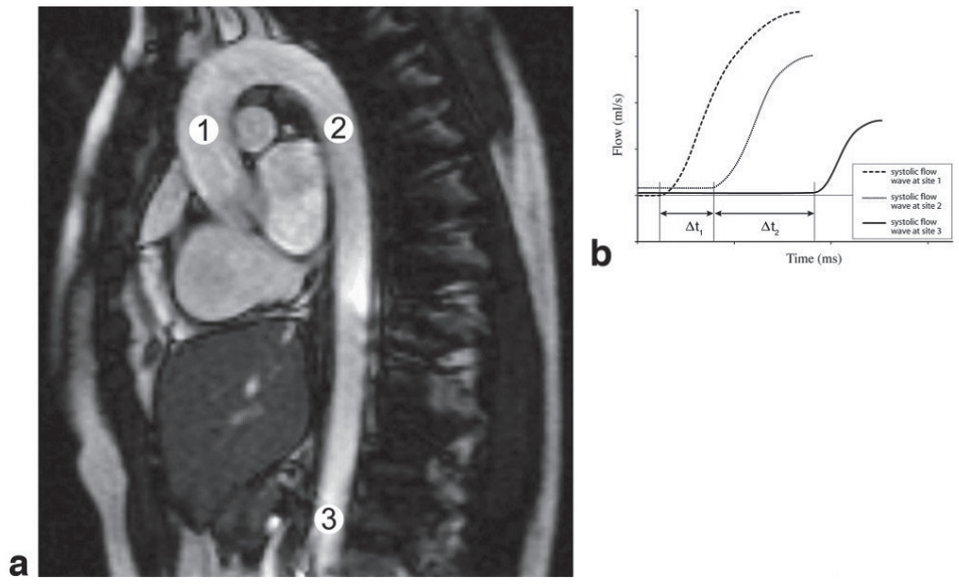

Analysis of pulse wave velocity with CMR. **a:** Oblique sagittal image covering the full course of the aorta, indicating the sites for the through-plane velocity-encoded pulse wave velocity assessments: the ascending aorta (1), the proximal descending aorta just distal to the aortic arch (2), and the most distal level of the abdominal aorta depicted in the oblique sagittal scout (3). Determination of the onset of the three systolic flow waves for pulse wave velocity at the measurement sites are depicted in **b,** The distance between these sites and the transit time between the individual onsets of the systolic flow waves determine the pulse wave velocity.

of patients presented with systemic RV failure after 25 years follow-up.(66) Other common clinical problems after atrial switch include tricuspid regurgitation, baffle obstruction, baffle leakage, and pulmonary venous or systemic venous obstruction.

L-transposition of the great arteries

L-transposition of the great arteries is a rare congenital cardiac anomaly, comprising less than 1% of all patients with CHD. L-transposition is characterized by atrio-ventricular and ventriculo-arterial discordance: the right atrium is connected the morphological LV, which is connected to the pulmonary artery, and the left atrium is coupled with the morphological RV, which is connected to the aorta. The 'L' refers to the levo-position of the embryonic bulboventricular loop (i.e. the morphological RV is on the left side). In L-transposition patients, the morphological RV is supporting the systemic circulation. Associated cardiac anomalies are very common in L-transposition and include tricuspid valve abnormalities (90%), ventricular septal defects (70%) and pulmonary stenosis (40%).(67) The clinical presentation and outcome of patients with L-transposition is largely determined by the nature and hemodynamic consequences of the associated lesions.(68)

Surgical management may be performed to improve outcome in patients with significant associated cardiac lesions. Most commonly, surgical repair for L-transposition of the great arteries includes closure of a ventricular septum defect, and/or tricuspid valve surgery or replacement. Alternatively, repair may be performed by means of the double switch procedure. The double switch procedure combines atrial rerouting (Senning or Mustard procedure) with the arterial switch. Hence, after the double switch operation, the morphological LV supports the systemic circulation. Currently, the double switch procedure is gaining ground in the surgical treatment of patients with L-transposition. During long term follow-up of L-transposition patients with a systemic RV, ventricular dysfunction and tricuspid regurgitation are common.(69) In a multi-center study by Graham and colleagues on 132 L-transposition patients with various associated cardiac lesions, 67% presented with systemic RV failure at the age of 45.(69)

CMR imaging plays an important prognostic role in the clinical follow-up of both patient subgroups with a systemic RV. Assessment of function and condition of the systemic RV can be studied in detail with various CMR techniques. CMR bright-blood GRE cines should be obtained to assess volumes and function of the systemic RV, as well as qualitative assessment of the presence of tricuspid regurgitation.(5) In systemic RV patients with progressive RV failure and significant tricuspid regurgitation, tricuspid valve replacement may be performed. The importance of close clinical follow-up of RV ejection fraction is underlined by the results of a study of Van Son et al., who observed increased mortality in systemic RV patients after tricuspid replacement when pre-operative ejection fraction was below 44%.(70) Image post-processing of the cine images requires special attention in systemic RV patients. During systemic RV analysis, hypertrophy of the RV myocardium may complicate identification of the endocardial border. When the hypertrophied RV trabeculations are included in the myocardial blood pool, RV volumes are may be significantly overestimated.(71) A recent investigation showed that delineation of endocardial contours outside the trabeculations yields more reproducible and probably more accurate measurements.(71)

Furthermore, stress MRI is of prognostic value in patients with a systemic RV. Winter et al. demonstrated that the inability of the systemic RV to increase ejection fraction and to reduce RV end-systolic volume upon exertion is significantly related to adverse outcome.(72) In addition, late enhancement imaging enables further prognostic classification of patients with a systemic RV. Areas of late enhancement in the systemic RV have been associated with RV dysfunction, poor exercise tolerance, arrhythmia, and progressive clinical deterioration.(73)

Finally, in D-transposition patients after the atrial switch operation and in L-transposition patients after the double switch procedure, another important goal of CMR imaging is the detailed assessment of baffle function and morphology. Obstruction of the intra-atrial baffle is frequently encountered during follow-up. Furthermore, baffle leaks may occur, causing left-to-right or right-to-left shunting at the atrial level. Baffle leaks may be quantified with phase-encoded flow imaging, by comparing aorta and pulmonary artery flow volumes (Qp/Qs). To delineate baffle obstruction, contiguous slices in the axial plane obtained by BBSE or bright-blood GRE cine imaging at the atrial level can be used.(74) Fogel et al. demonstrated that a 3D image display of the obtained contiguous

Figure 10. Post processing of 3D time-resolved flow images for volumetric assessment

From: van der Hulst et al. Radiology 2010; 256: 724-734. Copyright by RSNA.

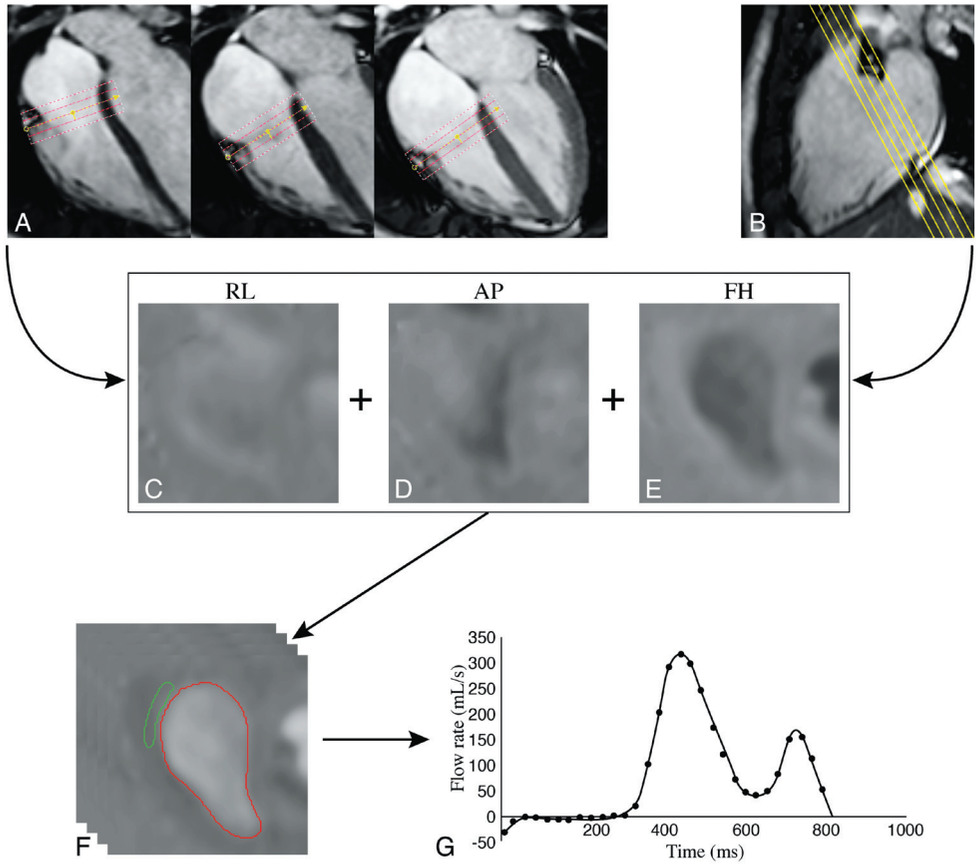

Post processing of 3D time-resolved flow images for volumetric assessment of the tricuspid valve. Retrospective tracking of the tricuspid valve is performed by positioning a plane of interest on the tricuspid valve perpendicular to the flow in every cardiac phase in a four-chamber **(a)** and two-chamber **(b)** view (cine images: repetition time (TR) 3.9 ms, echo time (TE) 1.5 ms, flip angle 50°). Velocity-encoded images from three orthogonal directions (TR/TE 7.5 ms/4.3 ms, flip angle 10°) **(c-e)**, reconstructed from the position of the valve determined with retrospective valve tracking based on the two-chamber **(b)** and four-chamber **(a)** views. Through-plane velocity-encoded images **(f)** are obtained by reformatting of the center valvular plane in each cardiac phase. The inner border of the tricuspid annulus is traced for flow analysis. A region within the free wall of the right ventricle is traced for background correction. Tricuspid flow velocity in time can be presented in a curve **(g)**, from which flow volume can be calculated. Abbreviations: AP: anterior-posterior velocity-encoded, FH: feet-head velocity-encoded, RL: right-left velocity-encoded.

Figure 11. Quantitative imaging of flow with 3D time resolved imaging

From: Hope et al. J. Magn. Reson. Imaging 2010;31:711–718. Copyright by Wiley-Blackwell.

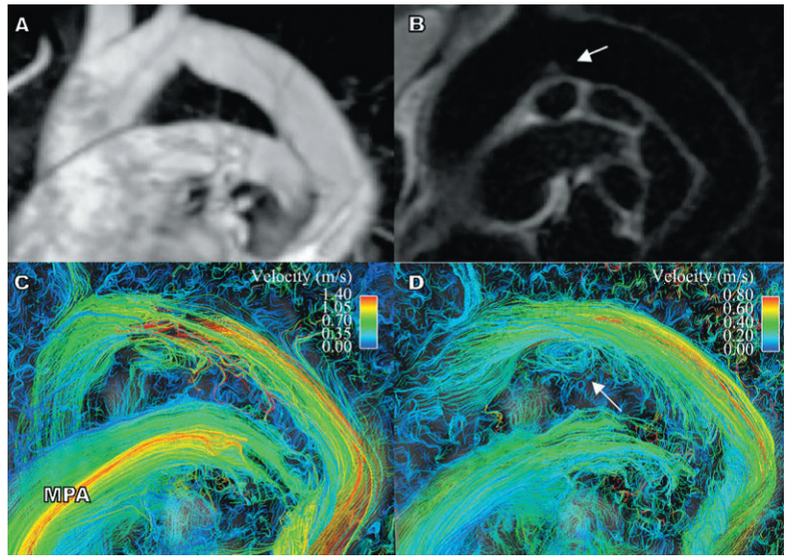

Abnormal vortical flow in a postoperative coarctation patient. Minimal residual narrowing (top arrow) of the mid aortic arch demonstrated with 3D-MRA (**a**) and BBSE (**b**) images images. Streamlines are presented in mid (**c**) and late (**d**) systole. Disturbed flow is revealed (secondary flow features), with acceleration and signal drop out secondary to aliasing, as well as vortical-type flow (bottom arrow) downstream of the focal region of mild aortic narrowing.

slices is useful for this purpose, as complex spatial relationships are more easily clarified.(74) Furthermore, 3D-MRA is a valuable technique for anatomic imaging of baffle morphology in patients with D-transposition after atrial switch.(74)

Single ventricle patients after the Fontan procedure

The subgroup of CHD patients with a single ventricle is heterogeneous, with diverse complex cardiac anomalies. There may be a true 'anatomic' single ventricle, or, more commonly, there may be one 'functional single ventricle' (such as in hypoplastic left heart syndrome or tricuspid atresia). The single ventricle can be of RV or LV morphology and a range of additional cardiac abnormalities may be present. The treatment of choice in patients with a single ventricle is the surgical construction of the Fontan circulation, performed in a staged process requiring at least two separate surgical interventions.(75) After completion of the Fontan circulation, the systemic and pulmonary circulations are separated and the single ventricle sustains the systemic circulation. Both caval veins are directly connected to the pulmonary arteries without interposition of a sub-pulmonary ventricle. Direct connection of the systemic venous return to the pulmonary arteries is constructed via an intra-atrial tunnel or an extra-cardiac conduit.(76) A fenestration may be created between the systemic venous return and the pulmonary venous pathways which allows for shunting towards the pulmonary venous circulation in case of increased pulmonary vascular resistance.

The Fontan procedure is a palliative procedure, although long term outcome is improving. In a recent report on 250 single ventricle patients who underwent the Fontan procedure, the 20-year survival after a successful Fontan procedure was 84%.(76) Failure of the Fontan circulation (defined as death, surgical 'takedown' of the Fontan, heart transplantation, or symptomatic heart failure in New York heart association (NYHA) functional class III or IV) was observed in 30% of patients after 20 years follow-up.(76) CMR evaluation can aid in the early recognition of single ventricle dysfunction. For this purpose, volumes, mass and ejection fraction can be studied by obtaining whole-heart bright blood GRE cines.(77) In addition to ventricular failure, other problems may complicate postoperative single ventricle with a Fontan circulation. Most commonly, obstruction of the pulmonary arteries or pulmonary veins occur, which can severely compromise the Fontan circulation. Flow obstruction to the pulmonary arteries may be due to anatomical narrowing or to increased pulmonary vascular resistance. Also, an enlarged right atrium or extra-cardiac conduit may compress the pulmonary veins.(78) Anatomic narrowing and obstruction in the pulmonary arterial and venous pathways can be visualized by static BBSE or bright-blood GRE cine acquisitions. Furthermore, obstruction can be revealed with the use of phase-encoded flow imaging by through-plane measurement of flow velocities. Of note, in Fontan patients, the maximum velocity-encoding during image acquisition should be anticipated upon the low flow velocities at the systemic venous side of the Fontan circulation. Moreover, as a result of the low blood flow velocities, the BBSE images should be comprehensively reviewed to identify possible thrombi.

In addition to the BBSE images, bright blood GRE images and phase-encoded images, 3D-MRA can reveal possible obstruction of the pulmonary and venous pathways in Fontan patients. Furthermore, 3D-MRA is helpful in delineating possible collateral arteries. The detection of the presence of collateral arteries is of clinical importance in Fontan patients as collateral blood flow causes volume overload to the vulnerable single ventricle. Goo and co-workers recently evaluated time-resolved 3D-MRA for the assessment of flow dynamics in Fontan patients. In 15 young patients (median age 10 years), time-resolved 3D-MRA yielded data on preferential lung flow and collateral arteries with high spatial resolution.(23)

Finally, imaging of bilateral lung perfusion is of clinical importance in Fontan patients.(79) Currently, perfusion scintigraphy is the method of choice to assess lung perfusion. However, Fratz and co-workers have demonstrated that in patients with a Fontan circulation, lung perfusion imaging with phase-encoded flow MRI is more accurate than perfusion scintigraphy.(79)

NOVEL CMR IMAGING TECHNIQUES IN CHD PATIENTS

In addition to the 'conventional' imaging sequences that are used during routine clinical follow-up, continuing research has provided several novel applications of CMR that have clinical value in postoperative CHD patients, including pulse wave velocity, 3D flow imaging, tissue velocity imaging and T1 mapping.

Aortic pulse wave velocity

The aortic pulse wave velocity is a surrogate marker for aortic wall compliance. It is defined as the velocity of the systolic wave front propagating through the aorta. Aortic pulse wave velocity, as assessed with Doppler echocardiography, is a strong predictor of cardiovascular mortality.(80,81) In hypertensive patients, the aortic pulse-wave velocity, as assessed with CMR, has been shown to be associated with LV mass and lacunar brain infarcts.(82) With CMR, the aortic pulse wave velocity can be assessed at any site of the aorta even in the presence of a tortuous aortic vessel. To obtain the aortic pulse wave velocity with CMR, 'conventional' phase-encoded flow images at various regions of the aorta are acquired (usually at the ascending aorta, descending aorta and at the abdominal aorta just proximal to the iliac bifurcation).(83) From the time-flow curves at each aortic region, the timing of the onset of the systolic flow wave can be obtained. (Figure 9) Subsequently, the time difference between the onset of flow between two aortic regions (transit time) is calculated. Finally, the pulse-wave velocity is obtained by dividing the distance measured between the two regions by the transit time. This CMR approach to assess the aortic pulse wave velocity was recently validated against intra-arterial pressure measurements during catheterization, and good agreement and high reproducibility were reported.(83)

The application of CMR to assess the aortic pulse wave velocity has been performed in postoperative CHD patients. Grotenhuis and colleagues assessed the aortic pulse wave velocity of the aortic arch in 15 D-transposition patients after arterial switch operation.(58) A reduced elasticity, reflected by an increased pulse wave velocity, was observed in the patients as compared with 15 age-matched controls (patients: 5.1 ± 1.2 m/s, controls: 3.9 ± 0.7 m/s, p=0.004).(58) Another study reported the aortic pulse wave velocity of 16 ToF patients after pulmonary valve replacement. The pulse wave

velocity at the aortic arch was increased in the ToF patients as compared with 16 healthy control subjects (5.5 ± 1.2 m/s vs. 4.6 ± 0.9 m/s, p=0.04).(47) Finally, Voges et al. assessed the aortic pulse wave velocity in 40 patients with a hypoplastic left heart syndrome and a Fontan circulation. In their study, the aortic pulse wave velocity was not significantly different in patients as compared with healthy controls.(84)

Current clinical research aims at further improvement of the assessment of the pulse wave velocity with CMR. Westenberg et al. recently validated the assessment of aortic pulse wave velocity by in-plane two-directional phase-encoded imaging of the aortic arch.(85) With this method, the entire aortic arch was depicted in three two-directional phase-encoded slices, which enabled the assessment of pulse-wave velocity among any two regions in the aorta.(85) The in-plane method was compared with the through-plane method and showed a better agreement with intra-arterial pressure measurement and an improved reproducibility.(85) Future follow-up studies using pulse wave velocity assessment with CMR are needed to reveal its prognostic value in CHD patients.

3D time-resolved flow imaging

Three-dimensional three-directional phase-encoded flow imaging (3D time-resolved flow imaging) enables quantification of valve flow as well as visualization of complex flow patterns. (86-90) Quantification of valve flow with conventional phase-encoded (two-dimensional) flow imaging is hampered by cardiac motion, since the acquisition plane is fixed throughout the cardiac cycle. Indeed, it has been shown that two-dimensional flow assessment of atrioventricular valve flow can lead to significant overestimation of flow volumes.(90) 3D time-resolved flow imaging solves the problem of valve motion by scanning a 3D volume with phase-encoding in three orthogonal directions.(87,90,91) This approach allows for 'retrospective valve tracking' during post-processing, a method that enables manual adjustment of the imaging plane in the 3D volume at any phase according to the angle and position of the valve of interest (Figure 10). (87,90) Furthermore, 3D time-resolved flow imaging allows simultaneous assessment of flow over all four valves, resulting in decreased scan time.(87) In postoperative ToF patients, 3D time-resolved flow has been validated against planimetry for the assessment of pulmonary and tricuspid flow.(89) As compared with two-dimensional flow MRI, 3D time-resolved flow imaging yielded better agreement with stroke volumes as assessed by SSFP planimetry.(89) Furthermore, the simultaneous assessment of flow over several valves enables evaluation of diastolic function of the RV in ToF patients with pulmonary regurgitation.(89) In the presence of pulmonary regurgitation, the flow pattern over the tricuspid valve does not reflect RV filling, since RV filling occurs also from the pulmonary regurgitation. Summation of the 3D time-resolved diastolic flow curves of the pulmonary valve and tricuspid valve allows the reconstruction of RV time-volume curves.(89) The RV time-volume curve represents RV filling and can be used to detect diastolic impairment in ToF patients.(89)

In addition to flow quantification, complex flow patterns can be visualized with 3D time resolved flow images.(86,88) This can be performed by particle tracing visualization in the 3D phase-encoded dataset. Particle tracing simulates the path taken in time by an imaginary particle (e.g. an erythrocyte in the vessel of interest). Particle tracing allows comprehensive visualization of complex flow pathways, for instance in patients with a Fontan circulation.(88) Furthermore, flow patterns can be characterized in static images with the use of so-called streamlines. Streamlines provide a snapshot of the instantaneous blood flow pattern in an image. In streamline images, laminar flow can be differentiated from 'secondary flow features' (e.g. vortices or helices) (Figure 11). Hope and colleagues performed 3D time-resolved systolic streamline imaging of the aorta in 26 coarctation patients and in eight healthy subjects. All healthy subjects showed laminar aortic flow patterns. However, vortical and helical flow patterns were observed in the descending aorta of 14 postoperative coarctation patients (54%).(86) Future studies are warranted to assess the clinical implications of flow visualization in postoperative CHD patients.

Tissue-velocity imaging

The echocardiographic assessment of peak systolic velocities with tissue Doppler imaging has shown to be of incremental value to conventional echocardiography to assess ventricular performance in various clinical conditions.(92-94) In addition, the assessment of the temporal occurrence of peak systolic velocities permits evaluation of mechanical dyssynchrony, which aids in the selection of heart failure patients that may benefit from cardiac resynchronization therapy. (95) With CMR, myocardial velocity (tissue-velocity) can be measured with phase-encoded imaging. (96-98) With tissue-velocity imaging, the maximum velocity is set at a lower threshold as compared to flow imaging (for example at 20 cm/s) which enables the assessment of myocardial motion velocity in time. Velocity can be encoded into any desired direction (usually along the longitudinal axis of the heart) and subsequently, regional time-velocity curves can be obtained. Tissue-velocity imaging with CMR has been validated against tissue Doppler imaging with echocardiography for the assessment of myocardial velocities and timings of myocardial velocities.(99-102) A recent study on tissue-velocity imaging of the RV with CMR in 33 ToF patients demonstrated significantly reduced peak systolic velocities at the RVFW and at the RVOT as compared with 19 healthy controls (RVFW: 8.2 cm/s (inter-quartile range 6.4-9.7) vs. 12.4 cm/s (10.8-13.8), p<0.01, RVOT: 4.7 cm/s (4.1-7.2) vs. 10.2 cm/s (8.7-11.2), p<0.01.(99) Furthermore, the mechanical activation pattern of the RV was evaluated and a significant time-delay within the healthy RV was observed, which was reduced in ToF patients.(99) Insight into RV mechanics may have clinical implications for future studies on pacing strategies in RV failure. In future trials, tissue-velocity MRI can provide detailed insight into myocardial performance, myocardial mechanics and possible dyssynchrony in postoperative CHD patients.

T1 mapping

The novel CMR application of clinical T1 mapping enables quantification of myocardial interstitial fibrosis. Interstitial fibrosis has been demonstrated within the myocardium of CHD patients(103) and may be an important substrate leading to heart failure. Currently, late enhancement imaging is the reference standard to image myocardial fibrosis or scar tissue.(5) However, with late enhancement imaging, diffuse myocardial fibrosis is not revealed, as the selected inversion time to

obtain late enhancement images is deliberately chosen to null 'normal' myocardium. Hence, with late enhancement imaging, only macroscopic scarring can be visualized. By the use of contrast-enhanced T1 mapping (regional assessment of T1 time throughout the myocardium of interest), diffuse interstitial fibrosis may be quantified. Recently, various methods to obtain T1 maps in clinical practice have been proposed.(104,105) In a heterogeneous group of adult CHD patients, Broberg et al. performed T1 mapping of the LV.(106) The authors assessed the ratio of T1 in the blood pool and in the LV myocardium before and after gadolinium-chelate administration with a multi-phase inversion recovery GRE sequence (Look-Locker sequence). In the presence of myocardial fibrosis, the gadolinium has a delayed wash-out from the extracellular matrix of the myocardium, altering the T1 ratio of the surrounding blood and myocardium. With this technique, the authors observed significantly more interstitial fibrosis in CHD patients as compared to healthy controls.(106) T1 mapping may be of great value in future research on the pathophysiology and treatment of heart failure in CHD patients.

CONCLUSION AND FUTURE PERSPECTIVE

Post-operative CHD patients constitute a heterogeneous group of patients that require life-long follow-up. In current clinical practice, noninvasive cardiac imaging with CMR plays an important role during follow-up of postoperative CHD patients, especially in those with complex CHD. CMR imaging yields 3D datasets that provide a comprehensive characterization of complex cardiac anatomy and reliable imaging of cardiac function. In addition, continuing clinical research on novel CMR techniques aims at providing new imaging parameters that may further improve clinical-decision making with regard to re-intervention and follow-up protocols in the growing CHD population.

REFERENCE LIST

1 Marelli AJ, Mackie AS, Ionescu-Ittu R, et al. Congenital heart disease in the general population: changing prevalence and age distribution. Circulation 2007;115:163-72.

2 Khairy P, Ionescu-Ittu R, Mackie AS, et al. Changing mortality in congenital heart disease. J Am Coll Cardiol 2010;56:1149-57.

3 Niwa K, Perloff JK, Webb GD, et al. Survey of specialized tertiary care facilities for adults with congenital heart disease. Int J Cardiol 2004;96:211-6.

4 Perloff JK, Warnes CA. Challenges posed by adults with repaired congenital heart disease. Circulation 2001;103:2637-43.

5 Pennell DJ, Sechtem UP, Higgins CB, et al. Clinical indications for cardiovascular magnetic resonance (CMR): Consensus Panel report. J Cardiovasc Magn Reson 2004;6:727-65.

6 Fratz S, Hess J, Schuhbaeck A, et al. Routine clinical cardiovascular magnetic resonance in paediatric and adult congenital heart disease: patients, protocols, questions asked and contributions made. J Cardiovasc Magn Reson 2008;10:46.

7 Roest AA, Helbing WA, van der Wall EE, et al. Postoperative evaluation of congenital heart disease by magnetic resonance imaging. J Magn Reson Imaging 1999;10:656-66.

8 The clinical role of magnetic resonance in cardiovascular disease. Task Force of the European Society of Cardiology, in collaboration with the Association of European Paediatric Cardiologists. Eur Heart J 1998;19:19-39.

9 Babar JL, Jones RG, Hudsmith L, et al. Application of MR imaging in assessment and follow-up of congenital heart disease in adults. Radiographics 2010;30:1145.

10 Hughes D, Siegel MJ. MRI of complex cyanotic congenital heart disease: pre- and post surgical considerations. Int J Cardiovasc Imaging 2010;26:333-43.

11 Ridgway JP. Cardiovascular magnetic resonance physics for clinicians: part I. J Cardiovasc Magn Reson 2010;12:71.

12 Tsai-Goodman B, Geva T, Odegard KC, et al. Clinical role, accuracy, and technical aspects of cardiovascular magnetic resonance imaging in infants. Am J Cardiol 2004;94:69-74.

13 Thiele H, Nagel E, Paetsch I, et al. Functional cardiac MR imaging with steady-state free precession (SSFP) significantly improves endocardial border delineation without contrast agents. J Magn Reson Imaging 2001;14:362-7.

14 Luijnenburg SE, Robbers-Visser D, Moelker A, et al. Intra-observer and interobserver variability of biventricular function, volumes and mass in patients with congenital heart disease measured by CMR imaging. Int J Cardiovasc Imaging 2010;26:57-64.

15 Plein S, Bloomer TN, Ridgway JP, et al. Steady-state free precession magnetic resonance imaging of the heart: comparison with segmented k-space gradient-echo imaging. J Magn Reson Imaging 2001;14:230-6.

16 Fratz S, Schuhbaeck A, Buchner C, et al. Comparison of accuracy of axial slices versus short-axis slices for measuring ventricular volumes by cardiac magnetic resonance in patients with corrected tetralogy of fallot. Am J Cardiol 2009;103:1764-9.

17 Rebergen SA, van der Wall EE, Doornbos J, et al. Magnetic resonance measurement of velocity and flow: technique, validation, and cardiovascular applications. Am Heart J 1993;126:1439-56.

18 Beerbaum P, Korperich H, Barth P, et al. Noninvasive quantification of left-to-right shunt in pediatric patients: phase-contrast cine magnetic resonance imaging compared with invasive oximetry. Circulation 2001;103:2476-82.

19 Caputo GR, Kondo C, Masui T, et al. Right and left lung perfusion: in vitro and in vivo validation with oblique-angle, velocity-encoded cine MR imaging. Radiology 1991;180:693-8.

20 Sridharan S, Derrick G, Deanfield J, et al. Assessment of differential branch pulmonary blood flow: a comparative study of phase contrast magnetic resonance imaging and radionuclide lung perfusion imaging. Heart 2006;92:963-8.

21 Geva T, Greil GF, Marshall AC, et al. Gadolinium-enhanced 3-dimensional magnetic resonance angiography of pulmonary blood supply in patients with complex pulmonary stenosis or atresia: comparison with x-ray angiography. Circulation 2002;106:473-8.

22 Didier D, Saint-Martin C, Lapierre C, et al. Coarctation of the aorta: pre and postoperative evaluation with MRI and MR angiography; correlation with echocardiography and surgery. Int J Cardiovasc Imaging 2006;22:457-75.

23 Goo HW, Yang DH, Park IS, et al. Time-resolved three-dimensional contrast-enhanced magnetic resonance angiography in patients who have undergone a Fontan operation or bidirectional cavopulmonary connection: initial experience. J Magn Reson Imaging 2007;25:727-36.

24 Shan K, Constantine G, Sivananthan M, et al. Role of cardiac magnetic resonance imaging in the assessment of myocardial viability. Circulation 2004;109:1328-34.

25 Oosterhof T, Mulder BJ, Vliegen HW, et al. Corrected tetralogy of Fallot: delayed enhancement in right ventricular outflow tract. Radiology 2005;237:868-71.

26 Rathod RH, Prakash A, Powell AJ, et al. Myocardial fibrosis identified by cardiac magnetic resonance late gadolinium enhancement is associated with adverse ventricular mechanics and ventricular tachycardia late after Fontan operation. J Am Coll Cardiol 2010;55:1721-8.

27 Tanous D, Benson LN, Horlick EM. Coarctation of the aorta: evaluation and management. Curr Opin Cardiol 2009;24:509-15.

28 Campbell M. Natural history of coarctation of the aorta. Br Heart J 1970;32:633-40.

29 Cohen M, Fuster V, Steele PM, et al. Coarctation of the aorta. Long-term follow-up and prediction of outcome after surgical correction. Circulation 1989;80:840-5.

30 Fawzy ME, Fathala A, Osman A, et al. Twenty-two years of follow-up results of balloon angioplasty for discreet native coarctation of the aorta in adolescents and adults. Am Heart J 2008;156:910-7.

31 Forbes TJ, Moore P, Pedra CA, et al. Intermediate follow-up following intravascular stenting for treatment of coarctation of the aorta. Catheter Cardiovasc Interv 2007;70:569-77.

32 Therrien J, Thorne SA, Wright A, et al. Repaired coarctation: a "cost-effective" approach to identify complications in adults. J Am Coll Cardiol 2000;35:997-1002.

33 Troost E, Gewillig M, Daenen W, et al. Behaviour of polyester grafts in adult patients with repaired coarctation of the aorta. Eur Heart J 2009;30:1136-41.

34 Steffens JC, Bourne MW, Sakuma H, et al. Quantification of collateral blood flow in coarctation of the aorta by velocity encoded cine magnetic resonance imaging. Circulation 1994;90:937-43.

35 Nielsen JC, Powell AJ, Gauvreau K, et al. Magnetic resonance imaging predictors of coarctation severity. Circulation 2005;111:622-8.

36 Hoffman JI, Kaplan S. The incidence of congenital heart disease. J Am Coll Cardiol 2002;39:1890-900.

37 Gatzoulis MA, Balaji S, Webber SA, et al. Risk factors for arrhythmia and sudden cardiac death late after repair of tetralogy of Fallot: a multicentre study. Lancet 2000;356:975-81.

38 Bouzas B, Kilner PJ, Gatzoulis MA. Pulmonary regurgitation: not a benign lesion. Eur Heart J 2005;26:433-9.

39 de Ruijter FT, Weenink I, Hitchcock FJ, et al. Right ventricular dysfunction and pulmonary valve replacement after correction of tetralogy of Fallot. Ann Thorac Surg 2002;73:1794-800.

40 Oosterhof T, van SA, Vliegen HW, et al. Preoperative thresholds for pulmonary valve replacement in patients with corrected tetralogy of Fallot using cardiovascular magnetic resonance. Circulation 2007;116:545-51.

41 Therrien J, Provost Y, Merchant N, et al. Optimal timing for pulmonary valve replacement in adults after tetralogy of Fallot repair. Am J Cardiol 2005;95:779-82.

42 Davlouros PA, Kilner PJ, Hornung TS, et al. Right ventricular function in adults with repaired tetralogy of Fallot assessed with cardiovascular magnetic resonance imaging: detrimental role of right ventricular outflow aneurysms or akinesia and adverse right-to-left ventricular interaction. J Am Coll Cardiol 2002;40:2044-52.

43 Wald RM, Haber I, Wald R, et al. Effects of regional dysfunction and late gadolinium enhancement on global right ventricular function and exercise capacity in patients with repaired tetralogy of Fallot. Circulation 2009;119:1370-7.

44 Babu-Narayan SV, Kilner PJ, Li W, et al. Ventricular fibrosis suggested by cardiovascular magnetic reso-

nance in adults with repaired tetralogy of fallot and its relationship to adverse markers of clinical outcome. Circulation 2006;113:405-13.
45 Schievano S, Coats L, Migliavacca F, et al. Variations in right ventricular outflow tract morphology following repair of congenital heart disease: implications for percutaneous pulmonary valve implantation. J Cardiovasc Magn Reson 2007;9:687-95.
46 Khambadkone S, Bonhoeffer P. Nonsurgical pulmonary valve replacement: why, when, and how? Catheter Cardiovasc Interv 2004;62:401-8.
47 Grotenhuis HB, Ottenkamp J, de BL, et al. Aortic elasticity and size are associated with aortic regurgitation and left ventricular dysfunction in tetralogy of Fallot after pulmonary valve replacement. Heart 2009;95:1931-6.
48 Muzzarelli S, Ordovas KG, Cannavale G, et al. Tetralogy of Fallot: Impact of the Excursion of the Interventricular Septum on Left Ventricular Systolic Function and Fibrosis after Surgical Repair. Radiology 2011; doi:10.1148/radiol.10100895.
49 van der Hulst AE, Delgado V, Holman ER, et al. Relation of left ventricular twist and global strain with right ventricular dysfunction in patients after operative "correction" of tetralogy of fallot. Am J Cardiol 2010;106:723-9.
50 Kang IS, Redington AN, Benson LN, et al. Differential regurgitation in branch pulmonary arteries after repair of tetralogy of Fallot: a phase-contrast cine magnetic resonance study. Circulation 2003;107:2938-43.
51 Mukherjee D, Lindsay M, Zhang Y, et al. Analysis of 8681 neonates with transposition of the great arteries: outcomes with and without Rashkind balloon atrial septostomy. Cardiol Young 2010;20:373-80.
52 Jatene AD, Fontes VF, Paulista PP, et al. Anatomic correction of transposition of the great vessels. J Thorac Cardiovasc Surg 1976;72:364-70.
53 Tobler D, Williams WG, Jegatheeswaran A, et al. Cardiac outcomes in young adult survivors of the arterial switch operation for transposition of the great arteries. J Am Coll Cardiol 2010;56:58-64.
54 Losay J, Touchot A, Serraf A, et al. Late outcome after arterial switch operation for transposition of the great arteries. Circulation 2001;104:I121-I126.
55 Schwartz ML, Gauvreau K, del NP, et al. Long-term predictors of aortic root dilation and aortic regurgitation after arterial switch operation. Circulation 2004;110:II128-II132.
56 Lalezari S, Mahtab EA, Bartelings MM, et al. The outflow tract in transposition of the great arteries: an anatomic and morphologic study. Ann Thorac Surg 2009;88:1300-5.
57 Grotenhuis HB, Kroft LJ, van Elderen SG, et al. Right ventricular hypertrophy and diastolic dysfunction in arterial switch patients without pulmonary artery stenosis. Heart 2007;93:1604-8.
58 Grotenhuis HB, Ottenkamp J, Fontein D, et al. Aortic elasticity and left ventricular function after arterial switch operation: MR imaging--initial experience. Radiology 2008;249:801-9.
59 Gutberlet M, Boeckel T, Hosten N, et al. Arterial switch procedure for D-transposition of the great arteries: quantitative midterm evaluation of hemodynamic changes with cine MR imaging and phase-shift velocity mapping-initial experience. Radiology 2000;214:467-75.
60 Bonhoeffer P, Bonnet D, Piechaud JF, et al. Coronary artery obstruction after the arterial switch operation for transposition of the great arteries in newborns. J Am Coll Cardiol 1997;29:202-6.
61 Legendre A, Losay J, Touchot-Kone A, et al. Coronary events after arterial switch operation for transposition of the great arteries. Circulation 2003;108 Suppl 1:II186-II190.
62 Taylor AM, Dymarkowski S, Hamaekers P, et al. MR coronary angiography and late-enhancement myocardial MR in children who underwent arterial switch surgery for transposition of great arteries. Radiology 2005;234:542-7.
63 Tulevski II, van der Wall EE, Groenink M, et al. Usefulness of magnetic resonance imaging dobutamine stress in asymptomatic and minimally symptomatic patients with decreased cardiac reserve from congenital heart disease (complete and corrected transposition of the great arteries and subpulmonic obstruction). Am J Cardiol 2002;89:1077-81.
64 Manso B, Castellote A, Dos L, et al. Myocardial perfusion magnetic resonance imaging for detecting coronary function anomalies in asymptomatic paediatric patients with a previous arterial switch operation for the transposition of great arteries. Cardiol Young 2010;20:410-7.
65 Dos L, Teruel L, Ferreira IJ, et al. Late outcome of Senning and Mustard procedures for correction of transposition of the great arteries. Heart 2005;91:652-6.
66 Roos-Hesselink JW, Meijboom FJ, Spitaels SE, et al. Decline in ventricular function and clinical condition after Mustard repair for transposition of the great arteries (a prospective study of 22-29 years). Eur Heart J 2004;25:1264-70.
67 Warnes CA. Transposition of the great arteries. Circulation 2006;114:2699-709.
68 Voskuil M, Hazekamp MG, Kroft LJ, et al. Postsurgical course of patients with congenitally corrected transposition of the great arteries. Am J Cardiol 1999;83:558-62.
69 Graham TP, Jr., Bernard YD, Mellen BG, et al. Long-term outcome in congenitally corrected transposition of the great arteries: a multi-institutional study. J Am Coll Cardiol 2000;36:255-61.
70 van Son JA, Danielson GK, Huhta JC, et al. Late results of systemic atrioventricular valve replacement in corrected transposition. J Thorac Cardiovasc Surg 1995;109:642-52.
71 Winter MM, Bernink FJ, Groenink M, et al. Evaluating the systemic right ventricle by CMR: the importance of consistent and reproducible delineation of the cavity. J Cardiovasc Magn Reson 2008;10:40.
72 Winter MM, Scherptong RW, Kumar S, et al. Ventricular response to stress predicts outcome in adult patients with a systemic right ventricle. Am Heart J 2010;160:870-6.
73 Giardini A, Lovato L, Donti A, et al. Relation between right ventricular structural alterations and markers of adverse clinical outcome in adults with systemic right ventricle and either congenital complete (after Senning operation) or congenitally corrected transposition of the great arteries. Am J Cardiol 2006;98:1277-82.
74 Fogel MA, Hubbard A, Weinberg PM. A simplified approach for assessment of intracardiac baffles and extracardiac conduits in congenital heart surgery with two- and three-dimensional magnetic resonance imaging. Am Heart J 2001;142:1028-36.
75 Fontan F, Baudet E. Surgical repair of tricuspid atresia. Thorax 1971;26:240-8.
76 d'Udekem Y, Iyengar AJ, Cochrane AD, et al. The Fontan procedure: contemporary techniques have improved long-term outcomes. Circulation 2007;116:I157-I164.
77 Fogel MA, Weinberg PM, Chin AJ, et al. Late ventricular geometry and performance changes of functional single ventricle throughout staged Fontan reconstruction assessed by magnetic resonance imaging. J Am Coll Cardiol 1996;28:212-21.
78 Lardo AC, del Nido PJ, Webber SA, et al. Hemodynamic effect of progressive right atrial dilatation in atriopulmonary connections. J Thorac Cardiovasc Surg 1997;114:2-8.
79 Fratz S, Hess J, Schwaiger M, et al. More accurate quantification of pulmonary blood flow by magnetic resonance imaging than by lung perfusion scintigraphy in patients with fontan circulation. Circulation 2002;106:1510-3.
80 Mitchell GF, Vita JA, Larson MG, et al. Cross-sectional relations of peripheral microvascular function, cardiovascular disease risk factors, and aortic stiffness: the Framingham Heart Study. Circulation 2005;112:3722-8.
81 Sutton-Tyrrell K, Najjar SS, Boudreau RM, et al. Elevated aortic pulse wave velocity, a marker of arterial stiffness, predicts cardiovascular events in well-functioning older adults. Circulation 2005;111:3384-90.
82 Brandts A, van Elderen SG, Westenberg JJ, et al. Association of aortic arch pulse wave velocity with left ventricular mass and lacunar brain infarcts in hypertensive patients: assessment with MR imaging. Radiology 2009;253:681-8.
83 Grotenhuis HB, Westenberg JJ, Steendijk P, et al. Validation and reproducibility of aortic pulse wave velocity as assessed with velocity-encoded MRI. J Magn Reson Imaging 2009;30:521-6.
84 Voges I, Jerosch-Herold M, Hedderich J, et al. Maladaptive aortic properties in children after palliation of hypoplastic left heart syndrome assessed by cardiovascular magnetic resonance imaging. Circulation 2010;122:1068-76.
85 Westenberg JJ, de Roos A., Grotenhuis HB, et al. Improved aortic pulse wave velocity assessment from multislice two-directional in-plane velocity-encoded magnetic resonance imaging. J Magn Reson Imaging 2010;32:1086-94.

86 Hope MD, Meadows AK, Hope TA, et al. Clinical evaluation of aortic coarctation with 4D flow MR imaging. J Magn Reson Imaging 2010;31:711-8.
87 Roes SD, Hammer S, van der Geest RJ, et al. Flow Assessment Through Four Heart Valves Simultaneously Using 3-Dimensional 3-Directional Velocity-Encoded Magnetic Resonance Imaging With Retrospective Valve Tracking in Healthy Volunteers and Patients With Valvular Regurgitation. Invest Radiol 2009.
88 Valverde I, Rachel C, Kuehne T, et al. Comprehensive four-dimensional phase-contrast flow assessment in hemi-Fontan circulation: systemic-to-pulmonary collateral flow quantification. Cardiol Young 2011;21:116-9.
89 van der Hulst AE, Westenberg JJ, Kroft LJ, et al. Tetralogy of fallot: 3D velocity-encoded MR imaging for evaluation of right ventricular valve flow and diastolic function in patients after correction. Radiology 2010;256:724-34.
90 Westenberg JJ, Roes SD, Ajmone MN, et al. Mitral valve and tricuspid valve blood flow: accurate quantification with 3D velocity-encoded MR imaging with retrospective valve tracking. Radiology 2008;249:792-800.
91 Nordmeyer S, Riesenkampff E, Crelier G, et al. Flow-sensitive four-dimensional cine magnetic resonance imaging for offline blood flow quantification in multiple vessels: a validation study. J Magn Reson Imaging 2010;32:677-83.
92 Alam M, Wardell J, Andersson E, et al. Right ventricular function in patients with first inferior myocardial infarction: assessment by tricuspid annular motion and tricuspid annular velocity. Am Heart J 2000;139:710-5.
93 Meluzin J, Spinarova L, Bakala J, et al. Pulsed Doppler tissue imaging of the velocity of tricuspid annular systolic motion; a new, rapid, and non-invasive method of evaluating right ventricular systolic function. Eur Heart J 2001;22:340-8.
94 Mogelvang R, Sogaard P, Pedersen SA, et al. Cardiac dysfunction assessed by echocardiographic tissue Doppler imaging is an independent predictor of mortality in the general population. Circulation 2009;119:2679-85.
95 Ypenburg C, Westenberg JJ, Bleeker GB, et al. Noninvasive imaging in cardiac resynchronization therapy--part 1: selection of patients. Pacing Clin Electrophysiol 2008;31:1475-99.
96 Delfino JG, Bhasin M, Cole R, et al. Comparison of myocardial velocities obtained with magnetic resonance phase velocity mapping and tissue Doppler imaging in normal subjects and patients with left ventricular dyssynchrony. J Magn Reson Imaging 2006;24:304-11.
97 Marsan NA, Westenberg JJ, Tops LF, et al. Comparison between tissue Doppler imaging and velocity-encoded magnetic resonance imaging for measurement of myocardial velocities, assessment of left ventricular dyssynchrony, and estimation of left ventricular filling pressures in patients with ischemic cardiomyopathy. Am J Cardiol 2008;102:1366-72.
98 Paelinck BP, de Roos A, Bax JJ, et al. Feasibility of tissue magnetic resonance imaging: a pilot study in comparison with tissue Doppler imaging and invasive measurement. J Am Coll Cardiol 2005;45:1109-16.
99 van der Hulst, Roest AA, Delgado V, et al. Corrected tetralogy of Fallot:comparison of tissue Doppler imaging and velocity-encoded MR for assessment of performance and temporal activation of right ventricle. Radiology 2011: doi: 10.1148/radiol.11101993
100 Paelinck BP, de Roos A, Bax JJ, et al. Feasibility of tissue magnetic resonance imaging: a pilot study in comparison with tissue Doppler imaging and invasive measurement. J Am Coll Cardiol 2005;45:1109-16.
101 Marsan NA, Westenberg JJ, Tops LF, et al. Comparison between tissue Doppler imaging and velocity-encoded magnetic resonance imaging for measurement of myocardial velocities, assessment of left ventricular dyssynchrony, and estimation of left ventricular filling pressures in patients with ischemic cardiomyopathy. Am J Cardiol 2008;102:1366-72.
102 Delfino JG, Bhasin M, Cole R, et al. Comparison of myocardial velocities obtained with magnetic resonance phase velocity mapping and tissue Doppler imaging in normal subjects and patients with left ventricular dyssynchrony. J Magn Reson Imaging 2006;24:304-11.
103 Jones M, Ferrans VJ. Myocardial degeneration in congenital heart disease. Comparison of morphologic findings in young and old patients with congenital heart disease associated with muscular obstruction to right ventricular outflow. Am J Cardiol 1977;39:1051-63.
104 Messroghli DR, Greiser A, Frohlich M, et al. Optimization and validation of a fully-integrated pulse sequence for modified look-locker inversion-recovery (MOLLI) T1 mapping of the heart. J Magn Reson Imaging 2007;26:1081-6.
105 Flett AS, Hayward MP, Ashworth MT, et al. Equilibrium contrast cardiovascular magnetic resonance for the measurement of diffuse myocardial fibrosis: preliminary validation in humans. Circulation 2010;122:138-44.
106 Broberg CS, Chugh SS, Conklin C, et al. Quantification of diffuse myocardial fibrosis and its association with myocardial dysfunction in congenital heart disease. Circ Cardiovasc Imaging 2010;3:727-34.

3.2

Direct comparison between tissue Doppler imaging and velocity-encoded magnetic resonance imaging for the assessment of performance and temporal activation of the right ventricle in corrected tetralogy of Fallot patients

Radiology 2011; 260: 88-97

A.E. van der Hulst
A.A.W. Roest
V. Delgado
L.J.M. Kroft
E.R. Holman
N.A. Blom
J.J. Bax
A. de Roos
J.J.M. Westenberg

ABSTRACT

Purpose: To compare velocity-encoded magnetic resonance imaging (VE-MRI) with tissue Doppler imaging (TDI) to assess right ventricular (RV) peak systolic velocities and timings in patients with corrected tetralogy of Fallot (cToF) and healthy subjects.

Materials and Methods: Local institutional review board approval was obtained, and patients or their parents gave informed consent. Thirty-three patients (20 male, 13 female; median age 12 years (11-15) [inter-quartile range]; range 8-18 years) and 19 controls (12 male, 7 female, median age 14 years (12-16), range 8-18 years) underwent VE-MRI and TDI. Peak systolic velocity and time to peak systolic velocity (expressed as percentage of cardiac cycle) were assessed at the RV free wall (RVFW) and RV outflow tract (RVOT). Data were analyzed using linear regression, paired and unpaired tests and Bland-Altman plots.

Results: Good correlation and agreement between the two techniques were observed. Peak systolic velocities: RVFW: r=0.95, mean difference -0.4cm/s, p<0.01, RVOT: r=0.95, mean difference -0.4 cm/s p=0.02. Timings: RVFW r=0.94, mean difference -0.2%, p=0.44, RVOT: r=0.89, mean difference -0.5%, p=0.01. Peak systolic velocities were reduced in cToF patients (RVFW: 8.2cm/s (6.4-9.7) vs. 12.4cm/s (10.8-13.8), p<0.01, RVOT: 4.7cm/s (4.1-7.2) vs. 10.2cm/s (8.7-11.2), p<0.01). A time delay between the RVFW and RVOT was observed, which was significantly shorter in cToF patients (5.9% (4.9-7.4) vs. 8.4% (6.6-12.4), p<0.01).

Conclusions: VE-MRI and TDI enable assessment of RV systolic performance and timing of velocities at the RVFW and RVOT in cToF patients. Both techniques can be used interchangeably to clinically assess velocities and timings of the RV.

INTRODUCTION

In patients after surgical correction of Tetralogy of Fallot (cToF), right ventricular (RV) dimensions and ejection fraction are important determinants of long-term outcome (1-3). However, these parameters evaluate RV function at a global level. In contrast, assessment of myocardial velocities with echocardiographic tissue Doppler imaging (TDI) permits evaluation of regional RV systolic function and characterization of the RV mechanical activation sequence by timing of peak systolic velocities. Previous studies have shown that assessment of RV myocardial velocities enables reliable quantification of RV performance in various clinical conditions (4-8). In cToF patients, abnormalities in timings of systolic events of the RV free wall (RVFW) and right ventricular outflow tract (RVOT) have been observed, which may contribute to RV failure in cToF patients (9,10). Therefore, comprehensive assessment of velocities and timings of the RVFW and RVOT may provide better understanding of RV failure in cToF patients. Cardiac magnetic resonance imaging (MRI) is the method of reference to assess RV dimensions and function in cToF patients (11). Recently, velocity- encoded MRI (VE-MRI) has been introduced to assess myocardial velocities. In the left ventricle (LV), VE-MRI has been validated against TDI for the assessment of myocardial velocities and timings of peak systolic velocities (12-15). In patients with cToF, the use of VE-MRI to assess myocardial velocities is of interest as it enables comprehensive assessment of RV function in cToF patients during a single integrated MRI examination. Thus far, the application of VE-MRI and TDI to assess RV velocities and timings in different regions of the RV has not been directly compared to our knowledge.
Accordingly, the aim of our study was to compare velocity-encoded magnetic resonance imaging with tissue Doppler imaging to assess peak systolic velocities and timings within the right ventricle in patients with a corrected tetralogy of Fallot and in healthy subjects.

MATERIALS AND METHODS

Study population

All participants or their parents gave written informed consent. Thirty-three patients with corrected tetralogy of Fallot (cToF) (mean age 13 years ± 3 [standard deviation]) were prospectively recruited. In addition, 19 healthy controls with a similar age range were enrolled in the study. All cToF patients and healthy controls underwent transthoracic echocardiography (including TDI) and MRI (including VE-MRI) on the same day. TDI and VE-MRI were performed to assess peak systolic velocities as well as the timing of peak systolic velocities at the RVFW and at the RVOT. The VE-MRI data and the TDI data were analyzed by A.E.v.d.H. (with 3 years experience in cardiac MRI and echocardiography). Inter-observer assessment of VE-MRI data was performed by A.A.W.R. (with 12 years experience in cardiac MRI). Correlation and agreement between TDI and VE-MRI measurements were assessed in the entire study cohort. Furthermore, the VE-MRI derived peak systolic velocities and the time difference between peak systolic velocities at the RVWF and RVOT were compared between cToF patients and controls.

Tissue Doppler imaging

Transthoracic echocardiography images were acquired by a single experienced sonographer (8 years experience in echocardiography) using a commercially available system equipped with a 3.5 MHz transducer (Vivid-7.0.0, GE Vingmed Ultrasound AS, Horten, Norway). Subjects were in the left lateral decubitus position during image acquisition. Acquisition of TDI images was performed with adjusted sector width and angle to align the ultrasound beam with the direction of the myocardial motion. The color frame rate was ≥120 frames/s, yielding a temporal resolution <8.3ms, and at least three consecutive beats were recorded. Analyses were performed off-line using EchoPac version 108.1.5 (General Electric Medical Systems). Longitudinal myocardial velocity curves were obtained by placing regions of interest (ROI) at the basal RVFW in the 4-chamber view (Figure 1, a and c) and at the lateral RVOT in a dedicated apical RVOT view (Figure 1, b and d), as previously reported (10). Semi-automated tissue tracking was used to maintain the sample area within the ROI throughout the cardiac cycle. Peak systolic velocity was measured at the RVFW (Figure 1c) and at the RVOT (Figure 1d).
In addition, time from R-wave of the ECG to peak systolic velocity was measured at both segments (Figure 1, c and d) and expressed as percentage of the RR interval to ensure accurate comparison of timings between the two techniques. Finally, the time difference between peak systolic velocity at the RVFW and peak systolic velocity at the RVOT was calculated in each cToF patient and control subject.

Magnetic resonance imaging

MRI was performed on a 1.5-Tesla pulsar gradient system (Intera, release 12; Philips Medical Systems, Best, the Netherlands) with 33 mT/m amplitude, 100 mT/m/ms slew rate, and 0.33 ms rise time. A five-element cardiac coil was used for signal reception. Multi-section transverse (16) cine imaging was performed to assess ventricular volumes and ejection fraction. A stack of slices was planned in the transversal plane, covering both ventricles throughout the cardiac cycle. Multi-section cine-images were acquired with a steady-state free precession sequence during breath hold at end-expiration, with scan parameters: repetition time (TR) 3.9ms, echo time (TE) 1.5ms, field of view 350mm; slice thickness 8mm; flip angle 50°; 1.8×2.0×8.0mm acquisition voxel reconstructed into a 1.4×1.4×8.0mm voxel; one signal acquired, 30 phases reconstructed, retrospective gating with 10% acceptance window.
VE-MRI was performed in a 4-chamber orientation for the assessment of longitudinal velocity data at the RVFW (Figure 2, a and c), and in a double oblique RVOT view for the assessment of longitudinal velocities at the RVOT (Figure 2, b and d). Imaging parameters for VE-MRI acquisition were: repetition time 5.4ms, echo time 3.4ms, flip angle 10°, slice thickness 8mm, matrix 128×128, field-of-view 370mm, actual temporal resolution 10.8ms. Retrospective triggering was used and data acquisition was performed during free breathing. Four signal averages were acquired to increase signal-to-noise ratio. Maximum velocity was set at 20cm/s to assess myocardial velocities. The maximum number of phases was reconstructed, yielding an effective temporal resolution in the velocity graph of approximately 10ms.

Magnetic resonance image analysis

All MRI data were analyzed using the MASS software package (Leiden University, Leiden, The Netherlands) (17). LV and RV end-systolic and end-diastolic volumes were calculated by summation of discs after manual tracing of the endocardial borders at end-systole and end-diastole in all transverse slices. RV and LV ejection fractions were then automatically calculated by the MASS software. For assessment of myocardial velocities, a ROI was placed in the VE-MRI images at the basal RVFW (Figure 2c) and the lateral wall of the RVOT (Figure 2d) in all phases. Manual positioning of the ROI was performed throughout the cardiac cycle to ensure data sampling within the myocardial wall. The average velocity within the ROI was recorded in every cardiac phase. Time-velocity graphs were constructed from the RVFW (Figure 2c) and lateral RVOT segments (Figure 2d). From these graphs, peak systolic velocity and time to peak systolic velocity were derived. Timings are expressed as percentage of the RR interval. In addition, the time difference between peak systolic velocity at the RVFW and peak systolic velocity at the RVOT was calculated in each cToF patient and control subject. Finally, intra-observer and inter-observer agreement for the VE-MRI measurements were assessed in a blinded manner, by re-measuring peak velocities and timings at the RVFW and RVOT in 15 randomly chosen individuals. Intra-observer agreement was evaluated by repeating measurements within one week interval.

Statistical analysis

Continuous variables were tested for normal ditriubution with the Kolmogorov-Smirnov test. Continuous variables with a normal distribution are expressed as mean ± standard deviation whereas those variables without normal distribution are expressed as median and IQR. Categorical variables are presented as numbers and percentages. Comparisons between cToF patients and controls were analyzed using the Mann-Whitney U-test for continuous data and the Fisher's exact test for categorical data. Comparisons between TDI and VE-MRI in the full population were analyzed using the paired t-test for normal distributed variables and with the Wilcoxon singed rank test for variables without a normal distribution. Linear regression analysis was used to evaluate the relation between TDI and VE-MRI. Logarithmic transformation was performed before linear regression analysis when variables were not normally distributed. Bland-Altman analysis was performed to assess the agreement between the two techniques. Intra-observer and inter-observer agreement of VE-MRI measurements was assessed using the intra-class correlation coefficient (ICC) for absolute agreement. Data were analyzed using the SPSS 17.0 software (SPSS Inc, Chicago, Illinois). A p-value of <0.05 was considered statistically significant and 95% confidence intervals (CI) were calculated.

RESULTS

Study population

Baseline characteristics of the cToF patients and controls are displayed in Table 1. cToF patients had significantly increased RV end-diastolic and RV end-systolic volumes (Table 1). Furthermore,

Table 1. Baseline characteristics

	cToF patient (n=33)	control (n=19)	p-value
Age (y)*	12 (11-15)	14 (12-16)	0.16
Gender male/female n (%)	20/13 (60/40)	12/7 (63/37)	0.55
QRS duration (ms)*	132 (120-150)	96 (90-100)	<0.01
Cardiac cycle (ms)	796 ± 127	848 ± 120	0.16
BSA (m^2)*	1.4 (1.2-1.7)	1.5 (1.4-1.7)	0.09
Age at corrective surgery (y)*	0.7 (0.5 - 1.1)	..	
Type of corrective surgery n (%)			
Infundibulectomy	7 (21)	..	
Transannular patch	20 (61)	..	
RVOT patch	3 (9)	..	
PA patch	3 (9)	..	
MRI			
LV-EDV (mL)*	117 (96-150)	141 (126-167)	0.03
LV-ESV (mL)*	52 (40-69)	62 (54-78)	0.05
LV-EF (%)*	57 (51-60)	55 (53-59)	0.89
RV-EDV (mL)*	171 (152-205)	149 (128-175)	0.03
RV-ESV (mL)*	90 (75-106)	72 (59-82)	0.02
RV-EF (%)*	48 (47-53)	53 (50-55)	0.01

Abbreviations: BSA: body surface area, EDV: end-diastolic volume, EF: ejection fraction, ESV: end-systolic volume, LV: left ventricle, PA: pulmonary artery, RV right ventricle, RVOT: right ventricular outflow tract. *median and inter-quartile range

RV ejection fraction was lower in cToF patients than in controls (median 48%, IQR: 47 to 53% vs. median 53% IQR 50 to 55%, p=0.01). All measurements at the RVFW and RVOT were feasible in each patient and control subject for both imaging techniques.

TDI versus VE-MRI: peak systolic velocities

Table 2 and Figure 3 summarize the relationship between TDI and VE-MRI to assess peak systolic velocities at the RVFW and RVOT. At the RVFW, a small difference between the techniques was observed. (Table 2) An excellent correlation between both techniques was observed in the full population (r=0.95, p<0.01) (Figure 3a). In addition, when the population was divided in cToF patients and controls, excellent correlations were observed between the two techniques (cToF patients r=0.91, p<0.01, controls r=0.90, p<0.01). Bland-Altman analysis showed limits of agreement of -2.3 to 1.5cm/s (Figure 3b). Finally, intra- and inter-observer agreement of VE-MRI assessment of peak systolic velocities at the RVFW yielded an intra-observer ICC of 0.97 (p<0.01) and an inter-observer ICC of 0.96 (p<0.01). At the RVOT, the assessment of peak systolic velocities yielded a small difference between the two techniques in the full population (Table 2). Furthermore, a strong correlation between TDI and VE-MRI was observed in the full population (r=0.95, p<0.01) (Figure 3c), as well as after dividing

the population in cToF patients and controls (cToF patients r=0.92, p<0.01, controls r=0.87, p<0.01). Figure 3d shows the Bland-Altman plots for VE-MRI and TDI agreement. Finally, good intra-observer and inter-observer agreement was noted for the assessment of peak systolic velocities at the RVOT (intra-observer ICC: 0.99, p<0.01, inter-observer ICC 0.97, p<0.01).

TDI versus VE-MRI: timing of peak systolic velocitis

Table 2 and Figure 4 show the relationship between TDI and VE-MRI to measure time to peak systolic velocity corrected by the RR interval. At the RVFW, no significant difference between the techniques was observed (Table 2). In addition, an excellent correlation between TDI and VE-MRI measurements at the RVFW was observed in the full population (r=0.94, p<0.01) (Figure 4a). Furthermore, good correlations between TDI and VE-MRI measurements were noted when the population was divided in cToF patients and controls (cToF patients r=0.86, p<0.01, controls r=0.92, p<0.01). Bland-Altman analysis showed narrow limits of agreement (-3.2 to 2.9%) (Figure 4b). Finally, intra-observer analysis of time to peak systolic velocity at the RVFW yielded an ICC of 0.96 (p<0.01). Assessment of inter-observer agreement of time to peak systolic velocity at the RVFW showed an ICC of 0.92 (p<0.01).

At the RVOT, a small difference between TDI and VE-MRI for time to peak systolic velocity at the RVOT was observed (Table 2). A strong correlation was observed between TDI and VE-MRI (r=0.89, p<0.01) (Figure 4c). After dividing the population in cToF patients and controls, good correlations between TDI and VE-MRI measurements were observed (cToF patients r=0.91, p<0.01, controls r=0.73, p<0.01). Bland-Altman analysis of agreement between VE-MRI and TDI to assess time to peak systolic velocity at the RVOT is displayed in Figure 4d. In addition, intra-observer agreement analysis of time to peak systolic velocity at the RVOT yielded an ICC of 0.89 (p<0.01). Inter-observer agreement of time to peak systolic velocity at the RVOT was 0.84 (p<0.01).

Table 2. Relationship between TDI and VE-MRI

	TDI	VE-MRI	mean difference	95% CI of difference	p-value	paired samples coefficient
Peak systolic velocity						
RVFW (cm/s)	9.1 ± 2.5	9.6 ± 3.0	-0.4 ± 1	-0.7 to -0.2	<0.01	0.95
RVOT (cm/s)*	6.4 (4.6-9.4)	6.6 (4.4-9.9)	-0.4 ± 1	..	0.02	0.95
Time to peak systolic velocity						
RVFW (%)	14.5 ± 4.3	14.7 ± 4.4	-0.2 ± 1.6	-0.6 to 0.3	0.44	0.94
RVOT (%)	6.7 ± 2.2	7.2 ± 2.4	-0.5 ± 1.1	-0.8 to -0.2	0.01	0.89
Time difference						
RVFW - RVOT (%)*	7.2 (5.1-10.1)	6.8 (5.3-9.2)	-0.4 ± 2	..	0.22	0.79

Timings are expressed as percentage of the RR interval. Abbreviations: CI: confidence interval, RVFW: right ventricular free wall, RVOT: right ventricular outflow tract, TDI: tissue Doppler imaging, VE-MRI: velocity encoded magnetic resonance imaging. *median and inter-quartile range

Figure 1.

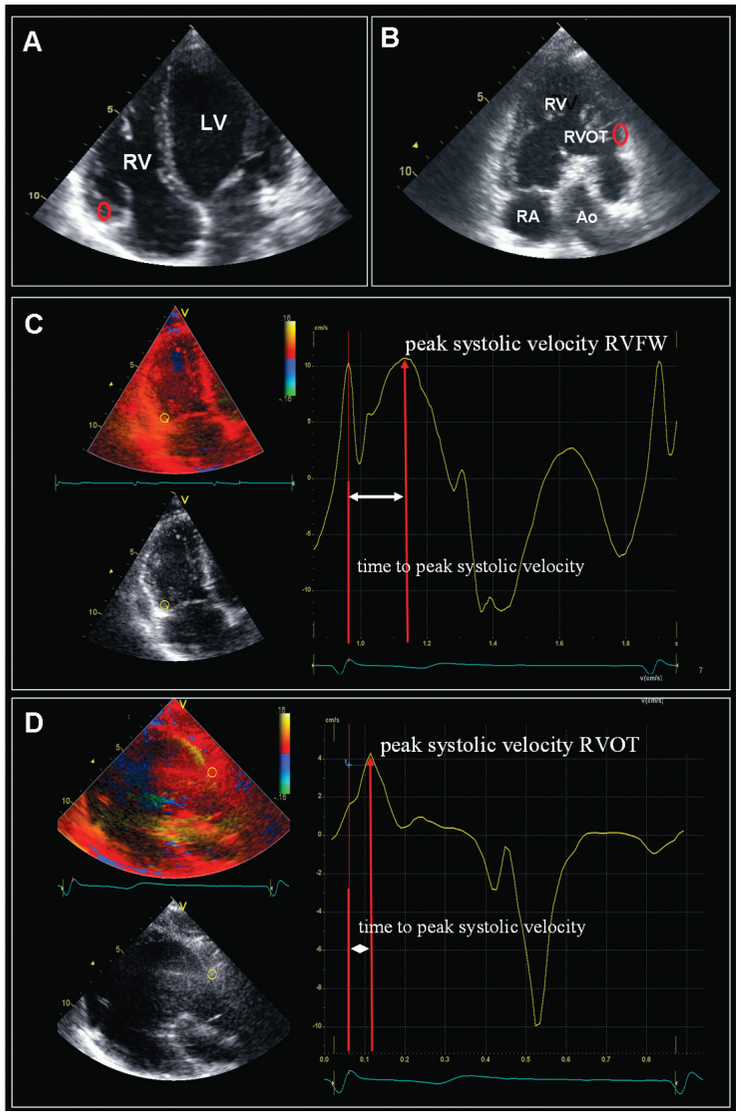

Image analysis of tissue Doppler images. **(a):** Echocardiographic 4-chamber view of a cToF patient. Red region of interest indicates RVFW myocardial segment where TDI measurements were performed. **(b):** Echocardiographic apical view of the RVOT of a cToF patient. Red region of interest indicates myocardial RVOT segment where TDI measurements were performed. **(c):** Example of TDI assessment of peak systolic velocity and time to peak systolic velocity at the RVFW in a cToF patient. Peak systolic velocity can be derived from the time-velocity curve (vertical arrow). Time to peak systolic velocity can be measured by calculating time from R to peak systolic velocity (horizontal arrow). **(d):** Example of TDI assessment of peak systolic velocity and time to peak systolic velocity at the RVOT in a cToF patient. Peak systolic velocity can be derived from the time-velocity curve (vertical arrow). Time to peak systolic velocity can be measured by calculating time from R to peak systolic velocity (horizontal arrow). Abbreviations: Ao: aorta, LV: left ventricle, RA: right atrium, RV: right ventricle, RVOT: right ventricular outflow tract.

Figure 2.

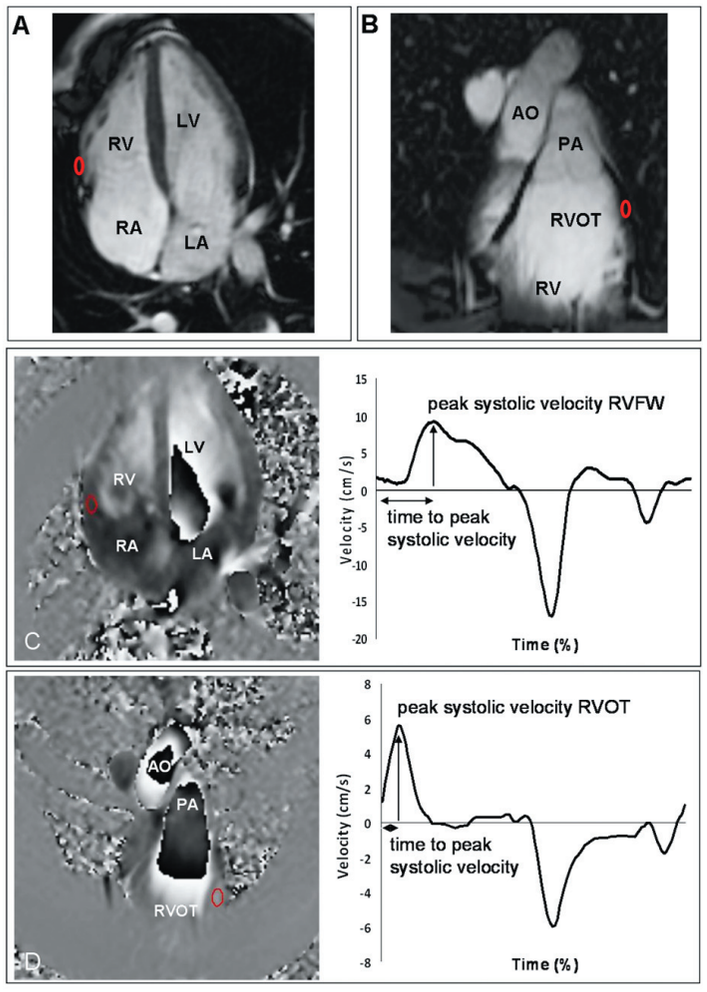

Image analysis of velocity-encoded MRI images. **(a):** Example of anatomic location of myocardial RVFW segment where measurements were performed. Cine image of 4-chamber view (repetition time (TR) 3.9 ms, echo time (TE) 1.5 ms, flip angle 50°). Red region of interest indicates myocardial segment where velocity-encoded measurements were performed. **(b):** Example of anatomic location of myocardial RVOT segment where measurements were performed. Cine image of double oblique RVOT view, red region of interest indicates myocardial segment where velocity-encoded measurements were performed. **(c):** Velocity-encoded image of 4-chamber view. (TR: 5.4 ms, TE: 3.4 ms, flip angle 10°) Velocity is encoded in longitudinal direction. A region of interest (red) is positioned at the basal RVFW in all cardiac phases. The average velocity at the region of interest is calculated in every phase, and can be displayed in a time-velocity curve, from which peak systolic velocity at the RVFW and time to peak systolic velocity at the RVFW can be derived. **(d):** Velocity-encoded image of RVOT. Velocity is encoded in longitudinal direction. A region of interest (red) is positioned at the lateral wall of the RVOT in all cardiac phases. The average velocity at the region of interest is calculated in every phase, and can be displayed in a time-velocity curve, from which peak systolic velocity at the RVOT and time to peak systolic velocity at the RVOT can be derived.
Abbreviations: Ao: Aorta, LA: left atrium, LV: left ventricle, PA: pulmonary artery, RA: right atrium, RV: right ventricle, RVFW: right ventricular free wall, RVOT: right ventricular outflow tract.

Finally, the time difference between time to peak systolic velocity at the RVFW and at the RVOT was calculated and compared between TDI and VE-MRI. The difference between the two techniques was not statistically significant (Table 2). An excellent correlation was observed between the two techniques for the overall population (r=0.79, p<0.01) and after dividing the population in patients and controls (cToF patient: r=0.75, p<0.01, control r=0.76, p<0.01). Finally, Bland-Altman analysis yielded narrow limits of agreement (-3.6 to 4.4%).

Patients versus controls: VE-MRI peak systolic velocities and timing of velocitiess

The VE-MRI derived peak systolic velocities and time differences between the RVWF and RVOT were compared between cToF patients and controls. The peak systolic velocity at the RVFW was significantly reduced in cToF patients (median: 8.2cm/s, IQR: 6.4 to 9.7cm/s vs. median 12.4cm/s, IQR 10.8 to 13.8cm/s, p<0.01). Similarly, at the RVOT, the peak systolic velocity was reduced in cToF patients (median 4.7cm/s, IQR: 4.1 to 7.2, vs. median 10.2cm/s, IQR: 8.7 to 11.2cm/s, p<0.01). Finally, the time difference between peak systolic velocity at the RVFW and the RVOT was significantly shorter in cToF patients as compared with controls (median 5.9%, IQR: 4.9 to 7.4%, vs. median 8.4%, IQR: 6.6 to 12.4%, p<0.01).

DISCUSSION

Our study provides a direct comparison of tissue Doppler imaging and velocity-encoded magnetic resonance imaging to assess peak systolic velocities and timings of the right ventricular free wall and right ventricular outflow tract in patients with a corrected tetralogy of Fallot and in healthy subjects. The main findings of the present study are: 1) velocity-encoded magnetic resonance imaging and tissue Doppler imaging have a strong correlation and a good agreement for the assessment of peak systolic velocities and timings at the right ventricular free wall and right ventricular outflow tract in patients with corrected tetralogy of Fallot as well as in healthy subjects 2) both velocity-encoded magnetic resonance imaging and tissue Doppler imaging showed reduced peak systolic velocities in patients with corrected tetralogy of Fallot at the right ventricular free wall as well as at the right ventricular outflow tract 3) velocity-encoded magnetic resonance imaging showed that the time difference between peak systolic velocity at the right ventricular free wall and the right ventricular outflow tract was significantly reduced in patients with corrected tetralogy of Fallot.

VE-MRI: peak systolic velocities

Evaluation of peak myocardial systolic velocities enables quantitative assessment of RV performance. Meluzin and co-workers demonstrated a close relationship between peak systolic velocity at the tricuspid valve annulus and RV ejection fraction in healthy subjects as well as in patients with LV failure (7). In addition, in patients with inferior myocardial infarction, Alam et al. demonstrated that measurement of tricuspid valve annular velocities with TDI enabled differentiation between patients

Figure 3.

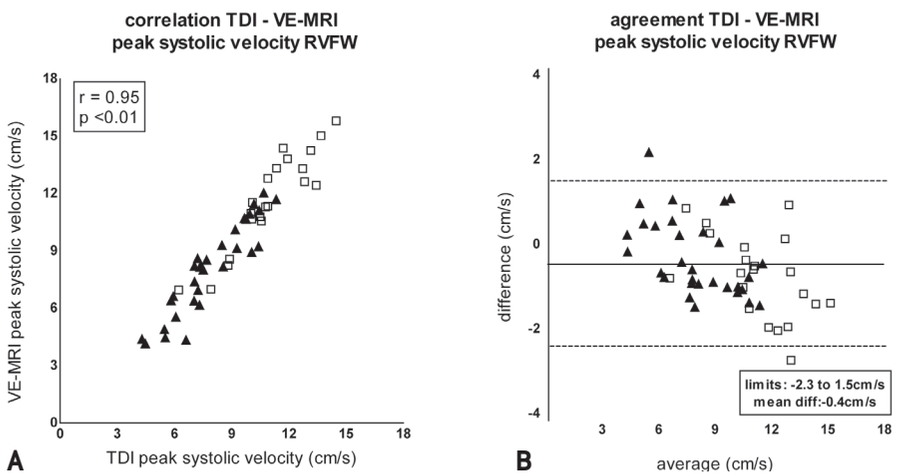

Correlation and agreement between TDI and VE-MRI for the assessment of peak systolic velocities at the RVFW and RVOT. **(a):** Correlation between TDI and VE-MRI for the assessment of peak systolic velocity at the RVFW. **(b):** Agreement between TDI and VE-MRI for the assessment of peak systolic velocity at the RVFW. **(c):** Correlation between log TDI and log VE-MRI for the assessment of peak systolic velocity at the RV outflow tract. **(d):** Agreement between TDI and VE-MRI for the assessment of peak systolic velocity at the RV outflow tract. Triangles: cToF patients, squares: controls.
Abbreviations: RVFW: right ventricular free wall, RVOT: right ventricular outflow tract, TDI: tissue Doppler imaging, VE-MRI: velocity-encoded magnetic resonance imaging.which peak systolic velocity at the RVOT and time to peak systolic velocity at the RVOT can be derived.
Abbreviations: RVFW: right ventricular free wall, RVOT: right ventricular outflow tract.

Figure 4.

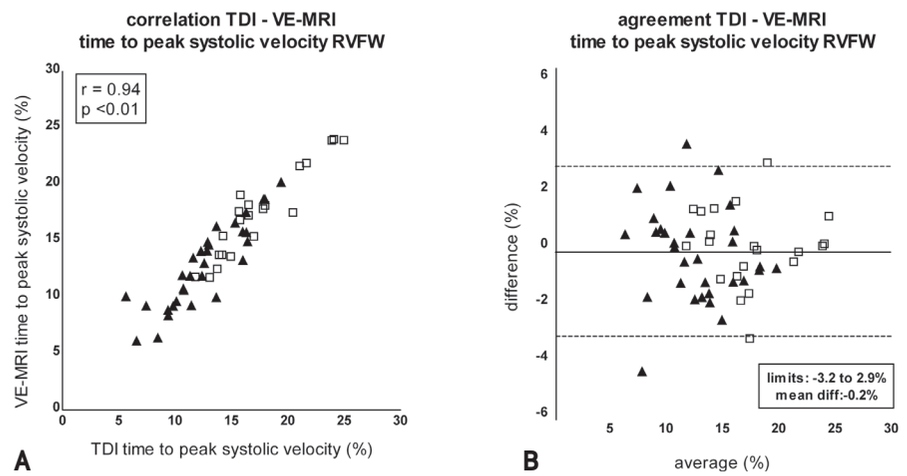

Correlation and agreement between TDI and VE-MRI for the assessment of time to peak velocity at the RVFW and at the RVOT. **(a):** Correlation between TDI and VE-MRI for the assessment of time to peak systolic velocity at the RVFW. **(b):** Agreement between TDI and VE-MRI for the assessment of time to peak systolic velocity at the RVFW. **(c):** Correlation between TDI and VE-MRI for the assessment of time to peak systolic velocity at the RV outflow tract. **(d):** Agreement between TDI and VE-MRI for the assessment of time to peak systolic velocity at the RV outflow tract. Timings are expressed as percentage of the RR interval. Triangles: cToF patients, squares: controls. Abbreviations: RVFW: right ventricular free wall, RVOT: right ventricular outflow tract, TDI: tissue Doppler imaging, Ts: time to peak systolic velocity, VE-MRI: velocity encoded magnetic resonance imaging.
Abbreviations: RVFW: right ventricular free wall, RVOT: right ventricular outflow tract.

with and without RV dysfunction (4). In cToF patients, RV dysfunction is commonly observed (1). Cardiac MRI currently is the reference standard to measure volumes and ejection fraction of the RV (11). However, this parameter of RV function may be influenced by pulmonary regurgitation, commonly observed in this group of patients (18). In contrast, assessment of myocardial velocities is much less affected by loading conditions (19) and, therefore, it may provide a more accurate and reliable quantification of RV performance. In addition, myocardial velocities can be assessed at the regional level, providing more detailed information on systolic performance of the different RV components.
Recently, VE-MRI was evaluated against TDI to assess LV myocardial velocities (12-15). However, no studies on VE-MRI for the assessment of RV myocardial velocities are available, to our knowledge. Our study provides a comparison of VE-MRI and TDI in healthy subjects and in cToF patients to assess myocardial velocities at the RVFW as well as at the RVOT. Excellent correlations between the two techniques were observed. A small difference between TDI and VE-MRI was observed, with VE-MRI slightly exceeding TDI velocities at both RV regions. The small bias may be explained by acoustic window limitations of TDI, preventing optimal alignment of the ultrasound beam with the myocardial wall in some patients. This may result in an underestimation of peak velocity. Other possible sources of bias may be phase errors or partial volume effects by VE-MRI, or technical differences between TDI (acquiring real-time velocities) and VE-MRI (acquiring a retrospectively-reconstructed time-velocity graph, averaged over 2-3 minutes). However, the observed statistical bias was small (≤0.7cm/s) and unlikely to be of any clinical relevance.

VE-MRI: timing of peak systolic velocities

In addition to the evaluation of myocardial velocities, VE-MRI has been shown to be a reliable tool for the assessment of timings and dyssynchrony of the LV (13,15). The use of VE-MRI to assess RV timings and possible dyssynchrony has not been studied, to our knowledge. Our study compared VE-MRI with TDI to assess timings of the RVFW and RVOT in healthy controls as well as in cToF patients. VE-MRI showed close correlation and agreement with TDI at both RV regions. At the RVOT, a small difference between VE-MRI and TDI was observed (0.5%). However, with an average cardiac cycle length of 800ms in our subjects, this difference equals approximately to 4ms, which is smaller than the temporal resolution of either technique. Moreover, the assessment of a time difference between the RVFW and the RVOT was highly concordant between TDI and VE-MRI, without a significant difference between the two techniques.

VE-MRI velocities and timings; cToF patients versus controls

In cToF patients, RV dysfunction is commonly observed as a result of volume overload due to pulmonary regurgitation (1,3). Although MRI derived RV end-diastolic volume and ejection fraction are important parameters for clinical decision making in these patients, the exact pathophysiological mechanisms leading to RV failure remain to be elucidated to our knowledge (20). The study of regional peak systolic velocities may contribute to a better understanding of RV failure. A recent study observed reduced velocities at the RVFW in 25 asymptomatic adult cToF patients as compared with 25 healthy controls (5). Our study confirms this finding in young cToF patients. In addition, our study extends these findings by assessing myocardial velocities and timings at the RVOT. In tetralogy of Fallot patients, surgical correction involves relief of the pulmonary stenosis by transannular patching or infundibulectomy. As a result, functional abnormalities of the RVOT are often observed, which have been related to RV performance (10,21). In our study, a reduced peak systolic velocity was observed in cToF patients, providing further evidence of abnormal mechanical performance of the RVOT in these patients.
Finally, time differences between peak systolic velocities at the RVFW and RVOT were evaluated. Investigation of the mechanical activation of the RV may help improve the results of different pacing strategies. The detrimental effects of RV apical pacing have been extensively demonstrated (22-24). In addition, the benefits of cardiac resynchronization therapy (CRT) may be maximized if the mechanical activation sequence of the RV is fully understood. Currently, little is known about the mechanical activation pattern of the different RV regions in either healthy subjects or cToF patients. In our study, a time delay between peak systolic velocity at the RVFW and RVOT was observed both cToF patients and controls. This presence of a time delay within the healthy RV confirms the findings of previous authors (9,10,25). In addition, the time delay within the RV was significantly shortened in cToF patients. These findings may have important clinical implications, as the pathophysiological basis of CRT is restoration of a synchronous contraction pattern and possibly, this concept may not be applied to the RV. In future studies, VE-MRI and TDI should be employed to investigate the RV mechanical activation pattern and its relation with RV performance.

Study limitations

The observed statistical differences in timings of peak systolic velocities at the RVFW and RVOT between VE-MRI and TDI could have resulted from a difference in temporal resolution between the techniques. Nevertheless, the difference in temporal resolution between the techniques was very small (2.5 ms) and therefore unlikely to be relevant in clinical practice.
In conclusion, VE-MRI and TDI can be used interchangeably for the clinical assessment of myocardial velocities and timings of the RV in healthy subjects as well as in cToF patients. Using VE-MRI, significant differences were detected in myocardial velocities as well as timings of the RVFW and RVOT between cToF patients and controls. The assessment of timings of peak velocities at the RVFW and RVOT can aid in future research on the mechanical activation pattern of the RV in healthy subjects and in cToF patients.

REFERENCE LIST

1. Geva T, Sandweiss BM, Gauvreau K, Lock JE, Powell AJ. Factors associated with impaired clinical status in long-term survivors of tetralogy of Fallot repair evaluated by magnetic resonance imaging. J Am Coll Cardiol 2004;43:1068-1074.
2. Knauth AL, Gauvreau K, Powell AJ, et al. Ventricular size and function assessed by cardiac MRI predict major adverse clinical outcomes late after tetralogy of Fallot repair. Heart 2008;94:211-216.
3. Niezen RA, Helbing WA, van der Wall EE, et al. Biventricular systolic function and mass studied with MR imaging in children with pulmonary regurgitation after repair for tetralogy of Fallot. Radiology 1996;201:135-140.
4. Alam M, Wardell J, Andersson E, Samad BA, Nordlander R. Right ventricular function in patients with first inferior myocardial infarction: assessment by tricuspid annular motion and tricuspid annular velocity. Am Heart J 2000;139:710-715.
5. Brili S, Alexopoulos N, Latsios G, et al. Tissue Doppler imaging and brain natriuretic peptide levels in adults with repaired tetralogy of Fallot. J Am Soc Echocardiogr 2005;18:1149-1154.
6. Ishii H, Harada K, Toyono M, Tamura M, Takada G. Usefulness of exercise-induced changes in plasma levels of brain natriuretic peptide in predicting right ventricular contractile reserve after repair of tetralogy of Fallot. Am J Cardiol 2005;95:1338-1343.
7. Meluzin J, Spinarova L, Bakala J, et al. Pulsed Doppler tissue imaging of the velocity of tricuspid annular systolic motion; a new, rapid, and non-invasive method of evaluating right ventricular systolic function. Eur Heart J 2001;22:340-348.
8. Rydman R, Larsen F, Caidahl K, Alam M. Right ventricular function in patients with pulmonary embolism: early and late findings using Doppler tissue imaging. J Am Soc Echocardiogr 2010;23:531-537.
9. Matsui H, Satomi G, Yasukochi S, Kaneko S, Haseyama K. Evaluation of right ventricular contraction by myocardial strain in children using a two-dimensional tissue tracking method. Pediatr Cardiol 2008;29:377-381.
10. Uebing A, Gibson DG, Babu-Narayan SV, et al. Right ventricular mechanics and QRS duration in patients with repaired tetralogy of Fallot: implications of infundibular disease. Circulation 2007;116:1532-1539.
11. Pennell DJ, Sechtem UP, Higgins CB, et al. Clinical indications for cardiovascular magnetic resonance (CMR): Consensus Panel report. J Cardiovasc Magn Reson 2004;6:727-765.
12. elfino JG, Bhasin M, Cole R, et al. Comparison of myocardial velocities obtained with magnetic resonance phase velocity mapping and tissue Doppler imaging in normal subjects and patients with left ventricular dyssynchrony. J Magn Reson Imaging 2006;24:304-311.
13. Marsan NA, Westenberg JJ, Tops LF, et al. Comparison between tissue Doppler imaging and velocity-encoded magnetic resonance imaging for measurement of myocardial velocities, assessment of left ventricular dyssynchrony, and estimation of left ventricular filling pressures in patients with ischemic cardiomyopathy. Am J Cardiol 2008;102:1366-1372.
14. Paelinck BP, de Roos A, Bax JJ, et al. Feasibility of tissue magnetic resonance imaging: a pilot study in comparison with tissue Doppler imaging and invasive measurement. J Am Coll Cardiol 2005;45:1109-1116.
15. Westenberg JJ, Lamb HJ, van der Geest RJ, et al. Assessment of left ventricular dyssynchrony in patients with conduction delay and idiopathic dilated cardiomyopathy: head-to-head comparison between tissue doppler imaging and velocity-encoded magnetic resonance imaging. J Am Coll Cardiol 2006;47:2042-2048.
16. Fratz S, Schuhbaeck A, Buchner C, et al. Comparison of accuracy of axial slices versus short-axis slices for measuring ventricular volumes by cardiac magnetic resonance in patients with corrected tetralogy of fallot. Am J Cardiol 2009;103:1764-1769.
17. van der Geest RJ, Buller VG, Jansen E, et al. Comparison between manual and semiautomated analysis of left ventricular volume parameters from short-axis MR images. J Comput Assist Tomogr 1997;21:756-765.
18. Vliegen HW, van Straten A, de Roos A, et al. Magnetic resonance imaging to assess the hemodynamic effects of pulmonary valve replacement in adults late after repair of tetralogy of fallot. Circulation 2002;106:1703-1707.
19. Royse CF, Connelly KA, MacLaren G, Royse AG. Evaluation of echocardiography indices of systolic function: a comparative study using pressure-volume loops in patients undergoing coronary artery bypass surgery. Anaesthesia 2007;62:109-116.
20. Henkens IR, van SA, Schalij MJ, et al. Predicting outcome of pulmonary valve replacement in adult tetralogy of Fallot patients. Ann Thorac Surg 2007;83:907-911.
21. Oosterhof T, Mulder BJ, Vliegen HW, de Roos A. Corrected tetralogy of Fallot: delayed enhancement in right ventricular outflow tract. Radiology 2005;237:868-871.
22. ops LF, Schalij MJ, Bax JJ. The effects of right ventricular apical pacing on ventricular function and dyssynchrony implications for therapy. J Am Coll Cardiol 2009;54:764-776.
23. Vanagt WY, Prinzen FW, Delhaas T. Physiology of cardiac pacing in children: the importance of the ventricular pacing site. Pacing Clin Electrophysiol 2008;31 Suppl 1:S24-S27.
24. Vatasescu R, Shalganov T, Paprika D, et al. Evolution of left ventricular function in paediatric patients with permanent right ventricular pacing for isolated congenital heart block: a medium term follow-up. Europace 2007;9:228-232.
25. Geva T, Powell AJ, Crawford EC, Chung T, Colan SD. Evaluation of regional differences in right ventricular systolic function by acoustic quantification echocardiography and cine magnetic resonance imaging. Circulation 1998;98:339-345.

3.3

Validation and application of tissue-velocity magnetic resonance imaging and tissue Doppler imaging for the assessment of regional myocardial diastolic velocities at the right ventricle in corrected tetralogy of Fallot patients

Submitted

A.E. van der Hulst
J.J.M. Westenberg
V. Delgado
L.J.M. Kroft
E.R. Holman
N.A. Blom
J.J. Bax
A. de Roos
A.A.W. Roest

ABSTRACT

Objectives: In patients with corrected tetralogy of Fallot (cToF), pulmonary regurgitation and subsequent increased right ventricular (RV) end-diastolic volume are diastolic parameters related to adverse outcome. In addition, abnormalities of the RV outflow tract (RVOT) independently promote RV dilatation in cToF patients. Tissue Doppler imaging (TDI) and tissue-velocity magnetic resonance imaging (TV-MRI) enable quantitative assessment of regional diastolic performance by measuring myocardial velocities. Assessment of regional diastolic velocities of the RV may provide insight into the relation between RVOT dysfunction and RV dilatation in cToF patients. The aim of the study was to perform a direct comparison of TV-MRI against TDI to assess regional RV diastolic velocities in cToF patients and control subjects. In addition, the relationship between regional RV diastolic velocities and RV dilatation was investigated.

Materials and methods: Thirty-four cToF patients (8-18 years) and 19 controls were studied. Early (E') and late (A') peak diastolic velocity and E'/A' were assessed with TDI and TV-MRI at the RV free wall (RVFW) and at the RVOT. RV volumes and pulmonary regurgitation were quantified with planimetric and three-dimensional flow MRI, respectively.

Results: Good correlation and agreement were observed between TDI and TV-MRI at both regions of the RV (RVFW: E': r=0.92, mean bias: 0.5 cm/s, A': r=0.92, mean bias: 0.4 cm/s; RVOT: E': r=0.92, mean bias: -0.3 cm/s, A': r=0.95, mean bias: 0.03 cm/s). With both imaging techniques, regional RV diastolic velocities were significantly reduced in cToF patients. The E'/A' ratio at the RVOT (assessed with both TDI and TV-MRI) was related to RV end-diastolic volume, even after correction for pulmonary regurgitation (TDI: $p<0.01$, TV-MRI: $p=0.05$).

Conclusions: TDI and TV-MRI can be used interchangeably for the assessment of regional diastolic velocities and performance of the RV in cToF patients and in healthy controls. Regional diastolic velocities at the RVOT are reduced in cToF patients as compared with controls. In addition to pulmonary regurgitation, impaired diastolic performance at the RVOT is independently related to RV dilatation.

INTRODUCTION

Tetralogy of Fallot (ToF) is the most common cyanotic congenital heart disease. Patients with ToF present with a ventricular septum defect (VSD), overriding of the aorta, pulmonary stenosis, and right ventricular hypertrophy. In current clinical practice, ToF patients are surgically corrected in the first year of life. Correction is performed by closure of the VSD and relief of the pulmonary stenosis by infundibulectomy and/or patch placement at the right ventricular outflow tract (RVOT). In ToF patients after surgical correction (cToF), pulmonary regurgitation is commonly observed.[1]
During long-term follow-up of cToF patients, right ventricular (RV) dilatation is related to poor clinical outcome in cToF patients.[1] Chronic volume overload due to pulmonary regurgitation is recognized as an important factor causing RV dilatation in cToF patients.[1,2] However, various studies have demonstrated that, in addition to pulmonary regurgitation, functional abnormalities of the RVOT after surgical repair independently promote RV dilatation in cToF patients.[3-5]In the presence of pulmonary regurgitation, the diastolic filling pattern of the RV is altered. Abnormalities of the RV diastolic function are commonly observed in cToF patients with pulmonary regurgitation. However, the clinical implications of global diastolic dysfunction, including a restrictive RV filling pattern, in cToF patients remain unclear.[6-9] In addition, regional diastolic function of the RV and specifically, of the RVOT has not been investigated so far. Therefore, assessment of diastolic velocities at the level of the RVOT may provide further insight into the relation between RVOT dysfunction and RV dilatation in cToF patients with pulmonary regurgitation.
Novel imaging techniques, such as tissue Doppler imaging (TDI) and tissue-velocity magnetic resonance imaging (TV-MRI) enable quantitative assessment of diastolic performance by measuring myocardial velocities.[10, 11] Regional diastolic myocardial velocities as assessed with TDI and TV-MRI have not been evaluated in cToF patients, to our knowledge. Accordingly, the aim of the current study was to perform a head-to-head comparison between TV-MRI and TDI to investigate the performance of these techniques to assess regional RV diastolic velocities at the RV free wall (RVFW) and at the RVOT in cToF patients and control subjects with structurally normal hearts. In addition, the relationship between regional RV diastolic velocities and RV dilatation was investigated.

METHODS

Patient population and data collection

Thirty-four cToF patients were prospectively enrolled in the current study. Patients after pulmonary valve replacement or any contraindications for cardiac MRI, such as claustrophobia, pacemaker devices and arrhythmia were excluded. In addition, 19 healthy controls with a similar age range were included in the study. Part of the population included in the present study formed part of the patient population of a previously published study.[9] All cToF patients and healthy controls underwent transthoracic echocardiography (including TDI) and cardiac MRI (including planimetry, TV-MRI and three-dimensional (3D) flow assessment) at the same day. With TDI and TV-MRI, early (E') and late (A') diastolic myocardial velocities and the E'/A' ratio were measured at the RVFW and at the RVOT. RV dilatation and pulmonary regurgitation were detected and quantified by planimetric MRI and novel 3D flow MRI, respectively.[9, 12]
A head-to-head comparison between TDI and TV-MRI for the assessment of regional diastolic velocities of the RV was performed. In addition, regional diastolic velocities measured with both techniques were compared between cToF patients and controls. Finally, the relationship between regional diastolic velocities and indexed RV end-diastolic volume was investigated, taking into account the relationship between pulmonary regurgitation and RV dilatation. The study protocol was approved by the institutional review board, and all cToF patients and controls or their parents gave written informed consent.

Table 1. cToF patient and control characteristics

	cToF patients	controls	p-value
Age (y)	13 ± 3	14 ± 2	0.254
Male/female n (%)	19/15 (60/40)	12/7 (63/37)	0.606
BSA (m²)	1.4 ± 0.3	1.6 ± 0.3	0.075
Age at surgical correction (y)*	0.8 ± 0.4	..	
Type of surgery n (%)*			
transannular patch	22 (67)	..	
Infundibulectomy	5 (15)	..	
RVOT or PA patch	6 (18)	..	
RV-EDV (ml/m²)	135 ± 35	99 ± 14	<0.001
RV-ESV (ml/m²)	69 ± 21	47 ± 10	<0.001
RV-EF (%)	50 ± 6	53 ± 4	0.027
PV forward flow (ml)	96 ± 30	77 ± 18	0.013
End diastolic forward flow n (%)	14 (41)	..	
PR fraction (%)	29 ± 15	0.2 ± 0.6	<0.001

Abbreviations: BSA: body surface area, EDV: end-diastolic volume, EF: ejection fraction; ESV: end-systolic volume, PR: pulmonary regurgitation, PV: pulmonary valve, RV: right ventricular. *Surgical records about age at correction and type of surgery were unknown for one patient.

Echocardiography: tissue Doppler imaging

Transthoracic echocardiography images were acquired by a single experienced sonographer using a commercially available system equipped with a 3.5 MHz transducer (Vivid-7, GE Vingmed Ultrasound AS, Horten, Norway). Subjects were in the left lateral decubitus position during image acquisition. Standard two-dimensional gray-scale images were acquired from the parasternal (long- and short-axis) and apical views (2-, 4-chamber and long-axis) and digitally stored in cine-loop format. Acquisition of TDI images was performed in the apical 4-chamber view for the assessment of diastolic velocities at the basal RVFW, (Figure 1, panel A) and in a dedicated apical RVOT view for the assessment of diastolic velocities at the RVOT as previous reported (Figure 1, panel

Table 2. Comparisons of flow volumes between 2D VE-MRI, 3D VE-MRI and planimetry

	cToF patients	controls	p-value
RVFW			
E' (cm/s)			
TDI	-9.9 ± 2.7	-12.6 ± 2.0	<0.001
TV-MRI	-10.2 ± 2.7	-13.3 ± 2.2	<0.001
A' (cm/s)			
TDI	-4.2 ± 1.5	-6.3 ± 1.4	<0.001
TV-MRI	-4.6 ± 1.8	-6.7 ± 1.6	<0.001
E'/A'			
TDI*	2.4 (2.0 – 3.1)	2.0 (1.7 – 2.4)	0.038
TV-MRI*	2.3 (1.8 – 2.9)	1.9 (1.7 – 2.6)	0.095
RVOT			
E' (cm/s)			
TDI	-6.6 ± 2.1	-7.9 ± 1.8	0.041
TV-MRI	-6.4 ± 2.1	-7.5 ± 2.1	0.071
A' (cm/s)			
TDI	-1.8 ± 1.3	-3.1 ± 1.1	0.002
TV-MRI	-1.9 ± 1.3	-3.1 ± 1.1	0.002
E'/A'			
TDI*	4.0 (2.6 – 7.7)	2.9 (1.9 – 3.7)	0.015
TV-MRI*	3.7 (2.5 – 5.8)	2.5 (1.9 – 3.3)	0.008

Abbreviations: A': peak late diastolic velocity, E': peak early diastolic velocity, RVFW: right ventricular free wall, RVOT: right ventricular outflow tract, TDI: tissue Doppler imaging, TV-MRI: tissue-velocity magnetic resonance imaging. * data presented as median and inter-quartile range.

B).[13, 14] The transducer was placed at the apex of the heart and then aligned with the longitudinal axis of the RVOT. A previous study published TDI data obtained from the apical RVOT view with good reproducibility.[13] Sector width and angle were adjusted to align the ultrasound beam with the direction of the myocardial motion. Images were recorded during breath-hold to minimize translational motion. The color frame rate was ≥120 frames/s (temporal resolution 8.3 ms), and three consecutive beats were recorded. The acquisition time of the TDI images was approximately one minute per image.

Analysis of TDI images was performed off-line using EchoPac version 108.1.5 (General Electric Medical Systems, Horten, Norway). Longitudinal myocardial velocity curves were obtained by placing regions of interest (5 x 5 mm) at the basal RVFW in the apical 4-chamber view (Figure 1A, right panel) and at the lateral RVOT in the apical RVOT view (Figure 1B, right panel). The basal RVFW

Figure 1. TDI images of RVFW and RVOT in a cToF patient

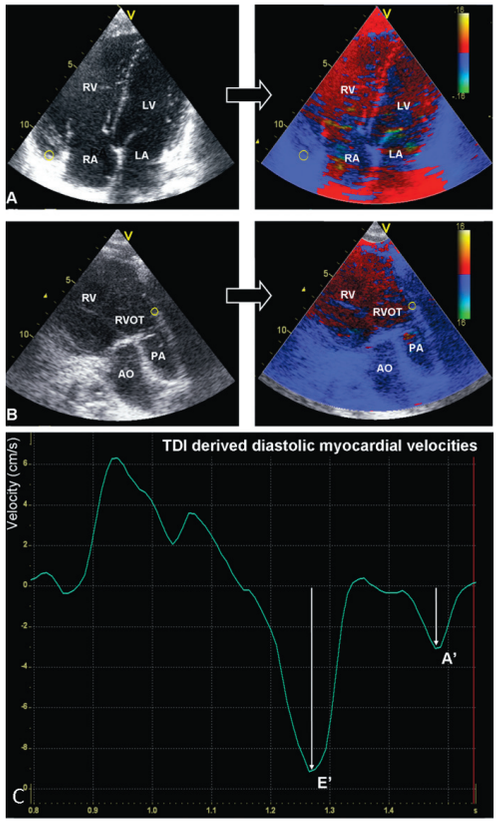

Panel A: Left: gray-scale echocardiographic image of a 4-chamber view. Right: TDI image of a 4-chamber view. A yellow region of interest is indicated at the myocardial wall of the basal RVFW, from which the velocity curve is derived. **Panel B:** Left: gray-scale echocardiographic of dedicated RVOT view. Right: TDI image of RVOT view. A yellow region of interest is indicated at the myocardial wall of the lateral RVOT, from which the velocity curve is derived. **Panel C:** TDI derived velocity curve of the RVFW in a cToF patient. White arrows indicate E' and A'.
Abbreviations: A': peak late diastolic velocity, AO: Aorta, E': peak early diastolic velocity, LA: left atrium, LV: left ventricle, PA: pulmonary artery, RA: right atrium, RV: right ventricle, RVOT: right ventricular outflow tract, TDI: tissue Doppler imaging.

Figure 2. TV-MRI images of RVFW and RVOT in a cToF patient

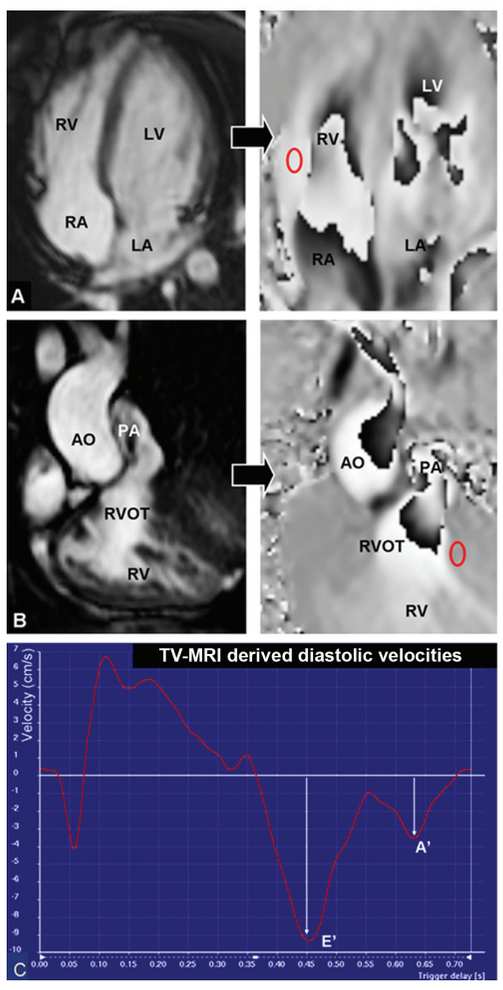

Panel A: Left: Cine image of a 4-chamber view, anatomical example of how TV-MRI images were planned. Right: TV-MRI image in a 4-chamber orientation. Velocity is encoded in the longitudinal direction. A red region of interest is indicated at the myocardial wall of the basal RVWF, from which the velocity curve is derived. **Panel B:** Left: Cine image of a double oblique RVOT view, anatomic example of how TV-MRI images were planned. Right: TV-MRI image in a double oblique RVOT orientation. Velocity is encoded in the longitudinal direction. A red region of interest is indicated at the myocardial wall of the lateral RVOT, from which the velocity curve is derived. **Panel C:** TV-MRI derived velocity curve of the RVFW in a cToF patient. White arrows indicate E' and A' Abbreviations: A': peak late diastolic velocity, AO: Aorta, E': peak early diastolic velocity, LA: left atrium, LV: left ventricle, PA: pulmonary artery, RA: right atrium, RV: right ventricle, RVOT: right ventricular outflow tract, TV-MRI: tissue-velocity magnetic resonance imaging.

was defined as the most basal region of the right ventricular free wall just apical to the tricuspid annulus in the 4-chamber view. The lateral RVOT was defined as the region of the RVOT opposite to the septum, just apical to the pulmonary valve annulus. The anatomical position of the ROI was identified at end-diastole. Semi-automated tissue tracking was used to maintain the sample area within the region of interest throughout the cardiac cycle. If needed, the sampling area was adjusted to fit within the region of interest. Myocardial velocity curves (Figure 1, panel C) were constructed by the software. From these curves, regional early diastolic velocity (E') and regional late diastolic velocity (A') were obtained at both RV regions. Finally, the ratio of E' and A' (E'/A'), was calculated for both regions of the RV. Previous authors have shown that an increased E'/A' ratio indicates early impairment of diastolic function.[15]

Magnetic resonance imaging: TV-MRI

MRI was performed on a 1.5-Tesla pulsar gradient system (Intera, release 12; Philips Medical Systems, Best, the Netherlands) with 33 mT/m amplitude, 100 mT/m/ms slew rate, and 0.33 ms rise time. A five-element cardiac coil was used for signal reception. TV-MRI was performed in a 4-chamber orientation to assess diastolic velocities at the RVFW (Figure 2, panel A), and in a double oblique coronal RVOT view, positioned along the longitudinal axis of the RVOT and through the pulmonary valve, for the assessment of diastolic velocities at the RVOT (Figure 2, panel B). Data acquisition was performed during free breathing and retrospective triggering was used. The acquisition time was approximately three minutes per TV-MRI image. The scan parameters were: repetition time (TR) 5.4 ms; echo time (TE): 3.4 ms; flip angle 10°; slice thickness 8 mm; field-of-view 370 mm; 2.9×2.9×8.0 mm acquisition voxel reconstructed into a 1.4×1.4×8.0 mm voxel. To optimize signal-to-noise ratio, four signal averages were acquired. The maximum velocity was set at 20 cm/s. The maximum number of phases was reconstructed, yielding an effective temporal resolution in the velocity graph of approximately 10 ms (true temporal resolution, defined by the number of acquisitions for velocity encoding and the repetition time, equals 2×5.4 = 10.8 ms). Image analysis was performed by placing regions of interest (5 x 5 mm) in the myocardium at the basal RVFW (the most basal region of the right ventricular free wall just apical to the tricuspid annulus in the 4-chamber view) (Figure 2A, right panel) and at the lateral wall of the RVOT opposite the septum and just apical to the pulmonary annulus (Figure 2B, right panel). The anatomical position of the ROI was identified at end-diastole in the modulus image and then copied into the corresponding TV-MRI image. Manual re-positioning of the regions of interest was performed on a frame by frame visual evaluation throughout the cardiac cycle to ensure data sampling within the myocardial region of interest. If needed, the sampling area was adjusted to fit within the region of interest. The average myocardial velocity within the region of interest was recorded in every phase for both segments, from which velocity graphs were constructed (Figure 2, panel C). From these graphs, E' (cm/s) and A' (cm/s) were derived at both regions of the RV. Finally, E'/A' was calculated at the RVFW and of the RVOT.

Figure 3. Correlation and agreement between TDI and TV-MRI for the assessment of regional diastolic velocities at the RVFW

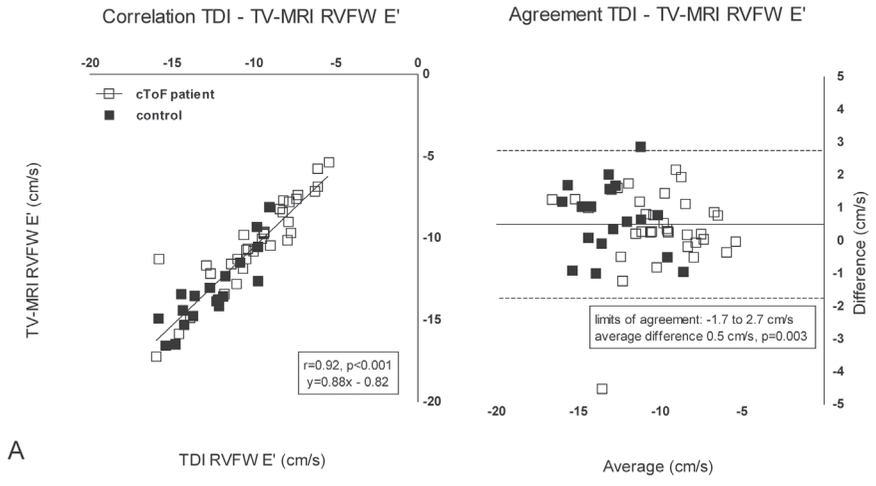

Panel A: Left: scatterplot depicting correlation between TDI and TV-MRI for the assessment of E' at the RVFW. Right: Bland-Altman plot showing agreement between TDI and TV-MRI for the assessment of E' at the RVFW. **Panel B:** Left: scatterplot depicting correlation between TDI and TV-MRI for the assessment of A' at the RVFW. Right: Bland-Altman plot showing agreement between TDI and TV-MRI for the assessment of A' at the RVFW. Abbreviations: A': peak late diastolic velocity, E': peak early diastolic velocity , RVFW: right ventricular free wall, TDI: tissue Doppler imaging, TV-MRI: tissue-velocity magnetic resonance imaging.

Figure 4. Correlation and agreement between TDI and TV-MRI for the assessment of regional diastolic velocities at the RVOT

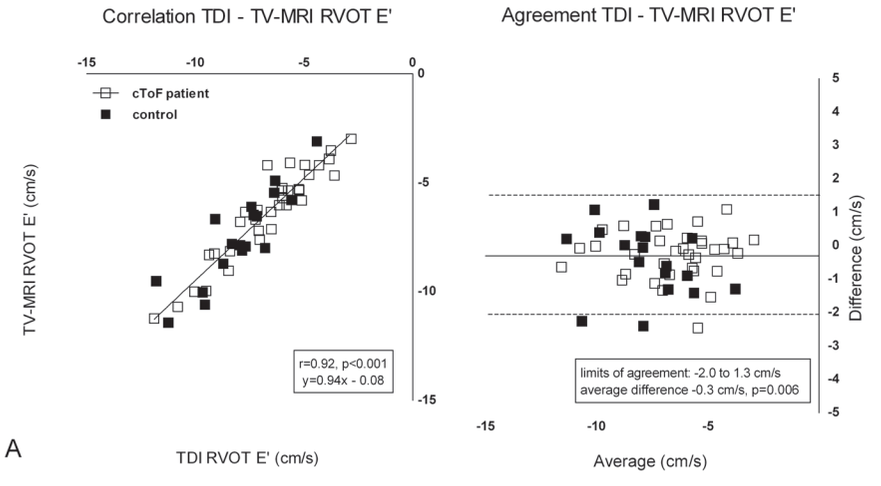

Panel A: Left: scatterplot depicting correlation between TDI and TV-MRI for the assessment of E' at the RVOT. Right: Bland-Altman plot showing agreement between TDI and TV-MRI for the assessment of E' at the RVOT. **Panel B:** Left: scatterplot depicting correlation between TDI and TV-MRI for the assessment of A' at the RVOT. Right: Bland-Altman plot showing agreement between TDI and TV-MRI for the assessment of A' at the RVOT. Abbreviations: A': peak late diastolic velocity, E': peak early diastolic velocity , RVFW: right ventricular free wall, TDI: tissue Doppler imaging, TV-MRI: tissue-velocity magnetic resonance imaging.

Magnetic resonance imaging: planimetry

RV volumes and ejection fraction were assessed with MRI planimetry. RV planimetry assessment was performed by transverse multi-section cine imaging. A stack of slices was planned in the transverse plane, covering the RV throughout the cardiac cycle. Cine images were acquired with a steady-state free precession sequence during breath hold at end-expiration. The scan parameters were: TR/TE: 3.9 ms/1.5 ms; flip angle 50°; slice thickness 8 mm; field of view 350 mm; 1.8×2.0×8.0 mm acquisition voxel reconstructed into a 1.4×1.4×8.0 mm voxel; one signal acquired; 30 phases reconstructed; retrospective gating with 10% acceptance window.

Image analysis was performed with the MASS software (Leiden University Medical Center, Leiden, the Netherlands). RV end-diastolic volume and RV end-systolic volume were calculated by manually tracing the endocardial border at end-systole and end-diastole in all transverse slices in which myocardium was visible and multiplying the area by slice thickness. Tracing of the endocardial border was aided by visualization of the multiple phases in cine mode in every slice. The RVOT was included in the volume calculations of the RV. From the obtained RV volumes, RV ejection fraction was automatically calculated.

Magnetic resonance imaging: 3D flow

Flow volume over the pulmonary valve was assessed with 3D velocity-encoded MRI. Detailed descriptions of the assessment of valvular flow and valvular function with 3D velocity-encoded MRI have been published recently.[9, 11, 16] In short, two orthogonal guide views of the pulmonary valve were obtained (double oblique coronal view and double oblique sagittal view of the RV outflow tract). In addition, a 3D volume slab was localized at the base of the heart covering the pulmonary valve throughout the cardiac cycle. In the 3D volume slab, velocity was encoded in three orthogonal directions during free breathing. The scan parameters were: TR/TE 7.5 ms/4.3 ms; flip angle 10°; 3D volume imaging with 48 mm slab thickness reconstructed into 12×4 mm slices; field-of-view 370 mm; 2.9×3.8×4.0 mm acquisition voxel reconstructed into a 1.4×1.4×4.0 mm voxel; one signal acquired; 30 phases reconstructed; retrospective gating with 10% acceptance window. A standard velocity-encoding of 150 cm/s was used in all three directions. Echo planar imaging was used with a factor of five. The acquisition time for 3D flow images was approximately five minutes.

For analysis of the 3D flow images of the pulmonary valve, first, the two orthogonal guide views of the pulmonary valve were used for 'retrospective valve tracking'. In both views, a reformatting plane was marked perpendicular to the flow at the level of the valve annulus in every cardiac phase. The three-directional velocity data from the 3D volume slab were reformatted in this plane, yielding 30 through-plane velocity-encoded images at the level of the pulmonary valve. Second, in these reformatted images, the inner border of the pulmonary annulus was traced to obtain flow volumes. Background correction was performed to correct for through-plane motion and local phase offset. Finally, a flow velocity curve was obtained by multiplying the valve area in each time frame by its average flow velocity. From this curve, pulmonary forward flow volume (ml), pulmonary regurgitation fraction (%) and the presence of end diastolic forward flow (EDFF) were derived. EDFF indicates a restrictive RV filling pattern, and is defined as the presence of late diastolic forward flow over the pulmonary valve that coincides with atrial contraction.[6]

Statistical analysis

Variables were tested for normal distribution by the Kolmogorov-Smirnov test. Continuous variables with a normal distribution are expressed as mean ± standard deviation. Continuous data with no normal distribution are expressed as median and inter-quartile range (IQR). Categorical variables are presented as numbers and percentages. Differences between TDI and TV-MRI, and differences between cToF patients and controls, and between cToF patients with and without EDFF were analyzed using the paired or unpaired t-test where appropriate for normally distributed continuous data. For continuous data with no normal distribution, the Mann-Whitney U-test (unpaired data) or Wilcoxon signed rank test (paired data) were used. Categorical data were analyzed with the Chi-square test. Bland-Altman analysis was performed to assess the agreement between the two techniques. Linear regression analysis was used to evaluate the correlation between TDI and TV-MRI measurements. In addition, univariate and multivariate linear regression analyses were performed to investigate the effect of various clinical parameters, including regional diastolic velocities, on RV end-diastolic volume. Only significant univariate parameters were entered as variables in the multivariate analysis. Data were analyzed using the SPSS 17.0 software (SPSS Inc, Chicago, Illinois). A p-value of <0.05 was considered statistically significant.

RESULTS

Study population

The characteristics of the patients and controls are summarized in Table 1. Age, gender and body surface area did not differ between cToF patients and controls. RV end-diastolic volume indexed for body surface area was significantly larger in cToF patients as compared with controls (135 ± 35 ml/m² vs. 99 ± 14 ml/m², $p<0.001$). In cToF patients, the mean pulmonary regurgitation fraction was 29 ± 15%. A total of 14 patients showed EDFF over the pulmonary valve. None of the patients showed an aneurysmatic or dyskinetic RVOT. Satisfactory TDI and TV-MRI images of the RVFW and RVOT were obtained in all patients and control subjects.

Diastolic velocities at the RVFW: TDI versus TV-MRI

Early and late diastolic velocities at the RVFW were compared between TDI and TV-MRI. Figure 3A shows a strong correlation between TDI and TV-MRI to measure E' at the RVFW in the full population (Figure 3A, left panel). After dividing the population in cToF patients and controls, the correlations between TDI and TV-MRI to assess E' at the RVFW were $r=0.91$ ($p<0.001$) and $r=0.87$ ($p<0.001$), respectively. In addition, the Bland-Altman analysis showed a small bias between TDI and TV-MRI and tight limits of agreement in the full population (Figure 3A, right panel) Subgroup analysis yielded an average difference of 0.4 cm/s (limits of agreement of -1.9 to 2.6 cm/s) in cToF

patients and an average difference of 0.7 cm/s (-1.4 to 2.8 cm/s) in the control subjects. Similarly, for the assessment of A' at the RVFW, TDI and TV-MRI showed a strong pooled correlation, as shown in Figure 3B (left panel). Assessing A' at the RVFW in the subgroups of cToF patients and control subjects yielded correlations of r=0.9 (p<0.001) and r=0.85 (p<0.001), respectively. Furthermore, Bland-Altman analysis yielded small differences with narrow limits of agreement in the full population (Figure 3B right panel) as well as in the subgroups of cToF patients (average difference: 0.4 cm/s, limits of agreement: -1.2 to 1.9 cm/s) and controls (0.4 cm/s, -1.3 to 2.12 cm/s).

Diastolic velocities at the RVOT: TDI versus TV-MRI

Figure 4A illustrates the correlation and agreement between TDI and TV-MRI-derived measurements of E' at the RVOT in the full population. When dividing the population in cToF patients and controls, strong correlations were observed (cToF patients: r=0.94, p<0.001, controls r=0.87 p<0.001). The Bland-Altman analysis to assess E' at the RVOT in the full population is shown in Figure 4A (right panel). Bland-Altman analysis in the subgroups of cToF patients and controls showed an average difference between TDI and TV-MRI of -0.3 cm/s in cToF patients (limits of agreement -1.7 to 1.1 cm/s) and of -0.4 cm/s (-2.5 to 1.6 cm/s) in controls.

Figure 4B shows the correlation and agreement between TDI and TV-MRI for the assessment of A' at the RVOT in the full population. In the subgroups of cToF patients and controls, excellent correlations (cToF patients r=0.94, p<0.001, controls r=0.96, p<0.001) were observed, with small differences between the two techniques (cToF patients: average difference 0.05 cm/s, limits of agreement -0.9 to 1.0 cm/s, controls: 0.04 cm/s, -0.5 to 0.5 cm/s).

RV regional diastolic velocities and performance: cToF patients versus controls

The regional diastolic velocities and the derived E'/A' ratio, as assessed with both TDI and TV- MRI, were compared between cToF patients and controls (Table 2).

At the RVFW, E' was significantly reduced in cToF patients as compared to controls, as assessed with both TDI and TV-MRI (TDI: -9.9 ± 2.7 cm/s vs. -12.6 ± 2.0 cm/s, p<0.001, TV-MRI: -10.2 ± 2.7 cm/s vs. -13.3 ± 2.2 cm/s, p<0.001). Likewise, A' at the RVFW was significantly decreased in cToF patients with both imaging techniques (Table 2). Finally, the E'/A' at the RVFW was increased in cToF patients as compared with controls, although with TV-MRI, the difference did not reach statistical significance (TDI: 2.4 (2.0 – 3.1) vs. 2.0 (1.7 – 2.4), p=0.038, TV-MRI: 2.3 (1.8 – 2.9) vs. 1.8 (1.7 – 2.6), p=0.095).

E' at the RVOT, as assessed with TDI, was reduced in patients (-6.6 ± 2.1 cm/s vs. -7.9 ± 1.8 cm/s, p=0.041). With TV-MRI, the reduction of E' in cToF patients was not statistically significant (-6.4 ± 2.1 cm/s vs. -7.5 ± 2.1 cm/s, p=0.071 cm/s). In addition, A' at the RVOT was significantly decreased in cToF patients as compared to controls with both TDI and TV-MRI (Table 2). Finally, the E'/A' at the RVOT was significantly increased in cToF patients with both imaging techniques (TDI: 4.0 (2.6 – 7.7) vs. 2.9 (1.9 – 3.7), p=0.015, TV-MRI: 3.7 (2.5 – 5.8) vs. 2.5 (1.9 – 3.3), p=0.008). Comparing the cToF patients with and without a restrictive RV filling pattern, no differences in diastolic velocities and performance were observed at the RVFW (TDI RVFW E': p=0.250, TV-MRI RVFW E': p=0.491, TDI RVFW A': p=0.101, TV-MRI A': p=0.119, TDI RVFW E'/A': p=0.299, TV-MRI RVFW E'/A': p=0.248). In addition, at the RVOT, no differences in diastolic velocity and performance were observed between patients with and without EDFF (TDI RVOT E': p=0.394, TV-MRI RVOT E': p=0.332, TDI RVOT A': p=0.887, TV-MRI A': p=0.985, TDI RVOT E'/A': p=0.241, TV-MRI RVOT E'/A': p=0.449).

Regional diastolic performance and RV dilatation

Univariate regression analysis was performed to investigate the relationship between various clinical parameters, including the diastolic performance parameters, and indexed RV end-diastolic volume. No significant relation was observed between RV end diastolic volume and gender (p=0.186), age at surgical correction (p=0.107) or type of surgery (p=0.367). In contrast, pulmonary regurgitation fraction was closely related to RV end-diastolic volume (r=0.71, p<0.01). Among the diastolic performance parameters at the RVFW, no significant relationship was observed between E'/A' ratio and RV end-diastolic volume (TDI: r=0.18, p=0.20, TV-MRI: r=0.14, p=0.31). In contrast, at the RVOT, a significant relation between the E'/A' ratio and RV end-diastolic volume was observed, with both TDI and TV-MRI (TDI: r=0.60, p<0.01, TV-MRI: r=0.48, p<0.01).

Subsequently, multivariate regression analysis was performed to further investigate the observed relationship between diastolic velocities at the RVOT and the indexed RV end-diastolic volume. After correction for the pulmonary regurgitation fraction, E'/A' ratio at the RVOT remained significantly related with indexed RV end-diastolic volume (TDI: p<0.01, TV-MRI: p=0.05).

DISCUSSION

The current study demonstrated that TDI and TV-MRI can be used interchangeably for the clinical assessment of regional diastolic velocities of the RV in cToF patients and in healthy controls. In addition, as assessed with both TDI and TV-MRI, regional diastolic velocities at the RVFW and RVOT are reduced in cToF patients as compared with healthy controls.

Finally, regional diastolic velocities at the RVOT were significantly related with RV end-diastolic volume, and this was independent of pulmonary regurgitation fraction.

Regional diastolic velocities of the RV

The assessment of diastolic velocities plays an essential role in the diagnosis of diastolic function in the left ventricle.[17] In the RV, recent data have shown that reduced diastolic velocities (as assessed at the tricuspid annulus) may be an early sign of compromised RV function.[18] However, no studies on the use of TV-MRI for the assessment of RV diastolic velocities are available. In addition, with both TDI and TV-MRI, the feasibility of the assessment of regional diastolic velocities of the RV has not been explored, to our knowledge. The current study provides a head-to-head comparison of TV-MRI and TDI in healthy subjects and in cToF patients to assess regional myocardial diastolic velocities at the RVFW and at the RVOT. Excellent correlations and a small bias between TDI and TV-MRI were observed at both RV regions. However, as the observed statistical difference was very small, it is unlikely to be relevant in clinical practice. Accordingly, for clinical purposes, both TDI and TV-MRI can be used interchangeably to assess regional RV diastolic velocities in healthy subjects and cToF patients.

Regional velocities and performance: cToF patients versus controls

Increased RV end-diastolic volume and pulmonary regurgitation are diastolic parameters strongly related with adverse outcome in cToF patients.[1, 2] Furthermore, global diastolic dysfunction as assessed with pulsed-waved Doppler recordings of the RV inflow, is commonly observed in cToF patients.[6-9] However, the clinical implications of global diastolic dysfunction in cToF patients with pulmonary regurgitation remain unclear, as conflicting results have been published.[6-9]

Previous studies have suggested that, in addition to pulmonary regurgitation, functional abnormalities of the RVOT may promote RV dilatation and RV dysfunction in cToF patients.[3-5, 19, 20] Therefore, comprehensive assessment of regional diastolic performance at the level of the RVOT in cToF patients may provide further insight into the pathophysiological mechanisms leading to RV dilatation in cToF patients with pulmonary regurgitation. In the current study, we observed significantly reduced early and late regional diastolic velocities at the RVFW and RVOT. The reduced diastolic velocities at the RVFW are in agreement with a recent study.[21] Brili et al. assessed diastolic velocities at the RV tricuspid annulus with TDI in 25 asymptomatic cToF patients.[21] Diastolic velocities were significantly reduced as compared with healthy controls. The current study extends these observations with the finding of reduced diastolic velocities at the RVOT in cToF patients. Furthermore, E'/A' ratio was evaluated in healthy controls and in cToF patients at both the RVFW and the RVOT. An increased E'/A' ratio has been demonstrated to reflect impaired myocardial relaxation.[15] In the present study, at both RV regions, E'/A' ratio was increased in cToF patients, indicating impaired diastolic performance at both RV regions in cToF patients. Finally, a total of 40% of patients showed a restrictive filling RV filling pattern, as assessed with 3D flow. Conflicting results on the clinical consequences of the occurrence of RV restriction in cToF patients have been published.[6, 8] In the present study, no differences were observed in diastolic myocardial velocities between patients with and without a restrictive RV filling pattern.

Relationship between diastolic performance and RV end-diastolic volume

In the current study, cToF patients showed significant pulmonary regurgitation and RV dilatation. A close relationship was observed between the pulmonary regurgitation and RV end-diastolic volume, which is in line with previous reports.[1, 2] Furthermore, increased E'/A' ratio at the RVOT, indicating impaired diastolic filling, was related to increased RV end-diastolic volume in the present analysis. This relationship between diastolic performance at the RVOT and indexed RV dilatation remained significant after correcting for pulmonary regurgitation and gender. At the RVFW, this relationship between diastolic performance and RV dilatation was not observed. These findings have important clinical implications, as RV dilatation in cToF patients is related with a poor clinical outcome. Furthermore, a recent study demonstrated that RV dilatation significantly increases over time in cToF patients.[22] A significant dilatation of the RV in cToF patients with pulmonary regurgitation is an indication for pulmonary valve replacement in order to reduce RV volume and improve clinical outcome.[23] However, various studies have demonstrated a lack of RV remodeling after pulmonary valve replacement in a substantial part of cToF patients.[24-26] The observed independent relationship between diastolic performance at the RVOT and RV end-diastolic volume in cToF patients suggests that RVOT dysfunction plays an additional role in the development of RV dilatation. This concept is supported by the results of a previous study by d'Udekem d'Acoz et al.[4] A total of 189 cToF patients were compared to 44 patients with pulmonary regurgitation after commissurotomy for pulmonary stenosis. The authors demonstrated that despite equal amounts of pulmonary regurgitation, cToF patients had larger RV end-diastolic volumes as compared with the patients after correction of pulmonary stenosis.[4] An important difference between surgical correction of tetralogy of Fallot and surgical correction of isolated pulmonary valve stenosis is the manipulation of the RVOT during tetralogy of Fallot correction. During surgical correction of tetralogy of Fallot, resection of infundibular muscle fibers or patch insertion at the RVOT is almost invariably needed to relieve the pulmonary stenosis. As a result, regional scar tissue may lead to functional abnormalities of the RVOT.[5, 20] Several studies have shown a relationship between regional RVOT abnormalities and RV systolic dysfunction in cToF patients.[13, 14, 20] The present study furthermore shows with two different imaging techniques that impaired RVOT diastolic performance is independently related to RV dilatation in cToF patients. Accordingly, in addition to pulmonary valve replacement, (surgical) treatment of cToF patients with pulmonary regurgitation and RV dilatation may need to target the RVOT. Additional studies to elucidate whether a targeted intervention on the RVOT in cToF patients undergoing pulmonary valve replacement may lead to improved outcomes are warranted.

Study limitations

The difference in temporal resolution between TDI and TV-MRI may have a small effect on the performance of peak diastolic velocity detection in the time-velocity graphs. However, as the difference in temporal resolution was very small (2.5 ms), this is unlikely to be relevant in clinical practice. Furthermore, myocardial velocity assessment with TDI and TV-MRI represents myocardial motion or displacement and does not image active myocardial deformation. Additional studies investigating regional diastolic myocardial deformation in cToF patients are needed. Finally, the manual repositioning of the regions of interest throughout the cardiac cycle may have introduced a small error in the velocity measurements, and furthermore the relatively small sampling area of the study may have influenced the results of the subgroup analyses. External validation of the observed diastolic myocardial velocities and the correlations and agreement between TDI and TV-MRI to assess diastolic velocities at the RVFW and RVOT is warranted.

Conclusions

TDI and TV-MRI can be used interchangeably for the clinical assessment of regional diastolic velocities of the RV in cToF patients and in healthy controls. Regional diastolic velocities and performance at the RVFW and RVOT are reduced in cToF patients as compared with healthy controls. The assessment of regional RV diastolic performance with TDI and TV-MRI provides further insight into the mechanism leading to RV dilatation in cToF patients, as regional diastolic performance at the RVOT was related to RV dilatation.

REFERENCE LIST

1 Gatzoulis MA, Balaji S, Webber SA, et al. Risk factors for arrhythmia and sudden cardiac death late after repair of tetralogy of Fallot: a multicentre study. Lancet 2000;356:975-81.
2 Bouzas B, Kilner PJ, Gatzoulis MA. Pulmonary regurgitation: not a benign lesion. Eur Heart J 2005;26:433-9.
3 d'Udekem d'Acoz Y, Ovaert C, Grandjean F, et al. Tetralogy of Fallot: transannular and right ventricular patching equally affect late functional status. Circulation 2000;102:III116-III122.
4 d'Udekem d'Acoz Y, Pasquet A, Lebreux L, et al. Does right ventricular outflow tract damage play a role in the genesis of late right ventricular dilatation after tetralogy of Fallot repair? Ann Thorac Surg 2003;76:555-61.
5 Oosterhof T, Mulder BJ, Vliegen HW, et al. Corrected tetralogy of Fallot: delayed enhancement in right ventricular outflow tract. Radiology 2005;237:868-71.
6 Gatzoulis MA, Clark AL, Cullen S, et al. Right ventricular diastolic function 15 to 35 years after repair of tetralogy of Fallot. Restrictive physiology predicts superior exercise performance. Circulation 1995;91:1775-81.
7 Helbing WA, Niezen RA, Le Cessie S, et al. Right ventricular diastolic function in children with pulmonary regurgitation after repair of tetralogy of Fallot: volumetric evaluation by magnetic resonance velocity mapping. J Am Coll Cardiol 1996;28:1827-35.
8 van den Berg J, Wielopolski PA, Meijboom FJ, et al. Diastolic function in repaired tetralogy of Fallot at rest and during stress: assessment with MR imaging. Radiology 2007;243:212-9.
9 van der Hulst AE, Westenberg JJ, Kroft LJ, et al. Tetralogy of fallot: 3D velocity-encoded MR imaging for evaluation of right ventricular valve flow and diastolic function in patients after correction. Radiology 2010;256:724-34.
10 Marsan NA, Westenberg JJ, Tops LF, et al. Comparison between tissue Doppler imaging and velocity-encoded magnetic resonance imaging for measurement of myocardial velocities, assessment of left ventricular dyssynchrony, and estimation of left ventricular filling pressures in patients with ischemic cardiomyopathy. Am J Cardiol 2008;102:1366-72.
11 Westenberg JJ, Roes SD, Ajmone MN, et al. Mitral valve and tricuspid valve blood flow: accurate quantification with 3D velocity-encoded MR imaging with retrospective valve tracking. Radiology 2008;249:792-800.
12 Pennell DJ, Sechtem UP, Higgins CB, et al. Clinical indications for cardiovascular magnetic resonance (CMR): Consensus Panel report. J Cardiovasc Magn Reson 2004;6:727-65.
13 Uebing A, Gibson DG, Babu-Narayan SV, et al. Right ventricular mechanics and QRS duration in patients with repaired tetralogy of Fallot: implications of infundibular disease. Circulation 2007;116:1532-9.
14 van der Hulst AE, Roest AA, Delgado V, et al. Relationship between temporal sequence of right ventricular deformation and right ventricular performance in patients with corrected tetralogy of Fallot. Heart 2011;97:231-6.
15 Mogelvang R, Sogaard P, Pedersen SA, et al. Cardiac dysfunction assessed by echocardiographic tissue Doppler imaging is an independent predictor of mortality in the general population. Circulation 2009;119:2679-85.
16 Roes SD, Hammer S, van der Geest RJ, et al. Flow Assessment Through Four Heart Valves Simultaneously Using 3-Dimensional 3-Directional Velocity-Encoded Magnetic Resonance Imaging With Retrospective Valve Tracking in Healthy Volunteers and Patients With Valvular Regurgitation. Invest Radiol 2009.
17 Paulus WJ, Tschope C, Sanderson JE, et al. How to diagnose diastolic heart failure: a consensus statement on the diagnosis of heart failure with normal left ventricular ejection fraction by the Heart Failure and Echocardiography Associations of the European Society of Cardiology. Eur Heart J 2007;28:2539-50.
18 Rydman R, Larsen F, Caidahl K, et al. Right ventricular function in patients with pulmonary embolism: early and late findings using Doppler tissue imaging. J Am Soc Echocardiogr 2010;23:531-7.
19 Davlouros PA, Karatza AA, Gatzoulis MA, et al. Timing and type of surgery for severe pulmonary regurgitation after repair of tetralogy of Fallot. Int J Cardiol 2004;97 Suppl 1:91-101.
20 Wald RM, Haber I, Wald R, et al. Effects of regional dysfunction and late gadolinium enhancement on global right ventricular function and exercise capacity in patients with repaired tetralogy of Fallot. Circulation 2009;119:1370-7.
21 Brili S, Alexopoulos N, Latsios G, et al. Tissue Doppler imaging and brain natriuretic peptide levels in adults with repaired tetralogy of Fallot. J Am Soc Echocardiogr 2005;18:1149-54.
22 Geva T. Indications and timing of pulmonary valve replacement after tetralogy of Fallot repair. Semin Thorac Cardiovasc Surg Pediatr Card Surg Annu 2006;11-22.
23 Henkens IR, van Straten A, Schalij MJ, et al. Predicting outcome of pulmonary valve replacement in adult tetralogy of Fallot patients. Ann Thorac Surg 2007;83:907-11.
24 Therrien J, Siu SC, McLaughlin PR, et al. Pulmonary valve replacement in adults late after repair of tetralogy of fallot: are we operating too late? J Am Coll Cardiol 2000;36:1670-5.
25 Therrien J, Provost Y, Merchant N, et al. Optimal timing for pulmonary valve replacement in adults after tetralogy of Fallot repair. Am J Cardiol 2005;95:779-82.

3.4

Tetralogy of Fallot: 3D velocity-encoded MR imaging for ealuation of right ventricular valve flow and diastolic function in patients after correction

Radiology 2010; 256: 724-734

A.E. van der Hulst
J.J.M. Westenberg
L.J.M. Kroft
J.J. Bax
N.A. Blom
A. de Roos
A.A.W. Roest

ABSTRACT

Purpose: To evaluate three-dimensional (3D) velocity-encoded (VE) magnetic resonance (MR) imaging, as compared with two-dimensional (2D) VE MR imaging, for assessment of pulmonary valve (PV) and tricuspid valve (TV) flow, with planimetry as the reference standard, and to evaluate diastolic function in patients with a corrected tetralogy of Fallot (TOF).

Materials and Methods: Local institutional review board approval was obtained, and patients or their parents gave informed consent. Twenty-five patients with a corrected TOF (12 male, 13 female; mean age, 13.1 years ± 2.7 [standard deviation]; age range, 8–18 years) and 19 control subjects (12 male, seven female; mean age, 14.1 years ± 2.4; age range, 8–18 years) underwent planimetric MR imaging, 2D VE MR imaging, and 3D VE MR imaging for TV and PV flow evaluation. For evaluation of diastolic function, PV and TV flow were summated. Data were analyzed by using linear regression analysis, paired and unpaired *t* testing, and Bland-Altman plots.

Results: Strong correlations between the 2D VE MR and 3D VE MR measurements of PV flow (for forward flow: $r = 0.87$, $P < .01$; for backward flow: $r = 0.97$, $P < .01$) were observed. With PV effective flow as a reference, 3D TV effective flow measurements were more accurate than 2D TV effective flow measurements: In patients, the mean 2D TV effective flow versus 2D PV effective flow difference was 17.6 mL ± 11 ($P < .001$), and the mean 3D TV effective flow versus 3D PV effective flow difference was −1.2 mL ± 4.7 ($P = .22$). Diastolic functional impairment in patients could be detected at 3D VE MR imaging diastolic assessment.

Conclusion: Three-dimensional VE MR imaging is accurate for PV flow assessment and is more accurate than 2D VE MR imaging for TV flow evaluation. Assessment of diastolic function with 3D VE MR imaging can facilitate ongoing research of diastolic dysfunction in patients with a corrected TOF.

INTRODUCTION

Tetralogy of Fallot (TOF) is one of the most common congenital heart diseases and consists of pulmonary stenosis, overriding of the aorta, ventricular septal defect, and right ventricular hypertrophy. Currently, surgical correction is performed in the first year of life by means of closure of the ventricular septal defect and relief of the pulmonary stenosis. After correction, pulmonary regurgitation is common. In a large multicenter study involving patients with corrected TOF, 54% of patients had at least moderate pulmonary regurgitation (1). Accurate assessment of pulmonary regurgitation is important, because this is a key determinant of the outcome of patients with a corrected TOF (1,2). In addition, right ventricular diastolic dysfunction is frequently observed (3-5), with the estimated percentage of patients with a right ventricular restrictive filling pattern ranging from 35% to 66% (3,5-9). Conflicting results regarding the implications of diastolic dysfunction—the role of right ventricular restriction in particular—in terms of the long-term prognosis for patients with a corrected TOF have been published (3,5-9). This disparity can be attributed in part to technical difficulties in the assessment of right ventricular diastolic function. Echocardiography is a simple and widely available imaging modality for the assessment of right ventricular systolic and diastolic function. However, in patients with pulmonary regurgitation, right ventricular diastolic function does not correspond to Doppler echocardiographic tricuspid valve (TV) inflow patterns, because early diastolic filling of the right ventricle occurs from two sources: normal inflow through the TV and pathologic pulmonary regurgitation.

In contrast, two-dimensional (2D) one-directional velocity-encoded magnetic resonance (MR) imaging enables evaluation of right ventricular diastolic function in the presence of pulmonary regurgitation by means of summation of the TV and pulmonary valve (PV) flow volumes obtained during two acquisitions (5,8). Currently, 2D velocity-encoded MR imaging is the method of choice for assessment of PV flow in clinical practice (10-13). However, 2D velocity-encoded MR evaluation of atrioventricular transvalvular flow is hampered by cardiac motion, because the acquisition plane is fixed throughout the cardiac cycle (14,15), whereas the TV may move up to 24 mm toward the apex during systole (16). As a result, correlations between atrioventricular transvalvular flow and aortic flow are only moderate (17). Moreover, it has been shown that 2D velocity-encoded MR imaging can lead to overestimations of TV flow volume of up to 25% (18). Finally, heart rate variability during separate flow acquisitions reduces the accuracy of the summation of TV and PV flow volumes in the assessment of diastolic function.

Three-dimensional (3D) three-directional velocity-encoded MR imaging has been introduced for the assessment of transvalvular flow (17-19). The use of 3D velocity-encoded MR imaging resolves the problem of valvular annulus motion owing to retrospective valve tracking and velocity encoding in three orthogonal directions. In addition, 3D velocity-encoded MR imaging enables flow assessment through all cardiac valves during the same acquisition, eliminating the error that results from heart rate variability. Accordingly, the purpose of our study was to evaluate 3D velocity-encoded MR imaging, as compared with 2D velocity-encoded MR imaging, for assessment of PV and TV flow, with planimetry as the reference standard, and to evaluate the diastolic function in patients with a corrected TOF.

MATERIALS AND METHODS

Subjects

All participants or their parents gave written informed consent. Twenty-five patients who had a corrected TOF with pulmonary regurgitation (mean age, 13.1 years ± 2.7 [standard deviation]) and 19 healthy control subjects (mean age, 14.1 years ± 2.4) underwent cardiac MR imaging, including MR planimetry (summation of disks from multisection 2D MR imaging) and both 2D velocity-encoded MR imaging and 3D velocity-encoded MR imaging assessment of PV and TV flow. The image quality with all three MR imaging sequences was satisfactory in all subjects enrolled in the study. Patients with a corrected TOF were prospectively recruited from an ongoing registry of the Center of Congenital Heart Disease Amsterdam-Leiden *(www.cahal.nl)* when they were scheduled for cardiac MR imaging evaluation. Patients who had a corrected TOF with a residual ventricular septal defect were excluded. None of the patients with a corrected TOF had signs of marked tricuspid regurgitation at echocardiographic assessment (20) performed on the same day as cardiac MR imaging.

Cardiac MR Imaging

MR imaging was performed by using a 1.5-T pulsar gradient system (Intera, release 12; Philips Medical Systems, Best, the Netherlands) with a 33 mT/m amplitude, a 100 ($mT \cdot m^{-1}$)/msec slew rate, and a 0.33-msec rise time. A five-element cardiac coil was used for signal reception. A series of localizing thoracic scout images were acquired for planning purposes. We assessed the ventricular volumes at multisection cine imaging by planning a stack of sections, in the transverse plane (21–24), that encompassed both ventricles throughout the cardiac cycle. Cine images were acquired with a steady-state free precession sequence during breath holding at end expiration by using the following parameters: 3.9/1.5 (repetition time msec/echo time msec), a 350-mm field of view, an 8-mm section thickness, a 50° flip angle, a 1.8 × 2.0 × 8.0-mm acquisition voxel reconstructed into a 1.4 × 1.4 × 8.0-mm voxel, one acquired signal, 30 phases reconstructed, and retrospective gating with a 10% acceptance window.

For 2D TV flow mapping, right ventricular two-chamber and four-chamber cine views were acquired. The 2D TV imaging plane was positioned at the valve at end systole, perpendicular to the inflow. For 2D PV flow mapping, a double-oblique coronal cine view and a double-oblique sagittal cine view of the right ventricular outflow tract were acquired. The 2D PV imaging plane was positioned perpendicular to the pulmonary artery, midway between the PV and the bifurcation at end diastole. Velocity was encoded in one direction during free breathing. Maximal velocity encoding of 150 cm/sec for PV flow and 100 cm/sec for TV flow was used. The velocity-encoded images

Table 1. patient and control characteristics

	cToF patient (mean ± SD)	control (mean ± SD)	p-value
n	25	19	
age (y)	13.1 ± 2.7	14.1 ± 2.4	0.22
male/female n (%)	12/13 (48/52)	12/7 (63/37)	0.3
heart rate (min-¹)	80 ± 14	78 ± 11	0.954
age at surgery	0.9 ± 0.5		
type of surgery n (%)			
TAP	16 (72)	na	
inf	2 (9)	na	
RVOT patch	2 (9)	na	
PA patch	2 (9)	na	
QRS (ms)	131 ± 19	94 ± 8	<0.001
BSA (m²)	1.4 ± 0.3	1.6 ± 0.3	0.11
Planimetry values			
LV-SV	67 ± 20	82 ± 18	0.01
RV-SV (mL)	93 ± 28	81 ± 19	0.12
PV backward (mL)	26 ± 24	1 ± 5	<0.001

BSA: body surface area, inf: infundibulectomy, LV-SV: left ventricular stroke volume, PA: pulmonary artery, PV: pulmonary valve, RVOT: right ventricular outflow tract, RV-SV right ventricular stroke volume, SD: standard deviation, TAP: transannular patch.

were reviewed immediately, and the maximal velocity was adjusted in cases of phase wrapping. Imaging parameters were as follows: 8.9/5.7, a 350-mm field of view, an 8-mm section thickness, a 20° flip angle, a 2.7 × 3.4 × 8.0-mm acquisition voxel reconstructed into a 1.4 × 1.4 × 8.0-mm voxel, two acquired signals, a 495-mHz sampling bandwidth, 36 phases reconstructed, and retrospective gating with a 10% acceptance window.

A detailed description of the 3D velocity-encoded MR imaging acquisition has been published recently (18,19). In short, a 3D volume slab was localized at the base of the heart and encompassed both valves throughout the cardiac cycle (visually verified on the right ventricular four- and two-chamber views and on the double-oblique coronal and sagittal views of the right ventricular outflow tract), in which the velocity was encoded in three orthogonal directions during free breathing. Imaging parameters were as follows: 7.5/4.3, a 370-mm field of view, 3D volume imaging with 48-mm slab thickness reconstructed into 12 × 4-mm sections, a 10° flip angle, a 2.9 × 3.8 × 4.0-mm acquisition voxel reconstructed into a 1.4 × 1.4 × 4.0-mm voxel, one acquired signal, a 237-Hz sampling bandwidth, retrospective gating with a 10% acceptance window, and 30 phases reconstructed. Standard velocity encoding of 150 cm/sec was used in all three directions. However, if the 2D velocity-encoded MR imaging PV acquisition required a higher maximal velocity, this velocity was also used with 3D velocity-encoded MR imaging in all three directions. Echo-planar imaging was performed with a factor of five, and the sampling bandwidth in the echo-planar imaging direction

Table 2. Comparisons of flow volumes between 2D VE-MRI, 3D VE-MRI and planimetry

	subject	r	mean diff (mL)	p-value	95% limits of agreement (mL)
2D PV forw / planimetry RV-SV	patients	0.84	1.3 ± 15.6	0.69	-29.3 to 31.9
	controls	0.96	5.6 ± 6.3	0.001	-6.7 to 17.9
3D PV forw / planimetry RV-SV	patients	0.87	1.5 ± 15.5	0.64	-28.9 to 31.9
	controls	0.92	-4.7 ± 7.6	0.02	-19.6 to 10.2
2D PV forw / 3D PV forw	patients	0.88	-0.3 ± 15.5	0.93	-30.7 to 30.1
	controls	0.93	10.4 ± 6.6	<0.001	-2.5 to 23.3
2D PV backw / planimetry PV backw	patients	0.83	11.0 ± 14.0	0.001	-16.4 to 38.4
3D PV backw / planimetry PV backw	patients	0.84	3.2 ± 12.5	0.22	-21.3 to 27.7
2D PV backw / 3D PV backw	patients	0.9	7.6 ± 6.7	<0.001	-5.5 to 20.7
2D TV effective / 2D PV effective	patients	0.84	17.6 ± 11	<0.001	-4.0 to 39.1
	controls	0.89	21.4 ± 12.8	<0.001	-3.7 to 46.5
3D TV effective/ 3D PV effective	patients	0.97	-1.2 ± 4.7	0.22	-10.4 to 8.0
	controls	0.95	2.0 ± 6.0	0.16	-9.8 to 13.8
2D TV forw / 3D TV forw	patients	0.87	9.8 ± 9.8	<0.001	-9.4 to 29.0

Abbreviations: 2D: two-dimensional velocity-encoded MRI, 3D: three-dimensional velocity-encoded MRI, backw: backward, CI: confidence interval, diff: difference, effective: forward minus backward flow, forw: forward, PV: pulmonary valve, r: correlation coefficient, TV tricuspid valve.

was 2.28 kHz. During image reconstruction, the local phase correction filter was switched on, and velocity offsets caused by Maxwell concomitant gradients were corrected.

Image Analysis

Image postprocessing was performed with in-house–developed (Leiden University, Leiden, the Netherlands) software packages: Flow (25) for 2D velocity-encoded MR imaging data and MR analytical software system (MASS) (26) for planimetric data. The 3D velocity-encoded MR imaging data were analyzed (A.E.v.d.H, J.J.M.W, L.J.M.K., 2, 14, and 13 years experience in cardiac MR imaging, respectively) with MASS research software developed at our institution. Image readings were performed by a single researcher (A.E.v.d.H.) and were checked by the other two (J.J.M.W, L.J.M.K.). Differences were resolved by consensus. We evaluated ventricular volumes by manually tracing the endocardial border at end systole and end diastole on all transverse sections and multiplying the area by the section thickness. Right ventricular and left ventricular stroke volumes were automatically calculated. The planimetric PV forward flow volume was assessed by using the right ventricular stroke volume. The planimetric PV backward flow volume was assessed by subtracting the left ventricular stroke volume from the right ventricular stroke volume (12).

A detailed description of 3D velocity-encoded MR image postprocessing was published recently (18). In short, the two orthogonal guide views of the TV and PV were used for retrospective valve tracking. A reformatting plane (five parallel planes with 5-mm distance) was marked at the level of the valve annulus in every cardiac phase, perpendicular to the flow (Fig 1a and 1b). The 3D velocity data were reformatted in the center reformatted plane (Fig 1c-1e) to yield 30 through-plane velocity-encoded images (Fig 1f), with which the flow analysis was performed (Fig 1g).

For both the 2D velocity-encoded images and the reformatted 3D velocity-encoded images, the inner border of the pulmonary or tricuspid annulus was traced during every phase. Two-dimensional velocity-encoded MR imaging contours were drawn on the corresponding modulus images and copied onto the velocity-encoded images (27). Background correction was performed on the 2D MR TV images and on the 3D MR PV and TV reformatted images to correct for through-plane motion and local phase offset (14,15,18). Through-plane motion correction was not possible for the 2D MR images of the PV, because no myocardium was present in the imaging plane. Background correction of the 3D MR TV images was performed by placing a region of interest at the center reformatted plane in the right ventricular free wall (Fig 1f). The background region of interest for 3D MR PV images was placed at the septum in the most caudal plane (at a 10-mm distance from the central plane) to warrant the presence of the myocardium for positioning the region of interest. Flow velocity curves were calculated by multiplying the valve area in each time frame by the average flow velocity to yield the following parameters, expressed as flow volumes in milliliters: PV forward flow volume, PV backward flow volume, PV effective flow volume (forward minus backward flow volume), TV forward flow volume, TV backward flow volume, and TV effective flow volume. The PV effective flow volume was used as a reference for evaluation of the TV effective flow volume, because these two values should be equal in the absence of intracardiac shunts.

Table 3. 3D VE-MRI and 2D VE-MRI diastolic functional data

	2D VE-MRI mean ± SD	**3D VE-MRI** mean ± SD	**p-value**	**95% CI of diff**
EPFR (mL/s)	506 ± 132	423 ± 133	<0.001	58 to 106
DT (%)	26 ± 10	25 ± 9	0.52	-2 to 5
APFR (mL/s)	289 ± 115	227 ± 79	<0.001	34 to 90
E/A	2.0 ± 0.8	2.0 ± 0.8	0.71	-0.2 to 1.5
FF (%)	44 ± 11	44 ± 12	0.53	-2 to 3
AFF (%)	23 ± 14	26 ± 10	0.01	-6 to -1

Comparsion of 2D VE-MRI with 3D VE-MRI data in all subjects (n=44)Abbreviations: AFF: atrial filling fraction, APFR: atrial peak filling rate, CI: confidence interval, DT: deceleration time, E/A: EPFR divided by APFR, EPFR: early peak filling rate, FF: early filling fraction, SD: standard deviation.

Table 4 . Diastolic functional data in cToF patients and controls

	Control (n=19)	**EDFF (n=10)**	**no EDFF (n=15)**
EPFR (mL/s)	388 ± 104	521 ± 175*	398 ± 104
DT (%)	22 ± 5	25 ± 14	28 ± 8*
APFR (mL/s)	283 ± 101	306 ± 118	275 ± 126
E/A	1.9 ± 0.6	2.5 ± 1.1	2.0 ± 1
FF (%)	44 ± 14	47 ± 9	40 ± 11
AFF (%)	24 ± 8	25 ± 11	31 ± 13

* indicates statistical significant difference with control subject. Abbreviations: AFF: atrial filling fraction, APFR: peak atrial filling rate, DT: deceleration time, EDFF: end diastolic forward flow, EPFR: early peak filling rate, FF: early filling fraction.

Diastolic Functional Data

Summation of the TV flow and PV flow (5) yielded right ventricular time-flow and time-volume curves (Fig 2) for 2D and 3D velocity-encoded MR imaging, at which diastolic functional data were calculated. The following measurements were derived from the time-flow curves (Fig 2, top panel): EPFR, in milliliters per second; deceleration time (expressed as a percentage of the R-R interval)—that is, the time from the early peak filling to the moment that an extrapolated deceleration-velocity line reaches 0 mL/sec; APFR, in milliliters per second; and EPFR/APFR ratio (EPFR divided by APFR). The following measurements were derived from the time-volume curves (Fig 2, bottom panel): early filling fraction (expressed as a percentage)—that is, the filling volume during the first one-third of diastole relative to the total filling volume—and atrial filling fraction (expressed as a percentage)—that is, the filling volume during atrial systole relative to the total filling volume. The patients who had a corrected TOF with end-diastolic forward flow (EDFF) were examined separately, because such patients are considered to have a restrictive right ventricular filling pattern (3). EDFF was defined as the presence of late-diastolic PV forward flow that coin-

cides with atrial contraction (3), as assessed with echocardiography on the same day as cardiac MR imaging.

Statistical Analyses

Data were analyzed by using SPSS, version 16.0 (SPSS, Chicago, Ill), software. Results are expressed as means ± standard deviations. Differences between the means of the continuous data were analyzed with *t* tests for unpaired or paired data, where appropriate. Categorical data were analyzed with χ^2 testing. Correlations between the 2D velocity-encoded MR imaging, 3D velocity-encoded MR imaging, and planimetric measurements were assessed by using Pearson correlation coefficient and linear regression analyses. Bland-Altman plots were constructed to assess agreement between 2D velocity-encoded MR imaging, 3D velocity-encoded MR imaging, and planimetric data (28). $P < .05$ indicated statistical significance.

RESULTS

The characteristics of the patients with a corrected TOF and the control subjects are cited in Table 1. The duration of the QRS complex was significantly longer in the patients with a corrected TOF (mean duration, 131 msec ± 19 versus 94 msec ± 8 for control subjects; $P < .001$). Mean right ventricular stroke volumes were 93 mL ± 28 for the patients with a corrected TOF and 81 mL ± 19 for the control subjects ($P = .12$). The mean PV backward flow volume in the corrected TOF group was 26 mL ± 24.

PV Forward Flow Volume

Pooled correlations and agreement between the 2D MR PV forward flow volume, 3D MR PV forward flow volume, and planimetric right ventricular stroke volume measurements for both the patients with a corrected TOF and the control subjects are illustrated in Figure 3. We observed strong pooled correlations between planimetric right ventricular stroke volume and both 2D MR PV forward flow volume ($r = 0.87$, $P < .01$) and 3D MR PV forward flow volume ($r = 0.88$, $P < .01$). Nevertheless, a significant difference between 2D MR PV forward flow volume and 3D MR PV forward flow volume was observed in the control subjects (mean difference, 10.4 mL ± 6.6; 95% limits of agreement: −2.5 mL, 23.3 mL) (Table 2). In contrast, in the patients with a corrected TOF, 2D PV forward flow volume and 3D PV forward flow volume measurements were not significantly different (Table 2).

PV Backward Flow Volume

Correlations and agreement between the different MR imaging–based measurements of PV backward flow volume in the patients with a corrected TOF are illustrated in Figure 4. Although an excellent correlation between 2D MR PV backward flow volume and 3D MR PV backward flow volume was observed ($r = 0.97$, $P < .01$), 2D MR and 3D MR PV backward flow volumes were significantly different (mean difference, 7.6 mL ± 6.7 mL; 95% limits of agreement: −5.5 mL, 20.7 mL; $P < .001$)

Figure 1:

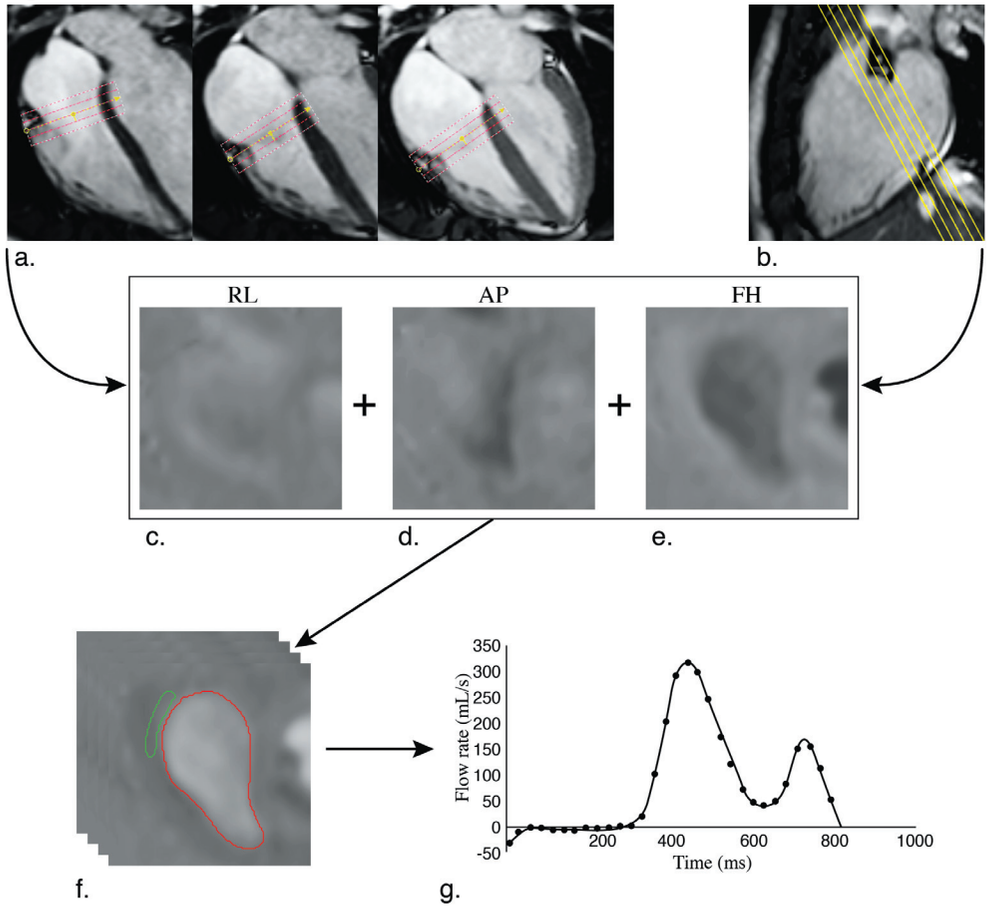

Post processing of 3D VE-MRI images. Schematic presentation of post processing of 3D VE-MRI images of the tricuspid valve in a healthy subject. Retrospective tracking of the tricuspid valve is performed by positioning a plane of interest on the tricuspid valve perpendicular to the flow in every cardiac phase in a four-chamber **(a)** and two-chamber **(b)** view (cine images: repetition time (TR) 3.9 ms, echo time (TE) 1.5 ms, flip angle 50°). Velocity-encoded images from three orthogonal directions (TR/TE 7.5 ms/4.3 ms, flip angle 10°) **(c-e)**, reconstructed from the position of the valve determined with retrospective valve tracking based on the two-chamber **(b)** and four-chamber **(a)** views. Through-plane velocity-encoded images **(f)** are obtained by reformatting of the center valvular plane in each cardiac phase. The inner border of the tricuspid annulus is traced for flow analysis. A region within the free wall of the right ventricle is traced for background correction. Tricuspid flow velocity in time can be presented in a curve **(g)**, from which flow volume can be calculated. Abbreviations: AP: anterior-posterior velocity-encoded, FH: feet-head velocity-encoded, RL: right-left velocity-encoded.Comparsion of 2D VE-MRI with 3D VE-MRI data in all subjects (n=44)Abbreviations: AFF: atrial filling fraction, APFR: atrial peak filling rate, CI: confidence interval, DT: deceleration time, E/A: EPFR divided by APFR, EPFR: early peak filling rate, FF: early filling fraction, SD: standard deviation.

(Table 2). With 2D MR velocity-encoded MR imaging, the PV backward flow volume was significantly overestimated compared with the planimetric measurement (mean difference, 11.0 mL ± 14.0; 95% limits of agreement: −16.4 mL, 38.4 mL; *P* = .001) (Table 2). In contrast, we observed no significant difference between the 3D MR PV and planimetric PV backward flow volumes (mean difference, 3.2 mL ± 12.5; 95% limits of agreement: −21.3 mL, 27.7 mL; *P* = .22).

TV Flow Volume

Pooled correlations and agreement regarding TV flow volume measurements are illustrated in Figure 5. A significant difference between 2D MR PV effective flow volume and 2D MR TV effective flow volume was observed in both the patients with a corrected TOF (mean difference, 17.6 mL ± 11; 95% limits of agreement: −4.0 mL, 39.1 mL; *P* < .001) and the control subjects (mean difference, 21.4 mL ± 12.8; 95% limits of agreement: −3.7 mL, 46.5 mL; *P* < .001) (Table 2). In contrast, 3D MR PV effective flow and 3D MR TV effective flow measurements were not significantly different, and limits of agreement were narrow in both the corrected TOF (mean difference, −1.2 mL ± 4.7; 95% limits of agreement: −10.4 mL, 8.0 mL; *P* = .22) and control (mean difference, 2.0 mL ± 6.0; 95% limits of agreement: −9.8 mL, 13.8 mL; *P* = .16) groups (Table 2). To further compare the accuracies of 2D velocity-encoded MR imaging and 3D velocity-encoded MR imaging for effective flow measurements, we compared the absolute value of the differences between TV effective flow and PV effective flow between the two techniques and observed a significant difference (mean difference, 19 mL ± 11; *P* < .001). Furthermore, 2D TV forward flow volume and 3D TV forward flow volume were significantly different in both the corrected TOF group (mean difference, 9.8 mL ± 9.8; 95% limits of agreement: −9.4 mL, 29.0 mL; *P* < .001) and control group (mean difference, 29.3 mL ± 15.0; 95% limits of agreement: −0.1 mL, 58.7 mL; *P* < .001).

Diastolic Functional Parameters

Comparison of diastolic data between 2D velocity-encoded MR imaging and 3D velocity-encoded MR imaging yielded similar EPFR/APFR ratios. However, significant differences in EPFR, APFR, and atrial filling fraction were observed (Table 3). In Table 4, 3D velocity-encoded MR imaging diastolic parameters are compared between the control subjects and both the patients with a corrected TOF who had EDFF and the patients with a corrected TOF who did not have EDFF. We observed no significant differences in baseline characteristics between the patients with a corrected TOF who had EDFF and those who did not. In the patients with EDFF, the EPFR was significantly increased compared with that in the control subjects (mean EPFRs, 521 mL/sec ± 175 versus 398 mL/sec ± 104; 95% confidence interval: 27 mL/sec, 238 mL/sec; *P* = .02). The deceleration time was increased in the patients without EDFF compared with that in the control subjects (mean deceleration times, 28% ± 8 versus 22% ± 5; 95% confidence interval: 0.6%, 11.3%; *P* = .03).

Figure 2:

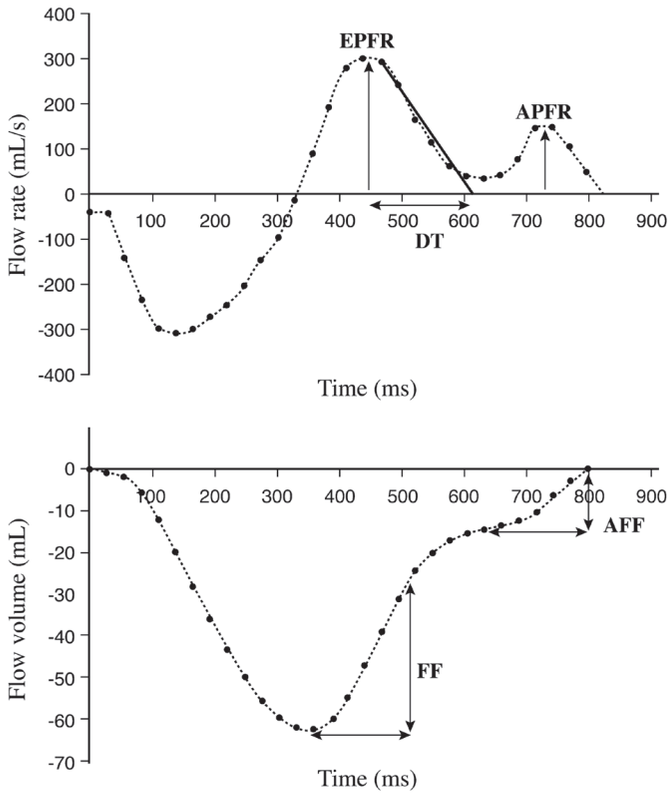

Right ventricular time-volume change and time-volume curve. Upper panel**:** 3D VE-MRI time-flow curve of the right ventricle of a healthy subject. The curve is constructed by summation of flow through the tricuspid valve and pulmonary valve. APFR: atrial peak filling rate, DT: deceleration time, EPFR: early peak filling rate**.** Lower panel**:** 3D VE-MRI time-volume curve of the right ventricle of a healthy subject. The curve is obtained by integration of the time-flow curve. Abbreviations: AFF: atrial filling fraction, FF: early filling fraction.

Figure 3:

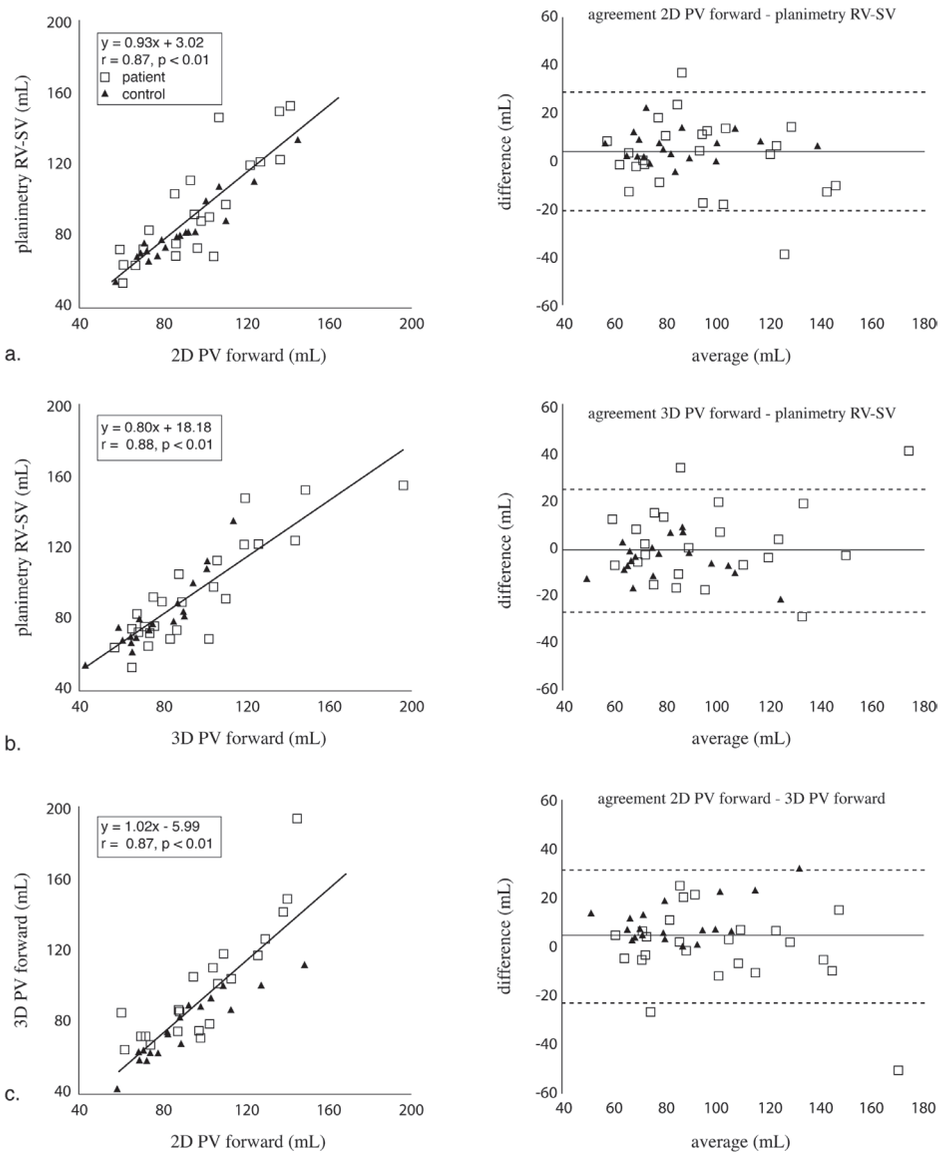

Pooled correlation and agreement of pulmonary forward flow assessed with 2D VE-MRI, 3D VE-MRI and planimetry**. (a)** Left: scatter plot depicting correlation between 2D PV forward flow and planimetry RV-SV, right: Bland-Altman plot depicting agreement between 2D PV forward flow and planimetry RV-SV. **(b)** Left: scatter plot depicting correlation between 3D PV forward flow and planimetry RV-SV, right: Bland-Altman plot depicting agreement between 3D PV forward flow and planimetry RV-SV. (**c)** Left: scatter plot depicting correlation between 2D PV forward flow and 3D PV forward flow, right: Bland-Altman plot depicting agreement between 2D PV forward flow and 3D PV forward flow. Squares: cToF patients, triangles: control subjects. Abbreviations: PV: pulmonary valve, RV-SV: right ventricular stroke volume.

DISCUSSION

Our study represents a comprehensive evaluation of PV and TV flow during one acquisition by using 3D velocity-encoded MR imaging with retrospective valve tracking in patients with a corrected TOF and healthy control subjects. Our study findings show that 3D velocity-encoded MR imaging is a reliable tool for assessment of PV forward and backward flow. Furthermore, 3D velocity-encoded MR imaging assessment of TV flow proved to be more accurate than 2D velocity-encoded MR imaging assessment. Finally, 3D velocity-encoded MR imaging enabled evaluation of right ventricular diastolic function in the patients who had a corrected TOF with pulmonary regurgitation.

PV Flow

Three-dimensional velocity-encoded MR imaging has been evaluated in vitro and in vivo for assessment of valvular flow in healthy adults and adult patients, and accurate flow assessment was demonstrated with this technique (17,19). In children, high steady-state heart rate and respiration frequency potentially influence flow measurement accuracy. Our data demonstrate the feasibility of 3D velocity-encoded MR imaging for assessment of PV flow in children, with excellent correlations between the 3D velocity-encoded MR imaging and planimetric measurements. A significant difference between 2D PV forward flow volume and 3D PV forward flow volume was observed in the healthy control subjects. It has been demonstrated that systolic displacement of the PV annulus is significantly greater in healthy subjects than in patients with a corrected TOF (29). We suggest that the greater pulmonary movement in the control subjects may have caused the observed differences. To our knowledge, our study is the first in which 3D velocity-encoded MR imaging was evaluated for assessment of pulmonary backward flow. Strong correlations between 2D velocity-encoded MR imaging and 3D velocity-encoded MR imaging were observed. However, 2D velocity-encoded MR imaging, as compared with planimetry, yielded a significant overestimation of the PV backward flow volume, whereas such a difference was not observed with 3D velocity-encoded MR imaging. Our data indicate that 3D velocity-encoded MR imaging is an accurate tool for assessment of PV backward flow. One of the advantages of 3D velocity-encoded MR imaging in the assessment of pulmonary backward flow is the possibility to angulate the imaging plane according to the direction of the flow jet. We hypothesize that alterations in the direction of the regurgitant flow and movement of the pulmonary artery with respect to a fixed imaging plane caused the observed differences.

TV Flow

Assessment of TV flow with 2D velocity-encoded MR imaging is hampered by movement of the TV annulus of up to 24 mm through the fixed imaging plane (14-16), which results in a 15%–25% overestimation of the TV forward flow despite through-plane motion correction (18). Three-dimensional velocity-encoded MR imaging enables flow assessment at the level of the valve and perpendicular to the flow direction throughout the cardiac cycle with retrospective valve tracking. In accordance with a previous study (19), our study revealed that 3D velocity-encoded MR ima-

Figure 4:

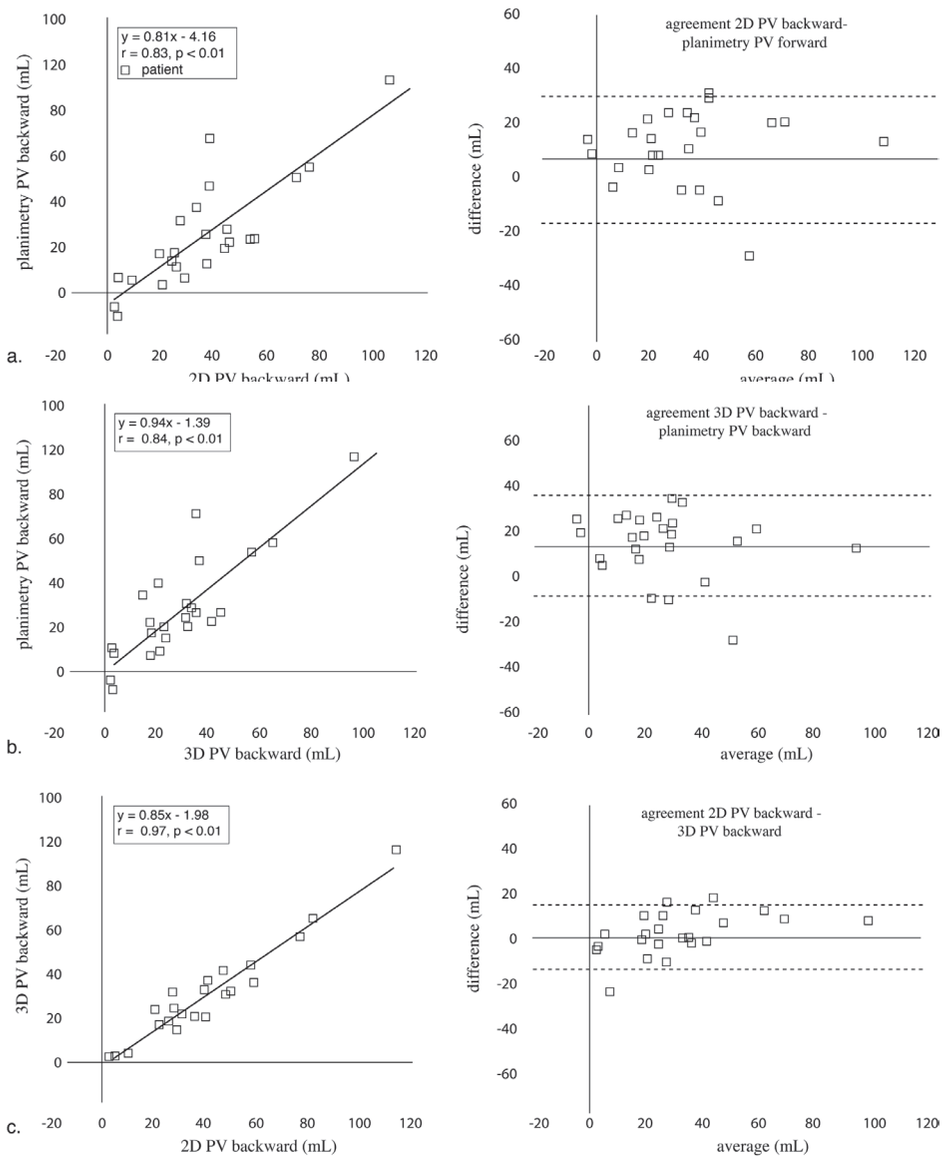

Pooled correlation and agreement of pulmonary backward flow assessed with 2D VE-MRI, 3D VE-MRI and planimetry **(a)** left: scatter plot depicting correlation between 2D PV backward flow and planimetry PV backward flow, right: Bland-Altman plot depicting agreement between 2D PV backward flow and planimetry PV backward flow. (**b):** left: scatter plot depicting correlation between 3D PV backward flow and planimetry PV backward flow, right: Bland-Altman plot depicting agreement between 3D PV backward flow and planimetry PV backward flow. **(c):** left: scatter plot depicting correlation between 2D PV backward flow and 3D PV backward flow, right: Bland-Altman plot depicting agreement between 2D PV backward flow and 3D PV backward flow. Squares: cToF patients. Abbreviations: PV: pulmonary valve, TV: tricuspid valve.

Figure 5:

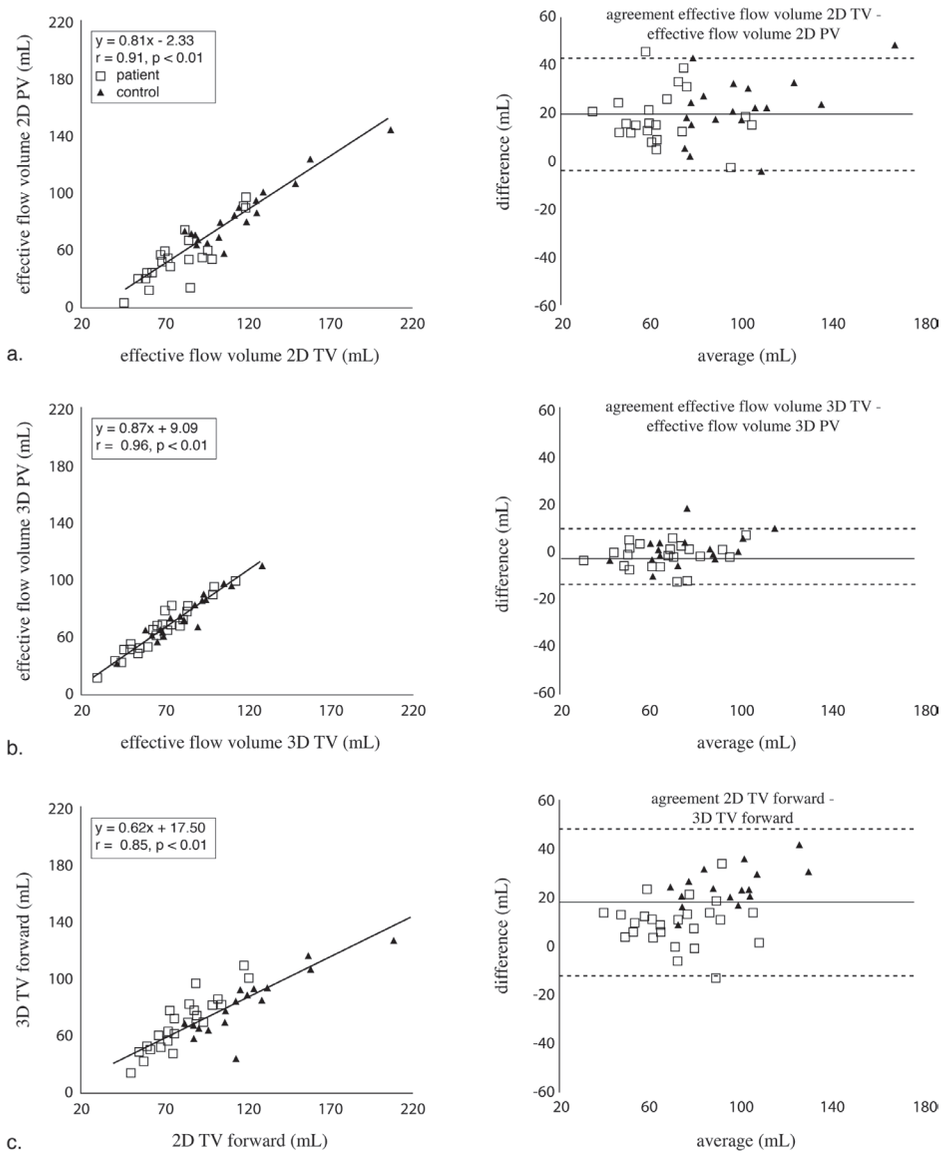

Pooled correlation and agreement of tricuspid flow assessed with 2D VE-MRI and 3D VE-MRI. **(a):** left: scatter plot depicting correlation between 2D TV forward flow and 3D TV forward flow, right: Bland-Altman plot depicting agreement between 2D PV forward and 3D TV forward flow. **(b):** left: scatter plot depicting correlation between 2D PV effective flow and 2D TV effective flow, right: Bland-Altman plot depicting agreement between 2D PV effective flow and 2D TV effective flow. **(c):** left: scatter plot depicting correlation between 3D PV effective flow and 3D TV effective flow, right: Bland-Altman plot depicting agreement between 3D PV effective flow and 3D TV effective flow. Squares: cToF patients, triangles: controls. Abbreviations: PV: pulmonary valve, TV: tricuspid valve.

ging is more accurate than 2D velocity-encoded MR imaging in the assessment of TV flow volumes. Two-dimensional velocity-encoded MR imaging yielded a significant difference between PV and TV effective flow volumes, mainly owing to an overestimation of the TV flow volume. In contrast, 3D velocity-encoded MR imaging yielded excellent correlation and agreement between PV and TV effective flow volumes. In addition to retrospective valve tracking, 3D velocity-encoded MR imaging assessment of flow through both valves during one acquisition enabled us to rule out heart rate variability errors, further improving accuracy. According to our data, 3D velocity-encoded MR imaging can play a future role in quantitative assessment of atrioventricular transvalvular flow in children with congenital heart disease.

Diastolic Right Ventricular Function

Directly after surgery, a restrictive right ventricular filling pattern correlates with a slower clinical recovery in patients with a corrected TOF (30). The clinical implications of right ventricular diastolic dysfunction during long-term follow-up remain unclear. Right ventricular restriction has been related to improved exercise capacity, less right ventricular dilatation, and less arrhythmia (3). However, others have observed a reduced tolerance for exercise and impaired right ventricular filling at dobutamine-induced stress in patients who have a corrected TOF with a restrictive right ventricle (8). The use of different diagnostic tools to assess diastolic function may have caused these conflicting results (8). The Doppler echocardiographic assessment of right ventricular diastolic function in patients with a corrected TOF is often hampered by pulmonary regurgitation. With velocity-encoded MR imaging, summation of PV flow and TV flow enables assessment of right ventricular diastolic function in the presence of pulmonary regurgitation (23). In our study, 2D and 3D velocity-encoded MR imaging time-volume curves were compared and yielded similar EPFR/APFR ratios, a parameter widely used for diastolic functional assessment (31). Nevertheless, significant differences in EPFR, APFR, and AFF were observed. Although no reference standard is available, on the basis of the more accurate diastolic flow volume measurements obtained with 3D velocity-encoded MR imaging, we speculate that the diastolic functional data derived with this technique are also more reliable. With use of 3D velocity-encoded MR imaging, restrictive right ventricular filling was confirmed in the patients who had a corrected TOF with EDFF, as evidenced by a higher EPFR (9,32). In addition, 3D velocity-encoded MR imaging detected impaired right ventricular relaxation, indicated by an increase in deceleration time, in the patients without EDFF. In the future, 3D velocity-encoded MR imaging will aid in the assessment of both right ventricular diastolic function and the clinical implications of this abnormality in patients with a corrected TOF.

Study Limitations

The postprocessing time in 3D velocity-encoded MR imaging, as compared with that in 2D velocity-encoded MR imaging, is increased because retrospective valve tracking and reformatting are performed manually and have been estimated to take 5 minutes per valve (19). Nevertheless, an advantage of 3D velocity-encoded MR imaging is the reduced imaging time. Two-dimensional velocity-encoded MR imaging with free breathing requires 3 minutes for each valve. With 3D velocity-encoded MR imaging, all valves can be addressed in one acquisition of approximately 5 minutes, depending on the heart rate (19). Especially in children, the reduced imaging time may improve the success rate of MR imaging assessment.

No reference standard is available for the estimation of flow volumes. However, compared with 2D velocity-encoded MR imaging, planimetry is hampered much less by cardiac motion and is a widely accepted technique for cardiac volumetric assessment. Our study provided an internal validation to compare PV effective and TV effective flow volumes and yielded no marked differences among the 3D velocity-encoded MR imaging measurements, with narrow limits of agreement.

In conclusion, 3D velocity-encoded MR imaging is a valid recently introduced technique for assessing PV forward and backward flow in patients with a corrected TOF and healthy children. Three-dimensional velocity-encoded MR imaging assessment of TV flow in patients with a corrected TOF is more accurate than 2D velocity-encoded MR imaging. Finally, the evaluation of diastolic function with 3D velocity-encoded MR imaging can facilitate ongoing research of the implications of diastolic dysfunction during long-term follow-up in patients with a corrected TOF.

REFERENCE LIST

1. Bouzas B, Kilner PJ, Gatzoulis MA. Pulmonary regurgitation: not a benign lesion. Eur Heart J 2005;26(5):433-439.
2. Gatzoulis MA, Balaji S, Webber SA, et al. Risk factors for arrhythmia and sudden cardiac death late after repair of tetralogy of Fallot: a multicentre study. Lancet 2000;356(9234):975-981.
3. Gatzoulis MA, Clark AL, Cullen S, Newman CG, Redington AN. Right ventricular diastolic function 15 to 35 years after repair of tetralogy of Fallot. Restrictive physiology predicts superior exercise performance. Circulation 1995;91(6):1775-1781.
4. Gatzoulis MA, Norgard G, Redington AN. Biventricular long axis function after repair of tetralogy of Fallot. Pediatr Cardiol. 1998;19(2):128-132.
5. Helbing WA, Niezen RA, Le Cessie S, van der Geest RJ, Ottenkamp J, de Roos A. Right ventricular diastolic function in children with pulmonary regurgitation after repair of tetralogy of Fallot: volumetric evaluation by magnetic resonance velocity mapping. J Am Coll Cardiol 1996;28(7):1827-1835.
6. Choi JY, Kwon HS, Yoo BW, et al. Right ventricular restrictive physiology in repaired tetralogy of Fallot is associated with smaller respiratory variability. Int J Cardiol 2008;125(1):28-35.
7. Gatzoulis MA, Till JA, Somerville J, Redington AN. Mechanoelectrical interaction in tetralogy of Fallot. QRS prolongation relates to right ventricular size and predicts malignant ventricular arrhythmias and sudden death. Circulation 1995;92(2):231-237.
8. van den Berg J, Wielopolski PA, Meijboom FJ, et al. Diastolic function in repaired tetralogy of Fallot at rest and during stress: assessment with MR imaging. Radiology 2007;243(1):212-219.
9. van Straten A, Vliegen HW, Hazekamp MG, de Roos A. Right ventricular function late after total repair of tetralogy of Fallot. Eur Radiol 2005;15(4):702-707.
10. Oosterhof T, Mulder BJ, Vliegen HW, de Roos A. Cardiovascular magnetic resonance in the follow-up of patients with corrected tetralogy of Fallot: a review. Am Heart J 2006;151(2):265-272.
11. Rebergen SA, van der Wall EE, Doornbos J, de Roos A. Magnetic resonance measurement of velocity and flow: technique, validation, and cardiovascular applications. Am Heart J 1993;126(6):1439-1456.
12. Rebergen SA, Chin JG, Ottenkamp J, van der Wall EE, de Roos A. Pulmonary regurgitation in the late postoperative follow-up of tetralogy of Fallot. Volumetric quantitation by nuclear magnetic resonance velocity mapping. Circulation 1993;88(5 Pt 1):2257-66.
13. Weber OM, Higgins CB. MR evaluation of cardiovascular physiology in congenital heart disease: flow and function. J Cardiovasc Magn Reson 2006;8(4):607-617.
14. Kayser HW, Stoel BC, van der Wall EE, van der Geest RJ, de Roos A. MR velocity mapping of tricuspid flow: correction for through-plane motion. J Magn Reson Imaging 1997;7(4):669-673.
15. Kilner PJ, Gatehouse PD, Firmin DN. Flow measurement by magnetic resonance: a unique asset worth optimising. J Cardiovasc Magn Reson 2007;9(4):723-728.
16. Morcos P, Vick GW 3rd, Sahn DJ, Jerosch-Herold M, Shurman A, Sheehan FH. Correlation of right ventricular ejection fraction and tricuspid annular plane systolic excursion in tetralogy of Fallot by magnetic resonance imaging. Int J Cardiovasc Imaging 2009;25(3):263-270.
17. Westenberg JJ, Danilouchkine MG, Doornbos J, et al. Accurate and reproducible mitral valvular blood flow measurement with three-directional velocity-encoded magnetic resonance imaging. J Cardiovasc Magn Reson 2004;6(4):767-776.
18. Westenberg JJ, Roes SD, Ajmone MN, et al. Mitral valve and tricuspid valve blood flow: accurate quantification with 3D velocity-encoded MR imaging with retrospective valve tracking. Radiology 2008;249(3):792-800.
19. Roes SD, Hammer S, van der Geest RJ, et al. Flow Assessment Through Four Heart Valves Simultaneously Using 3-Dimensional 3-Directional Velocity-Encoded Magnetic Resonance Imaging With Retrospective Valve Tracking in Healthy Volunteers and Patients With Valvular Regurgitation. Invest Radiol 2009;44(10):669-675
20. Zoghbi WA, Enriquez-Sarano M, Foster E, et al. Recommendations for evaluation of the severity of native valvular regurgitation with two-dimensional and Doppler echocardiography. J Am Soc Echocardiogr 2003;16(7):777-802.
21. Alfakih K, Plein S, Bloomer T, Jones T, Ridgway J, Sivananthan M. Comparison of right ventricular volume measurements between axial and short axis orientation using steady-state free precession magnetic resonance imaging. J Magn Reson Imaging 2003;18(1):25-32.
22. Fratz S, Schuhbaeck A, Buchner C, et al. Comparison of accuracy of axial slices versus short-axis slices for measuring ventricular volumes by cardiac magnetic resonance in patients with corrected tetralogy of fallot. Am J Cardiol 2009;103(12):1764-1769.
23. Helbing WA, Rebergen SA, Maliepaard C, et al. Quantification of right ventricular function with magnetic resonance imaging in children with normal hearts and with congenital heart disease. Am Heart J 1995;130(4):828-837.
24. Sechtem U, Pflugfelder PW, Gould RG, Cassidy MM, Higgins CB. Measurement of right and left ventricular volumes in healthy individuals with cine MR imaging. Radiology 1987;163(3):697-702.
25. van der Geest RJ, Niezen RA, van der Wall EE, de Roos A, Reiber JH. Automated measurement of volume flow in the ascending aorta using MR velocity maps: evaluation of inter- and intraobserver variability in healthy volunteers. J Comput Assist Tomogr 1998;22(6):904-911.
26. van der Geest RJ, Buller VG, Jansen E, et al. Comparison between manual and semiautomated analysis of left ventricular volume parameters from short-axis MR images. J Comput Assist Tomogr 1997;21(5):756-765.
27. Buonocore MH, Bogren H. Factors influencing the accuracy and precision of velocity-encoded phase imaging. Magn Reson Med 1992;26(1):141-154.
28. Bland JM, Altman DG. Statistical methods for assessing agreement between two methods of clinical measurement. Lancet 1986;1(8476):307-310.
29. Uebing A, Gibson DG, Babu-Narayan SV, et al. Right ventricular mechanics and QRS duration in patients with repaired tetralogy of Fallot: implications of infundibular disease. Circulation 2007;116(14):1532-1539.
30. Sachdev MS, Bhagyavathy A, Varghese R, Coelho R, Kumar RS. Right ventricular diastolic function after repair of tetralogy of Fallot. Pediatr Cardiol 2006;27(2):250-255.
31. Nagueh SF, Appleton CP, Gillebert TC,et al. Recommendations for the evaluation of left ventricular diastolic function by echocardiography. J Am Soc Echocardiogr 2009;22(2):107-133.
32. Mittal SR, Barar RV, Arora H. Echocardiographic evaluation of left and right ventricular function in mild hypertension. Int J Cardiovasc.Imaging 2001;17(4):263-270.

CHAPTER 4

Prediction of outcome of congenital heart disease patients patients with echocardiography

4.1

Mild residual pulmonary stenosis after correction of tetralogy of Fallot reduces the risk of pulmonary valve replacement during follow-up

Submitted

A.E. van der Hulst*
M.G. Hylkema*
H.W. Vliegen
V. Delgado
M.G. Hazekamp
M.E.B. Rijlaarsdam
E.R. Holman
N.A. Blom
A.A.W. Roest
* equal authorship

ABSTRACT

Objective: Current surgical strategies that aim at preventing pulmonary regurgitation in patients with corrected tetralogy of Fallot (cToF) may result in a certain grade of residual pulmonary stenosis (PS). The clinical implications of a postoperative residual PS in cToF patients remain unclear. Pulmonary valve replacement (PVR) due to pulmonary regurgitation is frequently needed during follow-up of cToF patients. The aim of the current study was to determine the role of residual PS on the need for PVR during follow-up in cToF patients.

Design and patients: cToF patients were included if clinical follow-up after primary surgical correction had taken place for a minimum of five years. Patient characteristics, surgical parameters and postoperative parameters were reviewed, with special focus on the transpulmonic valve systolic gradient.

Main outcome measure: Cox proportional hazards regression analysis was performed to identify predictors of PVR.

Results: Out of 171 cToF patients, 71 (41.5%) underwent PVR after 24.2 years (inter-quartile range: 16.8 - 31.6 years). Year of birth, older age at corrective surgery and patch use significantly predicted PVR during follow-up. In contrast, a mild residual PS in cToF patients (peak systolic gradient 15 to 30 mmHg) independently reduced the risk of PVR, as compared with patients without PS (hazard ratio: 0.47, p=0.02) and with moderate-to-severe PS (hazard ratio: 0.35, p=0.01).

Conclusion: In addition to known risks factors for PVR, a postoperative mild residual PS reduces the risk of PVR during follow-up of cToF patients. This finding provides clinical evidence for a conservative PS relief during correction of ToF patients.

Table 1. Patient characteristics and surgical parameters

	PVR (n=71)	no PVR (n=100)	p-value
Patient characteristics			
Follow-up (y)	24.3 (16.5-31.6)	21.3 (12.1-37)	0.59
Year of birth (y)	1972 (1963-1986)	1985 (1961-1996)	<0.01
Male/female n (%)	37/34	44/56	0.30
Chromosomal abnormalities n (%)	8 (11)	10 (10)	0.79
Pre-/peri-operative			
Palliative procedure n (%)	24 (33)	28 (28)	0.42
Age at repair (y)	4.9 (1.5-6.7)	1.6 (0.7-8.1)	0.05
Surgical approach n (%)			<0.01
Transventricular	48 (81)	11 (12)	
Transatrial/transpulmonary	11 (18)	50 (54)	
Type of PS relief n (%)			<0.01
No patch	13 (20)	52 (80)	
RVOT and/or PApatch	18 (62)	10 (36)	
Transannular patch	38 (54)	33 (46)	
Valve morphology n (%)			0.91
Bicuspid	20 (33)	40 (70)	
Tricuspid	8 (29)	17 (30)	
Valve intervention n (%)	41 (65)	34 (38)	<0.01
Pulmonary annulus (z-score)	-0.84 (-2.0-0.17)	-0.295 (-0.1-0.17)	0.136
Cross-clamp time (min), mean (SD)	62 ± 30	61 ± 28	0.98
Minimum temp (°C)	25 (23-27)	27 (25-28)	0.02

Continuous data presented as median and inter-quartile range unless specified. Abbreviations: PA: pulmonary artery, PS: pulmonary stenosis, PVR: pulmonary valve replacement, RVOT: right ventricular outflow tract, temp: temperature.

Table 2. Postoperative parameters

	PVR (n=71)	no PVR (n=100)	p-value
QRS duration (s)	0.12 (0.10-0.14)	0.10 (0.80-0.13)	0.05
Pulmonary insufficiency, n (%)			0.05
None	2 (13)	14 (87)	
Mild	40 (44)	51 (56)	
Moderate-to-severe	28 (45)	34 (55)	
Pulmonary stenosis, n (%)			0.15
None (0-15 mmHg)	31 (45)	38 (55)	
Mild (>15-30 mmHg)	20 (30)	46 (69)	
Moderate-to-severe (>30 mmHg)	13 (46)	15 (53)	

Continous data presented as median and inter-quartile range. Abbreviation: IQR: inter-quartile range.

Table 3. Univariate analysis of determinants of PVR in cToF patients at follow-up

	HR	95% CI	p-value
Patient characteristics			
Year of birth (y)	1.10	1.07 - 1.14	<0.01
Male sex	1.19	0.74 - 1.89	0.48
Chromosomal abnormalities	1.84	0.87 - 3.88	0.11
Pre-/peri operative			
Palliation	0.68	0.42 -1.12	0.13
Age at repair (y)	0.90	0.85 - 0.96	<0.01
Transatrial/transpulmonary	3.35	1.53 - 7.36	<0.01
Patch use			
Non-transannular	5.07	2.45 - 10.51	<0.01
Transannular	9.2	4.79 - 17.83	<0.01
Bicuspid valve	2.81	1.20 - 6.59	0.02
Valve intervention	1.31	0.78 - 2.20	0.31
Pulmonary annulus (z-score)	0.90	0.78 - 1.04	0.16
Cross-clamp time (min)	1.02	1.01 - 1.03	<0.01
Minimum temp (°C)	1.00	0.93 - 1.08	0.97
Postoperative			
QRS interval (s)	0.15	0.00 - 439.47	0.64
Pulmonary regurgitation			
Mild	3.62	0.87 - 14.97	0.76
Moderate-to-severe	6.20	1.48 - 28.10	0.01
Pulmonary stenosis			
Mild vs. none	0.73	0.42 - 1.29	0.28
Mild vs. moderate-to-severe	0.55	0.27 - 1.11	0.09
None vs. moderate-to-severe	0.75	0.39 - 1.43	0.38

Abbreviations: CI: confidence interval, HR: hazard ratio, temp: temperature

Table 4. Multivariate analysis determinants of PVR in cToF patients at follow-up

	HR	95% CI	p-value
Patient characteristics			
Year of birth (y)	1.19	1.12 - 1.26	<0.01
Male sex	..	..	..
Chromosomal abnormalities	..	..	..
Pre/ peri-operative			
Palliation	..	..	..
Age at repair (y)	1.18	1.10 - 1.27	<0.01
Transatrial/transpulmonary	0.82	0.31 - 2.18	0.70
Patch use			
Non-transannular	5.24	2.28 - 12.06	<0.01
Transannular	8.13	3.73 - 17.68	<0.01
Bicuspid valve	..	..	..
Valve intervention	..	..	..
Pulmonary annulus (z-score)	..	..	..
Cross-clamp time (min)	..	..	..
Minimum temp (°C)	...	..	..
Postoperative			
QRS interval (s)	..	..	..
Pulmonary regurgitation			
Mild	1.66	0.36 - 7.65	0.51
Moderate-to-severe	1.54	0.33 – 7.28	0.59
Pulmonary stenosis			
Mild vs. none	0.47	0.25 - 0.88	0.02
Mild vs. moderate-to-severe	0.35	0.15- 0.81	0.01
None vs. moderate-to-severe	0.75	0.35 - 1.59	0.45

Abbreviations: CI: confidence interval, HR: hazard ratio, temp: temperature

INTRODUCTION

Surgical repair in patients with tetralogy of Fallot (ToF) is performed by closure of the ventricular septal defect and relief of pulmonary stenosis (PS) by infundibulectomy and/or valvotomy. In addition, surgical enlargement of the pulmonary annulus and right ventricular outflow tract (RVOT) with a patch may be needed. However, this surgical approach often results in significant pulmonary regurgitation, especially when a patch is used.(1) Chronic volume overload secondary to significant pulmonary valve regurgitation may lead to RV dilatation and dysfunction with important prognostic implications.(2;3) In the last decade, pulmonary valve replacement (PVR) has been increasingly used in cToF patients during follow-up in order to prevent or reverse adverse RV remodelling and dysfunction. Furthermore, to limit the amount of pulmonary regurgitation and its adverse effects on the RV, current surgical strategies to relieve PS during repair of ToF aim to limit the use of a patch whenever possible.(2;4-6) However, this conservative surgical approach may result in a certain degree of residual PS in post-operative cToF patients. Although the benefits of this conservative approach have been demonstrated(6), there are no data on the clinical implications of a postoperative residual pulmonary systolic gradient in cToF patients.

A mild residual PS could limit the amount of pulmonary regurgitation in cToF patients and consequently, reduce the need for PVR.(4) However, a moderate or severe residual PS is related to tricuspid insufficiency and RV failure.(7) Accordingly, the aim of the current study was to investigate the influence of various grades of PS on the need for PVR in cToF patients among several clinical, surgical and echocardiographic parameters during long-term follow-up in cToF patients.

METHODS

Study population and design

The study population was selected from a clinical database of the Center for Congenital Heart disease Amsterdam-Leiden (CAHAL). In this database, all patients that have undergone surgery for congenital heart disease at the Leiden University Medical Center and the Amsterdam Academic Medical Center are registered. Patients were included in the current analysis if their diagnosis was ToF, and if clinical follow-up had taken place at our institution for a minimum of five years postoperatively. Patients with pulmonary atresia, absent pulmonary valve or a complete atrioventricular septal defect and patients who received a surgical pulmonary conduit or PVR at the time of corrective surgery were excluded.

Various pre-operative and peri-operative parameters were retrospectively evaluated in the study population. Furthermore, the included cToF patients were followed-up from corrective surgery until PVR occurred and this time interval was recorded. In the cToF patients who did not undergo PVR, the follow-up duration ended at the last clinical visit prior to August 2010. From this follow-up period, clinical notes, surgical reports and echocardiographic studies were comprehensively reviewed and various parameters were recorded. The first available postoperative echocardiographic study

Figure 1. Relationship between time to PVR and year of birth

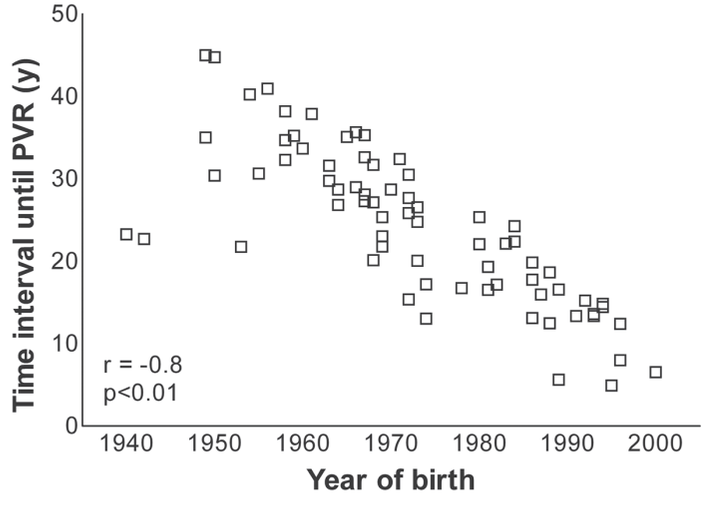

Scatterplot depicting the relationship between the time interval between corrective surgery and pulmonary valve replacement and the year of birth. The more recently born cToF patients had a significant shorter time-interval between corrective surgery and PVR.
Abbreviation: PVR: pulmonary valve replacement.

Figure 2. Relationship between age at corrective surgery and year of birth

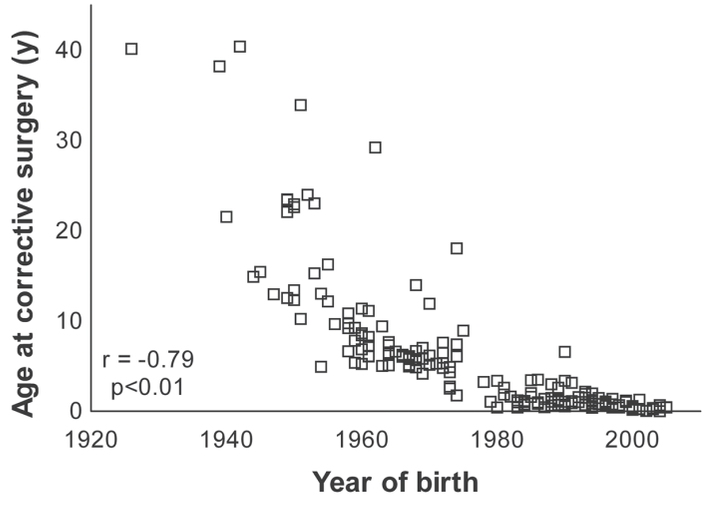

Scatterplot depicting the relation between age at corrective surgery and the year of birth. The more recently born cToF patients were significantly younger at corrective surgery.Abbreviation: PVR: pulmonary valve replacement.

was selected to evaluate pulmonary regurgitation and residual PS. Finally, the influence of clinical, surgical and echocardiographic parameters on the risk for PVR was evaluated, with a particular focus on the various grades of postoperative residual PS.

Pre-operative and peri-operative parameters

All palliative procedures prior to the corrective operation (such as Blalock-Taussig shunt placement) were noted. In addition, the surgical and anaesthetic reports concerning the corrective operation of all included patients were recorded. From these reports, the following parameters were reviewed: operation date, pulmonary valve morphology (bicuspid or tricuspid pulmonary valve), pulmonary artery size, transventricular or transatrial surgery, use of a patch (transannular or non-transannular), pulmonary valve interventions (valvotomy, commissurotomy or valve dilatation). The pulmonary artery size was assessed with Hegar dilators after relief of the PS during surgery. Pulmonary artery size was expressed as z-score, taking into account the patient's body surface area at the time of surgery. Finally, the aortic cross-clamp time and lowest body temperature during the corrective surgery were obtained from the anaesthetic reports.

Postoperative parameters

From the earliest postoperative electrocardiographic (ECG) recordings, the maximum QRS duration was obtained. In addition, the earliest postoperative echocardiographic studies were comprehensively reviewed. If the echocardiographic study was available in digital format, it was reviewed with the use of EchoPac (version 108.1.5 General Electric Medical Systems). Alternatively, the data regarding pulmonary regurgitation and stenosis were obtained from the echocardiographic notes. Presence and severity of pulmonary regurgitation were recorded. The severity of pulmonary regurgitation was assessed and categorized as absent, mild, and moderate-to-severe. In addition, with continuous wave Doppler flow recordings, the peak pressure gradient across the RVOT/pulmonary artery was assessed. Peak systolic pulmonary gradients were arbitrarily categorized in none, mild and moderate-to-severe PS (0-15 mmHg, 15-30 mmHg and >30 mmHg, respectively).

Statistical analysis

Data were tested for the normal distribution by the Kolmogorov-Smirnov test. Continuous data with a normal distribution are presented as mean ± standard deviation. Continuous data with no normal distribution are presented as median and inter-quartile range (IQR). Categorical data are presented as numbers and percentages. Differences between the group of patients with PVR and the group of patients without PVR were assessed with the Student's t-test or Mann-Whitney U-test, where appropriate, for continuous variables and with the Chi-square test for categorical variables. Linear regression analysis was performed to investigate the relationship between year of birth and the time interval between surgical correction and PVR, and the relationship between year of birth and age at surgical correction. Univariate and multivariate Cox proportional hazards regression analyses were performed to identify pre-operative, peri-operative and post-operative predictors of PVR during follow-up. Univariate predictors with p-values <0.1 and ≥70% complete data were entered as predictors in the multivariate analysis. Hazard ratios (HR) and 95% confidence intervals (CI) were calculated for each variable. A value of $p<0.05$ was considered significant. Data analysis was performed with SPSS software for Windows (version 17.0, SPSS Inc, Chicago, Illinois).

RESULTS

Patient characteristics and follow-up

A total of 171 cToF patients were included in the present analysis. Of these patients, 71 (41.5%) underwent PVR during follow-up. Table 1 summarizes the characteristics of all included cToF patients. The overall median follow-up duration between corrective surgery and PVR was 24.2 years (IQR: 16.8 - 31.6 years). Of all PVR procedures, 55 (77.5%) were performed during the last decade (2000 to 2010). The age at corrective surgery significantly decreased over the study period ($r = -0.79$, $p<0.01$; Figure 1). Furthermore, as a result of an earlier re-intervention, the more recently born patients had a shorter interval to PVR ($r = -0.80$, $p<0.01$), as shown in Figure 2. Finally, the overall survival during follow-up after corrective surgery was 95.4%.

Pre-operative and peri-operative parameters

Table 1 depicts the pre-operative and peri-operative parameters of the included cToF patients. Palliative surgical shunts procedures prior to the corrective surgery were performed in 52 patients at a median age of 2.3 years (IQR: 7 months - 3.8 years). In 4 patients, 2 palliative procedures were performed. Corrective surgery was performed between 1959 and 2005. The median age at corrective surgery was 4.9 years in the PVR group, and 1.6 years in the group without PVR ($p=0.05$). Finally, patch use was significantly different in the two groups. In the PVR group, 13 (20%) patients had no patch and 38 (54%) patients received a transannular patch. In contrast, in the group without PVR, 80% of patients did not have a patch whereas 46% had a transannular patch ($p<0.01$).

Post-operative parameters

Table 2 shows the postoperative data, obtained from ECG and echocardiographic recordings. In the PVR group, 2 patients (13%) showed no pulmonary regurgitation at the earliest post-operative examination, whereas 40 (44%) and 28 (45%) patients presented with mild and moderate-to-severe pulmonary regurgitation, respectively. In contrast, in the group of patients without PVR, these percentages were 87%, 56% and 34% ($p=0.05$). Finally, the earliest post-operative peak systolic gradient across the RVOT/pulmonary artery was recorded. Among the 71 patients that underwent PVR, 31 patients (45%) had no residual pulmonary gradient.

Furthermore, 20 of the PVR patients (30%) had a mild PS and 13 patients (46%) had a moderate-to-severe residual PS. In the patients without PVR during follow-up, these percentages were 55%, 69% and 53%, respectively.

Prediction of PVR during follow-up

Table 3 and Table 4 summarize the results of the univariate and multivariate regression analysis. After multivariate regression analysis, the risk of PVR was significantly higher in the cToF patients that were more recently born (HR: 1.19, 95% CI: 1.12 - 1.26, p<0.01). In addition, of the surgical parameters, older age at surgical repair (HR: 1.18, 95% CI: 1.10 - 1.27, p<0.01) and the use of patch to relieve PS during the corrective surgery (non-transannular: HR: 5.24, 95% CI: 2.28 - 12.06, p<0.01, transannular patch: HR: 8.13, 95% CI: 3.73 - 17.68, p<0.01) significantly increased the risk of PVR. Finally, of the postoperative variables, the group of patients with mild PS showed a significantly reduced risk of PVR as compared with the patients without PS (HR: 0.47, 95% CI: 0.25 - 0.88, p=0.02) and as compared with the patients with moderate-to-severe PS (HR: 0.35, 95% CI: 0.35 – 1.59, p=0.01).

DISCUSSION

The current study shows that in cToF patients, an older age at corrective surgery and the use of a patch are independent predictors of PVR during long-term follow-up. Furthermore, increasing age at surgical correction and a more recent year of birth independently predicted PVR, reflecting altered surgical indications over time. Finally, our results demonstrate that a mild postoperative residual PS independently reduces the risk of PVR in cToF patients.

PVR in cToF patients

PVR in cToF patients with pulmonary regurgitation and RV dilatation has proven its benefits. After PVR, pulmonary regurgitation decreases, RV volumes normalize and clinical status improves. (8-10) According to these current insights, the number of cToF patients undergoing PVR has increased, and the age at PVR has decreased, as was observed in the results of the present study. Nevertheless, PVR is an invasive procedure and furthermore, it places cToF patients at risk for late prosthetic valve failure.(11) Accordingly, comprehensive knowledge about predictors of the need for PVR in cToF patients is of value to refine clinical counselling, to improve follow-up protocols and ultimately, to prevent the need for PVR in cToF patients.

Risk factors for PVR in cToF patients

Previous studies have identified clinical parameters that determine outcome in cToF patients, such as age at surgical repair and the use of patch.(1;12;13) Accordingly, these parameters significantly predicted PVR in the present study. In addition, the current investigation focused on the role of a residual pulmonary systolic gradient during follow-up of cToF patients. To prevent pulmonary regurgitation in cToF patients and its adverse effects on the RV, current surgical strategies advocate a conservative relief of PS in ToF patients, primarily by limiting patch use.(4-6) However, this conservative surgical approach may lead to a residual PS, and the long-term clinical implications of a residual PS remain unclear. In the present analysis, a postoperative mild residual PS was observed in 39% of patients, and a moderate-to-severe PS was observed in 16% of patients. According to our results, the presence of a mild residual PS independently reduced the need for PVR at follow-up. In a recent experimental study, Kilner and colleagues demonstrated that an increasing pulmonary gradient was closely correlated with a reduced regurgitation fraction.(14) Furthermore, in a clinical study including 67 cToF patients, Uebing et al. reported a significant relation between a smaller postoperative pulmonary annulus area and a reduced severity of pulmonary regurgitation.(4) These studies indicate that after surgical correction of ToF, a mild residual PS reduces the need for PVR during follow-up of cToF patients. In contrast, the presence of a moderate-to-severe residual PS significantly increased the risk for PVR in the current report. A moderate-to-severe outflow tract obstruction is related with reduced RV performance and tricuspid regurgitation(7), which are concomitant indications for PVR in cToF patients with pulmonary regurgitation.(15)
Finally, in the present study, the absence of a residual PS increased the risk of PVR during follow-up of cToF patients. Extensive infundibulectomy and patching to relieve PS in cToF patients, resulting in the absence of a residual gradient, may lead to dilatation and impaired contractility of the RVOT. (16-18) In a previous report by d'Udekem d'Acoz et al., a total of 189 cToF patients with pulmonary regurgitation were compared to 44 PS patients with pulmonary regurgitation after commissurotomy. (16) Despite similar grades of pulmonary regurgitation in the two groups, the cToF patients showed more RV dilatation.(16) An important difference between surgical correction of ToF and surgical correction of isolated PS is the manipulation of the RVOT during ToF correction. The authors concluded that the resultant postoperative RVOT dilatation and dysfunction in cToF patients aggravates the deleterious effect of pulmonary regurgitation on the RV.(16) Based on these observations and the results of the current study, there is a delicate equilibrium among the pulmonary gradient, the use of a patch and the severity of pulmonary regurgitation, ultimately leading to RV dilatation and RV failure which culminates into the decision to perform PVR in cToF patients.

CONCLUSION

This study provides novel insights into the predictive value of peri-operative parameters on the need of PVR during follow-up in cToF patients. In addition to known risk factors for PVR, a mild residual PS independently reduced the need for PVR. This finding provides clinical evidence underscoring the importance of current surgical strategies, advocating a conservative relief of PS in ToF patients.

REFERENCE LIST

1 d'Udekem Y, Ovaert C, Grandjean F, Gerin V, Cailteux M, Shango-Lody P, et al. Tetralogy of Fallot: transannular and right ventricular patching equally affect late functional status. Circulation 2000 Nov 7;102(19 Suppl 3):III116-III122.

2 Gatzoulis MA, Balaji S, Webber SA, Siu SC, Hokanson JS, Poile C, et al. Risk factors for arrhythmia and sudden cardiac death late after repair of tetralogy of Fallot: a multicentre study. Lancet 2000 Sep 16;356(9234):975-81.

3 Bouzas B, Kilner PJ, Gatzoulis MA. Pulmonary regurgitation: not a benign lesion. Eur Heart J 2005 Mar;26(5):433-9.

4 Uebing A, Fischer G, Bethge M, Scheewe J, Schmiel F, Stieh J, et al. Influence of the pulmonary annulus diameter on pulmonary regurgitation and right ventricular pressure load after repair of tetralogy of Fallot. Heart 2002 Nov;88(5):510-4.

5 Stewart RD, Backer CL, Young L, Mavroudis C. Tetralogy of Fallot: results of a pulmonary valve-sparing strategy. Ann Thorac Surg 2005 Oct;80(4):1431-8.

6 Voges I, Fischer G, Scheewe J, Schumacher M, Babu-Narayan SV, Jung O, et al. Restrictive enlargement of the pulmonary annulus at surgical repair of tetralogy of Fallot: 10-year experience with a uniform surgical strategy. Eur J Cardiothorac Surg 2008 Nov;34(5):1041-5.

7 Bonow RO, Carabello BA, Chatterjee K, de LA, Jr., Faxon DP, Freed MD, et al. 2008 Focused update incorporated into the ACC/AHA 2006 guidelines for the management of patients with valvular heart disease: a report of the American College of Cardiology/American Heart Association Task Force on Practice Guidelines (Writing Committee to Revise the 1998 Guidelines for the Management of Patients With Valvular Heart Disease): endorsed by the Society of Cardiovascular Anesthesiologists, Society for Cardiovascular Angiography and Interventions, and Society of Thoracic Surgeons. Circulation 2008 Oct 7;118(15):e523-e661.

8 Cheung EW, Wong WH, Cheung YF. Meta-analysis of pulmonary valve replacement after operative repair of tetralogy of fallot. Am J Cardiol 2010 Aug 15;106(4):552-7.

9 Geva T. Indications and timing of pulmonary valve replacement after tetralogy of Fallot repair. Semin Thorac Cardiovasc Surg Pediatr Card Surg Annu 2006;11-22.

10 Vliegen HW, van SA, de RA, Roest AA, Schoof PH, Zwinderman AH, et al. Magnetic resonance imaging to assess the hemodynamic effects of pulmonary valve replacement in adults late after repair of tetralogy of fallot. Circulation 2002 Sep 24;106(13):1703-7.

11 Zubairi R, Malik S, Jaquiss RD, Imamura M, Gossett J, Morrow WR. Risk factors for prosthesis failure in pulmonary valve replacement. Ann Thorac Surg 2011 Jan 1;91(2):561-5.

12 Pigula FA, Khalil PN, Mayer JE, del Nido PJ, Jonas RA. Repair of tetralogy of Fallot in neonates and young infants. Circulation 1999 Nov 9;100(19 Suppl):II157-II161.

13 Walsh EP, Rockenmacher S, Keane JF, Hougen TJ, Lock JE, Castaneda AR. Late results in patients with tetralogy of Fallot repaired during infancy. Circulation 1988 May;77(5):1062-7.

14 Kilner PJ, Balossino R, Dubini G, Babu-Narayan SV, Taylor AM, Pennati G, et al. Pulmonary regurgitation: the effects of varying pulmonary artery compliance, and of increased resistance proximal or distal to the compliance. Int J Cardiol 2009 Apr 3;133(2):157-66.

15 Park CS, Lee JR, Lim HG, Kim WH, Kim YJ. The long-term result of total repair for tetralogy of Fallot. Eur J Cardiothorac Surg 2010 Sep;38(3):311-7.

16 d'Udekem dY, Pasquet A, Lebreux L, Ovaert C, Mascart F, Robert A, et al. Does right ventricular outflow tract damage play a role in the genesis of late right ventricular dilatation after tetralogy of Fallot repair? Ann Thorac Surg 2003 Aug;76(2):555-61.

17 Davlouros PA, Kilner PJ, Hornung TS, Li W, Francis JM, Moon JC, et al. Right ventricular function in adults with repaired tetralogy of Fallot assessed with cardiovascular magnetic resonance imaging: detrimental role of right ventricular outflow aneurysms or akinesia and adverse right-to-left ventricular interaction. J Am Coll Cardiol 2002 Dec 4;40(11):2044-52.

18 Wald RM, Haber I, Wald R, Valente AM, Powell AJ, Geva T. Effects of regional dysfunction and late gadolinium enhancement on global right ventricular function and exercise capacity in patients with repaired tetralogy of Fallot. Circulation 2009 Mar 17;119(10):1370-7.

4.2

Prediction of atrial arrhythmia in adult patients with congenital heart disease with tissue Doppler imaging

Submitted

A.E. van der Hulst
A.A.W. Roest
E.R. Holman
H.W. Vliegen
M.G. Hazekamp
J.J. Bax
N.A. Blom
V. Delgado

ABSTRACT

Aims: Atrial arrhythmia (AA) is common in adult patients with congenital heart disease (CHD). To enable prevention of AA or its complications, timely identification of adult CHD patients at risk for AA is crucial. Long total atrial activation times have been related to AA. Tissue Doppler imaging permits non-invasive evaluation of the total atrial conduction time (PA-TDI duration). The present study evaluated the role of PA-TDI duration in adult CHD patients to predict AA.

Methods and Results: A total of 223 adult CHD patients were followed-up for the occurrence of AA after PA-TDI duration assessment. The PA-TDI duration was defined as the time interval from the onset of the P-wave on the electrocardiogram to the peak of the A' wave at the lateral atrial wall on TDI tracings. Among various clinical and echocardiographic parameters, the value of the PA-TDI duration to predict AA occurrence was investigated. Median follow-up was 39 months (inter-quartile range 21 to 57 months). A PA-TDI duration ≥126 ms predicted AA during follow-up (log rank p<0.001). At multivariate analysis, PA-TDI duration (hazard ratio (HR) 2.02, 95% confidence interval (CI) 1.07-3.83), prior history of AA (HR 4.85, 95% CI 2.71-8.69) and surgical procedures during follow-up (HR 2.33 95% CI 1.26-4.33) independently predicted the occurrence of AA.

Conclusion: The PA-TDI duration, prior history of AA and surgical procedures during follow-up are independent predictors of the occurrence of AA in adult CHD patients. PA-TDI duration is a useful tool to identify CHD patients at risk for AA during follow-up.

INTRODUCTION

Improvements in cardiac surgery have led to increased survival of patients with congenital heart disease (CHD). Consequently, the population of adult patients with CHD is growing and aging.[1] During follow-up, atrial arrhythmia (AA) is a frequent clinical problem in this group of patients with a lifetime risk over 50% in patients with severe CHD.[2] AA in adult patients with CHD is related to thrombo-embolic complications, heart failure and increased mortality.[2] To enable prevention of AA or its complications, timely identification of adult CHD patients at risk for AA is essential. In CHD patients, longstanding altered atrial hemodynamics, increased atrial pressure and surgical atrial scarring promote atrial remodeling and electrical conduction abnormalities.[3] These electrical disturbances include prolonged atrial conduction time, favoring the onset of AA.[4, 5] Recently, a novel echocardiographic tool using tissue Doppler imaging (TDI), has shown to be a fast, easy and reliable method to assess the total atrial conduction time.[6] With color-coded TDI of the atria, the time interval from the onset of the P-wave on the electrocardiogram to the peak of the A' wave on the TDI tracings of the lateral atrial wall can be measured (so-called PA-TDI duration). The PA-TDI duration reflects the total atrial conduction time, and has been shown to be a predictor of AA in patients with cardiac disease.[6-8] However, the value of the PA-TDI duration to predict AA in CHD patients has not been evaluated. The current study investigated the clinical and echocardiographic predictors of AA in adult CHD patients. Specifically, the value of PA-TDI duration to predict the occurrence of AA in adult CHD patients was assessed.

METHODS

Patient population and data collection

The present population included adult patients with CHD, who were followed-up for the occurrence of AA from the first available TDI echocardiogram in sinus rhythm (baseline) until November 2010. Patients without sinus rhythm at baseline or without further clinical follow-up visits were excluded from the analysis. AA was defined as atrial tachycardia, atrial flutter, or atrial fibrillation on surface electrocardiogram (ECG), 24 or 48 hours Holter ECG or implantable cardioverter-defibrillator device recordings.

Clinical and echocardiographic data were retrieved from the departmental Cardiology Information System (EPD-Vision®, Leiden University Medical Center) and the echocardiographic database, respectively. All adult CHD patients underwent a complete clinical evaluation at baseline. The CHD diagnosis was specified to be 'severe CHD' or 'not severe CHD', as described previously.[9] In addition, the use of beta-blockers, anti-arrhythmic medication or angiotensin-converting enzyme (ACE) inhibitors at baseline was recorded. Furthermore, the presence of hypertension at baseline (systolic pressure >140 mmHg and/or diastolic pressure >90 mmHg) and any surgical procedures during follow-up were documented. In addition, baseline echocardiographic variables included dimensions

Table 1. Patient characteristics at baseline and during follow-up

	AA (n= 57)	No AA (n=166)	p-value
Clinical parameters			
Age (y)	51 ± 13	48 ± 12	0.245
Male/female, n (%)	30/27 (53/47)	79/87 (48/52)	0.511
Severe CHD*, n (%)	30 (53)	57 (34)	0.015
Prior history of AA, n (%)	35 (61)	26 (16)	<0.001
Medication, n (%)			
Beta-blocker	31 (54)	25 (15)	<0.001
Anti-arrhythmic	5 (9)	10 (6)	0.475
ACE inhibitor	21 (36)	32 (19)	0.007
Hypertension, n (%)	5 (9)	23 (14)	0.318
Surgical procedure during follow-up, n (%)	14 (25)	15 (9)	0.003
Echocardiographic parameters			
Systemic ventricle EDV (ml)	124 ± 46	118 ± 49	0.441
Systemic ventricle ESV (ml)	68 ± 34	61 ± 32	0.187
Systemic ventricle EF (%)	46 ± 13	48 ± 11	0.118
PA-TDI (ms)	152 ± 33	121 ± 24	<0.001

* 'Severe CHD' included the following diagnoses: atrioventricular septum defect, tetralogy of Fallot, D-transposition after arterial switch, D-transposition after atrial switch, L-transposition, truncus arteriosus, and tricspid atresia. 'Not severe CHD' included: anomalous pulmonary venous return, aortic stenosis, ventricular septum defect, atrial septum defect, atrial septum defect and ventricular septum defect, coarctation of the aorta, Ebstein's anomaly, patent ductus arteriosus, pulmonary stenosis, pulmonary stenosis and atrial septum defect, pulmonary stenosis and ventricular septum defect. Abbreviations: AA: atrial arrhythmia, ACE: angiotensin-converting enzyme, CHD: congenital heart disease, EDV: end-diastolic volume, EF: ejection fraction, ESV: end-systolic volume, FU: follow-up, PA-TDI: total atrial activation time, as assessed with tissue Doppler imaging.

Table 2. Univariate and multivariate predictors of atrial arrhythmia in patients with congenital heart disease

Predictor	Univariate analysis			Multivariate analysis		
	HR	95% CI	p-value	HR	95% CI	p-value
Severity of CHD	1.61	0.96 - 2.71	0.074			
History of AA	6.38	3.69 - 11.03	<0.001	4.85	2.71 - 8.69	<0.001
Gender	0.84	0.50 -1.41	0.510	…	…	…
Hypertension	0.74	0.29 - 1.84	0.512	…	…	…
Surgical procedure	2.91	1.58 - 5.34	0.001	2.33	1.26 - 4.33	0.007
Systemic ventricle EDV	1.00	0.99 -1.01	0.554	…		
Systemic ventricle ESV	1.00	0.99 - 1.01	0.316			
Systemic ventricle EF	0.99	0.96 - 1.01	0.247			
PA-TDI dichotomized	3.66	2.03 - 6.61	<0.001	2.02	1.07 - 3.83	0.031

Abbreviations: AA: atrial arrhythmia, CHD: congenital heart disease, CI: confidence interval, EDV: end-diastolic volume, ESV: end-systolic volume, EF: ejection fraction, HR: hazard ratio, PA-TDI: total atrial activation time, as assessed with tissue Doppler imaging.

and systolic function of the systemic ventricle and the total atrial conduction time as measured with TDI (PA-TDI). Among the several clinical and echocardiographic parameters, the independent determinants of AA occurrence during follow-up were identified. Subsequently, the value of the PA-TDI duration to predict the occurrence of AA in adult CHD was assessed.

Echocardiography

Transthoracic echocardiographic images were acquired with a commercially available system equipped with a 3.5 MHz transducer (Vivid-7, GE Vingmed Ultrasound AS, Horten, Norway). Subjects were in the left lateral decubitus position during image acquisition. Standard two-dimensional images were acquired from the parasternal (long- and short-axis) and apical views (2-, 4-chamber and long-axis) and digitally stored in cine-loop format. Analyses were performed off-line using EchoPac version 108.1.5 (General Electric Medical Systems). The end-diastolic and end-systolic volumes of the systemic ventricle were measured in the apical 2- and 4-chamber views, and the ejection fraction was calculated. Furthermore, TDI images from the apical 4-chamber view were obtained. The color frame rate was ≥120 frames/s, and at least three consecutive beats were recorded. The PA-TDI duration was determined, as previously described.[6] In brief, a sample volume was placed at the lateral wall of the left-sided atrium, just above the atrioventricular valve annulus. Next, the PA-TDI duration, defined as the time from onset of the P-wave of the surface ECG to the peak of the A' wave on the TDI tracings of the lateral atrial wall was assessed (Figure 1). The PA-TDI duration was averaged from three cardiac cycles.

Atrial arrhythmia

Patients were followed-up at six to12 monthly intervals for the occurrence of AA. AA was determined on the basis of electrocardiographic findings consistent with the diagnosis of atrial flutter, atrial tachycardia or atrial fibrillation on 12-lead electrocardiograms and 24 hours electro-cardiogram Holter recordings.[10] In patients with an ICD, stored electrocardiographic information was interrogated every six months, and episodes of AA were recorded.

Statistical Analysis

Continuous variables are expressed as mean ± standard deviation. Categorical variables are presented as numbers and percentages. Differences between the patients with and without AA during follow-up were analyzed using the unpaired Student t-test for continuous data and the Chi-square test for categorical data. The study population was divided according to the optimal PA-TDI duration cut-off value for the prediction of AA occurrence. The optimal PA-TDI cut-off value was determined with receiver operating characteristic (ROC) curve analysis. Cumulative event rates were calculated with the Kaplan-Meier survival analysis and the time-to-event data with respect to the occurrence of AA were compared with the log-rank test between the two groups of patients, dichotomized based on the PA-TDI cut-off value. In addition, univariate and multivariate Cox proportional hazards regression analyses were performed to identify clinical and echocardiographic predictors for the occurrence of AA. Only significant univariate predictors were

Figure 1. PA-TDI duration measurement

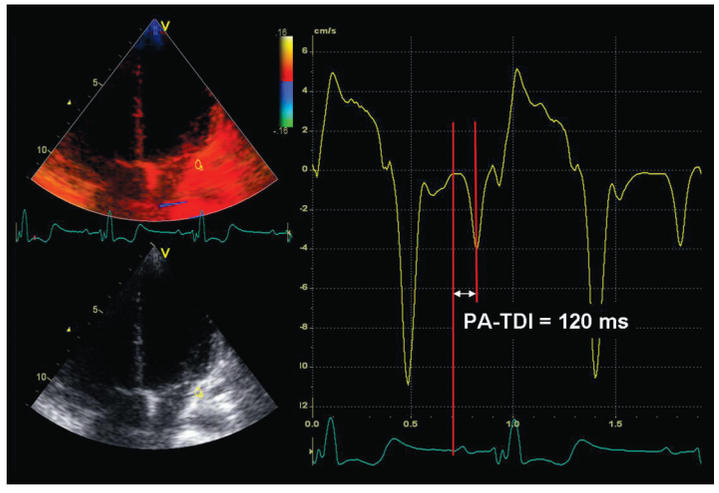

Example of the assessment of PA-TDI duration in a Tetralogy of Fallot patient. A sample volume is placed on the lateral wall of the left atrium just above the mitral valve. The PA-TDI duration is the time from the onset of the P-wave to the peak of the A' wave in the velocity graph (white arrow). In this patient, the PA-TDI duration is 120 ms. Abbreviation: PA-TDI: total atrial activation time, as assessed with tissue Doppler imaging.

entered as variables in the multivariate analysis using the enter method. None of the significant univariate predictors had a linear correlation coefficient >0.7 and therefore, multicollinearity between the parameters was unlikely. Hazard ratios and 95% confidence intervals (CI) were calculated for each independent variable. Data were analyzed using the SPSS 17.0 software (SPSS Inc, Chicago, Illinois). A p-value of <0.05 was considered statistically significant.

RESULTS

Patient population

A total of 223 adult CHD patients were included (mean age 49 ± 12 years, 49% male). During a median follow-up duration of 39 months (inter-quartile range 21 to 57 months), a total of 57 (26%) patients presented with AA. Table 1 displays the clinical and echocardiographic characteristics of both groups of adult CHD patients (AA during follow-up vs. no AA during follow-up). The proportion of patients with severe CHD was significantly larger in the group of patients with AA compared to the group of patients without AA (53% vs. 34%, p=0.015). A total of 61% of patients with AA during follow-up had a prior history of AA. No differences between the two groups were observed for the presence of hypertension. Surgical procedures were performed during follow-up in 29 patients (5 atrioventricular valve repairs or replacements, 17 pulmonary or aortic valve replacements, 5 atrial septum defect closures, 2 other procedures). In the group with AA during follow-up, surgical procedures were more frequently performed (25% vs. 9%, p=0.003).

On echocardiography, no significant differences in dimensions and ejection fraction of the systemic ventricle were observed between the two groups (Table 1). Interestingly, the PA-TDI duration was significantly longer in the group with AA during follow-up as compared with the group with no AA during follow-up (152 ± 33 ms vs. 121 ± 24 ms, p<0.001).

Prediction of AA during follow-up

The ROC curve analysis to identify the optimal PA-TDI cut-off value to predict AA yielded a cut-off value of 126 ms (area under the curve 0.76). Subsequently, this cut-off value for PA-TDI duration was used to dichotomize the population, and the time-to-event data with respect to the occurrence of AA was evaluated with Kaplan-Meier survival analysis.

The Kaplan-Meier curves showed a significantly higher cumulative event rate in the group of adult CHD patients with longer PA-TDI duration (≥126 ms) as compared with adult CHD patients with a shorter PA-TDI duration (<126 ms) (Chi-square: 21.10, log rank p<0.001) (Figure 2). The cumulative event rates in the group with a PA-TDI duration ≥126 ms were 20%, 26%, 36% and 43% at 12, 24, 36 and 48 months, respectively. In contrast, in the group of patients with a PA-TDI duration <126 ms, these event rates were 5%, 6%, 8% and 8%, for the respective time frames.

Table 2 shows the hazard ratios for the univariate predictors for the occurrence of AA during follow-up. Prior history of AA, surgical procedure during follow-up and PA-TDI duration were significant univariate predictors. Finally, at multivariate analysis, prior history of AA (hazard ratio: 4.85, 95% CI: 2.71 to 8.69, p<0.001) surgical procedure during follow-up (hazard ratio: 2.33, 95% CI: 1.26 to 4.33, p=0.007) and the PA-TDI duration (hazard ratio: 2.02, 95% CI: 1.07 to 3.83, p=0.031) were independent predictors of the occurrence of AA during follow-up.

Figure 2. Kaplan-Meier curve for freedom from atrial arrh ythmia

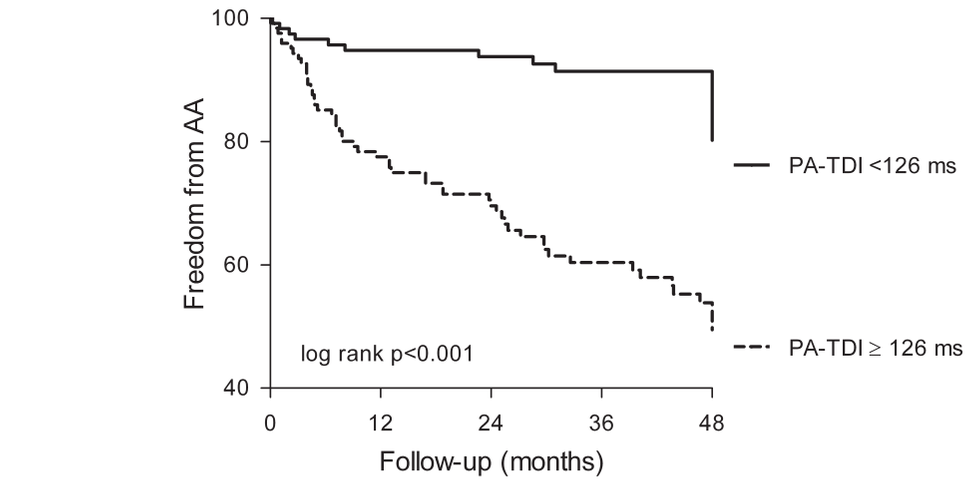

Patients at risk:

PA-TDI < 126 ms	117	104	90	72	49
PA-TDI ≥ 126 ms	106	81	67	48	33

Kaplan-Meier curve depicting freedom from atrial arrhythmia of CHD patients according to PA-TDI duration, dichotomized based on ROC curve analysis. Abbreviations: AA atrial arrhythmia, PA-TDI: total atrial activation time, as assessed with tissue Doppler imaging.

DISCUSSION

The present evaluation demonstrates that in adult CHD patients, long total atrial activation time as assessed with echocardiographic techniques (PA-TDI duration) is associated with increased risk of AA occurrence during follow-up. Particularly, the risk of AA occurrence during follow-up was twofold in adult CHD patients with a PA-TDI duration ≥126 ms compared with adult CHD patients with a PA-TDI duration <126 ms.

Atrial arrhythmia in CHD patients

AA is common during long-term follow-up in adult CHD patients. In a recent population-based study, Bouchardy et al. reported a lifetime risk of AA of 63% in patients with severe CHD and of 47% in patients without severe CHD.[2] AA is an important clinical burden in adult CHD patients as it is associated with the occurrence of stroke, heart failure, cardiac interventions and increased mortality.[2] Particularly, in patients with severe CHD, the occurrence of AA may further impair a compromised hemodynamic condition.[2, 11] Previous studies have identified various clinical predictors of AA in adult patients with CHD, such as CHD diagnosis and type and number of surgical repairs.[12-14] In the current study, prior history of AA and surgical procedures during follow-up were related to AA. Furthermore, the present evaluation showed that the assessment of PA-TDI duration with echocardiography provided an additional parameter to further improve the stratification of CHD patients for AA occurrence.

PA-TDI duration in CHD patients

In CHD patients, the principal pathophysiological substrate for AA is provided by electrical re-entry through atrial areas with delayed electrical conduction.[3, 15-17] These areas result from surgical atrial scar tissue (e.g. after Fontan and Mustard/Senning procedure, closure of atrial septal defect, or atriotomy in tetralogy of Fallot correction) or atrial fibrosis in patients with longstanding pressure or volume overload of the atria.[3, 15-17] These sites of delayed electrical conduction prolong the time required for atrial electrical activation. Prolonged total atrial conduction time is a reliable predictor of AA.[4, 5] Currently, the gold standard for assessing total atrial conduction time is the P-wave duration as assessed with signal-averaged electrocardiograms.[4, 5] However, this is a time-consuming technique and therefore not suitable for routine clinical use. The novel echocardiographic modality of TDI enables assessment of the total atrial activation time by measuring the PA-TDI duration, a readily and feasible noninvasive method to identify patients with a prolonged atrial conduction

time. Recently, Merckx and co-workers validated PA-TDI duration against the P-wave duration on signal-averaged electrocardiograms.[6] The authors observed a strong correlation between the two techniques (r=0.91). In addition, subsequent studies demonstrated the value of PA-TDI to predict AA in various groups of patients with heart disease with or without prior AA.[7, 8, 18] In the current study, the PA-TDI duration independently predicted the occurrence of AA during follow-up of CHD patients. This finding may have important implications. Timely identification of CHD patients at risk for AA provides an opportunity for preventive measures for AA occurrence (such as anti-tachycardia pacing or surgical treatment of an underlying hemodynamic problem)[10, 16, 19, 20] or for indication of anticoagulant therapy to prevent complications of AA (such as stroke).[10, 16] Future studies are warranted to identify the cut-off values of PA-TDI duration for risk stratification of AA in the various diagnostic subgroups with CHD.

CONCLUSION

In conclusion, the PA-TDI duration, prior history of AA and surgical procedures during follow-up were independently associated with the occurrence of AA in adult CHD patients. PA-TDI duration is a useful tool for the identification of CHD patients at risk for AA during clinical follow-up.

REFERENCE LIST

1 Marelli AJ, Mackie AS, Ionescu-Ittu R, Rahme E, Pilote L. Congenital heart disease in the general population: changing prevalence and age distribution. Circulation 2007;115:163-172.

2 Bouchardy J, Therrien J, Pilote L, Ionescu-Ittu R, Martucci G, Bottega N, Marelli AJ. Atrial arrhythmias in adults with congenital heart disease. Circulation 2009;120:1679-1686.

3 Walsh EP, Cecchin F. Arrhythmias in adult patients with congenital heart disease. Circulation 2007;115:534-545.

4 Fukunami M, Yamada T, Ohmori M, Kumagai K, Umemoto K, Sakai A, Kondoh N, Minamino T, Hoki N. Detection of patients at risk for paroxysmal atrial fibrillation during sinus rhythm by P wave-triggered signal-averaged electrocardiogram. Circulation 1991;83:162-169.

5 Guidera SA, Steinberg JS. The signal-averaged P wave duration: a rapid and noninvasive marker of risk of atrial fibrillation. J Am Coll Cardiol 1993;21:1645-1651.

6 Merckx KL, De Vos CB, Palmans A, Habets J, Cheriex EC, Crijns HJ, Tieleman RG. Atrial activation time determined by transthoracic Doppler tissue imaging can be used as an estimate of the total duration of atrial electrical activation. J Am Soc Echocardiogr 2005;18:940-944.

7 Antoni ML, Bertini M, Atary JZ, Delgado V, ten Brinke EA, Boersma E, Holman ER, van der Wall EE, Schalij MJ, Bax JJ, van de Veire NR. Predictive value of total atrial conduction time estimated with tissue Doppler imaging for the development of new-onset atrial fibrillation after acute myocardial infarction. Am J Cardiol 2010;106:198-203.

8 De Vos CB, Weijs B, Crijns HJ, Cheriex EC, Palmans A, Habets J, Prins MH, Pisters R, Nieuwlaat R, Tieleman RG. Atrial tissue Doppler imaging for prediction of new-onset atrial fibrillation. Heart 2009;95:835-840.

9 Mackie AS, Pilote L, Ionescu-Ittu R, Rahme E, Marelli AJ. Health care resource utilization in adults with congenital heart disease. Am J Cardiol 2007;99:839-843.

10 Camm AJ, Kirchhof P, Lip GY, Schotten U, Savelieva I, Ernst S, Van G, I, Al-Attar N, Hindricks G, Prendergast B, Heidbuchel H, Alfieri O, Angelini A, Atar D, Colonna P, De CR, De SJ, Goette A, Gorenek B, Heldal M, Hohloser SH, Kolh P, Le Heuzey JY, Ponikowski P, Rutten FH, Vahanian A, Auricchio A, Bax J, Ceconi C, Dean V, Filippatos G, Funck-Brentano C, Hobbs R, Kearney P, McDonagh T, Popescu BA, Reiner Z, Sechtem U, Sirnes PA, Tendera M, Vardas PE, Widimsky P, Vardas PE, Agladze V, Aliot E, Balabanski T, Blomstrom-Lundqvist C, Capucci A, Crijns H, Dahlof B, Folliguet T, Glikson M, Goethals M, Gulba DC, Ho SY, Klautz RJ, Kose S, McMurray J, Perrone FP, Raatikainen P, Salvador MJ, Schalij MJ, Shpektor A, Sousa J, Stepinska J, Uuetoa H, Zamorano JL, Zupan I. Guidelines for the management of atrial fibrillation: The Task Force for the Management of Atrial Fibrillation of the European Society of Cardiology (ESC). Eur Heart J 2010.

11 Li W, Somerville J. Atrial flutter in grown-up congenital heart (GUCH) patients. Clinical characteristics of affected population. Int J Cardiol 2000;75:129-137.

12 Khairy P, Aboulhosn J, Gurvitz MZ, Opotowsky AR, Mongeon FP, Kay J, Valente AM, Earing MG, Lui G, Gersony DR, Cook S, Ting JG, Nickolaus MJ, Webb G, Landzberg MJ, Broberg CS. Arrhythmia burden in adults with surgically repaired tetralogy of Fallot: a multi-institutional study. Circulation 2010;122:868-875.

13 Stephenson EA, Lu M, Berul CI, Etheridge SP, Idriss SF, Margossian R, Reed JH, Prakash A, Sleeper LA, Vetter VL, Blaufox AD. Arrhythmias in a contemporary fontan cohort: prevalence and clinical associations in a multicenter cross-sectional study. J Am Coll Cardiol 2010;56:890-896.

14 Trojnarska O, Grajek S, Kramer L, Gwizdala A. Risk factors of supraventricular arrhythmia in adults with congenital heart disease. Cardiol J 2009;16:218-226.

15 Delacretaz E, Ganz LI, Soejima K, Friedman PL, Walsh EP, Triedman JK, Sloss LJ, Landzberg MJ, Stevenson WG. Multi atrial maco-re-entry circuits in adults with repaired congenital heart disease: entrainment mapping combined with three-dimensional electroanatomic mapping. J Am Coll Cardiol 2001;37:1665-1676.

16 Triedman JK. Arrhythmias in adults with congenital heart disease. Heart 2002;87:383-389.

17 Zrenner B, Ndrepepa G, Schneider MA, Karch MR, Brodherr-Heberlein S, Kaemmerer H, Hess J, Schomig A, Schmitt C. Mapping and ablation of atrial arrhythmias after surgical correction of congenital heart disease guided by a 64-electrode basket catheter. Am J Cardiol 2001;88:573-578.

18 Bertini M, Borleffs CJ, Delgado V, Ng AC, Piers SR, Shanks M, Antoni ML, Biffi M, Boriani G, Schalij MJ, Bax JJ, van de Veire.N.R. Prediction of atrial fibrillation in patients with an implantable cardioverter-defibrillator and heart failure. Eur J Heart Fail 2010;12:1101-1110.

19 Collins KK, Love BA, Walsh EP, Saul JP, Epstein MR, Triedman JK. Location of acutely successful radiofrequency catheter ablation of intraatrial reentrant tachycardia in patients with congenital heart disease. Am J Cardiol 2000;86:969-974.

20 Deal BJ, Mavroudis C, Backer CL, Johnsrude CL, Rocchini AP. Impact of arrhythmia circuit cryoablation during Fontan conversion for refractory atrial tachycardia. Am J Cardiol 1999;83:563-568.

CHAPTER 5

Summary and conclusions

Nederlandse samenvatting

5.1

Summary and conclusions

RIGHT VENTRICULAR IMAGING: ECHOCARDIOGRAPHY

The first part of this thesis aimed to characterize ventricular mechanics and performance with advanced echocardiographic imaging techniques in patients with congenital heart disease (CHD), with particular focus on the right ventricle (RV). In **chapter 2.1**, an overview was provided on the current role of cardiac resynchronization therapy (CRT) in CHD and pediatric patients with heart failure. CRT is a novel therapy and typically involves atrio-biventricular pacing. CRT has demonstrated to improve left ventricular (LV) function and outcome of adult patients with LV failure by inducing a more synchronous contraction pattern. Based on the current clinical evidence, CRT is a promising therapy to improve cardiac performance and clinical outcome of CHD and pediatric patients with heart failure, in particular in those with LV failure as a result of chronic RV pacing. However, trials reporting on the long-term effects of CRT in CHD and pediatric patients are warranted. Furthermore, no trials have been performed to assess the adult selection criteria for CRT (New York Heart Association functional class III or IV despite optimized pharmacological therapy, left ventricular ejection fraction (LVEF) <35% and QRS duration >120 ms) in CHD and pediatric patients. The various anatomical substrates in CHD patients (systemic LV, systemic RV, single ventricle) may result in patterns of cardiac dyssynchrony that are not accurately characterized by the adult criteria. Future trials are needed to establish appropriate guidelines for CHD patient selection for CRT, taking into account the different anatomical subgroups.

Subsequently, the role of conventional and advanced echocardiographic techniques to response to CRT in CHD and pediatric patients was discussed in detail in chapter 2.1. In adult trials, the assessment of dyssynchrony with echocardiography has been shown to predict a favorable response to CRT. At present, few studies are available on cardiac mechanics and dyssynchrony parameters that predict CRT response in CHD and pediatric patients. Therefore, studying LV and RV mechanics with various (advanced) imaging modalities can provide a definition of cardiac dyssynchrony in CHD and pediatric patients.

Accordingly, the promising results of CRT have encouraged the research on LV and RV mechanics in pediatric and CHD patients, which was the focus of the subsequent chapters of this thesis. First, understanding ventricular mechanics in healthy children can help optimize the benefits of pacing strategies such as CRT in pediatric and CHD patients with heart failure. **Chapter 2.2** aimed to provide reference values of peak systolic velocities and timings of peak systolic velocities of the LV and RV, as assessed with tissue Doppler imaging (TDI) in healthy children. Peak systolic velocities increased significantly with age at both ventricles, reflecting cardiac maturation. Within the LV, no relevant intra-ventricular time differences were observed at any age. This observation of a synchronous contraction of the LV is in agreement with adult studies, and provides an empirical basis for the application of CRT in pediatric candidates with LV failure.

In contrast, within the RV of healthy children, a significant mechanical time delay was observed between the peak systolic velocity at the RV free wall (RVFW) and the intra-ventricular septum (IVS) and between the RVOT and the RV free wall (RVFW). In a subsequent study, this phenomenon of a mechanical time delay between the outlet and inlet regions of the RV was also observed with speckle tracking strain imaging, as described in **chapter 2.3.** In this study, the longitudinal deformation pattern of the RVFW and RVOT was evaluated in healthy children and in patients with corrected tetralogy of Fallot (cToF). As assessed with speckle tracking strain imaging, longitudinal deformation of the RVOT preceded longitudinal deformation of the RVFW in children with a structurally normal RV. In cToF patients, this mechanical activation sequence was also observed. However, in the cToF patients, the RVOT deformation was significantly delayed, causing a reduction of the mechanical time delay within the RV. Furthermore, the reduced time delay was related to impairment in RV performance.

The observed mechanical activation pattern of the healthy RV, with longitudinal motion and deformation of the RVOT preceding that of the RVFW, seems to conflict with the theory of a peristalsis-like contraction pattern of the RV segments. This peristalsis theory postulates that the RV body contracts prior to the RVOT and was mainly derived from experimental animal studies. However, data from these experiments did not uniformly point towards a peristalsis-like pattern of RV contraction. Importantly, two directions of motion of the RVOT have been explored in these studies: transversal and longitudinal. In individuals with a structurally normal RV, a peristalsis-like pattern of RV contraction was only observed in the transversal direction. However, in the longitudinal direction, the peristalsis-like pattern was not observed, which is in agreement with our data. The presence of a mechanical delay during contraction of the structurally normal RV has important clinical implications for the treatment of RV dysfunction with CRT. The pathophysiological basis of CRT is the restoration of electromechanical dyssynchrony. With the observed mechanical delay within the healthy RV, this concept of resynchronization may not be applicable to the RV. Additional studies to confirm this model of RV sequential contraction are warranted prior to the application of CRT in patients with RV failure.

In **chapter 2.4,** ventricular-ventricular interaction was studied with speckle tracking strain imaging by assessing the relationship between longitudinal RV and LV strain and LV rotation in cToF patients and in healthy subjects. Despite a normal LV ejection fraction (as assessed with cardiac magnetic resonance [CMR]), subclinical dysfunction of both the RV and LV was observed with speckle tracking strain imaging in the cToF patients. At a regional level, analysis with two-dimensional speckle tracking revealed a homogeneous reduction of longitudinal RV strain in cToF patients in all segments, whereas at the LV, impairment in longitudinal strain and rotational mechanics was only observed at the mid and apical levels. Furthermore, a close relationship was observed between global RV and LV mechanics. This close relationship was most pronounced at the apical levels of the RV and LV, indicating that the observed adverse ventricular-ventricular interactions may start at the apical level in cToF patients.

These conclusions were endorsed by a subsequent study in **chapter 2.5** that showed pronounced volume increase in cToF patients with chronic volume overload at the apical level of the RV**.** In this study, a segmental analysis of the RV was performed with real-time three-dimensional echocardiography (RT3DE). In healthy subjects as well as in cToF patients, RV volumes and ejection fraction were analysed at a global and regional (inlet, apical trabecular and outlet) level. Global RV volumes were significantly increased in cToF patients. The segmental analysis pointed out that the volume increase in cToF patients was most pronounced at the apical trabecular segment. According to these results and the results of chapter 2.4, the apical trabecular part plays a central role in the adaptive response of the RV to volume overload in cToF patients. Furthermore, the regional volume increase at the apex of the RV may account for the observed adverse ventricular-ventricular interaction at the apex. As a result of the volume increase at the apex, altered apical geometry of the RV may distort regional fiber orientation, which could have a deleterious effect on systolic biventricular performance. Future studies in cToF and other CHD patients with RV dilatation may need to focus on the apical trabecular segment of the RV to determine criteria for therapeutic intervention.

RIGHT VENTRICULAR IMAGING: CARDIAC MAGNETIC RESONANCE

The second part of this thesis aimed to investigate the role of advanced cardiac magnetic resonance (CMR) techniques to characterize RV mechanics in CHD patients. CMR plays an increasing role during clinical follow-up of CHD patients, especially in those with complex CHD. **Chapter 3.1** provided an overview of the current clinical applications of CMR in various subgroups of post-operative CHD patients. Furthermore, an overview of advanced CMR techniques in CHD patients and their clinical value was presented in this chapter. One of these advanced CMR techniques is the assessment of myocardial velocities and timings with tissue-velocity magnetic resonance imaging (TV-MRI). In **chapter 3.2** a direct comparison between TV-MRI and TDI was performed to assess peak systolic velocities and timings of peak systolic velocities within the RV in cToF patients and in healthy subjects. The results demonstrated that TV-MRI and TDI can be used interchangeably for the clinical evaluation of RV mechanics in healthy subjects and in cToF patients. Furthermore, with both TV-MRI and TDI, the peak systolic velocity at the RVOT occurred prior to the peak systolic velocity at the RVFW in cToF patients as well as in healthy subjects. These results underpin the observations on the temporal activation pattern of the RV as described in chapters 2.2 and 2.3.

Chapter 3.3 extended the validation of TV-MRI to assess RV mechanics by comparing diastolic velocities between TV-MRI and TDI in cToF patients and healthy subjects. The assessment of diastolic function is relevant in cToF patients, since RV end-diastolic volume and pulmonary regurgitation (two parameters strongly related to adverse outcome in cToF patients) are diastolic parameters. Conflicting results have been published on the clinical implications of global diastolic dysfunction in cToF patients. However, TV-MRI enables the assessment of diastolic performance of the RV at a regional level. Diastolic velocities of the RVOT had not been investigated previously. During surgical correction of tetralogy of Fallot, manipulation of the RVOT is almost invariably needed to relieve the pulmonary stenosis. As a result, regional scar tissue may lead to functional abnormalities of the RVOT. In chapter 3.3, regional diastolic velocities (early diastolic velocity: E', late diastolic velocity: A' and diastolic performance: E'/ A') were measured at the RVFW and at the RVOT with TV-MRI and with TDI in cToF patients and in controls. It was demonstrated that TV-MRI and TDI can be used interchangeably for the assessment of regional diastolic velocities and performance of the RV. Furthermore, the regional diastolic velocities and diastolic performance at the RVFW and RVOT were impaired in cToF patients. At the RVOT, the observed impaired diastolic performance was independently related to RV dilatation. This observation was in accordance with previous studies that pointed out the independent role of RVOT integrity to prevent RV dilatation in cToF patients. Accordingly, the assessment of regional RV diastolic performance with TDI and TV-MRI yielded insight into the pathophysiological mechanism leading to RV dilatation in cToF patients. More trials are needed to further investigate the observed relation between diastolic performance of the RVOT and RV dilatation.

In **chapter 3.4,** novel three-dimensional three-directional velocity-encoded flow imaging with retrospective valve tracking (3D flow) was validated for the assessment of RV flow volumes. 3D flow was compared with conventional two-dimensional velocity-encoded flow imaging (2D flow) for the assessment of flow volumes over the pulmonary valve and the tricuspid valve in cToF patients and in healthy subjects. Planimetry was used as the reference standard. The study demonstrated that 3D flow is more accurate than 2D flow for the assessment of both pulmonary valve flow volumes as well as for tricuspid valve flow volumes. An important advantage of 3D flow is the retrospective valve tracking, enabling angulation of the imaging plane according to the position and the direction of the flow jet. Adjustment of the imaging plane is especially important for the assessment of flow at the tricuspid valve, since this valve may move up to 24 mm during image acquisition. Furthermore, during 3D flow assessment, the pulmonary and tricuspid valve flow is acquired simultaneously. The simultaneous assessment of various valves during 3D flow acquisition reduces scan time. Furthermore, with the use of 3D flow, global diastolic function of the RV in cToF patients with pulmonary regurgitation can be evaluated. The assessment of diastolic function of the RV in patients with pulmonary regurgitation is complicated, since diastolic filling occurs from two sources; the tricuspid valve and the pulmonary valve. The simultaneous assessment of flow over both valves during 3D flow enables accurate summation of both flow volume curves during diastole. Summation of the tricuspid and pulmonary flow volumes during diastole provides time-volume curves, reflecting the diastolic filling pattern of the RV. Hence, 3D flow-derived RV time-volume curves permit the evaluation of global diastolic function of the RV in patients with pulmonary regurgitation. It was shown in chapter 3.4 that diastolic assessment with 3D flow was able to discriminate between patients and controls. Furthermore, 3D flow assessment of diastolic function discriminated cToF patients with a restrictive RV filling pattern from those without RV restriction. In conclusion, the advanced MRI applications of 3D flow and TV-MRI provide novel parameters for the assessment of RV diastolic function at a global and regional level, respectively. The evaluation of global and regional diastolic RV function with these advanced CMR techniques can facilitate ongoing research on the clinical implications of RV diastolic dysfunction during long-term follow-up in CHD patients.

PREDICTION OF OUTCOME

The prediction of clinical outcome is an important goal of clinical studies on cardiac imaging techniques. The last part of this thesis focused on the prediction of clinical outcome of CHD patients with the use of conventional and advanced echocardiographic techniques. **Chapter 4.1** investigated clinical predictors for the need for pulmonary valve replacement. In particular the relation between residual pulmonary stenosis, as assessed with conventional Doppler echocardiography, and the need for pulmonary valve replacement during long term follow-up of cToF patients was investigated. Current surgical strategies to relieve pulmonary stenosis in cToF patients aim to limit the amount of patch use whenever possible, since patch use is related to pulmonary regurgitation. However, this 'restrictive approach' may result into a (mild) degree of residual pulmonary stenosis in post-operative cToF patients. A mild residual pulmonary stenosis may reduce the amount of pulmonary regurgitation and consequently, may reduce the need for pulmonary valve replacement during follow-up of cToF patients. Indeed, the results of our study indicated that a mild gradient over the pulmonary artery is independently associated with a reduced risk of pulmonary valve replacement. These findings underscore the importance of the current surgical strategies in cToF patients that advocate a restrictive surgical relief of the pulmonary stenosis in ToF patients. Furthermore, knowledge on the clinical implications of a mild residual pulmonary stenosis improves patient-based counseling during clinical follow-up of cToF patients.

Finally, in **chapter 4.2**, the advanced echocardiographic application of TDI was used for the prediction of atrial arrhythmias in a cohort of adult CHD patients. With TDI of the atria, the time interval from the onset of the P-wave on the electrocardiogram to the peak of the A' wave on the TDI tracings of the lateral atrial wall can be measured (PA-TDI duration). In CHD patients, the principal pathophysiological substrate for atrial arrhythmias is provided by electrical re-entry through atrial areas with delayed electrical conduction. These sites of delayed electrical conduction prolong the time required for atrial electrical activation. Prolonged total atrial conduction time is a reliable predictor of atrial arrhythmias. The PA-TDI duration reflects the total atrial conduction time, and has been shown to be a predictor of atrial arrhythmias in adult patients with 'acquired' heart disease. In our study, the PA-TDI duration was independently associated with the occurrence of atrial arrhythmia in adult CHD patients. Therefore, the PA-TDI duration can be a useful tool for the identification of CHD patients at risk for atrial arrhythmias during clinical follow-up.

CONCLUSIONS

In this thesis, important new insights were gained in the electromechanical activation and deformation pattern of the RV with the use of advanced echocardiographic and MRI techniques. The obtained insights have clinical implications for future treatment strategies in CHD patients with RV failure. The population of patients with CHD is growing, and RV failure is frequently observed in this population. Nevertheless, the pathophysiology of RV failure remains incompletely understood. In current clinical practice, the application of CRT has recently gained ground in the treatment of patients with LV failure. The beneficial results of CRT in adult patients with LV failure have encouraged studies on RV mechanics and performance, as presented in this thesis. With the use of three different noninvasive advanced imaging techniques (TDI, speckle tracking strain imaging, TV-MRI) it was demonstrated in this thesis that a considerable mechanical delay during longitudinal systolic contraction is present in the healthy RV. In addition, this mechanical delay was related to the performance of the RV. Accordingly, the concept of resynchronization by the application of CRT seems not directly applicable in patients with RV failure, and this should be an important starting point for future studies on pacing strategies in patients with RV failure.

Additional insight into RV mechanics and performance in the presence of volume overload was obtained by studying the RV of cToF patients at a regional level. It was demonstrated that adverse RV remodeling after chronic volume overload in cToF patients starts at the apical level. Furthermore, adverse ventricular-ventricular interaction, leading to subclinical LV dysfunction, was also most apparent at the apical level. At present, there is ongoing debate on the optimal cut-off values for pulmonary valve replacement in cToF patients. The results of this thesis indicate that future trials on cut-off values may need to focus specifically on the apical trabecular part of the RV. Finally, novel insight was obtained on the role of the (surgically remodeled) RVOT in the pathophysiological pathway leading to RV dilatation in cToF patients. Both the study on regional diastolic velocities as well as the report on the clinical predictors of the need for pulmonary valve replacement pointed out that in cToF patients, the integrity and function of the RVOT is important in the pathophysiological mechanism leading to RV dilatation. Accordingly, a targeted intervention on the RVOT in cToF patients undergoing pulmonary valve replacement could lead to improved outcomes.

5.2

Nederlandse samenvatting

Beeldvorming van de rechter hartkamer: echocardiografie

Het eerste deel van dit proefschrift had als doel om met behulp van echocardiografie het elektromechanische activatiepatroon van de hartkamers in kaart te brengen bij patiënten met aangeboren hartafwijkingen. In het bijzonder werd in dit proefschrift gefocust op de rechter hartkamer. **Hoofdstuk 2.1** geeft een overzicht van de gepubliceerde onderzoeken over cardiale resynchronisatietherapie (CRT) bij patiënten met aangeboren hartafwijkingen en kinderen met hartfalen. CRT is een nieuwe therapie die veel gebruikt wordt bij volwassen patiënten met hartfalen. Bij CRT wordt gebruikgemaakt van een pacemaker die op beide hartkamers is aangesloten. Met deze pacemakertherapie wordt een synchrone contractie van het hart beoogd, wat een positief effect heeft bij mensen met een falende linker hartkamer. Uit de huidige gepubliceerde onderzoeken over CRT bij patiënten met aangeboren hartafwijkingen en kinderen met hartfalen kan worden geconcludeerd dat CRT een veelbelovende therapie is in deze patiëntenpopulatie. Echter, onderzoek naar de langetermijneffecten is vereist. Daarnaast zijn de inclusiecriteria voor CRT bij volwassenen (New York Heart Assoccation functioneren in klasse III of IV ondanks optimale medicamenteuze therapie, linker hartkamer ejectiefractie <35%, QRS duur >120 ms) niet onderzocht bij patiënten met aangeboren hartafwijkingen en kinderen met hartfalen. Vervolgens werd in hoofdstuk 2.1 beschreven of conventionele en geavanceerde echocardiografietechnieken kunnen voorspellen welke patiënten met aangeboren hartafwijkingen en kinderen met hartfalen baat hebben bij CRT. De groep patiënten met aangeboren hartafwijkingen is zeer heterogeen en kan worden onderverdeeld in anatomische subgroepen: patiënten waarbij de linker hartkamer de grote bloedsomloop ondersteunt, patiënten waarbij de rechter hartkamer de grote bloedsomloop ondersteunt en patiënten met één hartkamer. Deze subgroepen kunnen afwijkende contractiepatronen van de hartkamers vertonen die niet worden ondervangen door de inclusiecriteria voor CRT bij volwassenen met hartfalen. Vervolgstudies moeten zich richten op inclusiecriteria voor CRT bij patiënten met congenitale hartafwijkingen en kinderen met hartfalen. Met behulp van geavanceerde beeldvormende technieken kan het contractiepatroon van de hartkamers bij kinderen en patiënten met aangeboren hartafwijkingen gedetailleerd in kaart worden gebracht.

Primair is inzicht in het contractiepatroon van de hartkamers bij gezonde kinderen van belang om het resultaat van CRT en eventuele andere pacemakertherapieën te optimaliseren. In **hoofdstuk 2.2** werd een studie beschreven naar referentiewaarden van pieksnelheden tijdens de contractie van de hartkamer, tijd tot pieksnelheid, en tijdsverschillen tussen de pieksnelheden op verschillende locaties binnen de hartkamers bij gezonde kinderen gemeten met 'tissue Doppler imaging' echocardiografie (TDI). In de studie werd een leeftijdsafhankelijke toename van pieksnelheden tijdens contractie in beide hartkamers geobserveerd. Daarnaast werden in de linker hartkamer zeer kleine tijdsverschillen geobserveerd tussen pieksnelheden tijdens contractie bij kinderen van alle leeftijden. Deze data over het contractiepatroon van de linker hartkamer vormen een empirische onderbouwing voor studies naar afwijkende contractiepatronen (dissynchronie) en CRT voor de linker hartkamer bij kinderen met hartfalen. In tegenstelling tot de bevindingen in de linker hartkamer, werd in de rechter hartkamer een groot tijdsverschil geobserveerd tussen het optreden van de pieksnelheden tussen de rechterkamerintstroom en het interventrikulaire septum, alsook tussen de rechterkamerinstroombaan en de rechterkameruitstroombaan. Dit tijdsverschil werd ook geobserveerd in een studie naar deformatie van hartspierweefsel met 'speckle tracking' echocardiografie in **hoofdstuk 2.3.** In deze studie werd het deformatiepatroon van het hartspierweefsel van de rechter hartkamer onderzocht bij gezonde kinderen en bij patiënten met een chirurgische gecorrigeerde tetralogie van Fallot (cToF) (een aangeboren hartafwijking waarbij frequent disfunctie van de rechter hartkamer word gezien). De longitudinale samentrekking van hartspierweefsel tijdens contractie werd bestudeerd in the rechterkamerinstroombaan en in de rechterkameruitstroombaan. De maximale longitudinale verkorting tijdens contractie had eerder plaats in de uitstroombaan dan in de instroombaan bij gezonde kinderen. Dit deformatiepatroon van de rechter hartkamer werd ook geobserveerd bij de cToF patiënten. Echter, het geobserveerde tijdsverschil was veel korter bij de patiënten, en dit was gerelateerd met een slechtere functie van de rechter hartkamer. De observatie dat de rechterkameruitstroombaan eerder samentrekt dan de rechterkamerinstroombaan is in tegenspraak met de theorie dat rechter hartkamercontractie volgens een peristaltisch patroon verloopt. Volgens deze theorie, die voornamelijk gebaseerd is op dierexperimenteel onderzoek, contraheert de rechterkamerinstroombaan vóór de rechterkameruitstroombaan. Echter, de data van deze onderzoeken wijzen niet eenduidig op een peristaltische contractie van de rechter hartkamer. Het contractieparoon van de rechter hartkamer werd in twee richtingen geanalyseerd; longitudinaal en transversaal. Het peristaltische contractiepatroon werd alleen geobserveerd in de transversale richting, en niet in de longitudinale richting. Deze data komen overeen met de observaties in onze studie.

De observatie van een tijdsverschil in het longitudinale contractiepatroon van de gezonde rechter hartkamer heeft belangrijke consequenties voor eventuele behandeling van rechter hartkamerdisfunctie met CRT. De insteek voor behandeling met CRT is het resynchroniseren van een dissynchroon contractiepatroon. Echter, dit concept lijkt niet van toepassing op de rechter hartkamer wanneer er van nature een tijdsverschil bestaat tijdens contractie. Meer studies zijn nodig naar het contractiepatroon van de rechter hartkamer alvorens CRT kan worden toegepast bij patiënten met een falende rechter hartkamer.

In **hoofdstuk 2.4** werd speckle tracking echocardiografie gebruikt om de interactie tussen beide hartkamers te bestuderen. Met behulp van speckle tracking werd de longitudinale samentrekking van beide hartkamers en de rotatie van de linker hartkamer bestudeerd bij gezonde kinderen en bij cToF patiënten. Ondanks een normale ejectiefractie van de linker hartkamer, was de longitudinale samentrekking verminderd in beide hartkamers. Analyse van de longitudinale samentrekking op

regionaal niveau liet zien dat de samentrekking van de rechter hartkamer van cToF patiënten in zijn geheel was verminderd, terwijl in de linker hartkamer de longitudinale samentrekking alsook de rotatie alleen was verminderd in het midden en aan de punt van het hart. Daarnaast werd en nauwe relatie geobserveerd tussen de longitudinale samentrekking van de linker- en rechter hartkamer. Deze relatie was het sterkst aan de punt van het hart. Dit wijst erop dat een nadelige interactie tussen beide hartkamers bij cToF patiënten aanvangt aan de punt van het hart. Deze conclusie werd bevestigd door een studie naar volumetoename van de rechter hartkamer bij cToF patiënten in **hoofdstuk 2.5**. In dit hoofdstuk werd segmentele volumeanalyse van de rechter hartkamer met 'real time' driedimensionale echocardiografie (RT3DE) verricht. Volumina en ejectiefractie van de gehele rechter hartkamer en van de regionale segmenten (instroom, apicale segment [punt van rechter hartkamer], uitstroom) werden geanalyseerd met RT3DE bij gezonde kinderen en bij cToF patiënten. Bij de cToF patiënten werd een toename in het globale volume van de rechter hartkamer geobserveerd. Met de segmentele analyse werd aangetoond dat deze toename het grootst was in het apicale segment.

Naar aanleiding van de observaties in de hoofdstukken 2.4 en 2.5 kan worden geconcludeerd dat het apicale segment een belangrijke rol speelt in de respons van de rechter hartkamer op chronische volumebelasting (zoals bij cToF patiënten, als gevolg van lekkage van de longslagader). Daarnaast zou de regionale toename in volume in het apicale segment de oorzaak kunnen zijn van de nadelige interactie tussen beide hartkamers die werd geobserveerd in hoofdstuk 2.4. Een veranderde geometrie van de rechter hartkamer door volumetoename aan de punt van het hart kan de oriëntatie van de hartspiervezels ter plaatse verstoren, wat een negatief effect heeft op de functie van beide hartkamers. Toekomstige studies naar grenswaarden (volumina) voor interventie bij cToF patiënten en andere patiënten met volumetoename van de rechter hartkamer zou zich wellicht moeten richten op het apicale segment van de rechter hartkamer.

Beeldvorming van de rechter hartkamer: magnetic resonance imaging (MRI)

In het tweede deel van dit proefschrift werd de rol van conventionele en geavanceerde MRI technieken voor het in kaart brengen van het contractiepatroon van de rechter hartkamer onderzocht. MRI van het hart speelt een steeds belangrijkere rol tijdens de controle van patiënten met aangeboren hartafwijkingen, in het bijzonder bij patiënten met complexe aangeboren hartafwijkingen. In **hoofdstuk 3.1** werd een overzicht gegeven van de huidige toepassingen van MRI in verschillende subgroepen van patiënten met aangeboren hartafwijkingen. Verder werd een overzicht gegeven van nieuwe MRI technieken en wat deze kunnen betekenen bij patiënten met aangeboren hartafwijkingen. Eén van deze nieuwe MRI technieken is 'tissue-velocity MRI' (TV-MRI) waarmee pieksnelheid en tijd tot pieksnelheid, naar analogie van de TDI techniek, in het hartspierweefsel kunnen worden gemeten. In **hoofdstuk 3.2** werden TV-MRI en TDI metingen van de rechter hartkamer bij cToF patiënten en gezonde kinderen met elkaar vergeleken. De studie liet zien dat beide MRI technieken dezelfde resultaten genereren. Daarnaast werd in zowel cToF patiënten als in gezonde kinderen met beide technieken geobserveerd dat de pieksnelheid van de rechterkameruitstroombaan eerder plaats heeft dan de pieksnelheid van de rechterkamerinstroombaan. Deze resultaten onderschrijven de eerdere observaties met betrekking tot het contractiepatroon van de rechter hartkamer in de hoofdstukken 2.2 en 2.3.

Vervolgens werd in **hoofdstuk 3.3** TV-MRI verder gevalideerd door pieksnelheden tijdens de relaxatie van de rechter hartkamer te vergelijken tussen TDI en TV-MRI bij cToF patiënten en gezonde kinderen. De relaxatiefunctie van de rechter hartkamer bij cToF patiënten is relevant omdat twee belangrijke parameters die de prognose cToF patiënten sterk beïnvloeden (lekkage van de longslagader en volume van de rechter hartkamer) gemeten worden tijdens de relaxatiefase van de rechter hartkamer. Echter, de resultaten van eerder onderzoek naar de prognostische waarde van disfunctie van de rechter hartkamer tijdens relaxatie spraken elkaar tegen. TV-MRI kan nieuw inzicht geven in de relaxatie van de rechter hartkamer doordat het kan worden toegepast op regionaal niveau. Het relaxatiepatroon van de uitstroombaan van de rechter hartkamer was niet eerder onderzocht. Bij cToF patiënten is de uitstroombaan van de rechter hartkamer bijna altijd chirurgisch gemodelleerd. Daardoor kan littekenweefsel zijn ontstaan dat ter plaatse van de uitstroombaan het relaxatiepatroon verstoort. In hoofdstuk 3.3 werden met behulp van TDI en TV-MRI regionale pieksnelheden tijdens relaxatie van de rechter hartkamer gemeten ter plaatse van de uitstroombaan en instroombaan bij cToF patiënten en bij gezonde kinderen. De gemeten relaxatiefunctie was significant verminderd in de instroombaan en de uitstroombaan bij de cToF patiënten. Bovendien was de relaxatiefunctie in de uitstroombaan onafhankelijk gerelateerd aan de volumetoename van de rechter hartkamer. Geconcludeerd kan worden dat het meten van de regionale relaxatiefunctie van de rechter hartkamer met TDI en TV-MRI inzicht kan geven in het ziekteproces van de rechter hartkamer bij cToF patiënten. Toekomstige onderzoeken zouden zich moeten richten op de relatie tussen de relaxatiefunctie van de rechterkameruitstroombaan en het volume van de rechter hartkamer.

Hoofdstuk 3.4 beschreef de validatie van driedimensionale MRI voor meting van bloedstroom-volumina in de rechter hartkamer. Driedimensionale MRI werd vergeleken met conventionele tweedimensionale MRI voor het meten van bloedstroomvolumina over de longslagaderklep en de tricuspidalisklep (de klep tussen rechterboezem en rechter hartkamer) bij cToF patiënten en bij gezonde kinderen. Planimetrie, de gouden standaard voor volumemetingen met MRI, werd gebruikt als referentie. De resultaten van de studie lieten zien dat driedimensionale MRI nauwkeuriger is dan de conventionele tweedimensionale MRI metingen. Een belangrijk voordeel van de driedimensionale MRI techniek is de mogelijkheid om de bloedstroommetingen gedurende de gehele contractie op de exacte locatie van de (bewegende) hartklep te laten plaatsvinden. Eerder is aangetoond dat de verplaatsing van de tricuspidalisklep tijdens de contractie een belangrijke beperking vormt van tweedimensionale MRI voor het meten van bloedstroomvolumina. Daarnaast worden de metingen van de longslagaderklep en de tricuspidalisklep bij driedimensionale MRI simultaan verkregen. Dit biedt, naast verkorting van de scantijd, als voordeel dat de bloedstroomcurves van beide metingen bij elkaar opgeteld kunnen worden voor een nauwkeurige weergave van de volumeveranderingen van de rechter hartkamer tijdens de relaxatie (vullingsfase). Bij cToF patiënten met lekkage van de longslagader wordt de rechter hartkamer

tijdens de relaxatiefase niet alleen gevuld met bloed door de tricuspidalisklep, maar ook met bloed door de longslagaderklep (de lekkage). Het optellen van de beide bloedstroomcurves tijdens de relaxatiefase geeft bij deze patiënten een nauwkeurige weergave van de het vullingpatroon van de rechter hartkamer, wat de globale relaxatiefunctie van de rechter hartkamer reflecteert. Samengevat kunnen zowel 3D MRI metingen van bloedstroomvolumina en TV-MRI worden toegepast om relaxatiefunctie van de rechter hartkamer op respectievelijk globaal en regionaal niveau te meten. Door de validatie van deze geavanceerde MRI technieken wordt toekomstig onderzoek naar de prognostische waarde van globale en regionale afwijkingen in relaxatie van de rechter hartkamer in cToF patiënt mogelijk gemaakt.

Prognostische waarde van echocardiografie

Een belangrijk doel van studies naar beeldvormende technieken van het hart is het verkrijgen van inzicht in de prognostische waarde van de verkregen beelden. Het laatste deel van dit proefschrift had als doel om de prognostische waarde van conventionele en nieuwe echocardiografische technieken in kaart te brengen. In **hoofdstuk 4.1** wordt de relatie tussen restvernauwing van de longslagader, welke wordt gemeten met conventionele Doppler echocardiografie, en de noodzaak tot longslagaderklepvervanging op de lange termijn bij cToF patiënten. De huidige chirurgische technieken die gebruikt worden om de vernauwing van de longslagader van ToF patiënten te behandelen zijn erop gericht om zo weinig mogelijk gebruik te maken van prothesemateriaal, omdat dit gerelateerd is aan het optreden van lekkage van de longslagaderklep. Echter, deze chirurgische strategie kan ertoe leiden dat de vernauwing van de longslagader niet helemaal wordt opgeheven, en er een lichte restvernauwing overblijft. Deze lichte vernauwing kan als gevolg hebben dat minder lekkage van de longslagader optreedt. Dit zou de noodzaak tot vervanging van de longslagaderklep op de lange termijn kunnen doen verminderen. De resultaten van onze studie in hoofdstuk 4.1 wezen er inderdaad op dat minder longslagaderklepvervangingen werden verricht in de groep cToF patiënten met een lichte vernauwing van de longslagader. Deze resultaten onderschrijven het belang van de huidige chirurgische strategieën, en geven daarnaast houvast voor de counseling van cToF patiënten met een lichte vernauwing van de longslagader.

Tot slot werd in **hoofdstuk 4.2** een studie beschreven naar de toepassing van TDI om boezemaritmieën (ritmestoornissen van de boezem) te voorspellen bij volwassen patiënten met aangeboren hartafwijkingen. Met TDI van de boezems kan het tijdsinterval tussen de elektrische relaxatiefase van de boezem (P) en de mechanische relaxatiefase van de boezem (A) worden gemeten (het zogenoemde PA-TDI interval). Het belangrijkste ziekteproces dat ten grondslag ligt aan boezemaritmieën is een verminderde elektrische geleiding in de boezems. Verminderde elektrische geleiding voorspelt boezemaritmieën en kan kwantitatief worden weergegeven met het PA-TDI interval bij volwassen patiënten zonder aangeboren hartafwijkingen. In onze studie in hoofdstuk 4.2 was het PA-TDI interval ook onafhankelijk gerelateerd aan het optreden van boezemaritmieën bij volwassen patiënten met aangeboren hartafwijkingen. Het PA-TDI interval is dus een bruikbare toepassing voor de identificatie van patiënten met aangeboren hartafwijkingen met een verhoogd risico op boezemaritmieën.

Conclusies

Door dit proefschrift zijn de inzichten in het mechanische activatiepatroon van de rechter hartkamer sterk verbeterd. De resultaten van de studies in dit proefschrift hebben consequenties voor de toekomstige behandeling van patiënten met een falende rechter hartkamer. De groep van patiënten met aangeboren hartafwijkingen wordt steeds groter, en falen van de rechter hartkamer komt in deze populatie frequent voor. Toch wordt het exacte mechanisme achter falen van de rechter hartkamer nog niet helmaal begrepen. De goede resultaten na behandeling met CRT bij patiënten met een falende linker hartkamer hebben ertoe geleid dat er meer onderzoek wordt gedaan naar het mechanische activatiepatroon van de rechter hartkamer in relatie tot de functie van de rechter hartkamer, zoals in dit proefschrift. Met behulp van drie verschillende non-invasieve geavanceerde beeldvormende technieken (TDI, speckle tracking en TV-MRI) werd in dit proefschrift aangetoond dat er een aanzienlijk tijdsverschil in mechanische activatie binnen de gezonde rechter hartkamer plaatsvindt. Dit tijdsverschil is bovendien gerelateerd aan de functie van de rechter hartkamer. Daarom is het concept van 'resynchronisatie' van de contractie, zoals wordt beoogd met CRT in de linker hartkamer, niet direct toepasbaar op patiënten met een falende rechter hartkamer. Deze bevinding zal in toekomstige studies naar pacemakerstrategieën voor patiënten met een falende rechter hartkamer als uitgangspunt moeten worden gebruikt.

Door de rechter hartkamer op regionaal niveau te bestuderen, werd nog meer inzicht verkregen in de functie en mechanische activatie van de rechter hartkamer. Bij patiënten met een vergrote rechter hartkamer als gevolg van volume overbelasting (door longslagaderkleplekkage) werd met RT3DE geobserveerd dat het apicale segment (punt van het hart) het meest was vergroot. Verder werd met 'speckle tracking' de nadelige invloed van de vergrote rechter hartkamer op de linker hartkamer op regionaal niveau bestudeerd. Deze nadelige invloed was het meest uitgesproken aan de punt van het hart. Op dit moment is er discussie over het juiste moment (welke afkapwaarde) van ingrijpen (bijv door middel van longslagaderklepvervanging) bij cToF patiënten met een vergrote rechter hartkamer. De resultaten van dit proefschrift suggereren dat toekomstige studies zich specifiek zouden moeten richten op de punt van het hart om afkapwaarden te formuleren die het tijdstip van interventie kunnen markeren.

Tot slot werden nieuw inzichten verkregen in de rol van de uitstroombaan van de rechter hartkamer in het mechanisme dat leidt tot een vergrote rechter hartkamer bij cToF patiënten. Twee afzonderlijke studies in dit proefschrift suggereren dat de integriteit en functie van de uitstroombaan van de rechter hartkamer een belangrijke rol spelen bij patiënten met een vergrote rechter hartkamer. Een gerichte interventie aan de uitstroombaan van de rechter hartkamer bij patiënten die een longslagaderklepvervanging ondergaan zou daarom kunnen leiden tot een verbetering van de prognose van cToF patiënten.

List of publications

AE van der Hulst, AA Roest, V Delgado, LJ Kroft, ER Holman, NA Blom, JJ Bax, A de Roos, JJ Westenberg. Corrected Tetralogy of Fallot: Comparison of Tissue Doppler Imaging and Velocity-encoded MR for Assessment of Performance and Temporal Activation of Right Ventricle. Radiology. 2011 Jul;260(1):88-97

AE van der Hulst, V Delgado, NA Blom, NR van de Veire, , MJ Schalij, JJ Bax, AAW Roest, ER Holman. Review: cardiac resynchronization therapy in pediatric and congenital heart disease patients. European Heart Journal 2011, doi: 10.1093/eurheartj/ehr093

A.E. van der Hulst, AAW Roest, V. Delgado, LJM Kroft, ER Holman, NA Blom, JJ Bax, A de Roos, JJM Westenberg. Direct Comparison between Tissue Doppler Imaging and Velocity-encoded Magnetic Resonance Imaging for the Assessment of Performance and Temporal Activation of the Right Ventricle in Corrected Tetralogy of Fallot Patients.Radiology 2011; doi: 10.1148/radiol.11101993

AE van der Hulst, AAW Roest, V Delgado, ER Holman, A de Roos, NA Blom, JJ Bax. Relationship between temporal sequence of right ventricular deformation and right ventricular performance in patients with corrected tetralogy of Fallot. Heart 2011;97:231-6.

AE van der Hulst, V Delgado, ER Holman, LJM Kroft, A de Roos, MG Hazekamp, NA Blom, JJ Bax, AAW Roest. Relation of Left Ventricular Twist and Global Strain with Right Ventricular Dysfunction in Patients after Operative "Correction" of Tetralogy of Fallot. Am J Cardiol 2010;106:723-9

AE van der Hulst, JJM Westenberg, LJM Kroft, JJ Bax, NA Blom, A de Roos, AAW Roest. Tetralogy of Fallot: 3D Velocity-encoded MR Imaging for Evaluation of Right Ventricular Valve Flow and Diastolic Function in Patients after Correction. Radiology, 2010;256:724-34

AE van der Hulst, RN Sukhai. A Red Ear. J Pediatr. 2009;154:624

AE van der Hulst, H Klip, PLP Brand. Risk of developing asthma in children with atopic eczema, a systematic review. J Allergy Clin Immunol. 2007;120(3)565-9

GC Hawkins, MH Bennett, AE van der Hulst. The outcome of chronic wounds following hyperbaric oxygen therapy: a prospective cohort study – the first year interim report. Diving and Hyperbaric Medicine 2006; 36(2)94-98.